The role of Medin, the most common human amyloid, in cerebrovascular disease and cerebral β-amyloidosis

Dissertation

zur Erlangung des Grades eines
Doktors der Naturwissenschaften

der Mathematisch-Naturwissenschaftlichen Fakultät
und
der Medizinischen Fakultät
der Eberhard-Karls-Universität Tübingen

vorgelegt
von

Jessica Wagner
aus Bitburg, Deutschland

2021

Tag der mündlichen Prüfung: 21.06.2021

Dekan der Math.-Nat. Fakultät: Prof. Dr. Thilo Stehle
Dekan der Medizinischen Fakultät: Prof. Dr. Bernd Pichler

1. Berichterstatter: Dr. Jonas J. Neher
2. Berichterstatter: Prof. Dr. Alexander N.R. Weber

Prüfungskommission: Dr. Jonas J. Neher
                             Prof. Dr. Alexander N.R. Weber
                             Prof. Dr. Mathias Jucker
                             Prof. Dr. Thomas Gasser

Ich erkläre, dass ich die zur Promotion eingereichte Arbeit mit dem Titel:

„The role of Medin, the most common human amyloid, in cerebrovascular disease and cerebral β-amyloidosis"

selbständig verfasst, nur die angegebenen Quellen und Hilfsmittel benutzt und wörtlich oder inhaltlich übernommene Stellen als solche gekennzeichnet habe. Ich versichere an Eides statt, dass diese Angaben wahr sind und dass ich nichts verschwiegen habe. Mir ist bekannt, dass die falsche Abgabe einer Versicherung an Eides statt mit Freiheitsstrafe bis zu drei Jahren oder mit Geldstrafe bestraft wird.

I hereby declare that I have produced the work entitled "The role of Medin, the most common human amyloid, in cerebrovascular disease and cerebral β-amyloidosis", submitted for the award of a doctorate, on my own (without external help), have used only the sources and aids indicated and have marked passages included from other works, whether verbatim or in content, as such. I swear upon oath that these statements are true and that I have not concealed anything. I am aware that making a false declaration under oath is punishable by a term of imprisonment of up to three years or by a fine.

Tübingen, den _____   _____

Datum   Unterschrift

Für meine Eltern

TABLE OF CONTENTS

1. Summary

Amyloids occur as localized or systemic deposits composed of compact β-sheet fibrils of abnormally folded proteins that may disrupt the physiological function of the afflicted tissue by loss-of-function or gain-of-toxicity. The best characterized amyloid, amyloid-β (Aβ) is a known trigger of the molecular and cellular cascade leading to Alzheimer's disease (AD). Aβ aggregation can amplify via a prion-like seeding mechanism and rapidly spread in the brain connectome. Several downstream processes potentiate the toxic cascade, ultimately resulting in brain damage and memory loss. Interestingly, vascular dysfunction is described as an early symptom of AD in humans.

Recently, a study identified another protein that deposits in the vasculature of the AD brain – Medin amyloid (an internal fragment of MFG-E8). Medin is the most common human vascular amyloid known to date, as it can be detected within the thoracic aorta and the upper body arteries of nearly everyone above 50 years of age. As the name Medin suggests, it predominantly deposits along the elastic fibers of the tunica media. Because of its vascular localization and potential role in arterial aging it has been suggested as a possible risk factor of AD. However, despite its high prevalence in the aging population, no causal role in human pathogenesis was previously reported. Nevertheless, *in vitro* studies have described common structural, physicochemical and cytotoxic amyloid properties for Medin, and analyses of human tissue derived from autopsy or surgery implicate a role for Medin in vascular diseases. However, the question of a mechanistic link between the presence of Medin, cerebrovascular dysfunction and AD pathology remains elusive due to lack of appropriate experimental *in vivo* models, which would enable mechanistic studies.

In this dissertation, a suitable animal model to investigate the influence of Medin aggregates on cerebrovascular function was established. In particular, we found that with advancing age wild-type mice develop endogenous Medin aggregates in the aorta and cerebral arteries that resemble the sequence, biochemical properties, and morphology of human Medin amyloid. We also showed in our first study that age-associated decline in cerebral vascular function (evident by impaired artery elasticity) in living mice was rescued by prevention of vascular Medin aggregate formation through a genetic knockout of the Medin-containing C2 domain of MFG-E8 (*Mfge8* C2 KO). These observations implicate Medin as a causal factor in age-associated cerebrovascular dysfunction for the first time.

Given the fact that Medin was recently shown to template aggregation of serum amyloid A, our second study addressed whether potential co-aggregation of Medin and Aβ may exacerbate AD pathology. Indeed, our study provided first evidence for a direct amyloid-amyloid interaction of Medin and Aβ in two mouse models for cerebral β-amyloidosis. Medin did not only co-localize substantially with Aβ deposits in the brain, but the genetic deletion of Medin also altered plaque and fibril structure *in vitro* and *in vivo*, prevented MFG-E8/Medin accumulation within plaques and vasculature, and slowed the onset of pathology in cerebral β-amyloidosis. It is further important to note that in line with its vascular localization in humans, genetic Medin deficiency reduced cerebral β-amyloid angiopathy (CAA) and related microhemorrhages even at end-stage amyloid pathology. Additionally, aorta-derived Medin 'seeds' promoted pre-mature Aβ aggregation in the brain, suggesting that Medin promotes Aβ by a heterologous seeding mechanism.

To analyze the translational relevance of a potential heterologous seeding mechanism between Medin and Aβ, we also examined data from the dorsolateral prefrontal cortex of >500 patients from the ROS/MAP cohorts, two longitudinal clinical studies on aging, cognitive decline and AD. Importantly, AD patients showed significantly increased *MFGE8* expression compared to non-demented patients. Moreover, *MFGE8* gene expression levels predicted cognitive decline independent of amyloid neuropathology, namely Aβ plaques and neurofibrillary tangles. Notably, Medin was previously reported to be increased within cerebral arteries of AD patients in comparison to non-demented controls, and levels of arteriole Medin predicted risk for AD independent of amyloid pathology, age, sex and ApoE status.

In summary, this thesis demonstrates the importance to develop new technologies and models to study amyloid pathobiology and cross-talk, as amyloids contribute to common age-related damage and dysfunction, but also affect progression, heterogeneity and co-morbidity of other diseases. Our studies demonstrate a new mechanism that may drive age-associated vascular disease and cerebral β-amyloid angiopathy, highlighting Medin as a potential therapeutic target to maintain vascular health and cognitive function with age.

2. Synopsis

2.1 Amyloids

The German pathologist Rudolf Virchow was the first one to use the term 'corpora amylacea' (amylum and amylon are Latin and Greek words for starch, referring to starch-like) based on his discovery that cerebral deposits stain for iodine and sulfuric acid, a typical blue reaction of starch (Iadanza et al., 2018; Virchow, 1854). Only five years later, two scientists demonstrated that these deposits originate from proteins and not carbohydrates (Friedreich & Kekulé, 1859). At the time, amyloidosis was described as a pathological state associated with the formation of (extracellular) amyloid deposits and originally classified as a rare disease. With advancing insight into human aging processes it was discovered that several diseases are associated with protein aggregation and amyloid formation, many of which are major threats to health and socioeconomic burden of the aging population in the 21st century (Alzheimer's Association Report, 2020; Knowles et al., 2014). Which symptoms develop from amyloid deposition is usually dependent on the tissue, where amyloid or prefibrillar aggregates are localized (Benson et al., 2020; Knowles et al., 2014). Amyloids in the brain can be neurotoxic and cause neuronal damage and cognitive decline, while the aggregates in the pancreatic islets of Langerhans can cause failure of insulin-producing β-cells, triggering type-2 diabetes (T2D) (Alzheimer, 1911; Opie, 1901). Other than their implications in disease, amyloids have many functions in material sciences (Knowles & Mezzenga, 2016); however, discussing these is out of scope of this thesis and they will therefore not be discussed further.

2.1.1 Overview of amyloid characteristics

In 2018, the Amyloidosis Nomenclature Committee stated that the term 'amyloid fibril' should be used for any cross β-sheet fibril (Benson et al., 2018). Such fibrils consist of intertwined, unbranched filaments composed of tightly stacked sheets of β-strands perpendicular to the main axis (Iadanza et al., 2018; R. Nelson et al., 2005; Shirahama & Cohen, 1965). These fibrils are insoluble and resistant to degradation by enzymes (Pras et al., 1968; Sipe & Cohen, 2000). By definition, all amyloids are structurally dominated by the distinct X-ray diffraction pattern that is produced by the repeated arrangement and spacing between β-sheets and β-strands (Eanes & Glenner, 1968; Makin & Serpell, 2005; Sunde & Blake, 1997). Multidisciplinary approaches and

increasing resolution of the amyloid structure have started to provide a better understanding of the complex appearance and function of amyloids and even allow identification of varying amyloid species and morphotypes in different neurodegenerative diseases (Rasmussen et al., 2017; Gallardo et al., 2020).

Although they have different primary structures and affect specific organs and cell types, amyloid deposits share the above-described structural features, and common fluorescent amyloid ligands can be applied for histology but also kinetic aggregation assays (Benson et al., 2020). These dyes undergo a shift in their conformation or absorbance when binding to cross β-sheet rich structures, which change their optical characteristics (Glenner et al., 1972; Maiti et al., 2016; G. T. Westermark et al., 1999). Two prominent examples are Congored and Thioflavin. Routinely, Congored is used as a qualitative readout to confirm the presence of amyloid species by a typical green birefringence under polarized light (Benson et al., 2018; Puchtler et al., 1962; Sipe & Cohen, 2000). Meanwhile, thioflavin T (ThT) becomes fluorescent upon amyloid binding and can be used in fluorescence assays to monitor aggregation kinetics (LeVine, 1993; Marzesco et al., 2016; Naiki et al., 1989). Moreover, a relatively new group of amyloid-binding dyes can differentiate between different amyloid conformations, enabling the identification of specific neurological phenotype-associated amyloid species and their implication for pathology (Gallardo et al., 2020; Klingstedt et al., 2019; Rasmussen, Mahler, et al., 2017). These so-called luminescent conjugated oligothiophenes (LCOs), shift their emission spectra upon binding to amyloid rich-structures, and varying the number of thiophene rings on their flexible backbones allows the design of amyloid conformation-specific binding ligands (Åslund et al., 2009; Klingstedt et al., 2011). The combination of different LCOs and quantification of their spectral shift reflects the three-dimensional (3D) structure of the amyloid and was recently shown to be able to distinguish different clinical subtypes of cerebral β-amyloidosis (Rasmussen, Mahler, et al., 2017) and α-synucleinopathies (Klingstedt et al., 2019).

2.1.2 From native proteins to amyloid fibrils

In order to find new therapeutics to treat these devastating diseases associated with amyloid deposition, it is important to understand when and how amyloids form. The amino acid (aa) sequence of a protein encoded from the genetic information within the deoxyribonucleic acid (DNA) determines its native architecture and folding (Anfinsen, 1973; Dobson et al., 1998). It is a very well-orchestrated process from amino acid chain via intermediates to the native protein, with many quality check points in which molecular chaperones and protease systems ensure the

efficient production of functional proteins (Hartl, 1996; Hartl et al., 2011; Powers et al., 2009). Energetically, folding is the way of the unfolded polypeptide chain through a rugged, funnel-shaped energy landscape towards the final, native structure (Jahn & Radford, 2005). Thus, this is not a sequential process of increasingly native-like species but rather a random fluctuation of transient folded or unfolded intermediates until a thermodynamically stable form is reached (Jahn & Radford, 2005; Rumbley et al., 2001). Disbalance of this mechanism can result in accumulation of partially (intermediate) folded or misfolded proteins (Jahn & Radford, 2005). These proteins typically expose hydrophobic residues or regions of unstructured polypeptide back bone, which are energetically unfavorable forcing the peptide into forming amorphous aggregates or thermodynamically more stable highly-ordered amyloid fibrils (reviewed in Jahn and Radford, 2005; Onuchic and Wolynes, 2004; Hartl and Hayer-Hartl, 2009).

Even though hydrophobic interactions are thought to be a driving force in protein aggregation and fibril formation, we have to distinguish between (mis)folding and aggregation processes (Jahn & Radford, 2005). Folding requires the information of the whole amino acid sequence, whereas a few hydrophobic amino acids are sufficient to make a protein region more prone to aggregation (Fändrich & Dobson, 2002; Fernandez-Escamilla et al., 2004; Jahn & Radford, 2005; Rousseau et al., 2006). Usually, these aggregation-prone proteins are kept under control by molecular chaperones, proteasomal degradation and quality control processes (Hartl, 1996; Hartl et al., 2011; Powers et al., 2009; Stroo et al., 2017). However, genetic mutations, a rise in concentration or fragmentation (cleavage) of the precursor protein or alterations of folding conditions and molecular and cellular control systems by aging or environmental factors can shift peptides towards kinetically more stable aggregates and amyloid fibrils (Jahn & Radford, 2005).

2.2 Alzheimer's disease and the amyloid-β peptide

2.2.1 Characteristics of Alzheimer's disease

One of the most prominent examples of a peptide, which forms these kinetically stable amyloid fibrils, is amyloid-β (Aβ). Aβ peptides misfold and aggregate to form extracellular deposits in the brain and these are a characteristic hallmark for Alzheimer's disease (AD) (Alzheimer, 1911; Glenner & Wong, 1984). AD is the most common neurodegenerative disorder with high socioeconomic burden for family caregivers and society (Alzheimer's Association Report, 2020). Currently, 60-80% of all dementia cases have AD with an average age of onset of 65 years (y) and 8-10 y of disease duration (Masters et al., 2015). Around 10-30% of the population above 65 y are affected, with higher incidence in women (Kawas et al., 2000; Masters et al., 2015). In 2018, more than 1.5 million people in Germany (1.91% of the overall population) were affected by AD and this number is projected to almost double by 2050 due to the demographic shift in the aging population (Alzheimer Europe, 2019). AD has a long preclinical phase and pathological changes occur many years before onset of symptoms (Bateman et al., 2012; Buchhave et al., 2012). It is a progressive brain disorder with synaptic and neuronal loss in the hippocampus and cortex that slowly impairs memory and personal behavior of the patient (McKhann et al., 2011; Terry et al., 1991). Once the brain is damaged, it (currently) cannot be reversed or replaced.

2.2.1.1 Neuropathology

A diagnosis for AD is usually based on the results of positron emission tomography (PET) brain scans with Pittsburg compound B tracer (a radioactive analog of ThT; Klunk et al., 2004), cognitive testing and biomarker levels in cerebrospinal fluid (CSF) or blood (Alzheimer's Association Report, 2020; Masters et al., 2015). Post-mortem neuropathological diagnosis predominantly relies on parenchymal lesions of two different proteins, Aβ and tau (Alzheimer, 1911; Glenner & Wong, 1984; Grundke-Iqbal et al., 1986; Walker, 2020; Wood et al., 1986). More specifically, plaques mainly consist of Aβ and are highly diverse in their appearance (Thal et al., 2006; Walker, 2020). Their morphology ranges from highly structured plaques with a dense core, to more diffuse structures that can lack staining for amyloid dyes (Congored, ThT). These Aβ plaques can be locally accompanied by various other molecular and cellular changes (including abnormal neuronal processes and reactive gliosis) (Walker, 2020). In 80-95% of AD patients, cerebral β-amyloid angiopathy (Aβ-type CAA) can be observed that is caused by Aβ deposition (mainly consisting of $Aβ_{40}$ species) around/within the walls of leptomeningeal and small cerebral blood vessels, leading

to the destruction of the vessel wall and blood brain barrier, increasing risk for intracerebral hemorrhages or ischemic stroke (Boyle et al., 2015; DeTure & Dickson, 2019; Greenberg et al., 2020; Winkler et al., 2001). The second neuropathological distinct feature of AD are intracellular neurofibrillary tangles composed of highly phosphorylated tau proteins (Goedert et al., 1988; Grundke-Iqbal et al., 1986; Wood et al., 1986). Tau is produced by alternative splicing from the microtubule-associated protein (MAPT) gene and is important for the stabilization of microtubules of the axonal cytoskeleton (Grundke-Iqbal et al., 1986; Weingarten et al., 1975). The Braak scoring, a histopathological staging of the progression of neurofibrillary changes, is used to determine severity of AD-related pathology and cognitive decline (Braak & Braak, 1991). However, the relationship between both protein abnormalities remains ambiguous.

2.2.1.2 Familial and sporadic AD

In ~1% of estimated AD cases, Mendelian inheritance of missense mutations in the three genes of amyloid precursor protein (APP), Presenilin-1 or -2 (PSEN1/2) are responsible for the irregular increased Aβ production (Bekris et al., 2010; Goate et al., 1991; Mullan, 1992; Sherrington et al., 1995). Typical for this familial form of AD is an early onset of first cognitive symptoms (30-65 y) (Bekris et al., 2010). Since the gene of APP is located in chromosome 21, patients with Down syndrome can develop diffuse Aβ plaques already in their mid-teens due to multiplication of the APP gene (Giaccone et al., 1989; J. Kang et al., 1987; Tanzi et al., 1987).

In sporadic, late-onset AD (LOAD), more than 29 genetic risk factors but also non-genetic risk factors (such as cardiovascular disease or traumatic brain injury) have been described – with age being the highest risk factor (Alzheimer's Association Report, 2020; Bertram et al., 2007; Bertram & Tanzi, 2019; Jansen et al., 2019). Most of the AD risk-genes are associated with dysregulated Aβ clearance involving Apolipoprotein E (ApoE), cholesterol/sterol metabolism, inflammation and endosomal vesicle trafficking, emphasizing that AD is a multifactorial disease with Aβ as the main driver (reviewed in Van Cauwenberghe et al., 2016; Selkoe and Hardy, 2016; Alzheimer's Association Report, 2020).

2.2.1.3 Treatment

Despite more than a century of research on AD, in >95% of the reported cases the trigger for AD remains unknown. This lack of knowledge complicates treatment of AD. Currently, pharmacological intervention cannot prevent or halt the disease, but only temporarily reliefs symptoms such as neurotransmitter deficits (rivastigmine, galantamine, donepezil) or excess neuronal stimulation (memantine) (Alzheimer's Association Report, 2020). Results of human trials

with anti-amyloid therapeutics (Aducanumab, Solanezumab), that are developed to stop or slow down disease progression, have not yet produced clinical effects that would warrant their widespread use for treatment (Huang et al., 2020; Knopman et al., 2020; Sabbagh & Cummings, 2020). However, researchers argue that it is important to develop early biomarker and start therapy in early-stage/pre-symptomatic disease phase (Das et al., 2012; Selkoe & Hardy, 2016; Uhlmann et al., 2020).

2.2.2 Amyloid-β and the amyloid cascade hypothesis

2.2.2.1 Generation of Aβ from the amyloid precursor protein

The main component of plaque and vascular amyloid is the Aβ peptide. Aβ, a 4 kilodalton (kDa) protein fragment, was first purified from the brain vasculature in 1984 (Glenner & Wong, 1984) and one year later also from amyloid plaque cores (Masters et al., 1985). It is continuously cleaved by proteases from the 695-770 aa amyloid precursor protein (APP) (Haass et al., 1992; J. Kang et al., 1987; Selkoe, 1998; Tanzi et al., 1987). Although a neurogenic, -protective and -regenerative role was the suggested, the physiological function of APP and its fragments remains unclear (Chen & Tang, 2006; Müller et al., 2017). Meanwhile, APP knockout mice have a normal life span without severe phenotype (Z. W. Li et al., 1996; Zheng et al., 1995). Sequential intramembrane processing of APP by either α-secretase or cleavage by β-and γ-secretase decides the fate for either the non-amyloidogenic or amyloidogenic pathway (Haass et al., 2012; Müller et al., 2017; Roberts et al., 1994; Sinha et al., 1999; R. Yan et al., 1999) (Figure 1). More precisely, for Aβ generation, β-secretase initiates intramembrane proteolysis of the amyloid precursor protein into an APP C-terminal fragment (βCTF) and a soluble APP ectodomain fragment (APPsβ), and is the rate-limiting step of Aβ generation (Haass et al., 2012; Müller et al., 2017). Further cleavage by γ-secretase releases the Aβ peptide from the membrane. Interestingly, the resulting Aβ peptide can vary between 37-43 aa depending on the cleavage site (Haass et al., 2012). The high expression of APP (especially isoform APP695; Müller et al., 2017) and β-secretase (BACE1; Roßner et al., 2006) in neurons may explain why β-amyloidosis predominantly affects the brain, despite its relatively widespread expression also in other organs (Haass et al., 2012; Vassar & Cole, 2008). Missense mutations in substrate (APP) or protease (PSEN, catalytic site of γ-secretase) result in gradual build-up of a pool of Aβ species such as $A\beta_{42}$ and $A\beta_{40}$ (De Strooper et al., 1998; Goate et al., 1991; Mullan, 1992; Sherrington et al., 1995). Conversely, patients with protective APP (A673T) mutation with altered APP cleavage and reduced aggregation-propensity show reduced age-associated cognitive decline and AD risk (Jonsson et al., 2012; Kero et al., 2013).
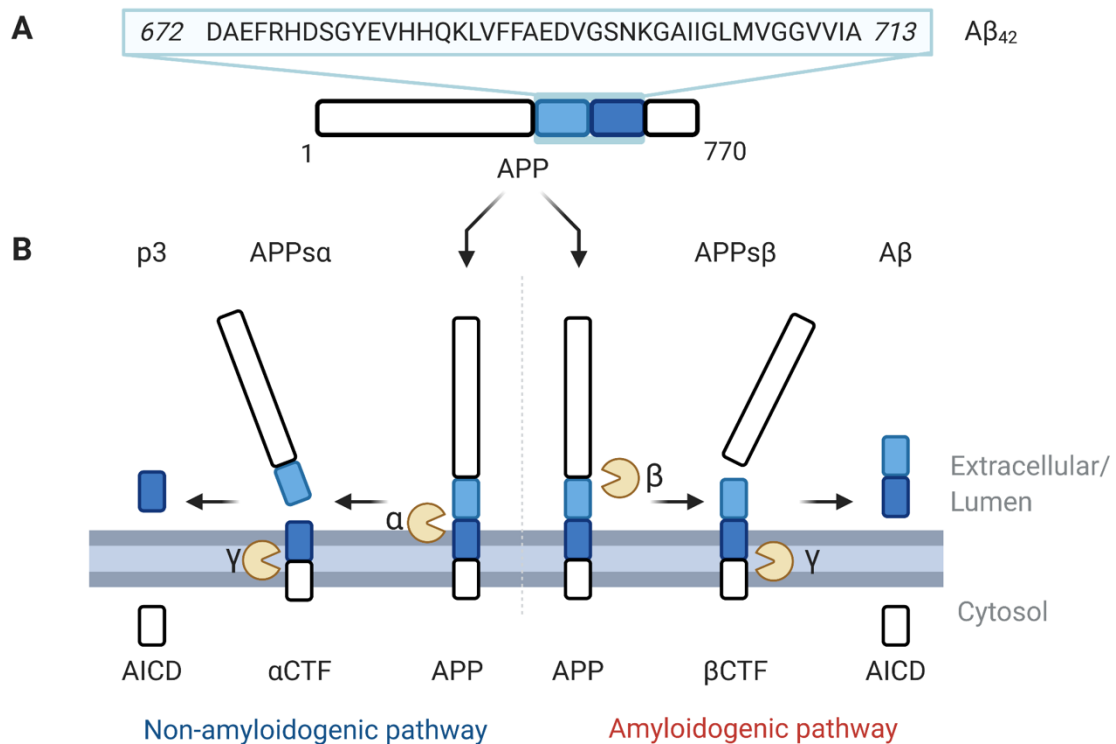
Figure 1: Generation of Aβ peptides. **A,** Aβ is cleaved from the 770 aa amyloid precursor protein, APP (UniProt P05067; Müller et al., 2017). **B,** Non-amyloidogenic processing of APP (left) involves the sequential cleavage of α-secretase followed by γ-secretase. For generation of Aβ, β-secretase initiates amyloidogenic processing of APP (right) and γ-secretase releases the Aβ peptide from the membrane. The resulting Aβ peptides can vary between 37-43 aa depending on the cleavage site. aa, amino acid; Aβ, Amyloid-β; CTF, C-terminal fragment; AICD, APP intracellular domain; APPs, soluble APP ectodomain fragment; p3, Aβ$_{17-40/42}$ fragment. Based on Haass et al., 2012; Müller et al., 2017.

2.2.2.2 The amyloid cascade hypothesis

The amyloid cascade hypothesis proposes a molecular sequence of events in AD ultimately causing neuronal death, with Aβ as the main initiator and driver (Hardy & Allsop, 1991; Hardy & Higgins, 1992; Hardy & Selkoe, 2002). Studies monitoring subjects with known familiar AD or other risk-gene mutations suggest that the disease progress starts with Aβ accumulation more than two decades before first cognitive deficits manifest (Bateman et al., 2012; Villemagne et al., 2013). Dysbalanced production and clearance of Aβ peptides in the brain results in a complex downstream cascade (Hardy & Selkoe, 2002; Selkoe & Hardy, 2016). First gradual effects on brain health and function are mediated by oligomeric species on synapses (Walsh & Selkoe, 2007). Aβ aggregates slowly accumulate and deposit as extracellular plaques, which in turn are thought to trigger the inflammatory response of astrocytes and microglia (Heneka et al., 2015; Heneka & O'Banion, 2007; Itagaki et al., 1989; Rogers et al., 1992). Oxidative stress, altered ionic homeostasis and enzymatic activity in neuronal cells lead to further synaptic and neuronal dysfunction (Selkoe

& Hardy, 2016). Although hyperphosphorylation of microtubule-associated protein tau but not Aβ plaques highly correlate with neuronal loss and cognitive decline (Braak & Braak, 1991; Giannakopoulos et al., 2003; P. T. Nelson et al., 2012), tau was proven to be a downstream target of the amyloid cascade (Selkoe & Hardy, 2016). Mutations in the tau gene (MAPT) cause frontotemporal dementia with Parkinson's disease (PD) but no Aβ deposition or related-dementia (Hutton et al., 1998; Roks et al., 1999), while mutations in the APP gene or processing clearly lead to early-onset AD (EOAD), as described. However, neurotoxicity of Aβ depends on expression of human tau (Jin et al., 2011; Roberson et al., 2011). The resulting neuronal loss clinically manifests as dementia (Selkoe & Hardy, 2016).

Besides the amyloid cascade hypothesis, there are various other potential mechanisms regarding AD pathogenesis, including tauopathy, cholinergic, mitochondrial cascade, calcium homeostasis, inflammatory, metal ion, lymphatic system and vascular hypothesis (reviewed in Liu et al., 2019). Consequently, it is important to keep in mind that AD is a multifactorial disease that will likely require therapeutic targeting of different pathological processes for successful treatment. The exact etiopathogenesis of sporadic, late-onset AD remains elusive and most of the proposed hypotheses show strong overlapping mechanism. And although the amyloid cascade cannot explain every pathological pathway and heterogeneity of the disease, it has remained the predominant, best-established model for 20 years now.

2.2.2.3 Experimental animal models of cerebral β-amyloidosis

The amyloid cascade hypothesis and the critical role of Aβ was validated by numerous studies in animal models. Although only ten physiological amyloids have been reported for domestic and wild animals, non-human primates and dogs but not mice or rats, can develop age-related Aβ plaques and CAA pathology (Benson et al., 2020; Jakob, 1971). However, animals rarely develop tauopathy or other aspects of AD such as memory decline (Jakob, 1971). Therefore, to study diseases specific pathology mechanism, humanized transgenic animal models are used and can resemble phenotypes of different disease-associated pathologies (Buxbaum, 2009; Dawson et al., 2018).

Given the relationship between APP expression/processing and AD pathology, overexpression of mutated APP forms the basis of animal models for cerebral β-amyloidosis, in some models combined with mutated PSEN1 genes (Games et al., 1995; Radde et al., 2006; Sturchler-Pierrat et al., 1997). Transgenic mouse models such as APPPS1 and APP23 overexpress the human APP gene, which differs in three amino-acids from the mouse sequence (Otvos et al., 1993), with described

familial mutations of AD (https://www.alzforum.org/mutations/app; Swedish mutations KM670/671NL and PSEN1 L166P under the control of the thymocyte differentiation antigen 1, Thy1, promoter). These models show typical AD-associated pathological features, such as plaque formation, tau-positive neuritic processes, gliosis, vascular uncoupling, synaptic, and cognitive impairment (Drummond & Wisniewski, 2017). However, they vary in composition of Aβ species, onset and morphology. In particular, APPPS1 transgenic animals preferentially generate the more hydrophobic $A\beta_{42}$ peptide resulting in numerous small amyloid plaques that start to appear around 6 weeks of age (Radde et al., 2006), while APP23 mice exhibit a later onset of plaque pathology (around 6 months of age) and a higher $A\beta_{40}$ to $A\beta_{42}$ ratio with additional cerebral amyloid angiopathy (CAA) of the Aβ peptide (Sturchler-Pierrat et al., 1997; Winkler et al., 2001). Similar to human cases, CAA in transgenic mice is often associated with destruction of the vessel wall and blood brain barrier, increasing risk for impaired cerebrovascular function and intracerebral microhemorrhages/strokes (Herzig et al., 2004; Kim, Ahn, et al., 2020; Kimbrough et al., 2015; Winkler et al., 2001). To mimic combined Aβ-tau pathology, tau transgenic mice can be cross-bred with APP tg mice (Lewis et al., 2001).

However, it has become evident that simplified models like APP overexpressing mouse models cannot capture the full spectrum of disease symptoms. AD-related behavioral changes are limited and other hallmarks, such as neurofibrillary tangles, local brain atrophy or comparable transcriptomic signatures have not been recapitulated (Calhoun et al., 1999; Hargis & Blalock, 2017; Wan et al., 2020). Moreover, it is criticized that APP overexpression does not resemble the physiological case and that only less than 5% of AD cases can be explained by familiar mutations (Bekris et al., 2010). Therefore, new knock-in and knock-out models are developed to investigate additional factors of the complex disease mechanism, such as other risk genes, environmental factors, coexisting medical conditions, life style and aging process to allow for studies of late-onset, idiopathic β-amyloidosis (Saito et al., 2014; Sukoff Rizzo et al., 2020).

2.2.2.4 Prion-like spreading of Aβ in the brain

Despite their limitations, these APP models are crucial for detailed studies of the temporo-spatial distribution and transmission of Aβ in the brain. Together with neuropathological staging in human brains, they show that Aβ accumulation and aggregation start long before first cognitive symptoms occur and may spread from a single nucleation site (Bateman et al., 2012; Lu et al., 2013; Villemagne et al., 2013). It has been noted that the temporal spread of brain amyloid is not random but rather follows a certain spatial pattern that appears to match brain activity and neuronal

connectivity (Iturria-Medina & Evans, 2015; Palmqvist et al., 2017) and may depend on selective cellular and regional vulnerability in the brain (Jucker & Walker, 2018; Mattsson et al., 2016; Selkoe & Hardy, 2016).

It is now widely accepted that formation and spreading of Aβ aggregates reflect the character of prion transmission (Condello et al., 2020; Lauwers et al., 2020). In particular, prion proteins (PrP) are described as 'proteinaceous infectious particles' (Prusiner, 1982). The native PrP misfolds to form the initial pathogenic seed, assembles further monomers for elongation and thereby rapidly spreads the misfolded conformation to other homologous proteins, leading to extra-/intracellular deposits that damage the surrounding tissue (Jucker & Walker, 2018; Prusiner, 1982; Rasmussen, Jucker, et al., 2017). Thus, a corruptive protein is sufficient to induce pathological changes in the infected tissue by gain of toxic and/or loss of physiological function (Winklhofer et al., 2008).

Several experimental studies have proven that the prion concept can be applied to AD and other neurodegenerative diseases. *In vitro* studies established that monomeric Aβ can rapidly self-assemble into amyloid fibrils. This process is divided into two main steps (Figure 2): the nucleation or lag-phase and the elongation or growth phase (reviewed in Jucker and Walker, 2013; Michaels et al., 2018). In the primary nucleation phase, monomers undergo conformational changes and assemble to form the first critical nucleus (also termed 'seed') composed of oligomer subunits with high β-sheet content. These initial seeds can act as a structural template and corrupt further native proteins to misfold. Subsequently, more Aβ species get recruited to the prefibrillary surface and become densely packed towards an energy-stable structure with β-sheets aligned parallel or anti-parallel, thereby elongating the (proto)fibril (Jarrett & Lansbury, 1993). The kinetics of this whole process follow an arithmetic sigmoidal-shape: the assembly into first oligmers is described by a lag phase, after which subunits are exponentially added until a saturated plateau is reached (Jarrett & Lansbury, 1993). Formation of the first nucleus is thermodynamically unfavorable and therefore, the rate-limiting step.
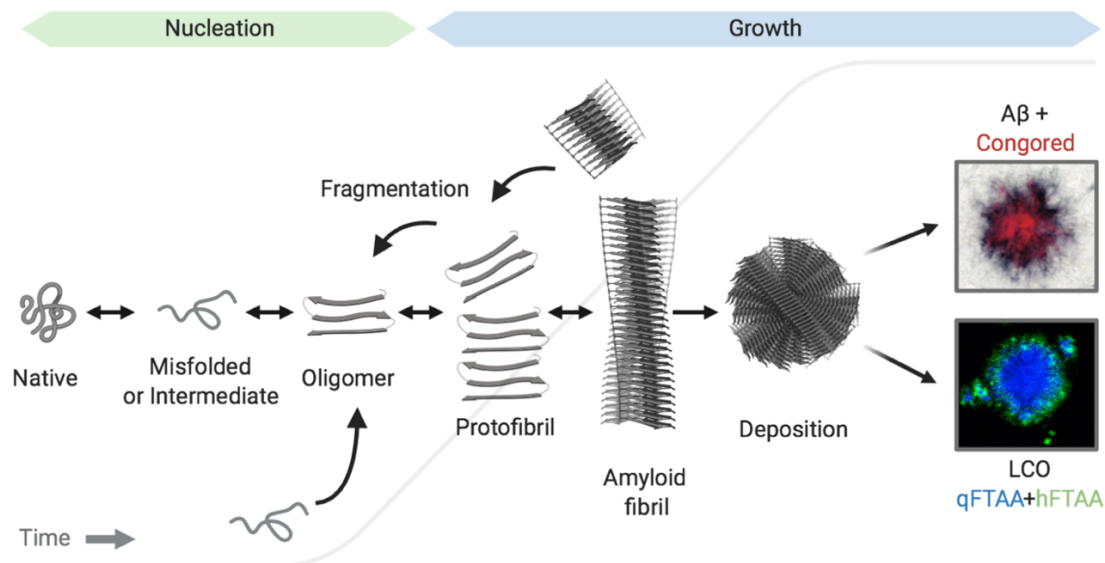
Figure 2: Nucleation-dependent assembly of amyloid aggregates. Formation of amyloid fibrils is divided into a slow nucleation or lag-phase and a rapid elongation or growth-phase (polymerization). The cross-β fibril structure is shared by all amyloid proteins and can be detected by common amyloid dyes such as Congored or LCOs. Aβ, amyloid-β; LCO, Luminescent conjugated oligothiophenes; qFTAA, quadro-formyl thiophene acetic acid; hFTAA, hepta-formyl thiophene acetic acid. Based on Jucker and Walker, 2013, and Karamanos et al., 2015.

In vivo experiments further showed that addition of preformed seeds can bypass the primary nucleation and shorten the lag-phase by template-assisted misfolding of homologous proteins (Friesen & Meyer-Luehmann, 2019; Jarrett & Lansbury, 1992; McAllister et al., 2020; Meyer-Luehmann et al., 2006; Ridley et al., 2006). In pre-depositing APP transgenic (tg) animals, inoculation with exogenous seeds derived from AD brain or Aβ rich extracts (by intracerebral injection) results in accelerated, pre-mature pathology of amyloid plaques and CAA and spreads in a prion-like mechanism through the neuronal connectome (Hamaguchi et al., 2012; Kane et al., 2000; Meyer-Luehmann et al., 2006; Walker et al., 2002; L. Ye et al., 2015). Of note, exogenous Aβ seeds can also travel from the periphery to the brain where they predominantly seed CAA (Burwinkel et al., 2018; Eisele et al., 2010; Jaunmuktane et al., 2015). Such a prion-like mechanism has been experimentally proven for Aβ, tau and α-synuclein, but evidence for several other proteins is emerging (huntingtin, SOD1, TDP-43) (Jucker & Walker, 2018).

These experimental models further enable the study of factors that define the morphology, toxicity and 'infectivity' of seeds. Given the structural variety of amyloid seeds (Cohen et al., 2015; Condello et al., 2018; Rasmussen, Mahler, et al., 2017; Watts et al., 2014), it may not come as a surprise that they differ in seeding potency. While synthetic or recombinant Aβ aggregates induce rather weak seeding (Meyer-Luehmann et al., 2006; Stöhr et al., 2012), early or oligomeric seeds derived from

tissue are highly infectious (Katzmarski et al., 2020; Langer et al., 2011; L. Ye et al., 2017). However, it is important to note that compared to α-synuclein and tau (Clavaguera et al., 2013; Masuda-Suzukake et al., 2013), propagation of Aβ depends on transgenic human APP expression in the host and does not occur in wild-type mice within their normal life span (Meyer-Luehmann et al., 2006; Morales et al., 2012).

First evidence for human-to-human transmission of amyloid seeds has been reported in patients that came into contact with contaminated material through neurosurgery, pituitary extracts or transplantation of dural grafts in early childhood (Banerjee et al., 2019; Giaccone et al., 2019; Hervé et al., 2018; Jaunmuktane et al., 2018; Purro et al., 2018). These cases developed cortical plaques and CAA, occasionally accompanied by microbleedings and intracerebral hemorrhages. However, they did not show tangles or other AD-typical neuritic or microglia pathology. It is interesting to note that these cases preferentially showed vascular amyloid pathology, suggesting a critical role of the cerebrovascular system, and that CAA may be transmissible (Giaccone et al., 2019; Masahito Yamada et al., 2019). Transmission seems to be dependent on direct exposure to human brain preparations and therefore, does not indicate a reason for isolation of demented patients (Lauwers et al., 2020).

2.2.3 Vascular hypothesis: Role of vascular dysfunction in Alzheimer's disease

A critical role of the vascular system in the development and progression of cerebral β-amyloidosis has been noted for some time. Back in the days of Alois Alzheimer, who was the first to present a senile dementia disease at a symposium in Tübingen in November 1906, dementias were primarily believed to originate from vascular dysfunction due to behavioral symptoms and evidence for vascular pathologies (Alzheimer, 1898; Libon et al., 2006; Liesz, 2019). Although nowadays there is convincing evidence for Aβ as a major driver of pathology, these early analyses highlight the relevance of cerebrovascular dysfunction for neuronal dysfunction and dementia. Vascular dysfunction in the brain and periphery is a strong risk factor and the earliest detected change in AD (Akoudad et al., 2016; Broce et al., 2019; Gottesman et al., 2017; Iturria-Medina et al., 2016; Korte et al., 2020).

During healthy aging, Aβ gets drained from the brain via the blood brain barrier (BBB), CSF, glymphatic system and perivascular space into the blood, degraded and/or removed by the liver

and kidneys (Cheng et al., 2020; Tarasoff-Conway et al., 2015; J. Wang et al., 2017; Zlokovic, 2011). In AD, vascular dysfunction is evident as (micro)structural and functional alterations that lead to dysregulated cerebral blood flow and hypoperfusion/hypoxia, BBB breakdown, secretion of endothelial neurotoxic and inflammatory factors, cellular dysfunction of the neurovascular unit and decreased clearance of proteinaceous or toxic metabolites (including Aβ) from the brain (De la Torre and Mussivand, 1993; Zlokovic, 2011; Cortes-Canteli and Iadecola, 2020; Steinman et al., 2021; Figure 3).
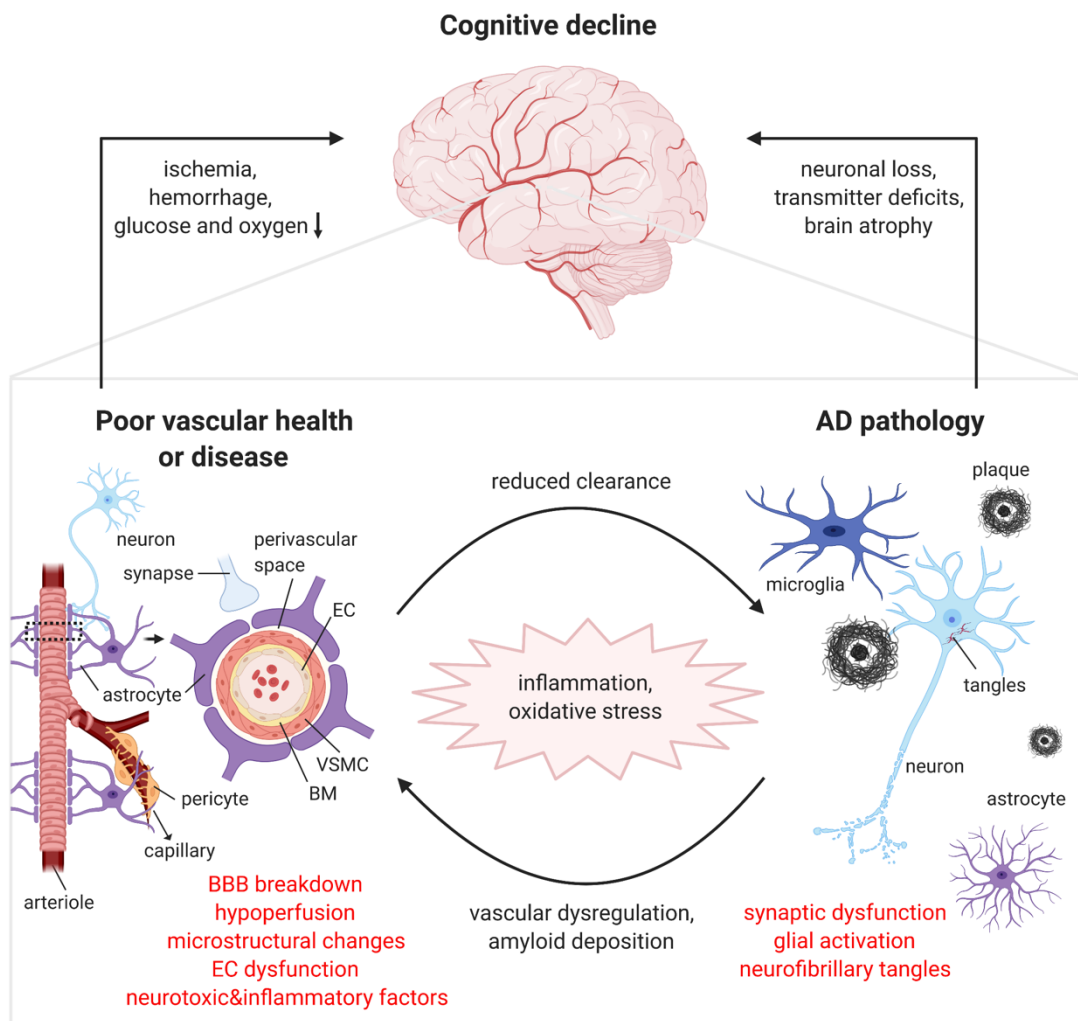

Figure 3: Vascular role in Alzheimer's disease. The neurovascular unit (consisting of vascular smooth muscle cells, astrocytes, neurons and endothelial cells) controls arterial and arteriolar blood flow. Pericytes are the gatekeepers of the blood-brain barrier and regulate the capillary tone. Age-related changes, genetic or environmental risk factors can lead to vascular damage and dysfunction favoring Aβ transport to and accumulation in the brain, which accelerates the Aβ-dependent mechanism of neuronal damage. In return, aggregating Aβ further damages cerebral blood vessels by uncoupling of the neurovascular unit, BBB disruption and amyloid deposition within the vessel wall. EC, endothelial cell; VSCM, vascular smooth muscle cell; BM, basement membrane; BBB, blood brain barrier. Based on Kisler et al., 2017; Iadecola and Gottesman, 2018; Lendahl et al., 2019.

In turn, Aβ accumulation and increased oxidative stress lead to dysregulation of the neurovascular unit via pericyte constriction, increased receptor for advanced glycation end products (RAGE) expression, effects on endothelial and innate immune cells, and reduced vascular reactivity/ vasodilation (Charidimou et al., 2017; Faraco et al., 2016; Nortley et al., 2019; Zlokovic, 2011). Aβ aggregates can accumulate in cerebral blood vessels, starting in the tunica media and adventitia of arteries and basement membrane of the capillaries, and further contribute to vascular pathology and degeneration (Cortes-Canteli & Iadecola, 2020; Thal et al., 2008). Cerebral β-amyloid angiopathy is associated with brain atrophy, cognitive decline and higher risk for dementia (Boyle et al., 2015; Fotiadis et al., 2016; Moulin et al., 2016; Smith, 2018). AD patients with CAA pathology frequently show atrophy of the vascular smooth muscle cell (VSMC) layer that causes rupture of the vessels and intracerebral (micro)hemorrhages and strokes (Charidimou et al., 2017; Pettersen et al., 2008; Viswanathan & Greenberg, 2011). Accordingly, vascular dysfunction and Aβ pathology can be two intertwined pathways in the AD brain (Figure 3).

2.2.4 Co-deposition of heterologous aggregates: An amyloid rarely comes alone

Although each type of amyloidosis is diagnosed by a predominant intra- or extracellular depositing protein, different misfolded proteins often co-exist in patients (Morales et al., 2013; Soto & Pritzkow, 2018; Spires-Jones et al., 2017). Amyloids can either deposit in the same or in separate organs. This may be purely coincidental but previous studies suggest that co-existence of several aggregated proteins influences disease onset, severity, vulnerability, progression and secondary phenotypes (Morales et al., 2013; Soto & Pritzkow, 2018; M. Yamada et al., 1988). For example, co-morbidity can lead to enhancement of cellular vulnerability, potentiation of immune-responses by cumulative toxicity and inflammation and/or impaired clearance (Morales et al., 2013; Soto & Pritzkow, 2018). The two amyloids Aβ and tau show clear synergy in AD. As mentioned earlier, Aβ is involved in downstream hyperphosphorylation of tau (C. Li & Götz, 2017; Wu et al., 2018), while tau mediates Aβ neurotoxicity (Ittner et al., 2010; Jin et al., 2011; Rapoport et al., 2002; Roberson et al., 2011). Neuropathological studies on post-mortem tissue further reported parenchymal deposition of α-synuclein or TDP-43 in AD brains (Josephs et al., 2016; Uchikado et al., 2006). Interestingly, despite its generation in the pancreas, amyloid polypeptide (IAPP; also called amylin), was detected in the brains and cerebrovasculature of AD patients and APP tg mice (Jackson et al., 2013; Ly et al., 2021; Moreno-Gonzalez et al., 2017). Epidemiologic studies show that diabetic

patients (T2D), which develop aggregates of IAPP in their pancreatic β-cells, are more likely to develop AD and cognitive impairment (Bourdel-Marchasson et al., 2010; Kopf & Frölich, 2009). Given the similar structural, kinetic and pathogenic characteristics of these amyloids, it may not be a surprise that they can show direct amyloid-amyloid interaction (Morales et al., 2013; Ren et al., 2019). This will be discussed in more detail at a later point (chapter 2.4.1).

A recent study has identified another protein to co-deposit in the AD brain – the most common human amyloid, Medin. In fact, arteriole Medin was significantly elevated in AD patients and correlated with AD-specific neuropathology (neurofibrillary tangles and amyloid plaques; Migrino et al., 2020). Because of its vascular localization and potential role in arterial aging, it was suggested to be a possible risk factor of vascular dementia and AD (Karamanova et al., 2020; Migrino et al., 2017, 2020). In contrast to IAPP, the precursor protein of Medin can be locally produced by astrocytic and vascular cells in the brain (MFG-E8, http://brainrnaseq.org/; Boddaert et al., 2007; Cahoy et al., 2008; Kranich et al., 2010). However, the question whether Medin could directly promote AD and may have an effect on cognitive decline has not been addressed so far. In the following, this dissertation provides an extensive summary of previous studies on Medin amyloid and implements first mechanistic evidence for a role of Medin as a causal link between age-associated cerebrovascular pathology and Alzheimer's disease.

2.3 Vascular pathobiology of Medin amyloid

2.3.1 Medin - localized amyloid of the vascular tunica media

The probably most common human amyloid Medin (also known as AMed) was first described in the aorta. In 1970, Schwartz et al. already noted that: „We are still searching for the case of a person older than 55 whose aorta contains no amyloid" (Schwartz, 1970; Figure 4). In fact, amyloids can be found in all three layers of the aortic wall: the media, intima and adventitia (Mucchiano et al., 1992; Takako, 1978). In the tunica intima, amyloid is derived from apolipoprotein A-I (Westermark et al., 1995; approximately 35% of patients above 50 years of age; related to atherosclerotic lesions). Meanwhile, amyloid in the tunica adventitia is found in the connective tissue or walls of the vasa vasorum and is often derived from systemic amyloidosis (Pitkänen et al., 1984; Cornwell et al., 1995; <5% of patients above 50 y). Both intimal and adventitial amyloids are less common (Cornwell et al., 1995; Mucchiano et al., 1992, 2001), whereas remarkably, the medial amyloid can be found in approximately 97 % of the Caucasian population above 50 years of age within the tunica media between the elastic fibers (Häggqvist et al., 1999; Mucchiano et al., 1992). Swedish scientists were the first to purify and sequence Medin amyloid from the aortic tunica media in 1999 (Häggqvist et al., 1999). The youngest case reported so far is a 42-year-old patient with juvenile diabetes mellitus (Mucchiano et al., 1992). There is no correlation to atherosclerotic lesions, although appearances of Medin and atherosclerotic deposits in blood vessels are strongly associated with aging (Mucchiano et al., 1992).

Aortic Medin amyloid fibrils are arranged extracellularly in compact bundles or many small spots in the tunica media and show green birefringence under polarized light upon Congored binding (Degenhardt et al., 2020; Peng et al., 2005). Medin is predominantly found in the thoracic aorta and to a lesser extent in the abdominal part (Mucchiano et al., 1992; Peng et al., 2005). In some cases, amyloid was also observed intracellularly in smooth muscle cells or occasionally as ring-like amyloid deposits surrounding individual muscle cells (Peng et al., 2005). These deposits were only weakly stained with Congored and showed low birefringence (Peng et al., 2005).

However, Medin was also described in the arteries of the upper body including the basilar, temporal and leptomeningeal arteries (Karamanova et al., 2020; Migrino et al., 2020; Peng et al., 2002) as well as arteries and arterioles in the brain parenchyma, which we confirmed in our recent study (Degenhardt et al., 2020). Medin aggregates in the head and brain appear later with

approximately 80-years-of-age and do not necessarily stain for Congored (Degenhardt et al., 2020; Peng et al., 2005). These differences in distribution and amyloid morphotype may indicate different age-of-onset or progression stages of Medin accumulation in the human body or alternatively, distinct vulnerability of different cells/organs to different Medin species.
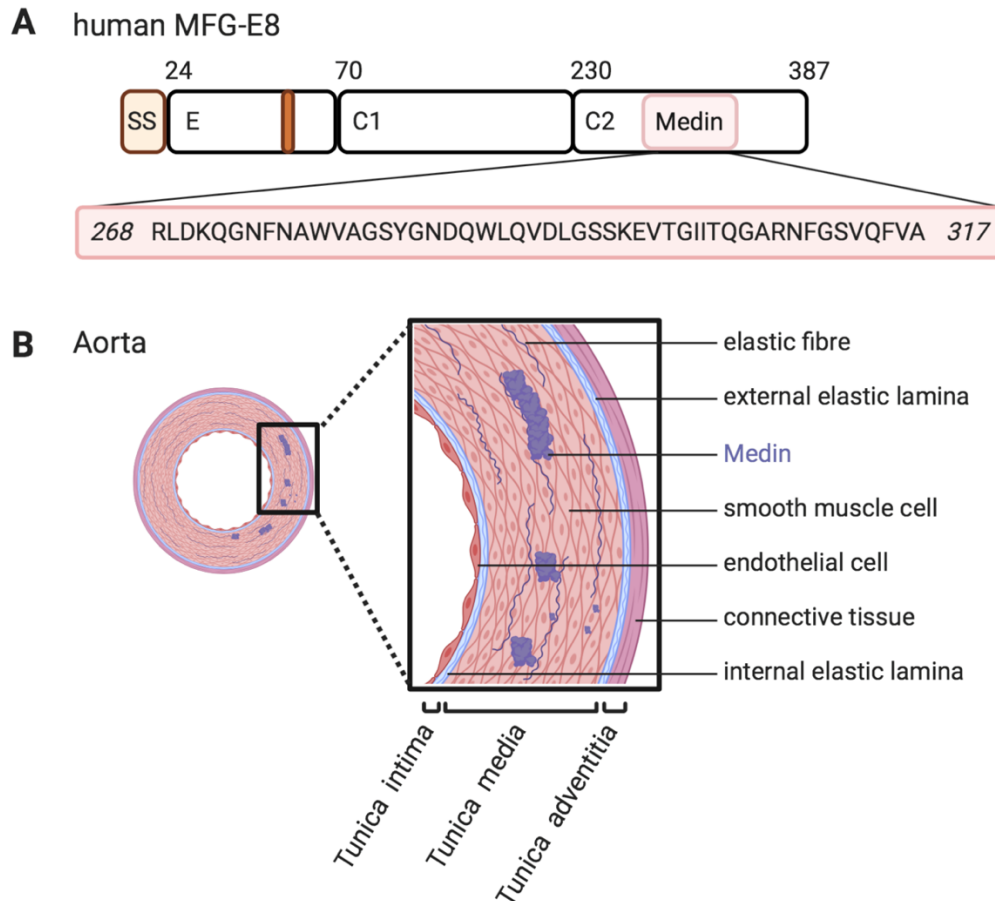

Figure 4: A, Structure of MFG-E8. The MFG-E8 protein has two main functional domains: The EGF-like domain that mediates integrin-binding via the RGD motif and two F5/8-type C domains that bind phospholipids. The Medin fragment is enzymatically cleaved by unknown events and sometimes has a ragged N-terminus with minor species starting at Pr-264 and Gly-273 (UniProt Q08431). **B**, Medin deposits along the elastic fibers in the tunica media of the aorta. SS, signal peptide sequence; E, EGF-like repeat; C1/2, F5/8-type C domains 1/2; RGD, arginine-glycine-aspartate.

2.3.1.1 Enzymatic cleavage of Medin from the precursor protein MFG-E8

The name of the protein 'milk fat globule-EGF factor-8' (MFG-E8; also called Lactadherin; Figure 4) was originally derived from its first discovery as a component of the milk fat globule in vertebrates (Stubbs et al., 1990). The *MFGE8* gene is mapped to chromosome 15 and encodes a 46 kDa membrane glycoprotein with four reported isoforms in humans (Gene ID 4240, UniProt Q08431; C. Collins et al., 1997; Yi, 2016). The N-terminal part of the protein contains a signal peptide sequence (SS) and one epidermal growth factor (EGF)-like domain (Couto et al., 1996; Stubbs et al., 1990). While the signal peptide is responsible for the release of the protein into the extracellular space, the EGF-like repeat contains the arginine-glycine-aspartate (RGD) motif that mediates its binding to $\alpha v \beta 3/\alpha v \beta 5$-integrins (Andersen et al., 1997; Hanayama et al., 2002; Taylor, 1997). The two C-terminal discoidin domains (F5/8-type C1 and C2 domains) are responsible for detection of amino-phospholipids, such as phosphatidylserine (Andersen et al., 1997; Couto et al., 1996; Hanayama et al., 2002). In mice, MFG-E8 is expressed in two isoforms that have an additional N-terminal EGF-like repeat, but without a second RGD motif (Figure 5; Hanayama et al., 2002; Watanabe et al., 2005).

MFG-E8 is expressed ubiquitously in various types of cells and tissues (Raymond et al., 2009; Yi, 2016). Several functions of MFG-E8 have been reported such as intestinal homeostasis, support of mucosal healing, inflammatory response as well as induction of vascular endothelial growth factor (VEGF)-mediated neo-vascularization, explaining its localization in the vasculature (reviewed in Raymond et al., 2009; Yi, 2016). Furthermore, MFG-E8 mediates phagocytosis of apoptotic cells in health and disease by acting as a bridging molecule (opsonin) between the phagocytes and the dying cell (Hanayama et al., 2002). The process of MFG-E8 mediated phagocytosis is likely to start with the apoptotic cells exposing phosphatidylserine on their surface, which represents a so called 'eat-me-signal' (Brown & Neher, 2014). MFG-E8 can facilitate phagocytic engulfment via binding to the $\alpha v \beta 3/\alpha v \beta 5$- integrin receptors that leads to a conformational change of the receptor (Akakura et al., 2004). Gene alterations and differentially regulated expression of MFG-E8 were implicated in several conditions including inflammatory, autoimmune (systemic lupus erythematosus), cancerous, vascular and neurodegenerative diseases (C. Y. Hu et al., 2009; B. Z. Li et al., 2013; Sapkota & Sanghera, 2020; Soubeyrand et al., 2019; Yamaguchi et al., 2008; Yu et al., 2012). For AD, it was reported that MFG-E8 might be involved in microglia-mediated Aβ phagocytosis (Boddaert et al., 2007; E. Li et al., 2012). However, whether MFG-E8 plays a protective or detrimental role in those diseases will require further investigation.

In the vasculature, MFG-E8 is expressed by smooth muscle cells of the tunica media in the aorta and arteries, and endothelial cells of small medial vessels (Häggqvist et al., 1999; Peng et al., 2002; Silvestre et al., 2005). Whether Medin is an abnormal cleavage product or is also produced under normal, physiological conditions (with a biological function) remains unknown. However, it was described that Medin is enzymatically cleaved from the C2-domain of its precursor protein MFG-E8 (Häggqvist et al., 1999). The co-localization of MFG-E8 and Medin with elastic fibers and the concentration-dependent binding to tropoelastin (the precursor of elastin and important for the cross-linking of the fiber network) mediated by the Medin-sequence *in vitro*, suggest a physiological function in anchoring of smooth muscle cells to elastic fibers (Larsson et al., 2006). So far it remains unknown whether the cleavage of Medin from MFG-E8 takes place intra- or extracellularly. The observation of intracellular amyloid in the smooth muscle cells in the aorta suggests a cleavage in the intracellular compartments (e.g. endoplasmic reticulum or Golgi; Peng et al., 2005). Another possible mechanism is that extracellular accumulation of MFG-E8 along elastic fibers or an excess of unbound MFG-E8 might be more vulnerable to proteolytic cleavage and thereby may generate more Medin fragments that have a high propensity to adopt a β-sheet structure (Häggqvist et al., 1999; Larsson et al., 2006). This hypothesis if further supported by the fact that Medin primarily deposits in arteries rich in elastin (Larsson et al., 2006).

2.3.1.2 Biochemical and -physical characteristics of Medin amyloid

The reported sequence of Medin consists of 50 aa at positions 268-317 of MFG-E8 (UniProt Q08431, identifier PRO_000000765; Häggqvist et al., 1999). In different patients and sample preparations, varying fragments starting before or after the main reported Medin sequence can be observed, usually with a ragged the N-terminus (Häggqvist et al., 1999). Protein extracts of amyloid-rich aortic media contain Medin monomers (4.5 to 6 kDa) and aggregates of different size, as well as its precursor protein MFG-E8 (Häggqvist et al., 1999; Mucchiano et al., 1992; Peng et al., 2005, 2007). These isolated Medin deposits are water-insoluble and resistant to proteinase digestion (Degenhardt et al., 2020; Häggqvist et al., 1999; Peng et al., 2007).

In vitro studies suggested that Medin appears largely unordered with a mixture of random-coil and approximately 30% β-sheet structures (Davies et al., 2018; Olofsson et al., 2007). Further, it was observed that monomeric Medin can adopt a stable core of three β-sheets while the termini are less well ordered (Davies et al., 2014, 2017). The self-assembly process may start from transient intermediates when the short C-terminal strand detaches from the soluble fold and thereby exposes the highly amyloidogenic C-terminal residues initiating nucleation and amyloid growth

(Davies et al., 2017). The binding to biological lipid interfaces might increase local Medin concentration and promote conformational changes into α-helical species/intermediates making it more prone for aggregation (Abedini & Raleigh, 2009; Byström et al., 2008; Olofsson et al., 2007), as previously described for Aβ and IAPP *in vitro* (Knight et al., 2006; Talafous et al., 1994; Terzi et al., 1997).

The resulting Medin fibrils have typical biochemical and biophysical/structural properties such as Congored staining and ThT fluorescence that bind β-rich structures (Ban et al., 2003; Häggqvist et al., 1999; Larsson et al., 2007; Reches & Gazit, 2004). Notably, preformed Medin fibrils are able to promote aggregation of soluble Medin *in vitro* (Davies et al., 2018). However, it is important to keep in mind that *in vitro* incubation conditions and sample preparation can alter amyloid aggregations characteristics, and could differ from physiological structures (Davies et al., 2018; Younger et al., 2020).

To perform mechanistic studies on the (patho-)physiological role of Medin *in vivo*, animal models are needed. Given the exceedingly high prevalence of Medin aggregates in the human population, we wondered if aging mice would also develop Medin deposition in their vasculature. This was the focus of the first study presented in the following.

2.3.1.3 Experimental model to study Medin pathology *in vivo*

In reference to:

Medin aggregation causes cerebrovascular dysfunction in aging wild-type mice

Karoline Degenhardt*, Jessica Wagner*, Angelos Skodras, Michael Candlish, Anna Julia Koppelmann, Katleen Wild, Rusheka Maxwell, Carola Rotermund, Felix von Zweydorf, Christian Johannes Gloeckner, Hannah A. Davies, Jillian Madine, Domenico Del Turco, Regina Feederle, Tammaryn Lashley, Thomas Deller, Philipp Kahle, Jasmin K. Hefendehl, Mathias Jucker, and Jonas J. Neher (2020). *PNAS* (DOI: 10.1073/pnas.2011133117) *contributed equally

---

The recent advances in the structural and biochemical characterization of Medin amyloid and its similarities to other amyloids, such as Aβ, indicate that it could have similar cytotoxic and inflammatory effects on tissue homeostasis and function. Correlative studies on post-mortem or surgical tissue highlight the age-associated localization of Medin amyloid in the vascular system of the human body and indicate a potential role in vascular dysfunction (Davies et al., 2019; Karamanova et al., 2020; Migrino et al., 2017; Muckle, 1988; Peng et al., 2007). However, these

techniques only provide limited mechanistic insight. Detailed studies in a more physiological, complex environment are needed to assess whether Medin could play a causal role in age-related vascular dysfunction.

In our recent study, we investigated whether mice could be a suitable candidate for *in vivo* studies. So far, no other species has been described to deposit Medin aggregates in blood vessels. However, age-associated increase of MFG-E8 levels in the aorta is conserved across species (Fu et al., 2009; Miura et al., 2019; M. Wang et al., 2012). Moreover, humans and mice share 78% sequence homology (Needle-Wunsch Global Alignment, BLAST) of the long isoform of the precursor protein MFG-E8. Importantly, we noted that the highest conservation can be observed in the aggregation-prone region, although the murine sequence is less hydrophobic according to TANGO predictions (Degenhardt et al., 2020; Fernandez-Escamilla et al., 2004). Similar to humans, wild-type (WT) mice show a significant increase of precursor MFG-E8 protein levels in an age-dependent manner as measured by ELISA of aorta homogenates and immunostaining intensity of MFG-E8 (Chiang et al., 2019; Degenhardt et al., 2020). We described that a significant difference in MFG-E8 levels can already be detected at midlife with 12 months by ELISA with even higher levels at older age (20-months; Degenhardt et al., 2020). In our study, immunostaining with a polyclonal antibody against mouse MFG-E8 (with high affinity for Medin-containing C2 domain and low affinity for C1) revealed amorphous, aggregate-like deposits along the aortic fibers with age in WT mice of the C57BL/6J strain (Degenhardt et al., 2020), resembling the findings of Medin deposits in the human aorta (Degenhardt et al., 2020; Mucchiano et al., 1992).

Furthermore, we confirmed specificity by absence of aggregates in *Mfge8* C2 knockout (KO) mice (Figure 5). These mice lack the Medin-containing C2-domain of MFG-E8 that is replaced by a β-galactosidase reporter gene fused to a transmembrane domain (Silvestre et al., 2005). *Mfge8* C2 KO mice still express the MFG-E8 protein, but without the Medin sequence. Because of the fused transmembrane domain, the truncated protein is trapped inside the cell and gets rapidly degraded, preventing any secretion or circulation of extracellular MFG-E8 or Medin (Silvestre et al., 2005).

Remarkably, in our study, purified aortic aggregates of aged wild-type mice had similar biochemical properties as human Medin and Aβ (Häggqvist et al., 1999; Peng et al., 2005, 2007; Stöhr et al., 2012). The enriched 5 kDa peptides were insoluble in aqueous medium and resistant to nuclease and protease digestion (Degenhardt et al., 2020). Shotgun-mass spectrometry analysis of mouse aorta homogenates identified small MFG-E8 peptides that could be assigned to the reported Medin sequence (Degenhardt et al., 2020). Of note, we did not detect any Medin aggregates in young WT

or aged *Mfge8* C2 KO mice. Having an animal model without overexpression of the protein of interest in a physiological aging-environment offers a unique opportunity to identify disease mechanisms that involve Medin but also to gain new insight about general amyloid biology *in vivo*.
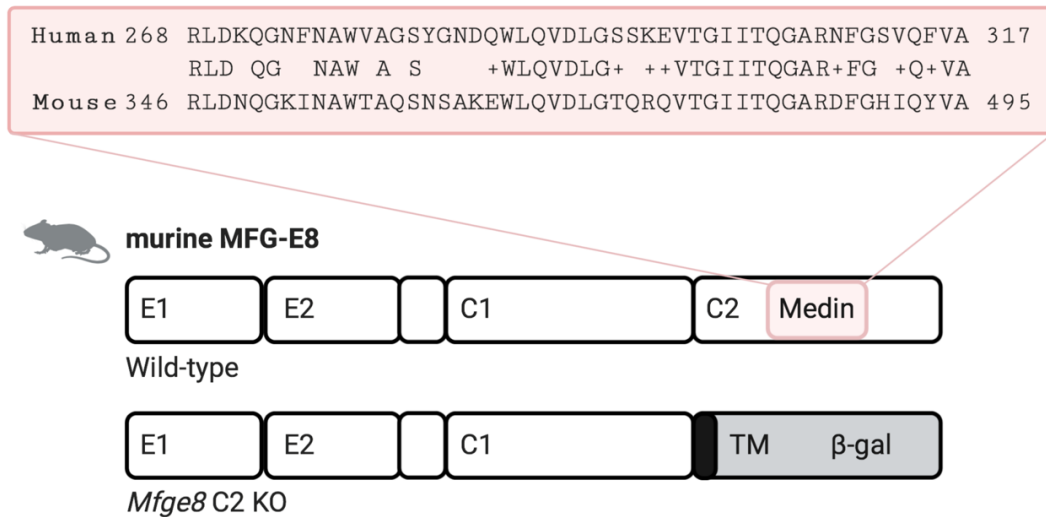


```
Human 268 RLDKQGNFNAWVAGSYGNDQWLQVDLGSSKEVTGIITQGARNFGSVQFVA 317
          RLD QG  NAW A S   +WLQVDLG+ ++VTGIITQGAR+FG +Q+VA
Mouse 346 RLDNQGKINAWTAQSNSAKEWLQVDLGTQRQVTGIITQGARDFGHIQYVA 495
```

Figure 5: In *Mfge8* C2 knockout (KO) animals, the Medin-containing C2 domain is replaced by a β-galactosidase (β-gal) reporter gene (fused to a transmembrane domain, TM) (Silvestre et al., 2005). *Mfge8* C2 KO mice still express the truncated MFG-E8 protein, but cannot develop Medin aggregates due to the missing sequence. E1/2, EGF-like repeat 1/2; C1/2, F5/8-type C domains 1/2. Based on Degenhardt et al., 2020.

2.3.2 Role of MFG-E8 and Medin in vascular diseases

The cardiovascular system is important for circulation of blood and efficient oxygen supply, especially to the brain, but also for the removal of metabolites and pathological proteins (such as Aβ) from the tissue. Approximately 85 % of all cardiovascular deaths are due to diseases of blood vessels supplying the heart or brain (fact sheet of World Health Organization, https://www.who.int/, March 2017). Several studies have established that aortic/arterial stiffness is a predictor of mortality (Laurent et al., 2001) as well as of cardiovascular diseases including aorta aneurysm and dissection, ischemia, stenosis and heart failure (reviewed in Xu et al., 2017; Collins et al., 2014). With age, the length, thickness, diameter and microstructural architecture of the aortic wall change (Fritze et al., 2011; Ohyama et al., 2018; Turkbey et al., 2014). In addition, oxidative stress, inflammation and cell death occur (Fritze et al., 2011). As a consequence, aortic stiffness significantly increases with >50 years of age leading to impaired vasodilation and blood pressure (Oishi et al., 2011; Wuyts et al., 1995).

Proteomic analysis of age-associated changes in the aortic tunica media show that Medin-precursor protein, MFG-E8, is an important marker for aging in the human aorta (Miura et al., 2019). Upregulation of MFG-E8 may play a role in arterial aging mediated via its effect on viability and function of smooth muscle cells and on microstructural alterations in rodents and nonhuman primates (Chiang et al., 2019; Fu et al., 2009). Furthermore, it was shown that the age-associated increase of MFG-E8 induces collagen and elastin degradation by matrix metalloproteinase 2 (MMP2), calcification and vessel wall damage in wild-type mice (Kim, Liu, et al., 2020). Importantly, this physiological aging process was attenuated by *Mfge8* KO (Kim, Liu, et al., 2020). Notably, strong labeling of human aortic media with MFG-E8 can already be observed with 24 and 28 years-of-age (Larsson et al., 2006). Interestingly, also apolipoprotein E (ApoE) seems to be upregulated with age in the tunica media and co-localizes with aortic Congored and MFG-E8 deposits (Miura et al., 2019). ApoE is known to protect endothelial cells from oxidative stress, but is also suggested to be an amyloid signature protein and play a role in amyloid pathology (Bales et al., 1997; Benson et al., 2020; Kanekiyo et al., 2014). However, it remains unknown whether increased MFG-E8 levels are a driver or consequence of the vascular aging processes.

In humans, altered MFG-E8 levels are not only induced by age but also by genetic susceptibility. While upregulation of MFGE8 expression increases risk for cardiovascular diseases, downregulation seems to be protective. A rare missense variant with upregulated expression of MFG-E8 is associated with increased atherosclerosis and arterial damage in diabetes (T2D) (Sapkota & Sanghera, 2020; Yu et al., 2012). Other previous studies identified an intergenic single nucleotide polymorphisms rs8042271 117kb upstream of MFGE8 (Nikpay et al., 2015; Soubeyrand et al., 2019) at the chromosome 15q26.1 locus (MFGE8-ABHD2) that is associated with decreased MFGE8 expression in coronary artery and protective against coronary artery disease.

In addition to the relationship of MFG-E8 with arterial aging, the occurrence and deposition of Medin amyloid is also strongly correlated with the physiological aging of the aorta. Binding of MFG-E8 and Medin deposits to elastic fibers in the tunica media could on the one hand new nucleation sites for further Medin amplification and on the other hand they affect the elasticity of the aorta (Larsson et al., 2006). Usually, elastin is extensible up to about 140% before failure (Wuyts et al., 1995). However, interference of Medin with the anchoring of smooth muscle cells to the elastic fibers and fiber degradation could alter the elasticity of the vessel wall (G. T. Westermark & Westermark, 2011). *In vitro*, Medin was shown to degrade elastin and collagen by upregulation of MMP2 production (Davies et al., 2019; Peng et al., 2007). Activity of MMPs was found to be

increased in aortic aneurysm and suggested as a potential biomarker for the progressive aortic dilation (Gallo et al., 2018; Ishii & Asuwa, 2000; Schmitt et al., 2019). In addition, Medin is toxic to smooth muscle and endothelial cells (Davies et al., 2018; Davies, Phelan, et al., 2015; Madine & Middleton, 2010; Peng et al., 2007). These structural and functional alterations of the vessel wall architecture predispose it to both rupture and arterial stiffness, leading to development of abnormal structures such as spontaneous thoracic aneurysms or aortic dissection (Davies et al., 2019; Peng et al., 2007). Furthermore, recent studies correlate aortic stiffness to cognitive decline and dementia (Cooper et al., 2016; Pase et al., 2016; Scuteri et al., 2013).

Altogether, the consequences of age-associated increase of MFG-E8 and its fragment Medin in the human aorta appear to be vascular stiffness and damage by altered viability and function of smooth muscle and endothelial cells, and extracellular matrix (ECM) remodeling (Davies et al., 2018, 2019; Larsson et al., 2006; Madine & Middleton, 2010; Peng et al., 2007).

2.3.3 Medin aggregates and cerebrovascular dysfunction

Medin is not exclusively found in the tunica media of the aorta but also in the arteries of the upper body, including the basilar, temporal and leptomeningeal arteries, as well as arteries and arterioles in the brain parenchyma (Karamanova et al., 2020; Migrino et al., 2020; Peng et al., 2002). Both aortic and arterial Medin deposits are closely associated with the elastic fibers (Larsson et al., 2006; Peng et al., 2005). The question therefore arises as to whether vascular deposits in the brain have pathological consequences different or similar to those previously described in the aorta.

Previously, 2D and 3D chip cell culture systems were used to analyze the effects of Medin on adipose and leptomeningeal arteries (Migrino et al., 2017). Acute exposure with Medin induced oxidative stress by increasing superoxide and peroxynitrite production and reduced bioavailable nitric oxide (NO) (Davies, Phelan, et al., 2015; Migrino et al., 2017). NO produced by endothelial cells, in response to shear stress or stimulation by acetylcholine, is an important signaling molecule for relaxation of smooth muscle cells and vasodilation (Furchgott & Zawadzki, 1980; Ignarro et al., 1987; Katsuki et al., 1977; Thijssen et al., 2016). In line with this, a reduced dilatory response to acetylcholine after Medin treatment was observed (Migrino et al., 2017, 2018). Furthermore, Medin-induced nitric and oxidative stress affected endothelial cell proliferation and migration (Migrino et al., 2017). Exposure to Medin additionally resulted in increased levels of interleukins, IL-6 and IL-8. The resulting pro-inflammatory signaling, likely mediated via RAGE and NFκB in

endothelial cells, further reduced cell viability and function (Migrino et al., 2017). Interestingly, similar effects of amyloid on vascular function have been described for Aβ (Cortes-Canteli & Iadecola, 2020; Iadecola, 2004; Migrino et al., 2018). Recent studies on Medin pathology in parenchymal arteries draw a similar picture. Here, Medin also induces activation of immune signaling by endothelial cells and astrocytes and cytotoxicity *in vitro* (Karamanova et al., 2020).

In order to translate *in vitro* findings into an *in vivo* setting, our recent study aimed to investigate whether Medin could have structural and functional effects on cerebral arteries and arterioles (Degenhardt et al., 2020). Brain arteries and arterioles are important for the regulation of blood flow to and blood pressure in the brain, ensuring the supply of oxygen and important metabolites. A healthy human brain consumes 20% of oxygen and 25% glucose circulating in the vascular system (although it comprises only 2% of total body mass; Zlokovic, 2011). This is controlled by functional hyperemia, a tightly regulated mechanism that spatially matches the cerebral blood flow to the local neuronal metabolic demands of the different brain regions (reviewed in Harder et al., 1998). Age- and disease-associated functional and structural alterations in the cerebrovasculature (including CAA; Peca et al., 2013; van Opstal et al., 2017) have been shown to lead to a reduction in functional hyperemia, independent of changes in neuronal activity (Girouard & Iadecola, 2006; Zlokovic, 2011).

We used wild-type mice as model to study Medin aggregates (see chapter 2.3.1.3) and found that protein levels of the precursor as well as vascular aggregate-like MFG-E8/Medin immunostaining were significantly increased with age in the mouse brain. The observed aggregates were absent in age-matched Medin deficient mice (*Mfge8* C2 KO) indicating that these endogenous murine deposits likely contained Medin (Degenhardt et al., 2020). Since PET and magnetic resonance imaging (MRI) are less suitable to measure subtle age-related changes in regional blood flow in mice (Maier et al., 2014), we performed two-photon imaging of the middle cerebral artery in mice with a cranial window allowing for *in vivo* measurements (Degenhardt et al., 2020). The hindlimb of the mouse was automatically mechanically stimulated to evoke increased regional blood flow to meet the neuronal activity in the sensorimotor cortex. Aged wild-type mice (>20-months-old) responded with a delayed dilation to the increased neuronal activity and slower constriction back to baseline afterwards in comparison to adult mice (5- to 6-months old). Genetic deficiency of Medin significantly improved vascular dilation and constriction in aged animals (Degenhardt et al., 2020). This delayed response supports the proposed effect of Medin on arterial stiffness (Davies et al., 2018, 2019; Larsson et al., 2006; Madine & Middleton, 2010; Peng et al., 2007) and provides

direct evidence that Medin deposition is causative for cerebrovascular dysfunction. However, the effects of Medin may potentiate or be intertwined with other age-associated structural and functional alterations in the arteries (H. M. Kang et al., 2016; Nicholson et al., 2017; Wheeler et al., 2015). Contrary to previous *in vitro* studies that showed cytotoxic effects of Medin on smooth muscle and endothelial cells (Davies et al., 2018; Davies, Phelan, et al., 2015; Madine & Middleton, 2010; Peng et al., 2007), we did not find any evidence for effects on the cells of the neurovascular unit (smooth muscle, endothelial or astrocytic cells), as vascular structure and coverage was unaltered. However, *in vitro* incubation conditions and sample preparation can alter amyloid aggregation characteristics and toxicity (Davies et al., 2018; Younger et al., 2020), and could differ from aorta aggregates; therefore, the cytotoxicity of Medin should be analyzed in more detail in future studies.

Since aortic/ arterial stiffness and chronic vascular inflammation are associated with cognitive decline and dementia (Oh et al., 2016; Rabkin, 2012; Singer et al., 2014; Taniguchi et al., 2015; Watson et al., 2011), Medin pathology could be a new risk factor for vascular cognitive impairment (VCI). The clinical presentation of VCI ranges from subjective cognitive decline to dementia and depends on type, extent and location of the underlying pathology (Van Der Flier et al., 2018). Dementia can be caused by vascular pathology only (<10% of dementia cases, referred to as vascular dementia), but is usually a mixed pathology with other diseases such as AD (Van Der Flier et al., 2018). Vascular dementia most often results from ischemic or hemorrhagic brain damage (Alzheimer's Association Report, 2020). Importantly, histological analysis of post-mortem tissue showed elevated arteriole Medin deposits in patients with vascular dementia (VaD) in comparison to non-demented cases and was also a reliable predictor of VaD diagnosis (Karamanova et al., 2020; Migrino et al., 2020), thereby implicating an independent contribution of Medin to cognitive decline. A pathogenic role for Medin is further supported by effects on endothelial dysfunction, immune activation and arterial stiffness in human cerebral arteries. These studies imply that Medin could be a biomarker or risk factor of cerebrovascular pathology and dementia.

2.4 Medin aggregates promote cerebral β-amyloidosis

In reference to:

Medin interacts with Aβ to promote cerebral β-amyloid angiopathy

Jessica Wagner*, Karoline Degenhardt*, Angelos Skodras, Ulrike Obermüller, Katleen Wild, Anupriya Dalmia, Lisa M. Häsler, Marius Lambert, Ping Liu, Marleen Veit, Hannah A. Davies, Jillian Madine, Regina Feederle, Domenico Del Turco, K. Peter R. Nilsson, Tammaryn Lashley, Thomas Deller, Lary C. Walker, Peter Heutink, Mathias Jucker, Jonas J. Neher. *Submitted* *contributed equally

2.4.1 Cross-talk between amyloids

The studies listed so far suggest an independent role of Medin in the intertwined pathways of age-associated vascular pathology in cognitive decline in vascular dementia and Alzheimer's disease. However, it is important to note that amyloid co-pathologies not only result in parallel downstream processes but can also directly interact (Morales et al., 2013; Ren et al., 2019). Direct amyloid-amyloid interaction can accelerate onset and progression of one primary or a mixed clinical phenotype. Experimental studies have shown that heterologous amyloids can cross-talk – either seeding (Johan et al., 1998; Moreno-Gonzalez et al., 2017) or inhibiting (Bachhuber et al., 2015; X. Li et al., 2013) each other's aggregation. Equivalent to homologous prion-like spreading (chapter 2.2.2), heterologous proteins can co-aggregate and grow via template-assisted or oligomer-nucleated induction (Figure 6; Ma and Nussinov, 2012; Farmer et al., 2017; Ren et al., 2019; Katzmarski et al., 2020). The biophysical and -chemical details of heterologous seeding mechanisms (also termed cross-seeding) are not fully understood yet. However, they seem to rely on sequence and conformation similarity between the binding partners ('conformational selection and population shift' model) and can lead to aggregation of both partners (bidirectional) or only one of the proteins (unidirectional) (Krebs et al., 2004; Morales et al., 2010; O'Nuallain et al., 2004). Whether amyloids cross-seed, -inhibit or show no interaction can also depend on the experimental conditions and can differ between *in vitro* and *in vivo* experiments (Morales et al., 2010; J. Yan et al., 2007). Most of the cross-seeding partners found *in vitro* or in experimental animals can be found co-depositing in humans but miss translational evidence for direct interaction and seeding potential.
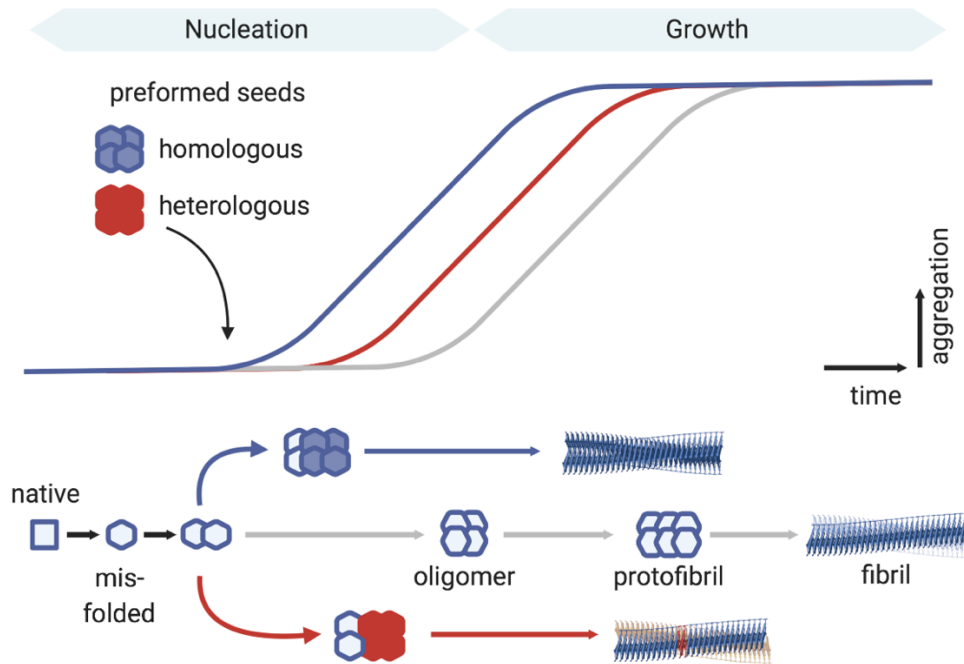
Figure 6: Misfolded or intermediate proteins can aggregate into amyloid fibrils (grey line). Addition of preformed homo-(blue) or heterologous seeds (red line) can template and speed up nucleation and growth of amyloid fibrils. Adapted from Morales et al., 2013.

2.4.2 Co-aggregation of Medin and Aβ

Given the recent finding that Medin levels correlate with Aβ plaque pathology in AD patients, we wondered if Medin and Aβ can directly interact and whether Medin deposition may be a consequence or a contributing factor of Aβ pathology (Migrino et al., 2020). To test this hypothesis first *in vitro*, we used ThT to monitor the potential co-aggregation kinetics in solution. In agreement with previous studies (Ban et al., 2003; Davies et al., 2018; Lindberg et al., 2015), we could demonstrate that soluble recombinant proteins of human Medin and $Aβ_{40}$ can spontaneously aggregate. Astonishingly, aggregation of Medin alone and co-aggregation of Aβ with Medin were significantly faster than Aβ alone and resulted in heterologous amyloid fibrils, as observed by transmission electron microscopy (Wagner et al., submitted). Both co-aggregation as well as inhibition of Aβ aggregation have been reported for other amyloids including transthyretin (TTR), IAPP, tau and α-synuclein (R. Hu et al., 2015; Köppen et al., 2020; X. Li et al., 2013; Luo et al., 2016; Moreno-Gonzalez et al., 2017; Qi et al., 2015). In the case of Medin, only one study investigated co-aggregation with another amyloid. Serum amyloid A (AA) is known as a systemic amyloid and develops due to high serum concentrations of the precursor protein AA after long-term chronic inflammation (Real de Asua et al., 2014; Sack, 2018). Interestingly, Medin aggregates were found

embedded in the core of AA deposits in the thoracic aorta of patients with systemic AA amyloidosis (Larsson et al., 2011). Furthermore, it was shown that Medin induced fibrillization of protein AA *in vitro* suggesting that Medin does not only assist serum AA as aggregation scaffold but rather acts through a heterologous seeding mechanism (Larsson et al., 2011). In case of Aβ and Medin, a common co-aggregation mechanism is further supported by shared structural, kinetic and cytotoxic characteristics (Davies, Madine, et al., 2015; Luo et al., 2016).

2.4.3 Heterologous seeding mechanism between Medin and Aβ promotes cerebral β-amyloidosis and vascular damage

2.4.3.1 Medin can cross-seed Aβ *in vivo*

Although the propensity of Medin and Aβ to co-aggregate *in vitro* was an interesting finding, it is important to determine whether they also interact *in vivo*. To study this potential mechanism, we examined Medin aggregates and related pathology in the brain of two APP transgenic mouse lines, APPPS1 and APP23 (Radde et al., 2006; Sturchler-Pierrat et al., 1997). Our study demonstrated strong co-localization of MFG-E8/Medin with parenchymal amyloid plaques and Aβ deposits in cerebral vessels (CAA) (Wagner et al., submitted). Importantly, genetic deficiency of Medin by cross-breeding APP tg mice with *Mfge8* C2 KO mice prevented deposition of Medin-aggregates and even significantly reduced amyloid pathology, mainly at onset of disease for plaques but robustly in the vasculature even at end-stage in APP23 mice (Wagner et al., submitted). These effects occurred despite indistinguishable APP processing or endogenous, murine Aβ production (Wagner et al., submitted). In contrast to previous studies (Boddaert et al., 2007), we did not observe effects on immune activation or microglia-mediated Aβ clearance by *Mfge8* deficiency.

We further demonstrated that the above effects on cerebral β-amyloidosis might be a result of direct amyloid-amyloid interaction as we found that the absence of MFG-E8/Medin aggregates altered Aβ fibril and plaque structure (Wagner et al., submitted). Notably, these effects of endogenous Medin-like aggregates were visible despite the 3-to-7-fold APP overexpression in these mice. In order to further test whether Medin could promote Aβ aggregation as a heterologous seed, we injected exogenous Medin aggregates from aged human and mouse aorta directly into the hippocampus of pre-depositing APP23 transgenic mice (Wagner et al., submitted). Strikingly, Medin in aged aorta seeding extracts induced pre-mature hippocampal Aβ-pathology after 6 months incubation, while seeding was absent or strongly reduced when using Medin-depleted or *Mfge8* C2 KO aorta extracts, respectively (Wagner et al., submitted). Of note, Medin

did not only promoted Aβ pathology in the hippocampus but also in distant but connected regions of the brain, e.g. the entorhinal cortex. This phenomenon was also reported for Aβ-derived extracts and is most-likely caused by active axonal transport and partially by passive diffusion of corruptive seeds (Eisele & Duyckaerts, 2016; Hamaguchi et al., 2012; Walker et al., 2002). Moreover, we noted the occurrence of CAA in hippocampus, thalamus and meninges after inoculation with exogenous Medin (data not shown), indicating an involvement of the vascular system (Eisele et al., 2009; Meyer-Luehmann et al., 2006). Previous studies detected low levels of Aβ in the human aorta (Kokjohn et al., 2011; Roher et al., 2009); however, sensitive ELISA measurements did not detect any $Aβ_{40}$ or $Aβ_{42}$ peptides in the human aorta extracts used for this study. Instead, immuno-electron microscopy of seeding extracts showed anti-human Medin labeling of 50-100 nm small particles. Some of these were tightly associated with collagen or elastic fibers and resisted protease treatment and sonification during the extraction from the fresh frozen aorta tissue (Degenhardt et al., 2020), underlining the strong binding capacity of Medin with the aortic fibers (Larsson et al., 2006). Of note, *in vitro* collagen fibers only have a minor effect on Aβ aggregation (Scherpelz et al., 2021).

2.4.3.2 MFG-E8 and Medin aggregates may contribute to cognitive decline by promoting cerebral amyloidosis and vascular damage in AD patients

Although these results enable a novel opportunity to study Medin pathology and highlight a possible amyloid-amyloid interaction via cross-seeding mechanism for Medin and Aβ, the relevance to the biology of the human disease remains to be proven. In the human brain, arteriole Medin was previously reported to correlate with AD pathology, namely tau pathology ('Braak score') and plaque load in post-mortem tissue (Migrino et al., 2020). Furthermore, Medin was found to be a reliable predictor of AD, vascular dementia (VaD) and mixed pathologies of VaD/AD; with even more robust correlation with AD diagnosis than CAA (Migrino et al., 2020).

Since no tools are currently available to monitor Medin aggregates in humans *in vivo*, analysis of the precursor MFG-E8 may be a suitable approach to monitor pathology progression, as MFG-E8 levels can be measured in CSF and blood of patients (Del Campo et al., 2018; Shimagaki et al., 2019; Yang et al., 2020). In our study, we wanted to ascertain the contribution of Medin to AD and to this end, we analyzed RNA-sequencing data of cortex samples from >500 patients of the ROSMAP cohort (De Jager et al., 2018). In this analysis, *MFGE8* expression was significantly increased in AD patients compared to non-demented controls. Notably, linear regression analysis revealed a significant impact of *MFGE8* expression on cognitive decline ('MMSE'; Folstein et al., 1975) that

was independent of amyloid plaque load ('CERAD score'; Chandler et al., 2005) and tau pathology ('Braak score'). These results imply that the physiological expression and function of MFG-E8 may be overturned by aging and disease, possibly through production of its fragment Medin. Notably, in our own and the previous data set, the effect of increased MFG-E8 and Medin in the AD brain were independent of age, sex, education, post-mortem interval, ApoE status and other related factors (Migrino et al., 2020; Wagner et al., submitted).

Immunostaining with our anti-human Medin (1H4) antibody further illustrated its localization in aggregate-like structures in leptomeninges and brain parenchymal arterioles out- or inside the smooth muscle cell layer in dementia patients but also in healthy, non-demented elderly (Degenhardt et al., 2020). We also observed localization of Medin in Aβ and Methoxy-positive leptomeninges and parenchymal arterioles of AD patients, with partial overlap of Medin and Aβ (Wagner et al., submitted). Although our study only analyzed a limited number of human cases, previous studies investigated cerebral Medin pathology in more than 90 participants (Karamanova et al., 2020; Migrino et al., 2020). In contrast to the APP transgenic mouse models, we did not observe Medin co-localization with amyloid plaques, supporting a predominant vascular role for Medin in human AD patients (Wagner et al., submitted). However, a correlation between vascular Medin and Aβ in the human AD brain needs to be analyzed in more detail in future studies.

Nevertheless, results from our mouse models support a predominant role for Medin in vascular pathology and heterologous seeding of CAA. In APP23 mice, MFG-E8 protein levels were positively correlated with CAA pathology at onset of the disease, while a negative correlation with plaque load was demonstrated (Wagner et al., submitted). Strikingly, genetic deficiency of MFG-E8 and Medin resulted in reduced vascular pathology in end-stage APP23 mice, as quantified by CAA frequency and severity. Furthermore, CAA-related microhemorrhages were reduced by more than half in Medin-deficient APP23 mice (Wagner et al., submitted), confirming a strong impact of Medin on vascular damage in AD.

In humans, CAA and microbleeds contribute to cognitive decline independent of plaque pathology (Akoudad et al., 2016; Boyle et al., 2015; Greenberg et al., 2020). Thus, these findings underline the unique contribution of Medin to age-associated cerebrovascular pathology and support synergistic effects of Medin on Aβ pathology especially in the brain vasculature. Medin does not only interact directly with Aβ, but through this interaction Medin may promote cerebral β-amyloid angiopathy and, in turn, vascular damage in AD. Medin is one of only two amyloids that have so far been reported to induce Aβ pathology *in vivo*. Only IAPP (amylin) was shown to cross-seed Aβ

(Moreno-Gonzalez et al., 2017), in contrast to Prion protein (Rasmussen et al., 2018) or α-synuclein (Bachhuber et al., 2015). Therefore, Medin may be a novel risk factor and potential therapeutic target for vascular dysfunction and cerebral β-amyloidosis.
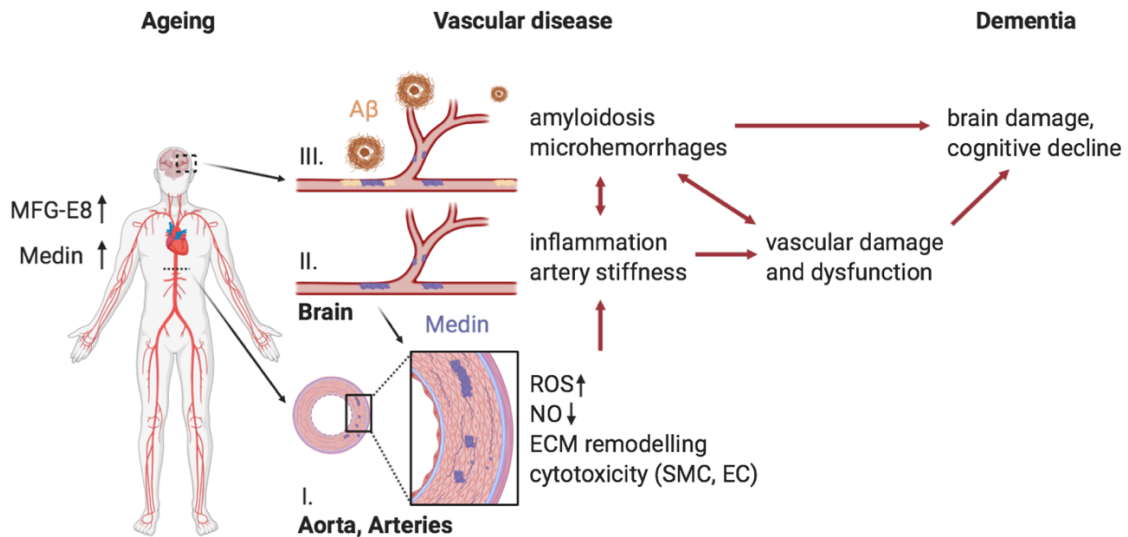

Figure 7: The role of Medin amyloid – one peptide, two potential pathways. Medin aggregates in the human aorta (**I**) and arteries (**II**) cause oxidative stress, cytotoxicity, and structural and functional alteration of the vessel wall resulting in aortic/artery stiffness and pro-inflammatory signaling. In the AD brain (**III**), local Medin aggregates may additionally promote amyloidosis, especially in the cerebral arteries, accelerating further vascular (micro)damage. Vascular damage and the amyloid cascade potentially contribute in a synergistic manner to neuronal damage and cognitive decline. EC, endothelial cell; ECM, extracellular matrix; NO, nitric oxide; ROS, reactive oxygen species; SMC, smooth muscle cell.

2.5 Concluding remarks and future perspectives

Up to now, thirty-six proteins have been described to misfold and aggregate into amyloid fibrils in humans (Benson et al., 2020). Although Medin is probably the most prevalent amyloid, a causal role in disease has not yet been addressed, and only a handful of research groups world-wide try to unravel its pathobiology (only 39 publications for 'Medin amyloid' since the first one in 1999 in comparison to more than 28.400 entries for 'Aβ amyloid' since 1994, according to https://pubmed.ncbi.nlm.nih.gov/, 06.01.2021). Medin aggregates deposit along the elastic fibers in the aorta and arteries of the upper body and correlate with vascular diseases like aortic aneurysm and dissection, and even vascular dementia (Davies et al., 2019; Häggqvist et al., 1999; Migrino et al., 2020; Peng et al., 2007). Understanding Medin pathology in more detail would offer new insights into amyloid biology and potential new strategies to target vascular disease and

dementia. The work of this dissertation established the first experimental *in vivo* model for Medin aggregation and suggests Medin as a potential mechanistic link between age-associated cerebro-vascular dysfunction, cognitive decline and Alzheimer's disease.

Because of the limited numbers of studies that have addressed Medin biology and pathology so far, fundamental questions still remain unanswered: i) what triggers increased MFG-E8 expression with age, ii) when, where, how and why is Medin produced, iii) which Medin species are relevant for disease and iv) despite the high prevalence in the aging population, what makes some elderly people more vulnerable to Medin deposition and pathology. The relatively sudden occurrence of Medin deposition in midlife also cannot be explained so far (Häggqvist et al., 1999; Migrino et al., 2017). Medin could be constantly produced and removed, or an initial nucleation sets off amplification and could be further driven by age-associated loss of protein homeostasis (Hipp et al., 2019; Labbadia & Morimoto, 2015) and increased local concentrations of the precursor protein (Davies et al., 2019; Degenhardt et al., 2020; Miura et al., 2019). Notably, the upregulation of MFG-E8 expression, the precursor of Medin, with age and its correlation with arterial aging is conserved across species (Chiang et al., 2019; Fu et al., 2009; Miura et al., 2019). However, identification of the molecular and cellular mechanisms will require further studies.

Our recent published study established wild-type mice as a powerful model to study Medin aggregates in the aorta and cerebral arteries in an age-dependent manner *in vivo* (Degenhardt et al., 2020). Although the murine Medin sequence is less aggregation-prone in comparison to the human one, murine aggregates show typical characteristics of human Medin including localization, sequence, morphology and biochemical properties (Degenhardt et al., 2020; Häggqvist et al., 1999). This novel model supports previous *in vitro* and *in situ* finding and suggests a causal role of Medin aggregates in age-associated decline in cerebrovascular dysfunction (Figure 7). Upregulation of the precursor protein MFG-E8 and accumulation of Medin aggregates expose endothelial and smooth muscle cells to oxidative and nitrative stress resulting in inflammatory signaling and cytotoxicity (Davies, Phelan, et al., 2015; Madine & Middleton, 2010; Migrino et al., 2017; Peng et al., 2007), while remodeling of the extracellular matrix by microstructural alteration (Davies et al., 2019; Larsson et al., 2006; Peng et al., 2007) and decreased levels of vasodilation-mediator NO (Migrino et al., 2017) increase aortic and artery stiffness. Chronically, vessel wall weakening and degeneration can lead to vascular damage and dysfunction. In the brain, artery stiffening and microstructural alterations reduce cerebral blood flow and consequently, supply with glucose and oxygen, associated with cognitive decline (Rabkin, 2012; Tarantini et al., 2017;

Waldstein et al., 2008). Notably, we demonstrated that age-associated cerebrovascular dysfunction was rescued by genetic deficiency of MFG-E8 and Medin (Degenhardt et al., 2020).

Vascular disease during midlife, a time window when also Medin deposition starts, is the earliest and strongest reported biomarker for late-onset of AD (Iturria-Medina et al., 2016). Only 24% of patients with dementia have 'pure' AD pathology (Aβ plaques and tangles), while the majority has vascular alteration or lesions, either alone (vascular dementia) or combined with AD pathology (Iadecola & Gottesman, 2018). Together, they are the most common cause of dementia in the elderly population (Attems & Jellinger, 2014). However, it remains unclear whether they contribute in an additive or synergistic manner to cognitive impairment. Previous studies suggest that cerebrovascular diseases (including different types of CAA and related microbleedings) affect cognitive decline and dementia through an independent pathway (Arvanitakis et al., 2011; Boyle et al., 2015; Greenberg et al., 2020; Revesz et al., 2003; Smith, 2018; Thal et al., 2008). Although the mechanistic details remain unclear, hypoperfusion, hypoxia, inflammation and ischemic/hemorrhagic damage were suggested to play a role in neuronal damage underlying brain atrophy and dementia, but no accountable protein or robust genetic risk factors have been described (Boyle et al., 2015; Greenberg et al., 2020). On the other hand, it was reported that AD patients with combined vascular and Aβ-pathology have more severe dementia and decreased survival rates (Azarpazhooh et al., 2018; Boyle et al., 2015; Goos et al., 2009). In particular, the fact that both amyloid plaques and CAA are often due to the common pathogenic Aβ peptide may explain why CAA is found preferentially in patients (80-95%) with AD, compared to ∼20-60 % of the aging population, and implicates a synergistic pathway for Aβ clearance and amplification (Boyle et al., 2015; Keage et al., 2009; Thal et al., 2008; M. Yamada et al., 1987). This suggests that vascular factors promote AD pathology and is further supported by the intertwined mechanisms of vascular and amyloid cascades in AD (vascular hypothesis, chapter 2.2.3).

Future research on Medin amyloid may provide new insights into the role of vascular disease in AD (Figure 7). MFG-E8 and its fragment Medin were found to be reliable, independent predictors of cognitive decline and AD (Migrino et al., 2020; Wagner et al., submitted); with even more robust correlation with AD diagnosis than CAA (Migrino et al., 2020). We and others demonstrated that the effect of increased MFG-E8 and Medin seems to be independent of amyloid/tau pathology, age, sex and ApoE status (Migrino et al., 2020; Wagner et al., submitted). In a mouse model of cerebral β-amyloidosis with severe vascular pathology, Medin aggregates seemed to further potentiate CAA severity and associated microhemorrhages, as vascular damage was attenuated by

genetic deficiency of MFG-E8 and Medin (Wagner et al., submitted). Since arterial stiffness, decreased perivascular drainage, neuroinflammation, CAA and hemorrhages are associated with brain damage, vascular cognitive impairment and dementia (Oh et al., 2016; Rabkin, 2012; Singer et al., 2014; Taniguchi et al., 2015; Watson et al., 2011), this could explain the independent contribution of MFG-E8 and Medin to vascular dementia and AD.

Interestingly, our recent studies imply a possible second pathway for a role of Medin in AD (Wagner et al., submitted). Medin aggregates were found co-localizing with parenchymal Aβ plaques and CAA in APP transgenic mice and interacted with Aβ *in vitro* and *in vivo*. Genetic deficiency of Medin decelerated Aβ pathology, while inoculation with exogenous Medin 'seeds' promoted pre-mature onset of cerebral β-amyloidosis. Although we cannot exclude other effects by genetic deficiency of MFG-E8 in the brain, these results provide first evidence that Medin and Aβ co-aggregation show synergistic effects on pathology: Medin and Aβ are not separate pathologies that distribute to the functional and cognitive decline by additive inflammatory, structural and toxic processes, but rather that Medin can directly promote cerebral amyloid angiopathy by a cross-seeding mechanism with Aβ. The possibility of prion-like seeding and transmission of CAA was already proven for human cases and experimental animal models following contamination or injection with exogenous Aβ seeds (Banerjee et al., 2019; Jaunmuktane et al., 2015; Meyer-Luehmann et al., 2006). Whether these finding show translational relevance to the pathobiology of Alzheimer's disease still needs to be investigated. However, we could confirm that Medin aggregates are prevalent in leptomeningeal vessels and parenchymal arterioles with partial overlap with Aβ in human brain tissue. Furthermore, an independent study demonstrated that arteriole Medin levels correlated with amyloid pathology and dementia diagnosis in AD patients (Migrino et al., 2020).

Nevertheless, we are just at the beginning of understanding Medin pathobiology and further studies are urgently needed. Human and murine Medin aggregates still show differences in aggregation-propensity and structure, with Medin aggregates in mice showing a less fibrillar and possibly pre-mature aggregation state. Therefore, a humanized model may offer better translation to the human pathology and would be an interesting vascular target for the sporadic AD (LOAD) mouse model project (Sukoff Rizzo et al., 2020).

Interestingly, we observed weak to no staining of Medin deposits in the human brain by the classical amyloid-binding dye Congored and its derivate Methoxy-X04 (Degenhardt et al., 2020; Wagner et al., submitted). Previous studies imply that oligomers are the main toxic Medin species involved in the pathophysiological processes (Davies et al., 2019; Peng et al., 2002, 2007). For

instance, an increased ratio of pre-fibrillar Medin oligomers to mature amyloid fibrils can be observed in cases of thoracic aortic aneurysm/dissection and temporal arteritis and may be involved in vascular wall weakening, cytotoxicity and reduced aortic elasticity (Davies et al., 2018, 2019; Larsson et al., 2006; Madine & Middleton, 2010; Peng et al., 2002, 2007; Younger et al., 2020). Also for other amyloids, oligomers are known to be potentially more toxic than the compact fibril species (oligomer hypothesis; Kayed et al., 2003; Breydo and Uversky, 2015; Sengupta et al., 2016). In case of Aβ, plaque compaction mediated by microglia or other factors prevents synaptotoxicity and neuritic dystrophy (Condello et al., 2015; Trujillo-Estrada et al., 2013; Yuan et al., 2016). Therefore, compaction of Medin into amyloid deposits may be a protective mechanism of the vasculature to prevent inflammation and degeneration in order to maintain vascular function.

Targeting these toxic species of Medin may offer new preventive, diagnostic and therapeutic strategies, especially for combined vascular and AD pathologies. The Lancet commission on dementia prevention concluded that 35% of dementia cases could be prevented by reducing modifiable cardiovascular (risk) factors and promoting cardiometabolic health (Baumgart et al., 2015; Livingston et al., 2020; Pase et al., 2017; Wahl et al., 2019). Future therapies may, therefore, target initial Medin formation and downstream pathways. Previous studies already reported beneficial effects of *Mfge8* deficiency on aortic extracellular matrix remodeling (elastin/collagen degradation), calcification and endothelial cell injury in mice (Kim, Liu, et al., 2020; Yu et al., 2012). Additionally, effects of toxic oligomeric species could be attenuated by interference with monomer assembly or promoting compaction into fibrils. Usage of heparin (Madine & Middleton, 2010), small complementary peptide or recombinant BRICHOS domains from proSP-C (CTC) (Nerelius et al., 2009; Willander et al., 2011) showed first promising results for an interference with Medin aggregation. Furthermore, *in vitro* experiments showed that oxidative stress conditions can result in nitration of tyrosine and tryptophan residues of Medin altering fibrilization kinetics and fibril morphology (Davies, Phelan, et al., 2015). Indeed, previous studies on Aβ showed that nitration can increase oligomeric species and synaptotoxicity (Guivernau et al., 2016). Prevention of oxidative and nitrative stress could therefore be an additional therapeutic strategy to reduce Medin oligomeric species, limit cytotoxicity and restore vascular function of smooth muscle and endothelial cells at the same time (Karamanova et al., 2020; Migrino et al., 2017). Finally, the previously published NMR structure of the Medin-containing C2 domain of MFG-E8 (Protein Data Bank ID code 2L9L; Ye et al., 2013) may offer targeted computational design of anti-Medin amyloid therapy and inhibition of Medin-Aβ interaction.

In conclusion, vascular dysfunction and disease significantly contribute to Aβ pathology and cognitive decline in AD patients. This dissertation provides a new experimental *in vivo* model and first mechanistic evidence that Medin may be involved on multiple levels of vascular dysfunction and cerebral β-amyloidosis in AD. Microstructural alterations of Medin in the cerebrovasculature affect cerebral blood flow and functional hyperemia, while a potential heterologous seeding mechanism further amplifies cerebral β-amyloidosis, vascular damage and cerebral microhemorrhages. In the future, Medin amyloid may emerge as common biomarker and/or therapeutic target to treat age-associated early vascular cognitive decline and Alzheimer's disease.

2.6 References

Abedini, A., & Raleigh, D. P. (2009). A role for helical intermediates in amyloid formation by natively unfolded polypeptides? *Physical Biology*, *6*(1), 15005. https://doi.org/10.1088/1478-3975/6/1/015005

Akakura, S., Singh, S., Spataro, M., Akakura, R., Kim, J.-I., Albert, M. L., & Birge, R. B. (2004). The opsonin MFG-E8 is a ligand for the alphavbeta5 integrin and triggers DOCK180-dependent Rac1 activation for the phagocytosis of apoptotic cells. *Experimental Cell Research*, *292*(2), 403–416. http://www.ncbi.nlm.nih.gov/pubmed/14697347

Akoudad, S., Wolters, F. J., Viswanathan, A., De Bruijn, R. F., Van Der Lugt, A., Hofman, A., Koudstaal, P. J., Arfan Ikram, M., & Vernooij, M. W. (2016). Association of cerebral microbleeds with cognitive decline and dementia. *JAMA Neurology*, *73*(8), 934–943. https://doi.org/10.1001/jamaneurol.2016.1017

Alzheimer's Association Report. (2020). Alzheimer's disease facts and figures. *Alzheimer's and Dementia*, *16*(3), 391–460. https://doi.org/10.1002/alz.12068

Alzheimer, A. (1898). Neuere Arbeiten über die Dementia senilis und die auf atheromatöser Gefässerkrankung basierenden Gehirnkrankheiten. *European Neurology*, *3*(1), 101–115. https://doi.org/10.1159/000228782

Alzheimer, A. (1911). Über eigenartige Krankheitsfälle des späteren Alters. *Zeitschrift Für Die Gesamte Neurologie Und Psychiatrie*, *4*(1), 356–385. https://doi.org/10.1007/BF02866241

Alzheimer Europe. (2019). *Dementia in Europe Yearbook. Estimating the prevalence of dementia in Europe.*

Andersen, M. H., Berglund, L., Rasmussen, J. T., & Petersen, T. E. (1997). Bovine PAS-6/7 binds $\alpha(v)\beta5$ integrin and anionic phospholipids through two domains. *Biochemistry*, *36*(18), 5441–5446. https://doi.org/10.1021/bi963119m

Anfinsen, C. B. (1973). Principles that govern the folding of protein chains. *Science*, *181*(4096), 223–230. https://doi.org/10.1126/science.181.4096.223

Arvanitakis, Z., Leurgans, S. E., Wang, Z., Wilson, R. S., Bennett, D. A., & Schneider, J. A. (2011). Cerebral amyloid angiopathy pathology and cognitive domains in older persons. *Annals of Neurology*, *69*(2), 320–327. https://doi.org/10.1002/ana.22112

Åslund, A., Sigurdson, C. J., Klingstedt, T., Grathwohl, S., Bolmont, T., Dickstein, D. L., Glimsdal, E., Prokop, S., Lindgren, M., Konradsson, P., Holtzman, D. M., Hof, P. R., Heppner, F. L., Gandy, S., Jucker, M., Aguzzi, A., Hammarström, P., & Nilsson, K. P. R. (2009). Novel pentameric thiophene derivatives for in vitro and in vivo optical imaging of a plethora of protein aggregates in cerebral amyloidoses. *ACS Chemical Biology*, *4*(8), 673–684. https://doi.org/10.1021/cb900112v

Attems, J., & Jellinger, K. A. (2014). The overlap between vascular disease and Alzheimer's disease - lessons from pathology. *BMC Medicine*, *12*(1), 206. https://doi.org/10.1186/s12916-014-0206-2

Azarpazhooh, M. R., Avan, A., Cipriano, L. E., Munoz, D. G., Sposato, L. A., & Hachinski, V. (2018). Concomitant vascular and neurodegenerative pathologies double the risk of dementia. *Alzheimer's and Dementia*, *14*(2), 148–156. https://doi.org/10.1016/j.jalz.2017.07.755

Bachhuber, T., Katzmarski, N., McCarter, J. F., Loreth, D., Tahirovic, S., Kamp, F., Abou-Ajram, C., Nuscher, B., Serrano-Pozo, A., Müller, A., Prinz, M., Steiner, H., Hyman, B. T., Haass, C., & Meyer-Luehmann, M. (2015). Inhibition of amyloid-β plaque formation by α-synuclein.

Nature Medicine, *21*(7), 802–807. https://doi.org/10.1038/nm.3885

Bales, K. R., Verina, T., Dodel, R. C., Du, Y., Altstiel, L., Bender, M., Hyslop, P., Johnstone, E. M., Little, S. P., Cummins, D. J., Piccardo, P., Ghetti, B., & Paul, S. M. (1997). Lack of apolipoprotein E dramatically reduces amyloid β-peptide deposition. In *Nature Genetics* (Vol. 17, Issue 3, pp. 263–264). https://doi.org/10.1038/ng1197-263

Ban, T., Hamada, D., Hasegawall, K., Naiki, H., & Goto, Y. (2003). Direct observation of amyloid fibril growth monitored by thioflavin T fluorescence. *Journal of Biological Chemistry*, *278*(19), 16462–16465. https://doi.org/10.1074/jbc.C300049200

Banerjee, G., Adams, M. E., Jaunmuktane, Z., Alistair Lammie, G., Turner, B., Wani, M., Sawhney, I. M. S., Houlden, H., Mead, S., Brandner, S., & Werring, D. J. (2019). Early onset cerebral amyloid angiopathy following childhood exposure to cadaveric dura. *Annals of Neurology*, *85*(2), 284–290. https://doi.org/10.1002/ana.25407

Bateman, R. J., Xiong, C., Benzinger, T. L. S., Fagan, A. M., Goate, A., Fox, N. C., Marcus, D. S., Cairns, N. J., Xie, X., Blazey, T. M., Holtzman, D. M., Santacruz, A., Buckles, V., Oliver, A., Moulder, K., Aisen, P. S., Ghetti, B., Klunk, W. E., McDade, E., … Morris, J. C. (2012). Clinical and Biomarker Changes in Dominantly Inherited Alzheimer's Disease. *New England Journal of Medicine*, *367*(9), 795–804. https://doi.org/10.1056/nejmoa1202753

Baumgart, M., Snyder, H. M., Carrillo, M. C., Fazio, S., Kim, H., & Johns, H. (2015). Summary of the evidence on modifiable risk factors for cognitive decline and dementia: A population-based perspective. *Alzheimer's and Dementia*, *11*(6), 718–726. https://doi.org/10.1016/j.jalz.2015.05.016

Bekris, L. M., Yu, C. E., Bird, T. D., & Tsuang, D. W. (2010). Genetics of Alzheimer disease. *Journal of Geriatric Psychiatry and Neurology*, *23*(4), 213–227. https://doi.org/10.1177/0891988710383571

Benson, M. D., Buxbaum, J. N., Eisenberg, D. S., Merlini, G., Saraiva, M. J. M., Sekijima, Y., Sipe, J. D., & Westermark, P. (2018). Amyloid nomenclature 2018: recommendations by the International Society of Amyloidosis (ISA) nomenclature committee. *Amyloid*, *25*(4), 215–219. https://doi.org/10.1080/13506129.2018.1549825

Benson, M. D., Buxbaum, J. N., Eisenberg, D. S., Merlini, G., Saraiva, M. J. M., Sekijima, Y., Sipe, J. D., & Westermark, P. (2020). Amyloid nomenclature 2020: update and recommendations by the International Society of Amyloidosis (ISA) nomenclature committee. *Amyloid*, *27*(4), 217–222. https://doi.org/10.1080/13506129.2020.1835263

Bertram, L., McQueen, M. B., Mullin, K., Blacker, D., & Tanzi, R. E. (2007). Systematic meta-analyses of Alzheimer disease genetic association studies: The AlzGene database. *Nature Genetics*, *39*(1), 17–23. https://doi.org/10.1038/ng1934

Bertram, L., & Tanzi, R. E. (2019). Alzheimer disease risk genes: 29 and counting. *Nature Reviews Neurology*, *15*(4), 191–192. https://doi.org/10.1038/s41582-019-0158-4

Boddaert, J., Kinugawa, K., Lambert, J.-C., Boukhtouche, F., Zoll, J., Merval, R., Blanc-Brude, O., Mann, D., Berr, C., Vilar, J., Garabedian, B., Journiac, N., Charue, D., Silvestre, J.-S., Duyckaerts, C., Amouyel, P., Mariani, J., Tedgui, A., & Mallat, Z. (2007). Evidence of a role for lactadherin in Alzheimer's disease. *The American Journal of Pathology*, *170*(3), 921–929. https://doi.org/10.2353/ajpath.2007.060664

Bourdel-Marchasson, I., Lapre, E., Laksir, H., & Puget, E. (2010). Insulin resistance, diabetes and cognitive function: consequences for preventative strategies. *Diabetes & Metabolism*, *36*(3), 173–181. https://doi.org/10.1016/j.diabet.2010.03.001

Boyle, P. A., Yu, L., Nag, S., Leurgans, S., Wilson, R. S., Bennett, D. A., & Schneider, J. A. (2015).

Cerebral amyloid angiopathy and cognitive outcomes in community-based older persons. *Neurology*, *85*(22), 1930–1936. https://doi.org/10.1212/WNL.0000000000002175

Braak, H., & Braak, E. (1991). Neuropathological stageing of Alzheimer-related changes. *Acta Neuropathologica*, *82*(4), 239–259. https://doi.org/10.1007/BF00308809

Breydo, L., & Uversky, V. N. (2015). Structural, morphological, and functional diversity of amyloid oligomers. *FEBS Letters*, *589*(19), 2640–2648. https://doi.org/10.1016/j.febslet.2015.07.013

Broce, I. J., Tan, C. H., Fan, C. C., Jansen, I., Savage, J. E., Witoelar, A., Wen, N., Hess, C. P., Dillon, W. P., Glastonbury, C. M., Glymour, M., Yokoyama, J. S., Elahi, F. M., Rabinovici, G. D., Miller, B. L., Mormino, E. C., Sperling, R. A., Bennett, D. A., McEvoy, L. K., … Desikan, R. S. (2019). Dissecting the genetic relationship between cardiovascular risk factors and Alzheimer's disease. *Acta Neuropathologica*, *137*(2), 209–226. https://doi.org/10.1007/s00401-018-1928-6

Brown, G. C., & Neher, J. J. (2014). Microglial phagocytosis of live neurons. *Nature Reviews Neuroscience*, *15*(4), 209–216. https://doi.org/10.1038/nrn3710

Buchhave, P., Minthon, L., Zetterberg, H., Wallin, Å. K., Blennow, K., & Hansson, O. (2012). Cerebrospinal fluid levels of β-amyloid 1-42, but not of tau, are fully changed already 5 to 10 years before the onset of Alzheimer dementia. *Archives of General Psychiatry*, *69*(1), 98–106. https://doi.org/10.1001/archgenpsychiatry.2011.155

Burwinkel, M., Lutzenberger, M., Heppner, F. L., Schulz-Schaeffer, W., & Baier, M. (2018). Intravenous injection of beta-amyloid seeds promotes cerebral amyloid angiopathy (CAA). *Acta Neuropathologica Communications*, *6*(1), 23. https://doi.org/10.1186/s40478-018-0511-7

Buxbaum, J. N. (2009). Animal models of human amyloidoses: Are transgenic mice worth the time and trouble? *FEBS Letters*, *583*(16), 2663–2673. https://doi.org/10.1016/j.febslet.2009.07.031

Byström, R., Aisenbrey, C., Borowik, T., Bokvist, M., Lindström, F., Sani, M. A., Olofsson, A., & Gröbner, G. (2008). Disordered proteins: Biological membranes as two-dimensional aggregation matrices. *Cell Biochemistry and Biophysics*, *52*(3), 175–189. https://doi.org/10.1007/s12013-008-9033-4

Cahoy, J. D., Emery, B., Kaushal, A., Foo, L. C., Zamanian, J. L., Christopherson, K. S., Xing, Y., Lubischer, J. L., Krieg, P. A., Krupenko, S. A., Thompson, W. J., & Barres, B. A. (2008). A transcriptome database for astrocytes, neurons, and oligodendrocytes: A new resource for understanding brain development and function. *Journal of Neuroscience*, *28*(1), 264–278. https://doi.org/10.1523/JNEUROSCI.4178-07.2008

Calhoun, M. E., Burgermeister, P., Phinney, A. L., Stalder, M., Tolnay, M., Wiederhold, K. H., Abramowski, D., Sturchler-Pierrat, C., Sommer, B., Staufenbiel, M., & Jucker, M. (1999). Neuronal overexpression of mutant amyloid precursor protein results in prominent deposition of cerebrovascular amyloid. *Proceedings of the National Academy of Sciences of the United States of America*, *96*(24), 14088–14093. https://doi.org/10.1073/pnas.96.24.14088

Chandler, M. J., Lacritz, L. H., Hynan, L. S., Barnard, H. D., Allen, G., Deschner, M., Weiner, M. F., & Cullum, C. M. (2005). A total score for the CERAD neuropsychological battery. *Neurology*, *65*(1), 102–106. https://doi.org/10.1212/01.wnl.0000167607.63000.38

Charidimou, A., Boulouis, G., Gurol, M. E., Ayata, C., Bacskai, B. J., Frosch, M. P., Viswanathan, A., & Greenberg, S. M. (2017). Emerging concepts in sporadic cerebral amyloid angiopathy. *Brain*, *140*(7), 1829–1850. https://doi.org/10.1093/brain/awx047

Chen, Y., & Tang, B. L. (2006). The amyloid precursor protein and postnatal neurogenesis/neuroregeneration. *Biochemical and Biophysical Research Communications*, *341*(1), 1–5. https://doi.org/10.1016/j.bbrc.2005.12.150

Cheng, Y., Tian, D. Y., & Wang, Y. J. (2020). Peripheral clearance of brain-derived Aβ in Alzheimer's disease: Pathophysiology and therapeutic perspectives. *Translational Neurodegeneration*, *9*(1), 16. https://doi.org/10.1186/s40035-020-00195-1

Chiang, H. Y., Chu, P. H., & Lee, T. H. (2019). MFG-E8 mediates arterial aging by promoting the proinflammatory phenotype of vascular smooth muscle cells. *Journal of Biomedical Science*, *26*(1), 1–14. https://doi.org/10.1186/s12929-019-0559-0

Clavaguera, F., Akatsu, H., Fraser, G., Crowther, R. A., Frank, S., Hench, J., Probst, A., Winkler, D. T., Reichwald, J., Staufenbiel, M., Ghetti, B., Goedert, M., & Tolnay, M. (2013). Brain homogenates from human tauopathies induce tau inclusions in mouse brain. *Proceedings of the National Academy of Sciences of the United States of America*, *110*(23), 9535–9540. https://doi.org/10.1073/pnas.1301175110

Cohen, M. L., Kim, C., Haldiman, T., ElHag, M., Mehndiratta, P., Pichet, T., Lissemore, F., Shea, M., Cohen, Y., Chen, W., Blevins, J., Appleby, B. S., Surewicz, K., Surewicz, W. K., Sajatovic, M., Tatsuoka, C., Zhang, S., Mayo, P., Butkiewicz, M., … Safar, J. G. (2015). Rapidly progressive Alzheimer's disease features distinct structures of amyloid-β. *Brain*, *138*(4), 1009–1022. https://doi.org/10.1093/brain/awv006

Collins, C., Nehlin, J. O., Stubbs, J. D., Kowbel, D., Kuo, W. L., & Parry, G. (1997). Mapping of a newly discovered human gene homologous to the apoptosis associated-murine mammary protein, MFG-E8, to chromosome 15q25. *Genomics*, *39*(1), 117–118. https://doi.org/10.1006/geno.1996.4425

Collins, J. A., Munoz, J. V., Patel, T. R., Loukas, M., & Tubbs, R. S. (2014). The anatomy of the aging aorta. *Clinical Anatomy*, *27*(3), 463–466. https://doi.org/10.1002/ca.22384

Condello, C., DeGrado, W. F., & Prusiner, S. B. (2020). Prion biology: implications for Alzheimer's disease therapeutics. *The Lancet Neurology*, *19*(10), 802–803. https://doi.org/10.1016/S1474-4422(20)30274-X

Condello, C., Lemmin, T., Stöhr, J., Nick, M., Wu, Y., Maxwell, A. M., Watts, J. C., Caro, C. D., Oehler, A., Keene, C. D., Bird, T. D., van Duinen, S. G., Lannfelt, L., Ingelsson, M., Graff, C., Giles, K., DeGrado, W. F., & Prusiner, S. B. (2018). Structural heterogeneity and intersubject variability of Aβ in familial and sporadic Alzheimer's disease. *Proceedings of the National Academy of Sciences of the United States of America*, *115*(4), E782–E791. https://doi.org/10.1073/pnas.1714966115

Condello, C., Yuan, P., Schain, A., & Grutzendler, J. (2015). Microglia constitute a barrier that prevents neurotoxic protofibrillar Aβ42 hotspots around plaques. *Nature Communications*, *6*(1), 6176. https://doi.org/10.1038/ncomms7176

Cooper, L. L., Woodard, T., Sigurdsson, S., Van Buchem, M. A., Torjesen, A. A., Inker, L. A., Aspelund, T., Eiriksdottir, G., Harris, T. B., Gudnason, V., Launer, L. J., & Mitchell, G. F. (2016). Cerebrovascular Damage Mediates Relations Between Aortic Stiffness and Memory. *Hypertension*, *67*(1), 176–182. https://doi.org/10.1161/HYPERTENSIONAHA.115.06398

Cornwell, G. G., Johnson, K. H., & Westermark, P. (1995). The age related amyloids: A growing family of unique biochemical substances. *Journal of Clinical Pathology*, *48*(11), 984–989. https://doi.org/10.1136/jcp.48.11.984

Cortes-Canteli, M., & Iadecola, C. (2020). Alzheimer's Disease and Vascular Aging: JACC Focus Seminar. *Journal of the American College of Cardiology*, *75*(8), 942–951.

https://doi.org/10.1016/j.jacc.2019.10.062

Couto, J. R., Taylor, M. R., Godwin, S. G., Ceriani, R. L., & Peterson, J. A. (1996). Cloning and sequence analysis of human breast epithelial antigen BA46 reveals an RGD cell adhesion sequence presented on an epidermal growth factor-like domain. *DNA and Cell Biology*, *15*(4), 281–286. https://doi.org/10.1089/dna.1996.15.281

Das, P., Verbeeck, C., Minter, L., Chakrabarty, P., Felsenstein, K., Kukar, T., Maharvi, G., Fauq, A., Osborne, B. A., & Golde, T. E. (2012). Transient pharmacologic lowering of A production prior to deposition results in sustained reduction of amyloid plaque pathology. *Molecular Neurodegeneration*, *7*(1), 39. https://doi.org/10.1186/1750-1326-7-39

Davies, H. A., Caamaño-Gutiérrez, E., Chim, Y. H., Field, M., Nawaytou, O., Ressel, L., Akhtar, R., & Madine, J. (2019). Idiopathic degenerative thoracic aneurysms are associated with increased aortic medial amyloid. *Amyloid*, *26*(3), 148–155. https://doi.org/10.1080/13506129.2019.1625323

Davies, H. A., Lee, C. F., Miller, L., Liu, L. N., & Madine, J. (2018). Insights into the origin of distinct medin fibril morphologies induced by incubation conditions and seeding. *International Journal of Molecular Sciences*, *19*(5). https://doi.org/10.3390/ijms19051357

Davies, H. A., Madine, J., & Middleton, D. A. (2015). Comparisons with Amyloid-β Reveal an Aspartate Residue That Stabilizes Fibrils of the Aortic Amyloid Peptide Medin. *Journal of Biological Chemistry*, *290*(12), 7791–7803. https://doi.org/10.1074/jbc.M114.602177

Davies, H. A., Phelan, M. M., Wilkinson, M. C., Migrino, R. Q., Truran, S., Franco, D. A., Liu, L.-N. N., Longmore, C. J., & Madine, J. (2015). Oxidative Stress Alters the Morphology and Toxicity of Aortic Medial Amyloid. *Biophysical Journal*, *109*(11), 2363–2370. https://doi.org/10.1016/j.bpj.2015.10.034

Davies, H. A., Rigden, D. J., Phelan, M. M., & Madine, J. (2017). Probing medin monomer structure and its amyloid nucleation using 13 C-direct detection NMR in combination with structural bioinformatics. *Scientific Reports*, *7*, 45224. https://doi.org/10.1038/srep45224

Davies, H. A., Wilkinson, M. C., Gibson, R. P., & Middleton, D. A. (2014). Expression and purification of the aortic amyloid polypeptide medin. *Protein Expression and Purification*, *98*, 32–37. https://doi.org/10.1016/j.pep.2014.02.009

Dawson, T. M., Golde, T. E., & Lagier-Tourenne, C. (2018). Animal models of neurodegenerative diseases. *Nature Neuroscience*, *21*(10), 1370–1379. https://doi.org/10.1038/s41593-018-0236-8

De Jager, P. L., Ma, Y., McCabe, C., Xu, J., Vardarajan, B. N., Felsky, D., Klein, H. U., White, C. C., Peters, M. A., Lodgson, B., Nejad, P., Tang, A., Mangravite, L. M., Yu, L., Gaiteri, C., Mostafavi, S., Schneider, J. A., & Bennett, D. A. (2018). Data descriptor: A multi-omic atlas of the human frontal cortex for aging and Alzheimer's disease research. *Scientific Data*, *5*(1), 180142. https://doi.org/10.1038/sdata.2018.142

De la Torre, J. C., & Mussivand, T. (1993). Can disturbed brain microcirculation cause Alzheimer's disease? *Neurological Research*, *15*(3), 146–153. https://doi.org/10.1080/01616412.1993.11740127

De Strooper, B., Saftig, P., Craessaerts, K., Vanderstichele, H., Guhde, G., Annaert, W., Von Figura, K., & Van Leuven, F. (1998). Deficiency of presenilin-1 inhibits the normal cleavage of amyloid precursor protein. *Nature*, *391*(6665), 387–390. https://doi.org/10.1038/34910

Degenhardt, K., Wagner, J., Skodras, A., Candlish, M., Koppelmann, A. J., Wild, K., Maxwell, R., Rotermund, C., Von Zweydorf, F., Gloeckner, C. J., Davies, H. A., Madine, J., Del Turco, D., Feederle, R., Lashley, T., Deller, T., Kahle, P., Hefendehl, J. K., Jucker, M., & Neher, J. J.

(2020). Medin aggregation causes cerebrovascular dysfunction in aging wild-type mice. *Proceedings of the National Academy of Sciences of the United States of America*, *117*(38), 23925–23931. https://doi.org/10.1073/pnas.2011133117

Del Campo, M., Galimberti, D., Elias, N., Boonkamp, L., Pijnenburg, Y. A., van Swieten, J. C., Watts, K., Paciotti, S., Beccari, T., Hu, W., & Teunissen, C. E. (2018). Novel CSF biomarkers to discriminate FTLD and its pathological subtypes. *Annals of Clinical and Translational Neurology*, *5*(10), 1163–1175. https://doi.org/10.1002/acn3.629

DeTure, M. A., & Dickson, D. W. (2019). The neuropathological diagnosis of Alzheimer's disease. *Molecular Neurodegeneration*, *14*(1), 32. https://doi.org/10.1186/s13024-019-0333-5

Dobson, C. M., Andrej, S., & Karplus, M. (1998). A knowledge of the potential energy surface that determines the dynamics of a polypeptide chain is as important for understanding protein folding as is the potential surface for Protein Folding : A Perspective from Theory and Experiment. *Angewandte Chemie*, *37*, 868–893.

Drummond, E., & Wisniewski, T. (2017). Alzheimer's disease: experimental models and reality. *Acta Neuropathologica*, *133*(2), 155–175. https://doi.org/10.1007/s00401-016-1662-x

Eanes, E. D., & Glenner, G. G. (1968). X-ray diffraction studies on amyloid filaments. *The Journal of Histochemistry and Cytochemistry : Official Journal of the Histochemistry Society*, *16*(11), 673–677. https://doi.org/10.1177/16.11.673

Eisele, Y. S., Bolmont, T., Heikenwalder, M., Langer, F., Jacobson, L. H., Yan, Z. X., Roth, K., Aguzzi, A., Staufenbiel, M., Walker, L. C., & Jucker, M. (2009). Induction of cerebral β-amyloidosis: Intracerebral versus systemic Aβ inoculation. *Proceedings of the National Academy of Sciences of the United States of America*, *106*(31), 12926–12931. https://doi.org/10.1073/pnas.0903200106

Eisele, Y. S., & Duyckaerts, C. (2016). Propagation of Aß pathology: hypotheses, discoveries, and yet unresolved questions from experimental and human brain studies. *Acta Neuropathologica*, *131*(1), 5–25. https://doi.org/10.1007/s00401-015-1516-y

Eisele, Y. S., Obermüller, U., Heilbronner, G., Baumann, F., Kaeser, S. A., Wolburg, H., Walker, L. C., Staufenbiel, M., Heikenwalder, M., & Jucker, M. (2010). Peripherally applied Aβ-containing inoculates induce cerebral β-amyloidosis. *Science*, *330*(6006), 980–982. https://doi.org/10.1126/science.1194516

Fändrich, M., & Dobson, C. M. (2002). The behaviour of polyamino acids reveals an inverse side chain effect in amyloid structure formation. *EMBO Journal*, *21*(21), 5682–5690. https://doi.org/10.1093/emboj/cdf573

Faraco, G., Sugiyama, Y., Lane, D., Garcia-Bonilla, L., Chang, H., Santisteban, M. M., Racchumi, G., Murphy, M., Van Rooijen, N., Anrather, J., & Iadecola, C. (2016). Perivascular macrophages mediate the neurovascular and cognitive dysfunction associated with hypertension. *Journal of Clinical Investigation*, *126*(12), 4674–4689. https://doi.org/10.1172/JCI86950

Farmer, K., Gerson, J. E., & Kayed, R. (2017). Oligomer Formation and Cross-Seeding: The New Frontier. *Israel Journal of Chemistry*, *57*(7), 665–673. https://doi.org/10.1002/ijch.201600103

Fernandez-Escamilla, A. M., Rousseau, F., Schymkowitz, J., & Serrano, L. (2004). Prediction of sequence-dependent and mutational effects on the aggregation of peptides and proteins. In *Nature Biotechnology* (Vol. 22, Issue 10, pp. 1302–1306). https://doi.org/10.1038/nbt1012

Folstein, M. F., Folstein, S. E., & McHugh, P. R. (1975). "Mini-mental state". A practical method for grading the cognitive state of patients for the clinician. *Journal of Psychiatric Research*, *12*(3), 189–198. https://doi.org/10.1016/0022-3956(75)90026-6

Fotiadis, P., van Rooden, S., van der Grond, J., Schultz, A., Martinez-Ramirez, S., Auriel, E., Reijmer, Y., van Opstal, A. M., Ayres, A., Schwab, K. M., Hedden, T., Rosand, J., Viswanathan, A., Wermer, M., Terwindt, G. M., Sperling, R. A., Polimeni, J. R., Johnson, K. A., van Buchem, M. A., … Gurol, M. E. (2016). Cortical atrophy in patients with cerebral amyloid angiopathy: A case-control study. *The Lancet Neurology*, *15*(8), 811–819. https://doi.org/10.1016/S1474-4422(16)30030-8

Friedreich, N., & Kekulé, A. (1859). Zur Amyloidfrage. *Archiv Für Pathologische Anatomie Und Physiologie Und Für Klinische Medicin*, *16*(1–2), 50–65. https://doi.org/10.1007/BF01945246

Friesen, M., & Meyer-Luehmann, M. (2019). Aβ Seeding as a Tool to Study Cerebral Amyloidosis and Associated Pathology. *Frontiers in Molecular Neuroscience*, *12*(October), 233. https://doi.org/10.3389/fnmol.2019.00233

Fritze, O., Romero, B., Schleicher, M., Jacob, M. P., Oh, D. Y., Starcher, B., Schenke-Layland, K., Bujan, J., & Stock, U. A. (2011). Age-related changes in the elastic tissue of the human aorta. *Journal of Vascular Research*, *49*(1), 77–86. https://doi.org/10.1159/000331278

Fu, Z., Wang, M., Gucek, M., Zhang, J., Wu, J., Jiang, L., Monticone, R. E., Khazan, B., Telljohann, R., Mattison, J., Sheng, S., Cole, R. N., Spinetti, G., Pintus, G., Liu, L., Kolodgie, F. D., Virmani, R., Spurgeon, H., Ingram, D. K., … Van Eyk, J. E. (2009). Milk fat globule protein epidermal growth factor-8: A pivotal relay element within the angiotensin II and monocyte chemoattractant protein-1 signaling cascade mediating vascular smooth muscle cells invasion. *Circulation Research*, *104*(12), 1337–1346. https://doi.org/10.1161/CIRCRESAHA.108.187088

Furchgott, R. F., & Zawadzki, J. V. (1980). The obligatory role of endothelial cells in the relaxation of arterial smooth muscle by acetylcholine. *Nature*, *288*(5789), 373–376. https://doi.org/10.1038/288373a0

Gallardo, R., Ranson, N. A., & Radford, S. E. (2020). Amyloid structures: much more than just a cross-β fold. *Current Opinion in Structural Biology*, *60*, 7–16. https://doi.org/10.1016/j.sbi.2019.09.001

Gallo, A., Agnese, V., Coronnello, C., Raffa, G. M., Bellavia, D., Conaldi, P. G., Pilato, M., & Pasta, S. (2018). On the prospect of serum exosomal miRNA profiling and protein biomarkers for the diagnosis of ascending aortic dilatation in patients with bicuspid and tricuspid aortic valve. *International Journal of Cardiology*, *273*, 230–236. https://doi.org/10.1016/j.ijcard.2018.10.005

Games, D., Adams, D., Alessandrini, R., Barbour, R., Borthelette, P., Blackwell, C., Carr, T., Clemens, J., Donaldson, T., Gillespie, F., Guido, T., Hagopian, S., Johnson-Wood, K., Khan, K., Lee, M., Leibowitz, P., Lieberburg, I., Little, S., Masliah, E., … Zhao, J. (1995). Alzheimer-type neuropathology in transgenic mice overexpressing V717F β-amyloid precursor protein. *Nature*, *373*(6514), 523–527. https://doi.org/10.1038/373523a0

Giaccone, G., Maderna, E., Marucci, G., Catania, M., Erbetta, A., Chiapparini, L., Indaco, A., Caroppo, P., Bersano, A., Parati, E., Di Fede, G., & Caputi, L. (2019). Iatrogenic early onset cerebral amyloid angiopathy 30 years after cerebral trauma with neurosurgery: vascular amyloid deposits are made up of both Aβ40 and Aβ42. *Acta Neuropathologica Communications*, *7*(1), 70. https://doi.org/10.1186/s40478-019-0719-1

Giaccone, G., Tagliavini, F., Linoli, G., Bouras, C., Frigerio, L., Frangione, B., & Bugiani, O. (1989). Down patients: Extracellular preamyloid deposits precede neuritic degeneration and senile plaques. *Neuroscience Letters*, *97*(1–2), 232–238. https://doi.org/10.1016/0304-3940(89)90169-9

Giannakopoulos, P., Herrmann, F. R., Bussière, T., Bouras, C., Kövari, E., Perl, D. P., Morrison, J. H., Gold, G., & Hof, P. R. (2003). Tangle and neuron numbers, but not amyloid load, predict cognitive status in Alzheimer's disease. *Neurology*, *60*(9), 1495–1500. https://doi.org/10.1212/01.WNL.0000063311.58879.01

Girouard, H., & Iadecola, C. (2006). Neurovascular coupling in the normal brain and in hypertension, stroke, and Alzheimer disease. *Journal of Applied Physiology*, *100*(1), 328–335. https://doi.org/10.1152/japplphysiol.00966.2005

Glenner, G. G., Eanes, E. D., & Page, D. L. (1972). The relation of the properties of Congo red-stained amyloid fibrils to the -conformation. *The Journal of Histochemistry and Cytochemistry : Official Journal of the Histochemistry Society*, *20*(10), 821–826. https://doi.org/10.1177/20.10.821

Glenner, G. G., & Wong, C. W. (1984). Alzheimer's disease: Initial report of the purification and characterization of a novel cerebrovascular amyloid protein. *Biochemical and Biophysical Research Communications*, *120*(3), 885–890. https://doi.org/10.1016/S0006-291X(84)80190-4

Goate, A., Chartier-Harlin, M. C., Mullan, M., Brown, J., Crawford, F., Fidani, L., Giuffra, L., Haynes, A., Irving, N., James, L., Mant, R., Newton, P., Rooke, K., Roques, P., Talbot, C., Pericak-Vance, M., Roses, A., Williamson, R., Rossor, M., … Hardy, J. (1991). Segregation of a missense mutation in the amyloid precursor protein gene with familial Alzheimer's disease. *Nature*, *349*(6311), 704–706. https://doi.org/10.1038/349704a0

Goedert, M., Wischik, C. M., Crowther, R. A., Walker, J. E., & Klug, A. (1988). Cloning and sequencing of the cDNA encoding a core protein of the paired helical filament of Alzheimer disease: Identification as the microtubule-associated protein tau. *Proceedings of the National Academy of Sciences of the United States of America*, *85*(11), 4051–4055. https://doi.org/10.1073/pnas.85.11.4051

Goos, J. D. C., Kester, M. I., Barkhof, F., Klein, M., Blankenstein, M. A., Scheltens, P., & Van Der Flier, W. M. (2009). Patients with alzheimer disease with multiple microbleeds: Relation with cerebrospinal fluid biomarkers and cognition. *Stroke*, *40*(11), 3455–3460. https://doi.org/10.1161/STROKEAHA.109.558197

Gottesman, R. F., Schneider, A. L. C., Zhou, Y., Coresh, J., Green, E., Gupta, N., Knopman, D. S., Mintz, A., Rahmim, A., Sharrett, A. R., Wagenknecht, L. E., Wong, D. F., & Mosley, T. H. (2017). Association between midlife vascular risk factors and estimated brain amyloid deposition. *JAMA - Journal of the American Medical Association*, *317*(14), 1443–1450. https://doi.org/10.1001/jama.2017.3090

Greenberg, S. M., Bacskai, B. J., Hernandez-Guillamon, M., Pruzin, J., Sperling, R., & van Veluw, S. J. (2020). Cerebral amyloid angiopathy and Alzheimer disease — one peptide, two pathways. *Nature Reviews Neurology*, *16*(1), 30–42. https://doi.org/10.1038/s41582-019-0281-2

Grundke-Iqbal, I., Iqbal, K., Quinlan, M., Tung, Y. C., Zaidi, M. S., & Wisniewski, H. M. (1986). Microtubule-associated protein tau. A component of Alzheimer paired helical filaments. *Journal of Biological Chemistry*, *261*(13), 6084–6089. https://doi.org/10.1016/s0021-9258(17)38495-8

Guivernau, B., Bonet, J., Valls-Comamala, V., Bosch-Morató, M., Godoy, J. A., Inestrosa, N. C., Perálvarez-Marín, A., Fernández-Busquets, X., Andreu, D., Oliva, B., & Muñoz, F. J. (2016). Amyloid-β peptide nitrotyrosination stabilizes oligomers and enhances NMDAR-mediated toxicity. *Journal of Neuroscience*, *36*(46), 11693–11703. https://doi.org/10.1523/JNEUROSCI.1081-16.2016

Haass, C., Kaether, C., Thinakaran, G., & Sisodia, S. (2012). Trafficking and proteolytic processing of APP. *Cold Spring Harbor Perspectives in Medicine*, *2*(5), a006270–a006270. https://doi.org/10.1101/cshperspect.a006270

Haass, C., Schlossmacher, M. G., Hung, A. Y., Vigo-Pelfrey, C., Mellon, A., Ostaszewski, B. L., Lieberburg, I., Koo, E. H., Schenk, D., Teplow, D. B., & Selkoe, D. J. (1992). Amyloid β-peptide is produced by cultured cells during normal metabolism. *Nature*, *359*(6393), 322–325. https://doi.org/10.1038/359322a0

Häggqvist, B. O., Näslund, J., Sletten, K., Westermark, G. T., Mucchiano, G., Tjernberg, L. O., Nordstedt, C., Engström, U., & Westermark, P. (1999). Medin: An integral fragment of aortic smooth muscle cell-produced lactadherin forms the most common human amyloid. *Proceedings of the National Academy of Sciences of the United States of America*, *96*(15), 8669–8674. https://doi.org/10.1073/pnas.96.15.8669

Hamaguchi, T., Eisele, Y. S., Varvel, N. H., Lamb, B. T., Walker, L. C., & Jucker, M. (2012). The presence of Aβ seeds, and not age per se, is critical to the initiation of Aβ deposition in the brain. *Acta Neuropathologica*, *123*(1), 31–37. https://doi.org/10.1007/s00401-011-0912-1

Hanayama, R., Tanaka, M., Miwa, K., Shinohara, A., Iwamatsu, A., & Nagata, S. (2002). Identification of a factor that links apoptotic cells to phagocytes. *Nature*, *417*(6885), 182–187. https://doi.org/10.1038/417182a

Harder, D. R., Alkayed, N. J., Lange, A. R., Gebremedhin, D., & Roman, R. J. (1998). Functional hyperemia in the brain: Hypothesis for astrocyte-derived vasodilator metabolites. *Stroke*, *29*(1), 229–234. https://doi.org/10.1161/01.STR.29.1.229

Hardy, J., & Allsop, D. (1991). Amyloid deposition as the central event in the aetiology of Alzheimer's disease. *Trends in Pharmacological Sciences*, *12*(C), 383–388. https://doi.org/10.1016/0165-6147(91)90609-V

Hardy, J., & Higgins, G. A. (1992). Alzheimer's disease: the amyloid cascade hypothesis. *Science (New York, N.Y.)*, *256*(5054), 184–185. http://www.ncbi.nlm.nih.gov/pubmed/1566067

Hardy, J., & Selkoe, D. J. (2002). The amyloid hypothesis of Alzheimer's disease: Progress and problems on the road to therapeutics. *Science*, *297*(5580), 353–356. https://doi.org/10.1126/science.1072994

Hargis, K. E., & Blalock, E. M. (2017). Transcriptional signatures of brain aging and Alzheimer's disease: What are our rodent models telling us? *Behavioural Brain Research*, *322*, 311–328. https://doi.org/10.1016/j.bbr.2016.05.007

Hartl, F. U. (1996). Molecular chaperones in cellular protein folding. *Nature*, *381*(6583), 571–580. https://doi.org/10.1038/381571a0

Hartl, F. U., Bracher, A., & Hayer-Hartl, M. (2011). Molecular chaperones in protein folding and proteostasis. *Nature*, *475*(7356), 324–332. https://doi.org/10.1038/nature10317

Hartl, F. U., & Hayer-Hartl, M. (2009). Converging concepts of protein folding in vitro and in vivo. *Nature Structural and Molecular Biology*, *16*(6), 574–581. https://doi.org/10.1038/nsmb.1591

Heneka, M. T., Carson, M. J., Khoury, J. El, Landreth, G. E., Brosseron, F., Feinstein, D. L., Jacobs, A. H., Wyss-Coray, T., Vitorica, J., Ransohoff, R. M., Herrup, K., Frautschy, S. A., Finsen, B., Brown, G. C., Verkhratsky, A., Yamanaka, K., Koistinaho, J., Latz, E., Halle, A., … Kummer, M. P. (2015). Neuroinflammation in Alzheimer's disease. *The Lancet Neurology*, *14*(4), 388–405. https://doi.org/10.1016/S1474-4422(15)70016-5

Heneka, M. T., & O'Banion, M. K. (2007). Inflammatory processes in Alzheimer's disease. *Journal*

of Neuroimmunology, *184*(1–2), 69–91. https://doi.org/10.1016/j.jneuroim.2006.11.017

Hervé, D., Porché, M., Cabrejo, L., Guidoux, C., Tournier-Lasserve, E., Nicolas, G., Adle-Biassette, H., Plu, I., Chabriat, H., & Duyckaerts, C. (2018). Fatal Aβ cerebral amyloid angiopathy 4 decades after a dural graft at the age of 2 years. In *Acta Neuropathologica* (Vol. 135, Issue 5, pp. 801–803). https://doi.org/10.1007/s00401-018-1828-9

Herzig, M., Winkler, D., & Bürki, K. (2004). Abeta is targeted to the vasculature in a mouse model of hereditary cerebral hemorrhage with amyloidosis. *Nature Neuroscience*, *7*(9), 954–960. https://doi.org/10.5167/uzh-10882

Hipp, M. S., Kasturi, P., & Hartl, F. U. (2019). The proteostasis network and its decline in ageing. *Nature Reviews Molecular Cell Biology*, *20*(7), 421–435. https://doi.org/10.1038/s41580-019-0101-y

Hu, C. Y., Wu, C. S., Tsai, H. F., Chang, S. K., Tsai, W. I., & Hsu, P. N. (2009). Genetic polymorphism in milk fat globule-EGF factor 8 (MFG-E8) is associated with systemic lupus erythematosus in human. *Lupus*, *18*(8), 676–681. https://doi.org/10.1177/0961203309103027

Hu, R., Zhang, M., Chen, H., Jiang, B., & Zheng, J. (2015). Cross-Seeding Interaction between β-Amyloid and Human Islet Amyloid Polypeptide. *ACS Chemical Neuroscience*, *6*(10), 1759–1768. https://doi.org/10.1021/acschemneuro.5b00192

Huang, L.-K., Chao, S.-P., & Hu, C.-J. (2020). Clinical trials of new drugs for Alzheimer disease. *Journal of Biomedical Science*, *27*(1), 18. https://doi.org/10.1186/s12929-019-0609-7

Hutton, M., Lendon, C. L., Rizzu, P., Baker, M., Froelich, S., Houlden, H. H., Pickering-Brown, S., Chakraverty, S., Isaacs, A., Grover, A., Hackett, J., Adamson, J., Lincoln, S., Dickson, D., Davies, P., Petersen, R. C., Stevena, M., De Graaff, E., Wauters, E., … Heutink, P. (1998). Association of missense and 5'-splice-site mutations in tau with the inherited dementia FTDP-17. *Nature*, *393*(6686), 702–704. https://doi.org/10.1038/31508

Iadanza, M. G., Jackson, M. P., Hewitt, E. W., Ranson, N. A., & Radford, S. E. (2018). A new era for understanding amyloid structures and disease. *Nature Reviews Molecular Cell Biology*, *19*(12), 755–773. https://doi.org/10.1038/s41580-018-0060-8

Iadecola, C. (2004). Neurovascular regulation in the normal brain and in Alzheimer's disease. *Nature Reviews Neuroscience*, *5*(5), 347–360. https://doi.org/10.1038/nrn1387

Iadecola, C., & Gottesman, R. F. (2018). Cerebrovascular alterations in Alzheimer disease incidental or pathogenic? *Circulation Research*, *123*(4), 406–408. https://doi.org/10.1161/CIRCRESAHA.118.313400

Ignarro, L. J., Byrns, R. E., Buga, G. M., & Wood, K. S. (1987). Endothelium-derived relaxing factor from pulmonary artery and vein possesses pharmacologic and chemical properties identical to those of nitric oxide radical. *Circulation Research*, *61*(6), 866–879. https://doi.org/10.1161/01.RES.61.6.866

Ishii, T., & Asuwa, N. (2000). Collagen and elastin degradation by matrix metalloproteinases and tissue inhibitors of matrix metalloproteinase in aortic dissection. *Human Pathology*, *31*(6), 640–646. https://doi.org/10.1053/hupa.2000.7642

Itagaki, S., McGeer, P. L., Akiyama, H., Zhu, S., & Selkoe, D. (1989). Relationship of microglia and astrocytes to amyloid deposits of Alzheimer disease. *Journal of Neuroimmunology*, *24*(3), 173–182. https://doi.org/10.1016/0165-5728(89)90115-X

Ittner, L. M., Ke, Y. D., Delerue, F., Bi, M., Gladbach, A., van Eersel, J., Wölfing, H., Chieng, B. C., Christie, M. J., Napier, I. A., Eckert, A., Staufenbiel, M., Hardeman, E., & Götz, J. (2010). Dendritic function of tau mediates amyloid-β toxicity in alzheimer's disease mouse models.

Cell, *142*(3), 387–397. https://doi.org/10.1016/j.cell.2010.06.036

Iturria-Medina, Y., & Evans, A. C. (2015). On the central role of brain connectivity in neurodegenerative disease progression. *Frontiers in Aging Neuroscience*, *7*(MAY), 90. https://doi.org/10.3389/fnagi.2015.00090

Iturria-Medina, Y., Sotero, R. C., Toussaint, P. J., Mateos-Pérez, J. M., Evans, A. C., Weiner, M. W., Aisen, P., Petersen, R., Jack, C. R., Jagust, W., Trojanowki, J. Q., Toga, A. W., Beckett, L., Green, R. C., Saykin, A. J., Morris, J., Shaw, L. M., Khachaturian, Z., Sorensen, G., … Furst, A. J. (2016). Early role of vascular dysregulation on late-onset Alzheimer's disease based on multifactorial data-driven analysis. *Nature Communications*, *7*(1), 11934. https://doi.org/10.1038/ncomms11934

Jackson, K., Barisone, G. A., Diaz, E., Jin, L. W., DeCarli, C., & Despa, F. (2013). Amylin deposition in the brain: A second amyloid in Alzheimer disease? *Annals of Neurology*, *74*(4), 517–526. https://doi.org/10.1002/ana.23956

Jahn, T. R., & Radford, S. E. (2005). The Yin and Yang of protein folding. *FEBS Journal*, *272*(23), 5962–5970. https://doi.org/10.1111/j.1742-4658.2005.05021.x

Jakob, W. (1971). Spontaneous amyloidosis of mammals. *Veterinary Pathology*, *8*(4), 292–306. https://doi.org/10.1177/030098587100800402

Jansen, I. E., Savage, J. E., Watanabe, K., Bryois, J., Williams, D. M., Steinberg, S., Sealock, J., Karlsson, I. K., Hägg, S., Athanasiu, L., Voyle, N., Proitsi, P., Witoelar, A., Stringer, S., Aarsland, D., Almdahl, I. S., Andersen, F., Bergh, S., Bettella, F., … Posthuma, D. (2019). Genome-wide meta-analysis identifies new loci and functional pathways influencing Alzheimer's disease risk. *Nature Genetics*, *51*(3), 404–413. https://doi.org/10.1038/s41588-018-0311-9

Jarrett, J. T., & Lansbury, P. T. (1992). Amyloid Fibril Formation Requires a Chemically Discriminating Nucleation Event: Studies of an Amyloidogenic Sequence from the Bacterial Protein OsmB. *Biochemistry*, *31*(49), 12345–12352. https://doi.org/10.1021/bi00164a008

Jarrett, J. T., & Lansbury, P. T. (1993). Seeding "one-dimensional crystallization" of amyloid: A pathogenic mechanism in Alzheimer's disease and scrapie? *Cell*, *73*(6), 1055–1058. https://doi.org/10.1016/0092-8674(93)90635-4

Jaunmuktane, Z., Mead, S., Ellis, M., Wadsworth, J. D. F., Nicoll, A. J., Kenny, J., Launchbury, F., Linehan, J., Richard-Loendt, A., Walker, A. S., Rudge, P., Collinge, J., & Brandner, S. (2015). Evidence for human transmission of amyloid-β pathology and cerebral amyloid angiopathy. *Nature*, *525*(7568), 247–250. https://doi.org/10.1038/nature15369

Jaunmuktane, Z., Quaegebeur, A., Taipa, R., Viana-Baptista, M., Barbosa, R., Koriath, C., Sciot, R., Mead, S., & Brandner, S. (2018). Evidence of amyloid-β cerebral amyloid angiopathy transmission through neurosurgery. *Acta Neuropathologica*, *135*(5), 671–679. https://doi.org/10.1007/s00401-018-1822-2

Jin, M., Shepardson, N., Yang, T., Chen, G., Walsh, D., & Selkoe, D. J. (2011). Soluble amyloid β-protein dimers isolated from Alzheimer cortex directly induce Tau hyperphosphorylation and neuritic degeneration. *Proceedings of the National Academy of Sciences of the United States of America*, *108*(14), 5819–5824. https://doi.org/10.1073/pnas.1017033108

Johan, K., Westermark, G., Engström, U., Gustavsson, Å., Hultman, P., & Westermark, P. (1998). Acceleration of amyloid protein A amyloidosis by amyloid-like synthetic fibrils. *Proceedings of the National Academy of Sciences of the United States of America*, *95*(5), 2558–2563. https://doi.org/10.1073/pnas.95.5.2558

Jonsson, T., Atwal, J. K., Steinberg, S., Snaedal, J., Jonsson, P. V., Bjornsson, S., Stefansson, H.,

Sulem, P., Gudbjartsson, D., Maloney, J., Hoyte, K., Gustafson, A., Liu, Y., Lu, Y., Bhangale, T., Graham, R. R., Huttenlocher, J., Bjornsdottir, G., Andreassen, O. A., … Stefansson, K. (2012). A mutation in APP protects against Alzheimer's disease and age-related cognitive decline. *Nature*, *488*(7409), 96. https://doi.org/10.1038/nature11283

Josephs, K. A., Murray, M. E., Whitwell, J. L., Tosakulwong, N., Weigand, S. D., Petrucelli, L., Liesinger, A. M., Petersen, R. C., Parisi, J. E., & Dickson, D. W. (2016). Updated TDP-43 in Alzheimer's disease staging scheme. *Acta Neuropathologica*, *131*(4), 571–585. https://doi.org/10.1007/s00401-016-1537-1

Jucker, M., & Walker, L. C. (2013). Self-propagation of pathogenic protein aggregates in neurodegenerative diseases. *Nature*, *501*(7465), 45–51. https://doi.org/10.1038/nature12481

Jucker, M., & Walker, L. C. (2018). Propagation and spread of pathogenic protein assemblies in neurodegenerative diseases. *Nature Neuroscience*, *21*(10), 1341–1349. https://doi.org/10.1038/s41593-018-0238-6

Kane, M. D., Lipinski, W. J., Callahan, M. J., Bian, F., Durham, R. A., Schwarz, R. D., Roher, A. E., & Walker, L. C. (2000). Evidence for seeding of β-amyloid by intracerebral infusion of Alzheimer brain extracts in β-amyloid precursor protein-transgenic mice. *Journal of Neuroscience*, *20*(10), 3606–3611. https://doi.org/10.1523/jneurosci.20-10-03606.2000

Kanekiyo, T., Xu, H., & Bu, G. (2014). ApoE and Aβ in Alzheimer's disease: Accidental encounters or partners? *Neuron*, *81*(4), 740–754. https://doi.org/10.1016/j.neuron.2014.01.045

Kang, H. M., Sohn, I., Jung, J., Jeong, J. W., & Park, C. (2016). Age-related changes in pial arterial structure and blood flow in mice. *Neurobiology of Aging*, *37*, 161–170. https://doi.org/10.1016/j.neurobiolaging.2015.09.008

Kang, J., Lemaire, H. G., Unterbeck, A., Salbaum, J. M., Masters, C. L., Grzeschik, K. H., Multhaup, G., Beyreuther, K., & Müller-Hill, B. (1987). The precursor of Alzheimer's disease amyloid A4 protein resembles a cell-surface receptor. *Nature*, *325*(6106), 733–736. https://doi.org/10.1038/325733a0

Karamanos, T. K., Kalverda, A. P., Thompson, G. S., & Radford, S. E. (2015). Mechanisms of amyloid formation revealed by solution NMR. *Progress in Nuclear Magnetic Resonance Spectroscopy*, *88–89*, 86–104. https://doi.org/10.1016/j.pnmrs.2015.05.002

Karamanova, N., Truran, S., Serrano, G. E., Beach, T. G., Madine, J., Weissig, V., Davies, H. A., Veldhuizen, J., Nikkhah, M., Hansen, M., Zhang, W., D'Souza, K., Franco, D. A., & Migrino, R. Q. (2020). Endothelial Immune Activation by Medin: Potential Role in Cerebrovascular Disease and Reversal by Monosialoganglioside-Containing Nanoliposomes. *Journal of the American Heart Association*, *9*(2), e014810. https://doi.org/10.1161/JAHA.119.014810

Katsuki, S., Arnold, W., Mittal, C., & Murad, F. (1977). Stimulation of guanylate cyclase by sodium nitroprusside, nitroglycerin and nitric oxide in various tissue preparations and comparison to the effects of sodium azide and hydroxylamine. *Journal of Cyclic Nucleotide Research*, *3*(1), 23–35.

Katzmarski, N., Ziegler-Waldkirch, S., Scheffler, N., Witt, C., Abou-Ajram, C., Nuscher, B., Prinz, M., Haass, C., & Meyer-Luehmann, M. (2020). Aβ oligomers trigger and accelerate Aβ seeding. *Brain Pathology*, *30*(1), 36–45. https://doi.org/10.1111/bpa.12734

Kawas, C., Gray, S., Brookmeyer, R., Fozard, J., & Zonderman, A. (2000). Age-specific incidence rates of Alzheimer's disease: The Baltimore longitudinal study of aging. *Neurology*, *54*(11), 2072–2077. https://doi.org/10.1212/WNL.54.11.2072

Kayed, R., Head, E., Thompson, J. L., McIntire, T. M., Milton, S. C., Cotman, C. W., & Glabel, C. G.

(2003). Common structure of soluble amyloid oligomers implies common mechanism of pathogenesis. *Science*, *300*(5618), 486–489. https://doi.org/10.1126/science.1079469

Keage, H. A. D., Carare, R. O., Friedland, R. P., Ince, P. G., Love, S., Nicoll, J. A., Wharton, S. B., Weller, R. O., & Brayne, C. (2009). Population studies of sporadic cerebral amyloid angiopathy and dementia: A systematic review. *BMC Neurology*, *9*, 3. https://doi.org/10.1186/1471-2377-9-3

Kero, M., Paetau, A., Polvikoski, T., Tanskanen, M., Sulkava, R., Jansson, L., Myllykangas, L., & Tienari, P. J. (2013). Amyloid precursor protein (APP) A673T mutation in the elderly Finnish population. *Neurobiology of Aging*, *34*(5), 1518.e1-1518.e3. https://doi.org/10.1016/j.neurobiolaging.2012.09.017

Kim, S. H., Ahn, J. H., Yang, H., Lee, P., Koh, G. Y., & Jeong, Y. (2020). Cerebral amyloid angiopathy aggravates perivascular clearance impairment in an Alzheimer's disease mouse model. *Acta Neuropathologica Communications*, *8*(1), 181. https://doi.org/10.1186/s40478-020-01042-0

Kim, S. H., Liu, L., Ni, L., Zhang, L., Zhang, J., Wang, Y., McGraw, K. R., Monticone, R., Telljohann, R., Lakatta, E. G., & Wang, M. (2020). MFG-E8 Signaling Promotes Elastolysis and Calcification in the Aging Aortic Wall. *BioRxiv*, 2020.10.05.326728. https://doi.org/10.1101/2020.10.05.326728

Kimbrough, I. F., Robel, S., Roberson, E. D., & Sontheimer, H. (2015). Vascular amyloidosis impairs the gliovascular unit in a mouse model of Alzheimer's disease. *Brain*, *138*(12), 3716–3733. https://doi.org/10.1093/brain/awv327

Kisler, K., Nelson, A. R., Montagne, A., & Zlokovic, B. V. (2017). Cerebral blood flow regulation and neurovascular dysfunction in Alzheimer disease. *Nature Reviews Neuroscience*, *18*(7), 419–434. https://doi.org/10.1038/nrn.2017.48

Klingstedt, T., Åslund, A., Simon, R. A., Johansson, L. B. G., Mason, J. J., Nyström, S., Hammarström, P., & Nilsson, K. P. R. (2011). Synthesis of a library of oligothiophenes and their utilization as fluorescent ligands for spectral assignment of protein aggregates. *Organic and Biomolecular Chemistry*, *9*(24), 8356–8370. https://doi.org/10.1039/c1ob05637a

Klingstedt, T., Ghetti, B., Holton, J. L., Ling, H., Nilsson, K. P. R., & Goedert, M. (2019). Luminescent conjugated oligothiophenes distinguish between α-synuclein assemblies of Parkinson's disease and multiple system atrophy. *Acta Neuropathologica Communications*, *7*(1), 193. https://doi.org/10.1186/s40478-019-0840-1

Klunk, W. E., Engler, H., Nordberg, A., Wang, Y., Blomqvist, G., Holt, D. P., Bergström, M., Savitcheva, I., Huang, G. F., Estrada, S., Ausén, B., Debnath, M. L., Barletta, J., Price, J. C., Sandell, J., Lopresti, B. J., Wall, A., Koivisto, P., Antoni, G., … Långström, B. (2004). Imaging Brain Amyloid in Alzheimer's Disease with Pittsburgh Compound-B. *Annals of Neurology*, *55*(3), 306–319. https://doi.org/10.1002/ana.20009

Knight, J. D., Hebda, J. A., & Miranker, A. D. (2006). Conserved and cooperative assembly of membrane-bound α-helical states of islet amyloid polypeptide. *Biochemistry*, *45*(31), 9496–9508. https://doi.org/10.1021/bi060579z

Knopman, D. S., Jones, D. T., & Greicius, M. D. (2020). Failure to demonstrate efficacy of aducanumab: An analysis of the EMERGE and ENGAGE trials as reported by Biogen, December 2019. *Alzheimer's and Dementia*, *n/a*(n/a). https://doi.org/10.1002/alz.12213

Knowles, T. P. J., & Mezzenga, R. (2016). Amyloid fibrils as building blocks for natural and artificial functional materials. *Advanced Materials*, *28*(31), 6546–6561. https://doi.org/10.1002/adma.201505961

Knowles, T. P. J., Vendruscolo, M., & Dobson, C. M. (2014). The amyloid state and its association with protein misfolding diseases. *Nature Reviews Molecular Cell Biology*, *15*(6), 384–396. https://doi.org/10.1038/nrm3810

Kokjohn, T. A., Van Vickle, G. D., Maarouf, C. L., Kalback, W. M., Hunter, J. M., Daugs, I. D., Luehrs, D. C., Lopez, J., Brune, D., Sue, L. I., Beach, T. G., Castaño, E. M., & Roher, A. E. (2011). Chemical characterization of pro-inflammatory amyloid-beta peptides in human atherosclerotic lesions and platelets. *Biochimica et Biophysica Acta - Molecular Basis of Disease*, *1812*(11), 1508–1514. https://doi.org/10.1016/j.bbadis.2011.07.004

Kopf, D., & Frölich, L. (2009). Risk of incident Alzheimer's disease in diabetic patients: a systematic review of prospective trials. *Journal of Alzheimer's Disease : JAD*, *16*(4), 677–685. https://doi.org/10.3233/JAD-2009-1011

Köppen, J., Schulze, A., Machner, L., Wermann, M., Eichentopf, R., Guthardt, M., Hähnel, A., Klehm, J., Kriegeskorte, M. C., Hartlage-Rübsamen, M., Morawski, M., von Hörsten, S., Demuth, H. U., Roßner, S., & Schilling, S. (2020). Amyloid-beta peptides trigger aggregation of alpha-synuclein in vitro. *Molecules*, *25*(3), 580. https://doi.org/10.3390/molecules25030580

Korte, N., Nortley, R., & Attwell, D. (2020). Cerebral blood flow decrease as an early pathological mechanism in Alzheimer's disease. *Acta Neuropathologica*, *140*(6), 793–810. https://doi.org/10.1007/s00401-020-02215-w

Kranich, J., Krautler, N. J., Falsig, J., Ballmer, B., Li, S., Hutter, G., Schwarz, P., Moos, R., Julius, C., Miele, G., & Aguzzi, A. (2010). Engulfment of cerebral apoptotic bodies controls the course of prion disease in a mouse strain-dependent manner. *Journal of Experimental Medicine*, *207*(10), 2271–2281. https://doi.org/10.1084/jem.20092401

Krebs, M. R. H., Morozova-Roche, L. A., Daniel, K., Robinson, C. V., & Dobson, C. M. (2004). Observation of sequence specificity in the seeding of protein amyloid fibrils. *Protein Science*, *13*(7), 1933–1938. https://doi.org/10.1110/ps.04707004

Labbadia, J., & Morimoto, R. I. (2015). The biology of proteostasis in aging and disease. *Annual Review of Biochemistry*, *84*, 435–464. https://doi.org/10.1146/annurev-biochem-060614-033955

Langer, F., Eisele, Y. S., Fritschi, S. K., Staufenbiel, M., Walker, L. C., & Jucker, M. (2011). Soluble aβ seeds are potent inducers of cerebral β-amyloid deposition. *Journal of Neuroscience*, *31*(41), 14488–14495. https://doi.org/10.1523/JNEUROSCI.3088-11.2011

Larsson, A., Malmström, S., & Westermark, P. (2011). Signs of cross-seeding: Aortic medin amyloid as a trigger for protein AA deposition. *Amyloid*, *18*(4), 229–234. https://doi.org/10.3109/13506129.2011.630761

Larsson, A., Peng, S., Persson, H., Rosenbloom, J., Abrams, W. R., Wassberg, E., Thelin, S., Sletten, K., Gerwins, P., & Westermark, P. (2006). Lactadherin binds to elastin - A starting point for medin amyloid formation? *Amyloid*, *13*(2), 78–85. https://doi.org/10.1080/13506120600722530

Larsson, A., Söderberg, L., Westermark, G. T., Sletten, K., Engström, U., Tjernberg, L. O., Näslund, J., & Westermark, P. (2007). Unwinding fibril formation of medin, the peptide of the most common form of human amyloid. *Biochemical and Biophysical Research Communications*, *361*(4), 822–828. https://doi.org/10.1016/j.bbrc.2007.06.187

Laurent, S., Boutouyrie, P., Asmar, R., Gautier, I., Laloux, B., Guize, L., Ducimetiere, P., & Benetos, A. (2001). Aortic stiffness is an independent predictor of all-cause and cardiovascular mortality in hypertensive patients. *Hypertension*, *37*(5), 1236–1241.

https://doi.org/10.1161/01.HYP.37.5.1236

Lauwers, E., Lalli, G., Brandner, S., Collinge, J., Compernolle, V., Duyckaerts, C., Edgren, G., Haïk, S., Hardy, J., Helmy, A., Ivinson, A. J., Jaunmuktane, Z., Jucker, M., Knight, R., Lemmens, R., Lin, I.-C. C., Love, S., Mead, S., Perry, V. H., … De Strooper, B. (2020). Potential human transmission of amyloid β pathology: surveillance and risks. *The Lancet Neurology*, *19*(10), 872–878. https://doi.org/10.1016/S1474-4422(20)30238-6

Lendahl, U., Nilsson, P., & Betsholtz, C. (2019). Emerging links between cerebrovascular and neurodegenerative diseases—a special role for pericytes. *EMBO Reports*, *20*(11), e48070. https://doi.org/https://doi.org/10.15252/embr.201948070

LeVine, H. (1993). Thioflavine T interaction with synthetic Alzheimer's disease β-amyloid peptides: Detection of amyloid aggregation in solution. *Protein Science*, *2*(3), 404–410. https://doi.org/10.1002/pro.5560020312

Lewis, J., Dickson, D. W., Lin, W. L., Chisholm, L., Corral, A., Jones, G., Yen, S. H., Sahara, N., Skipper, L., Yager, D., Eckman, C., Hardy, J., Hutton, M., & McGowan, E. (2001). Enhanced neurofibrillary degeneration in transgenic mice expressing mutant tau and APP. *Science*, *293*(5534), 1487–1491. https://doi.org/10.1126/science.1058189

Li, B. Z., Zhang, H. Y., Pan, H. F., & Ye, D. Q. (2013). Identification of MFG-E8 as a novel therapeutic target for diseases. *Expert Opinion on Therapeutic Targets*, *17*(11), 1275–1285. https://doi.org/10.1517/14728222.2013.829455

Li, C., & Götz, J. (2017). Somatodendritic accumulation of Tau in Alzheimer's disease is promoted by Fyn-mediated local protein translation. *The EMBO Journal*, *36*(21), 3120–3138. https://doi.org/10.15252/embj.201797724

Li, E., Noda, M., Doi, Y., Parajuli, B., Kawanokuchi, J., Sonobe, Y., Takeuchi, H., Mizuno, T., & Suzumura, A. (2012). The neuroprotective effects of milk fat globule-EGF factor 8 against oligomeric amyloid β toxicity. *Journal of Neuroinflammation*, *9*(1), 148. https://doi.org/10.1186/1742-2094-9-148

Li, X., Zhang, X., Ladiwala, A. R. A., Du, D., Yadav, J. K., Tessier, P. M., Wright, P. E., Kelly, J. W., & Buxbaum, J. N. (2013). Mechanisms of transthyretin inhibition of β-amyloid aggregation in vitro. *Journal of Neuroscience*, *33*(50), 19423–19433. https://doi.org/10.1523/JNEUROSCI.2561-13.2013

Li, Z. W., Stark, G., Götz, J., Rülicke, T., Müller, U., & Weissmann, C. (1996). Generation of mice with a 200-kb amyloid precursor protein gene deletion by Cre recombinase-mediated site-specific recombination in embryonic stem cells. *Proceedings of the National Academy of Sciences of the United States of America*, *93*(12), 6158–6162. https://doi.org/10.1073/pnas.93.12.6158

Libon, D. J., Price, C. C., Heilman, K. M., & Grossman, M. (2006). Alzheimer's "Other Dementia." *Cognitive and Behavioral Neurology*, *19*(2). https://journals.lww.com/cogbehavneurol/Fulltext/2006/06000/Alzheimer_s__Other_Dementia_.8.aspx

Liesz, A. (2019). The vascular side of Alzheimer's disease. *Science*, *365*(6450), 223–224. https://doi.org/10.1126/science.aay2720

Lindberg, D. J., Wranne, M. S., Gilbert Gatty, M., Westerlund, F., & Esbjörner, E. K. (2015). Steady-state and time-resolved Thioflavin-T fluorescence can report on morphological differences in amyloid fibrils formed by Aβ(1-40) and Aβ(1-42). *Biochemical and Biophysical Research Communications*, *458*(2), 418–423. https://doi.org/10.1016/j.bbrc.2015.01.132

Liu, P. P., Xie, Y., Meng, X. Y., & Kang, J. S. (2019). History and progress of hypotheses and clinical

trials for alzheimer's disease. *Signal Transduction and Targeted Therapy*, *4*(1), 29. https://doi.org/10.1038/s41392-019-0063-8

Livingston, G., Huntley, J., Sommerlad, A., Ames, D., Ballard, C., Banerjee, S., Brayne, C., Burns, A., Cohen-Mansfield, J., Cooper, C., Costafreda, S. G., Dias, A., Fox, N., Gitlin, L. N., Howard, R., Kales, H. C., Kivimäki, M., Larson, E. B., Ogunniyi, A., … Mukadam, N. (2020). Dementia prevention, intervention, and care: 2020 report of the Lancet Commission. *The Lancet*, *396*(10248), 413–446. https://doi.org/10.1016/S0140-6736(20)30367-6

Lu, J. X., Qiang, W., Yau, W. M., Schwieters, C. D., Meredith, S. C., & Tycko, R. (2013). XMolecular structure of β-amyloid fibrils in alzheimer's disease brain tissue. *Cell*, *154*(6), 1257. https://doi.org/10.1016/j.cell.2013.08.035

Luo, J., Wärmländer, S. K. T. S., Gräslund, A., & Abrahams, J. P. (2016). Cross-interactions between the Alzheimer disease amyloid-β peptide and other amyloid proteins: A further aspect of the amyloid cascade hypothesis. *Journal of Biological Chemistry*, *291*(32), 16485–16493. https://doi.org/10.1074/jbc.R116.714576

Ly, H., Verma, N., Sharma, S., Kotiya, D., Despa, S., Abner, E. L., Nelson, P. T., Jicha, G. A., Wilcock, D. M., Goldstein, L. B., Guerreiro, R., Craft, S., Murray, A. J., Zetterberg, H., Despa, F., Brás, J., Hanson, A. J., Biessels, G. J., & Troakes, C. (2021). *The association of circulating amylin with β -amyloid in familial Alzheimer ' s disease*. *September 2020*, 1–11. https://doi.org/10.1002/trc2.12130

Ma, B., & Nussinov, R. (2012). Selective molecular recognition in amyloid growth and transmission and cross-species barriers. *Journal of Molecular Biology*, *421*(2–3), 172–184. https://doi.org/10.1016/j.jmb.2011.11.023

Madine, J., & Middleton, D. A. (2010). Comparison of aggregation enhancement and inhibition as strategies for reducing the cytotoxicity of the aortic amyloid polypeptide medin. *European Biophysics Journal*, *39*(9), 1281–1288. https://doi.org/10.1007/s00249-010-0581-3

Maier, F. C., Wehrl, H. F., Schmid, A. M., Mannheim, J. G., Wiehr, S., Lerdkrai, C., Calaminus, C., Stahlschmidt, A., Ye, L., Burnet, M., Stiller, D., Sabri, O., Reischl, G., Staufenbiel, M., Garaschuk, O., Jucker, M., & Pichler, B. J. (2014). Longitudinal PET-MRI reveals β 2-amyloid deposition and rCBF dynamics and connects vascular amyloidosis to quantitative loss of perfusion. *Nature Medicine*, *20*(12), 1485–1492. https://doi.org/10.1038/nm.3734

Maiti, P., Hall, T. C., Paladugu, L., Kolli, N., Learman, C., Rossignol, J., & Dunbar, G. L. (2016). A comparative study of dietary curcumin, nanocurcumin, and other classical amyloid-binding dyes for labeling and imaging of amyloid plaques in brain tissue of 5×-familial Alzheimer's disease mice. *Histochemistry and Cell Biology*, *146*(5), 609–625. https://doi.org/10.1007/s00418-016-1464-1

Makin, O. S., & Serpell, L. C. (2005). Structures for amyloid fibrils. *FEBS Journal*, *272*(23), 5950–5961. https://doi.org/10.1111/j.1742-4658.2005.05025.x

Marzesco, A. M., Flötenmeyer, M., Bühler, A., Obermüller, U., Staufenbiel, M., Jucker, M., & Baumann, F. (2016). Highly potent intracellular membrane-associated Aβ seeds. *Scientific Reports*, *6*(1), 28125. https://doi.org/10.1038/srep28125

Masters, C. L., Bateman, R., Blennow, K., Rowe, C. C., Sperling, R. A., & Cummings, J. L. (2015). Alzheimer's disease. *Nature Reviews Disease Primers*, *1*(1), 15056. https://doi.org/10.1038/nrdp.2015.56

Masters, C. L., Simms, G., Weinman, N. A., Multhaup, G., McDonald, B. L., & Beyreuther, K. (1985). Amyloid plaque core protein in Alzheimer disease and Down syndrome. *Proceedings of the National Academy of Sciences of the United States of America*, *82*(12), 4245–4249.

https://doi.org/10.1073/pnas.82.12.4245

Masuda-Suzukake, M., Nonaka, T., Hosokawa, M., Oikawa, T., Arai, T., Akiyama, H., Mann, D. M. A., & Hasegawa, M. (2013). Prion-like spreading of pathological α-synuclein in brain. *Brain*, *136*(4), 1128–1138. https://doi.org/10.1093/brain/awt037

Mattsson, N., Schott, J. M., Hardy, J., Turner, M. R., & Zetterberg, H. (2016). Selective vulnerability in neurodegeneration: Insights from clinical variants of Alzheimer's disease. *Journal of Neurology, Neurosurgery and Psychiatry*, *87*(9), 1000–1004. https://doi.org/10.1136/jnnp-2015-311321

McAllister, B. B., Lacoursiere, S. G., Sutherland, R. J., & Mohajerani, M. H. (2020). Intracerebral seeding of amyloid-β and tau pathology in mice: Factors underlying prion-like spreading and comparisons with α-synuclein. *Neuroscience and Biobehavioral Reviews*, *112*, 1–27. https://doi.org/10.1016/j.neubiorev.2020.01.026

McKhann, G. M., Knopman, D. S., Chertkow, H., Hyman, B. T., Jack, C. R., Kawas, C. H., Klunk, W. E., Koroshetz, W. J., Manly, J. J., Mayeux, R., Mohs, R. C., Morris, J. C., Rossor, M. N., Scheltens, P., Carrillo, M. C., Thies, B., Weintraub, S., & Phelps, C. H. (2011). The diagnosis of dementia due to Alzheimer's disease: Recommendations from the National Institute on Aging-Alzheimer's Association workgroups on diagnostic guidelines for Alzheimer's disease. *Alzheimer's and Dementia*, *7*(3), 263–269. https://doi.org/10.1016/j.jalz.2011.03.005

Meyer-Luehmann, M., Coomaraswamy, J., Bolmont, T., Kaeser, S., Schaefer, C., Kilger, E., Neuenschwander, A., Abramowski, D., Frey, P., Jaton, A. L., Vigouret, J. M., Paganetti, P., Walsh, D. M., Mathews, P. M., Ghiso, J., Staufenbiel, M., Walker, L. C., & Jucker, M. (2006). Exogenous induction of cerebral β-amyloidogenesis is governed bf agent and host. *Science*, *313*(5794), 1781–1784. https://doi.org/10.1126/science.1131864

Michaels, T. C. T., Šarić, A., Habchi, J., Chia, S., Meisl, G., Vendruscolo, M., Dobson, C. M., & Knowles, T. P. J. (2018). Chemical Kinetics for Bridging Molecular Mechanisms and Macroscopic Measurements of Amyloid Fibril Formation. *Annual Review of Physical Chemistry*, *69*, 273–298. https://doi.org/10.1146/annurev-physchem-050317-021322

Migrino, R. Q., Davies, H. A., Truran, S., Karamanova, N., Franco, D. A., Beach, T. G., Serrano, G. E., Truong, D., Nikkhah, M., & Madine, J. (2017). Amyloidogenic medin induces endothelial dysfunction and vascular inflammation through the receptor for advanced glycation endproducts. *Cardiovascular Research*, *113*(11), 1389–1402. https://doi.org/10.1093/cvr/cvx135

Migrino, R. Q., Karamanova, N., Truran, S., Serrano, G. E., Davies, H. A., Madine, J., & Beach, T. G. (2020). Cerebrovascular medin is associated with Alzheimer's disease and vascular dementia. *Alzheimer's & Dementia: Diagnosis, Assessment & Disease Monitoring*, *12*(1), 1–10. https://doi.org/10.1002/dad2.12072

Migrino, R. Q., Truran, S., Karamanova, N., Serrano, G. E., Madrigal, C., Davies, H. A., Madine, J., Reaven, P., & Beach, T. G. (2018). Human cerebral collateral arteriole function in subjects with normal cognition, mild cognitive impairment, and dementia. *American Journal of Physiology - Heart and Circulatory Physiology*, *315*(2), H284–H290. https://doi.org/10.1152/ajpheart.00206.2018

Miura, Y., Tsumoto, H., Iwamoto, M., Yamaguchi, Y., Ko, P., Soejima, Y., Yoshida, S., Toda, T., Arai, T., Hamamatsu, A., Endo, T., & Sawabe, M. (2019). Age-associated proteomic alterations in human aortic media. *Geriatrics and Gerontology International*, *19*(10), 1054–1062. https://doi.org/10.1111/ggi.13757

Morales, R., Duran-Aniotz, C., Castilla, J., Estrada, L. D., & Soto, C. (2012). De novo induction of

amyloid-β deposition in vivo. *Molecular Psychiatry*, *17*(12), 1347–1353. https://doi.org/10.1038/mp.2011.120

Morales, R., Estrada, L. D., Diaz-Espinoza, R., Morales-Scheihing, D., Jara, M. C., Castilla, J., & Soto, C. (2010). Molecular cross talk between misfolded proteins in animal models of alzheimer's and prion diseases. *Journal of Neuroscience*, *30*(13), 4528–4535. https://doi.org/10.1523/JNEUROSCI.5924-09.2010

Morales, R., Moreno-Gonzalez, I., & Soto, C. (2013). Cross-seeding of misfolded proteins: implications for etiology and pathogenesis of protein misfolding diseases. *PLoS Pathogens*, *9*(9), e1003537–e1003537. https://doi.org/10.1371/journal.ppat.1003537

Moreno-Gonzalez, I., Edwards, G., Salvadores, N., Shahnawaz, M., Diaz-Espinoza, R., & Soto, C. (2017). Molecular interaction between type 2 diabetes and Alzheimer's disease through cross-seeding of protein misfolding. *Molecular Psychiatry*, *22*(9), 1327–1334. https://doi.org/10.1038/mp.2016.230

Moulin, S., Labreuche, J., Bombois, S., Rossi, C., Boulouis, G., Hénon, H., Duhamel, A., Leys, D., & Cordonnier, C. (2016). Dementia risk after spontaneous intracerebral haemorrhage: A prospective cohort study. *The Lancet Neurology*, *15*(8), 820–829. https://doi.org/10.1016/S1474-4422(16)00130-7

Mucchiano, G. I., Cornwell, G. G., & Westermark, P. (1992). Senile aortic amyloid: Evidence for two distinct forms of localized deposits. *American Journal of Pathology*, *140*(4), 871–877.

Mucchiano, G. I., Häggqvist, B., Sletten, K., & Westermark, P. (2001). Apoplipoprotein A-I-derived amyloid in atherosclerotic plaques of the human aorta. *Journal of Pathology*, *193*(2), 270–275. https://doi.org/10.1002/1096-9896(2000)9999:9999<::AID-PATH753>3.0.CO;2-S

Muckle, T. J. (1988). Giant cell inflammation compared with amyloidosis of the internal elastic lamina in temporal arteries. *Arthritis & Rheumatism*, *31*(9), 1186–1189. https://doi.org/10.1002/art.1780310916

Mullan, M. (1992). Familial Alzheimer's disease: Second gene locus located. *British Medical Journal*, *305*(6862), 1108–1109. https://doi.org/10.1136/bmj.305.6862.1108

Müller, U. C., Deller, T., & Korte, M. (2017). Not just amyloid: Physiological functions of the amyloid precursor protein family. *Nature Reviews Neuroscience*, *18*(5), 281–298. https://doi.org/10.1038/nrn.2017.29

Naiki, H., Higuchi, K., Hosokawa, M., & Takeda, T. (1989). Fluorometric determination of amyloid fibrils in vitro using the fluorescent dye, thioflavine T. *Analytical Biochemistry*, *177*(2), 244–249. https://doi.org/10.1016/0003-2697(89)90046-8

Nelson, P. T., Alafuzoff, I., Bigio, E. H., Bouras, C., Braak, H., Cairns, N. J., Castellani, R. J., Crain, B. J., Davies, P., Tredici, K. Del, Duyckaerts, C., Frosch, M. P., Haroutunian, V., Hof, P. R., Hulette, C. M., Hyman, B. T., Iwatsubo, T., Jellinger, K. A., Jicha, G. A., … Beach, T. G. (2012). Correlation of alzheimer disease neuropathologic changes with cognitive status: A review of the literature. *Journal of Neuropathology and Experimental Neurology*, *71*(5), 362–381. https://doi.org/10.1097/NEN.0b013e31825018f7

Nelson, R., Sawaya, M. R., Balbirnie, M., Madsen, A., Riekel, C., Grothe, R., & Eisenberg, D. (2005). Structure of the cross-β spine of amyloid-like fibrils. *Nature*, *435*(7043), 773–778. https://doi.org/10.1038/nature03680

Nerelius, C., Gustafsson, M., Nordling, K., Larsson, A., & Johansson, J. (2009). Anti-amyloid activity of the C-terminal domain of proSP-C against amyloid β-peptide and medin. *Biochemistry*, *48*(17), 3778–3786. https://doi.org/10.1021/bi900135c

Nicholson, C. J., Seta, F., Lee, S., & Morgan, K. G. (2017). MicroRNA-203 mimics age-related aortic smooth muscle dysfunction of cytoskeletal pathways. *Journal of Cellular and Molecular Medicine*, *21*(1), 81–95. https://doi.org/10.1111/jcmm.12940

Nikpay, M., Goel, A., Won, H. H., Hall, L. M., Willenborg, C., Kanoni, S., Saleheen, D., Kyriakou, T., Nelson, C. P., CHopewell, J., Webb, T. R., Zeng, L., Dehghan, A., Alver, M., MArmasu, S., Auro, K., Bjonnes, A., Chasman, D. I., Chen, S., … Farrall, M. (2015). A comprehensive 1000 Genomes-based genome-wide association meta-analysis of coronary artery disease. *Nature Genetics*, *47*(10), 1121–1130. https://doi.org/10.1038/ng.3396

Nortley, R., Korte, N., Izquierdo, P., Hirunpattarasilp, C., Mishra, A., Jaunmuktane, Z., Kyrargyri, V., Pfeiffer, T., Khennouf, L., Madry, C., Gong, H., Richard-Loendt, A., Huang, W., Saito, T., Saido, T. C., Brandner, S., Sethi, H., & Attwell, D. (2019). Amyloid b oligomers constrict human capillaries in Alzheimer's disease via signaling to pericytes. *Science*, *365*(6450), eaav9518. https://doi.org/10.1126/science.aav9518

O'Nuallain, B., Williams, A. D., Westermark, P., & Wetzel, R. (2004). Seeding Specificity in Amyloid Growth Induced by Heterologous Fibrils. *Journal of Biological Chemistry*, *279*(17), 17490–17499. https://doi.org/10.1074/jbc.M311300200

Oh, Y. S., Kim, J. S., Park, J. W., An, J. Y., Park, S. K., Shim, Y. S., Yang, D. W., & Lee, K. S. (2016). Arterial stiffness and impaired renal function in patients with Alzheimer's disease. *Neurological Sciences*, *37*(3), 451–457. https://doi.org/10.1007/s10072-015-2434-4

Ohyama, Y., Redheuil, A., Kachenoura, N., Venkatesh, B. A., & Lima, J. A. C. (2018). Advances in cardiovascular imaging imaging insights on the aorta in aging. *Circulation: Cardiovascular Imaging*, *11*(4), 1–11. https://doi.org/10.1161/CIRCIMAGING.117.005617

Oishi, Y., Miyoshi, H., Mizuguchi, Y., Iuchi, A., Nagase, N., & Oki, T. (2011). Aortic stiffness is strikingly increased with age ≥50 years in clinically normal individuals and preclinical patients with cardiovascular risk factors: Assessment by the new technique of 2D strain echocardiography. *Journal of Cardiology*, *57*(3), 354–359. https://doi.org/10.1016/j.jjcc.2010.12.003

Olofsson, A., Borowik, T., Gröbner, G., & Sauer-Eriksson, A. E. (2007). Negatively Charged Phospholipid Membranes Induce Amyloid Formation of Medin via an α-Helical Intermediate. *Journal of Molecular Biology*, *374*(1), 186–194. https://doi.org/10.1016/j.jmb.2007.08.064

Onuchic, J. N., & Wolynes, P. G. (2004). Theory of protein folding. *Current Opinion in Structural Biology*, *14*(1), 70–75. https://doi.org/10.1016/j.sbi.2004.01.009

Opie, E. L. (1901). The relation of diabetes mellitus to lesions of the pancreas. Hyaline degeneration of the islands of langerhans. *Journal of Experimental Medicine*, *5*(5), 527–540. https://doi.org/10.1084/jem.5.5.527

Otvos, L. J., Szendrei, G. I., Lee, V. M., & Mantsch, H. H. (1993). Human and rodent Alzheimer beta-amyloid peptides acquire distinct conformations in membrane-mimicking solvents. *European Journal of Biochemistry*, *211*(1–2), 249–257. https://doi.org/10.1111/j.1432-1033.1993.tb19893.x

Palmqvist, S., Schöll, M., Strandberg, O., Mattsson, N., Stomrud, E., Zetterberg, H., Blennow, K., Landau, S., Jagust, W., & Hansson, O. (2017). Earliest accumulation of β-amyloid occurs within the default-mode network and concurrently affects brain connectivity. *Nature Communications*, *8*(1), 1214. https://doi.org/10.1038/s41467-017-01150-x

Pase, M. P., Beiser, A., Himali, J. J., Tsao, C., Satizabal, C. L., Vasan, R. S., Seshadri, S., & Mitchell, G. F. (2016). Aortic Stiffness and the Risk of Incident Mild Cognitive Impairment and

Dementia. *Stroke*, *47*(9), 2256–2261. https://doi.org/10.1161/STROKEAHA.116.013508

Pase, M. P., Himali, J. J., Jacques, P. F., DeCarli, C., Satizabal, C. L., Aparicio, H., Vasan, R. S., Beiser, A. S., & Seshadri, S. (2017). Sugary beverage intake and preclinical Alzheimer's disease in the community. *Alzheimer's and Dementia*, *13*(9), 955–964. https://doi.org/10.1016/j.jalz.2017.01.024

Peca, S., McCreary, C. R., Donaldson, E., Kumarpillai, G., Shobha, N., Sanchez, K., Charlton, A., Steinback, C. D., Beaudin, A. E., Flück, D., Pillay, N., Fick, G. H., Poulin, M. J., Frayne, R., Goodyear, B. G., & Smith, E. E. (2013). Neurovascular decoupling is associated with severity of cerebral amyloid angiopathy. *Neurology*, *81*(19), 1659–1665. https://doi.org/10.1212/01.wnl.0000435291.49598.54

Peng, S., Glennert, J., & Westermark, P. (2005). Medin-amyloid: A recently characterized age-associated arterial amyloid form affects mainly arteries in the upper part of the body. *Amyloid*, *12*(2), 96–102. https://doi.org/10.1080/13506120500107006

Peng, S., Larsson, A., Wassberg, E., Gerwins, P., Thelin, S., Fu, X., & Westermark, P. (2007). Role of aggregated medin in the pathogenesis of thoracic aortic aneurysm and dissection. *Laboratory Investigation*, *87*(12), 1195–1205. https://doi.org/10.1038/labinvest.3700679

Peng, S., Westermark, G. T., Näslund, J., Häggqvist, B., Glennert, J., & Westermark, P. (2002). Medin and medin-amyloid in ageing inflamed and non-inflamed temporal arteries. *The Journal of Pathology*, *196*(1), 91–96. https://doi.org/10.1002/path.1014

Pettersen, J. A., Sathiyamoorthy, G., Gao, F. Q., Szilagyi, G., Nadkarni, N. K., St. George-Hyslop, P., Rogaeva, E., & Black, S. E. (2008). Microbleed topography, leukoaraiosis, and cognition in probable Alzheimer disease from the sunnybrook dementia study. *Archives of Neurology*, *65*(6), 790–795. https://doi.org/10.1001/archneur.65.6.790

Pitkänen, P., Westermark, P., & Cornwell 3rd, G. G. (1984). Senile systemic amyloidosis. *The American Journal of Pathology*, *117*(3), 391–399. https://pubmed.ncbi.nlm.nih.gov/6507586

Powers, E. T., Morimoto, R. I., Dillin, A., Kelly, J. W., & Balch, W. E. (2009). Biological and chemical approaches to diseases of proteostasis deficiency. *Annual Review of Biochemistry*, *78*(1), 959–991. https://doi.org/10.1146/annurev.biochem.052308.114844

Pras, M., Schubert, M., Zucker-Franklin, D., Rimon, A., & Franklin, E. C. (1968). The characterization of soluble amyloid prepared in water. *The Journal of Clinical Investigation*, *47*(4), 924–933. https://doi.org/10.1172/jci105784

Prusiner, S. B. (1982). Novel proteinaceous infectious particles cause scrapie. *Science*, *216*(4542), 136–144. https://doi.org/10.1126/science.6801762

Puchtler, H., Sweat, F., & Levine, M. (1962). On the Binding of Congo Red By Amyloid. *Journal of Histochemistry & Cytochemistry*, *10*(3), 355–364. https://doi.org/10.1177/10.3.355

Purro, S. A., Farrow, M. A., Linehan, J., Nazari, T., Thomas, D. X., Chen, Z., Mengel, D., Saito, T., Saido, T., Rudge, P., Brandner, S., Walsh, D. M., & Collinge, J. (2018). Transmission of amyloid-β protein pathology from cadaveric pituitary growth hormone. *Nature*, *564*(7736), 415–419. https://doi.org/10.1038/s41586-018-0790-y

Qi, R., Luo, Y., Wei, G., Nussinov, R., & Ma, B. (2015). Aβ "stretching-and-Packing" Cross-Seeding Mechanism Can Trigger Tau Protein Aggregation. *Journal of Physical Chemistry Letters*, *6*(16), 3276–3282. https://doi.org/10.1021/acs.jpclett.5b01447

Rabkin, S. W. (2012). Arterial stiffness: Detection and consequences in cognitive impairment and dementia of the elderly. *Journal of Alzheimer's Disease*, *32*(3), 541–549.

https://doi.org/10.3233/JAD-2012-120757

Radde, R., Bolmont, T., Kaeser, S. A., Coomaraswamy, J., Lindau, D., Stoltze, L., Calhoun, M. E., Jäggi, F., Wolburg, H., Gengler, S., Haass, C., Ghetti, B., Czech, C., Hölscher, C., Mathews, P. M., & Jucker, M. (2006). Abeta42-driven cerebral amyloidosis in transgenic mice reveals early and robust pathology. *EMBO Reports*, *7*(9), 940–946. https://doi.org/10.1038/sj.embor.7400784

Rapoport, M., Dawson, H. N., Binder, L. I., Vitek, M. P., & Ferreira, A. (2002). Tau is essential to β-amyloid-induced neurotoxicity. *Proceedings of the National Academy of Sciences of the United States of America*, *99*(9), 6364–6369. https://doi.org/10.1073/pnas.092136199

Rasmussen, J., Jucker, M., & Walker, L. C. (2017). Aβ seeds and prions: How close the fit? *Prion*, *11*(4), 215–225. https://doi.org/10.1080/19336896.2017.1334029

Rasmussen, J., Krasemann, S., Altmeppen, H., Schwarz, P., Schelle, J., Aguzzi, A., Glatzel, M., & Jucker, M. (2018). Infectious prions do not induce Aβ deposition in an in vivo seeding model. In *Acta Neuropathologica* (Vol. 135, Issue 6, pp. 965–967). https://doi.org/10.1007/s00401-018-1848-5

Rasmussen, J., Mahler, J., Beschorner, N., Kaeser, S. A., Häsler, L. M., Baumann, F., Nyström, S., Portelius, E., Blennow, K., Lashley, T., Fox, N. C., Sepulveda-Falla, D., Glatzel, M., Oblak, A. L., Ghetti, B., Nilsson, K. P. R., Hammarström, P., Staufenbiel, M., Walker, L. C., & Jucker, M. (2017). Amyloid polymorphisms constitute distinct clouds of conformational variants in different etiological subtypes of Alzheimer's disease. *Proceedings of the National Academy of Sciences of the United States of America*, *114*(49), 13018–13023. https://doi.org/10.1073/pnas.1713215114

Raymond, A., Ensslin, M. A., & Shur, B. D. (2009). SED1/MFG-E8: A Bi-motif protein that orchestrates diverse cellular interactions. *Journal of Cellular Biochemistry*, *106*(6), 957–966. https://doi.org/10.1002/jcb.22076

Real de Asua, D., Galvan, J. M., Filigghedu, M. T., Trujillo, D., Costa, R., & Cadinanos, J. (2014). Systemic AA amyloidosis: epidemiology, diagnosis, and management. *Clinical Epidemiology*, *6*, 369. https://doi.org/10.2147/clep.s39981

Reches, M., & Gazit, E. (2004). Amyloidogenic hexapeptide fragment of medin: Homology to functional islet amyloid polypeptide fragments. *Amyloid*, *11*(2), 81–89. https://doi.org/10.1080/13506120412331272287

Ren, B., Zhang, Y., Zhang, M., Liu, Y., Zhang, D., Gong, X., Feng, Z., Tang, J., Chang, Y., & Zheng, J. (2019). Fundamentals of cross-seeding of amyloid proteins: An introduction. *Journal of Materials Chemistry B*, *7*(46), 7267–7282. https://doi.org/10.1039/c9tb01871a

Revesz, T., Ghiso, J., Lashley, T., Plant, G., Rostagno, A., Frangione, B., & Holton, J. L. (2003). Cerebral amyloid angiopathies: A pathologic, biochemical, and genetic view. *Journal of Neuropathology and Experimental Neurology*, *62*(9), 885–898. https://doi.org/10.1093/jnen/62.9.885

Ridley, R. M., Baker, H. F., Windle, C. P., & Cummings, R. M. (2006). Very long term studies of the seeding of β-amyloidosis in primates. *Journal of Neural Transmission*, *113*(9), 1243–1251. https://doi.org/10.1007/s00702-005-0385-2

Roberson, E. D., Halabisky, B., Yoo, J. W., Yao, J., Chin, J., Yan, F., Wu, T., Hamto, P., Devidze, N., Yu, G. Q., Palop, J. J., Noebels, J. L., & Mucke, L. (2011). Amyloid-β/fyn-induced synaptic, network, and cognitive impairments depend on tau levels in multiple mouse models of alzheimer's disease. *Journal of Neuroscience*, *31*(2), 700–711. https://doi.org/10.1523/JNEUROSCI.4152-10.2011

Roberts, S. B., Ripellino, J. A., Ingalls, K. M., Robakis, N. K., & Felsenstein, K. M. (1994). Non-amyloidogenic cleavage of the β-amyloid precursor protein by an integral membrane metalloendopeptidase. *Journal of Biological Chemistry*, *269*(4), 3111–3116. https://doi.org/10.1016/s0021-9258(17)42055-2

Rogers, J., Cooper, N. R., Webster, S., Schultz, J., McGeer, P. L., Styren, S. D., Civin, W. H., Brachova, L., Bradt, B., Ward, P., & Lieberburg, I. (1992). Complement activation by β-amyloid in Alzheimer disease. *Proceedings of the National Academy of Sciences of the United States of America*, *89*(21), 10016–10020. https://doi.org/10.1073/pnas.89.21.10016

Roher, A. E., Esh, C. L., Kokjohn, T. A., Castaño, E. M., Van Vickle, G. D., Kalback, W. M., Patton, R. L., Luehrs, D. C., Daugs, I. D., Kuo, Y. M., Emmerling, M. R., Soares, H., Quinn, J. F., Kaye, J., Connor, D. J., Silverberg, N. B., Adler, C. H., Seward, J. D., Beach, T. G., & Sabbagh, M. N. (2009). Amyloid beta peptides in human plasma and tissues and their significance for Alzheimer's disease. *Alzheimer's and Dementia*, *5*(1), 18–29. https://doi.org/10.1016/j.jalz.2008.10.004

Roks, G., Dermaut, B., Heutink, P., Julliams, A., Backhovens, H., Van De Broeck, M., Serneels, S., Hofman, A., Van Broeckhoven, C., Van Duijn, C. M., & Cruts, M. (1999). Mutation screening of the tau gene in patients with early-onset Alzheimer's disease. *Neuroscience Letters*, *277*(2), 137–139. https://doi.org/10.1016/S0304-3940(99)00861-7

Roßner, S., Sastre, M., Bourne, K., & Lichtenthaler, S. F. (2006). Transcriptional and translational regulation of BACE1 expression-Implications for Alzheimer's disease. *Progress in Neurobiology*, *79*(2), 95–111. https://doi.org/10.1016/j.pneurobio.2006.06.001

Rousseau, F., Serrano, L., & Schymkowitz, J. W. H. (2006). How evolutionary pressure against protein aggregation shaped chaperone specificity. *Journal of Molecular Biology*, *355*(5), 1037–1047. https://doi.org/10.1016/j.jmb.2005.11.035

Rumbley, J., Hoang, L., Mayne, L., & Englander, S. W. (2001). An amino acid code for protein folding. *Proceedings of the National Academy of Sciences of the United States of America*, *98*(1), 105–112. https://doi.org/10.1073/pnas.98.1.105

Sabbagh, M. N., & Cummings, J. (2020). Open Peer Commentary to "Failure to demonstrate efficacy of aducanumab: An analysis of the EMRGE and ENGAGE Trials as reported by Biogen December 2019." *Alzheimer's and Dementia*, *n/a*(n/a). https://doi.org/10.1002/alz.12235

Sack, G. H. (2018). Serum amyloid A - A review. *Molecular Medicine*, *24*(1), 46. https://doi.org/10.1186/s10020-018-0047-0

Saito, T., Matsuba, Y., Mihira, N., Takano, J., Nilsson, P., Itohara, S., Iwata, N., & Saido, T. C. (2014). Single App knock-in mouse models of Alzheimer's disease. *Nature Neuroscience*, *17*(5), 661–663. https://doi.org/10.1038/nn.3697

Sapkota, B. R., & Sanghera, D. K. (2020). A rare missense variant in the milk fat globule-EGF factor 8 (MFGE8) increases T2DM susceptibility and cardiovascular disease risk with population-specific effects. *Acta Diabetologica*, *57*(6), 733–741. https://doi.org/10.1007/s00592-019-01463-x

Scherpelz, K. P., Wang, S., Pytel, P., Madhurapantula, R. S., Srivastava, A. K., Sachleben, J. R., Orgel, J., Ishii, Y., & Meredith, S. C. (2021). Atomic-level differences between brain parenchymal- and cerebrovascular-seeded Aβ fibrils. *Scientific Reports*, *11*(1), 247. https://doi.org/10.1038/s41598-020-80042-5

Schmitt, R., Tscheuschler, A., Laschinski, P., Uffelmann, X., Discher, P., Fuchs, J., Kreibich, M., Peyronnet, R., & Kari, F. A. (2019). A potential key mechanism in ascending aortic aneurysm

development: Detection of a linear relationship between MMP-14/TIMP-2 ratio and active MMP-2. *PLoS ONE*, *14*(2), e0212859–e0212859. https://doi.org/10.1371/journal.pone.0212859

Schwartz, P. (1970). Amyloidosis. Cause and manifestation of senile deterioration. *Springfield IL*.

Scuteri, A., Tesauro, M., Guglini, L., Lauro, D., Fini, M., & Di Daniele, N. (2013). Aortic stiffness and hypotension episodes are associated with impaired cognitive function in older subjects with subjective complaints of memory loss. *International Journal of Cardiology*, *169*(5), 371–377. https://doi.org/10.1016/j.ijcard.2013.09.009

Selkoe, D. J. (1998). The cell biology β-amyloid precursor protein and presenilin in Alzheimer's disease. *Trends in Cell Biology*, *8*(11), 447–453. https://doi.org/10.1016/S0962-8924(98)01363-4

Selkoe, D. J., & Hardy, J. (2016). The amyloid hypothesis of Alzheimer's disease at 25 years. *EMBO Molecular Medicine*, *8*(6), 595–608. https://doi.org/10.15252/emmm.201606210

Sengupta, U., Nilson, A. N., & Kayed, R. (2016). The Role of Amyloid-β Oligomers in Toxicity, Propagation, and Immunotherapy. *EBioMedicine*, *6*, 42–49. https://doi.org/10.1016/j.ebiom.2016.03.035

Sherrington, R., Rogaev, E. I., Liang, Y., Rogaeva, E. A., Levesque, G., Ikeda, M., Chi, H., Lin, C., Li, G., Holman, K., Tsuda, T., Mar, L., Foncin, J. F., Bruni, A. C., Montesi, M. P., Sorbi, S., Rainero, I., Pinessi, L., Nee, L., … St George-Hyslop, P. H. (1995). Cloning of a gene bearing missense mutations in early-onset familial Alzheimer's disease. *Nature*, *375*(6534), 754–760. https://doi.org/10.1038/375754a0

Shimagaki, T., Yoshio, S., Kawai, H., Sakamoto, Y., Doi, H., Matsuda, M., Mori, T., Osawa, Y., Fukai, M., Yoshida, T., Ma, Y., Akita, T., Tanaka, J., Taketomi, A., Hanayama, R., Yoshizumi, T., Mori, M., & Kanto, T. (2019). Serum milk fat globule-EGF factor 8 (MFG-E8) as a diagnostic and prognostic biomarker in patients with hepatocellular carcinoma. *Scientific Reports*, *9*(1), 15788. https://doi.org/10.1038/s41598-019-52356-6

Shirahama, T., & Cohen, A. S. (1965). Structure of amyloid fibrils after negative staining and high-resolution electron microscopy [38]. *Nature*, *206*(4985), 737–738. https://doi.org/10.1038/206737a0

Silvestre, J.-S., Théry, C., Hamard, G., Boddaert, J., Aguilar, B., Delcayre, A., Houbron, C., Tamarat, R., Blanc-Brude, O., Heeneman, S., Clergue, M., Duriez, M., Merval, R., Lévy, B., Tedgui, A., Amigorena, S., & Mallat, Z. (2005). Lactadherin promotes VEGF-dependent neovascularization. *Nature Medicine*, *11*(5), 499–506. https://doi.org/10.1038/nm1233

Singer, J., Trollor, J. N., Baune, B. T., Sachdev, P. S., & Smith, E. (2014). Arterial stiffness, the brain and cognition: A systematic review. *Ageing Research Reviews*, *15*(1), 16–27. https://doi.org/10.1016/j.arr.2014.02.002

Sinha, S., Anderson, J. P., Barbour, R., Basi, G. S., Caccaveffo, R., Davis, D., Doan, M., Dovey, H. F., Frigon, N., Hong, J., Jacobson-Croak, K., Jewett, N., Keim, P., Knops, J., Lieberburg, I., Power, M., Tan, H., Tatsuno, G., Tung, J., … John, V. (1999). Purification and cloning of amyloid precursor protein β-secretase from human brain. *Nature*, *402*(6761), 537–540. https://doi.org/10.1038/990114

Sipe, J. D., & Cohen, A. S. (2000). Review: History of the amyloid fibril. *Journal of Structural Biology*, *130*(2–3), 88–98. https://doi.org/10.1006/jsbi.2000.4221

Smith, E. E. (2018). Cerebral amyloid angiopathy as a cause of neurodegeneration. *Journal of Neurochemistry*, *144*(5), 651–658. https://doi.org/10.1111/jnc.14157

Soto, C., & Pritzkow, S. (2018). Protein misfolding, aggregation, and conformational strains in neurodegenerative diseases. *Nature Neuroscience*, *21*(10), 1332–1340. https://doi.org/10.1038/s41593-018-0235-9

Soubeyrand, S., Nikpay, M., Turner, A., Dang, A. T., Herfkens, M., Lau, P., & McPherson, R. (2019). Regulation of MFGE8 by the intergenic coronary artery disease locus on 15q26.1. *Atherosclerosis*, *284*, 11–17. https://doi.org/10.1016/j.atherosclerosis.2019.02.012

Spires-Jones, T. L., Attems, J., & Thal, D. R. (2017). Interactions of pathological proteins in neurodegenerative diseases. *Acta Neuropathologica*, *134*(2), 187–205. https://doi.org/10.1007/s00401-017-1709-7

Steinman, J., Sun, H.-S., & Feng, Z.-P. (2021). Microvascular Alterations in Alzheimer's Disease. *Frontiers in Cellular Neuroscience*, *14*(January). https://doi.org/10.3389/fncel.2020.618986

Stöhr, J., Watts, J. C., Mensinger, Z. L., Oehler, A., Grillo, S. K., DeArmond, S. J., Prusiner, S. B., & Giles, K. (2012). Purified and synthetic Alzheimer's amyloid beta (Aβ) prions. *Proceedings of the National Academy of Sciences of the United States of America*, *109*(27), 11025–11030. https://doi.org/10.1073/pnas.1206555109

Stroo, E., Koopman, M., Nollen, E. A. A., & Mata-Cabana, A. (2017). Cellular regulation of amyloid formation in aging and disease. *Frontiers in Neuroscience*, *11*(FEB), 1–17. https://doi.org/10.3389/fnins.2017.00064

Stubbs, J. D., Lekutis, C., Singer, K. L., Bui, A., Yuzuki, D., Srinivasan, U., & Parry, G. (1990). cDNA cloning of a mouse mammary epithelial cell surface protein reveals the existence of epidermal growth factor-like domains linked to factor VIII-like sequences. *Proceedings of the National Academy of Sciences of the United States of America*, *87*(21), 8417–8421. http://www.ncbi.nlm.nih.gov/pubmed/2122462

Sturchler-Pierrat, C., Abramowski, D., Duke, M., Wiederhold, K. H., Mistl, C., Rothacher, S., Ledermann, B., Bürki, K., Frey, P., Paganetti, P. A., Waridel, C., Calhoun, M. E., Jucker, M., Probst, A., Staufenbiel, M., & Sommer, B. (1997). Two amyloid precursor protein transgenic mouse models with Alzheimer disease-like pathology. *Proceedings of the National Academy of Sciences of the United States of America*, *94*(24), 13287–13292. http://www.ncbi.nlm.nih.gov/pubmed/9371838

Sukoff Rizzo, S. J., Masters, A., Onos, K. D., Quinney, S., Sasner, M., Oblak, A., Lamb, B. T., & Territo, P. R. (2020). Improving preclinical to clinical translation in Alzheimer's disease research. *Alzheimer's and Dementia: Translational Research and Clinical Interventions*, *6*(1), e12038. https://doi.org/10.1002/trc2.12038

Sunde, M., & Blake, C. (1997). The structure of amyloid fibrils by electron microscopy and x-ray diffraction. In F. M. Richards, D. S. Eisenberg, & P. S. B. T.-A. in P. C. Kim (Eds.), *Advances in Protein Chemistry* (Vol. 50, pp. 123–159). Academic Press. https://doi.org/10.1016/s0065-3233(08)60320-4

Takako, I. (1978). Pathological Study on Amyloidosis. *Pathology International*, *29*(6), 865–882. https://doi.org/10.1111/j.1440-1827.1979.tb00952.x

Talafous, J., Marcinowski, K. J., Klopman, G., & Zagorski, M. G. (1994). Solution Structure of Residues 1–28 of the Amyloid β-Peptide. *Biochemistry*, *33*(25), 7788–7796. https://doi.org/10.1021/bi00191a006

Taniguchi, Y., Fujiwara, Y., Nofuji, Y., Nishi, M., Murayama, H., Seino, S., Tajima, R., Matsuyama, Y., & Shinkai, S. (2015). Prospective study of arterial stiffness and subsequent cognitive decline among community-dwelling older Japanese. *Journal of Epidemiology*, *25*(9), 592–599. https://doi.org/10.2188/jea.JE20140250

Tanzi, R. E., Gusella, J. F., Watkins, P. C., Bruns, G. A. P., St. George-Hyslop, P., Van Keuren, M. L., Patterson, D., Pagan, S., Kurnit, D. M., & Neve, R. L. (1987). Amyloid β protein gene: CDNA, mRNA distribution, and genetic linkage near the Alzheimer locus. *Science*, *235*(4791), 880–884. https://doi.org/10.1126/science.2949367

Tarantini, S., Tran, C. H. T., Gordon, G. R., Ungvari, Z., & Csiszar, A. (2017). Impaired neurovascular coupling in aging and Alzheimer's disease: Contribution of astrocyte dysfunction and endothelial impairment to cognitive decline. *Experimental Gerontology*, *94*, 52–58. https://doi.org/10.1016/j.exger.2016.11.004

Tarasoff-Conway, J. M., Carare, R. O., Osorio, R. S., Glodzik, L., Butler, T., Fieremans, E., Axel, L., Rusinek, H., Nicholson, C., Zlokovic, B. V., Frangione, B., Blennow, K., Ménard, J., Zetterberg, H., Wisniewski, T., & De Leon, M. J. (2015). Clearance systems in the brain - Implications for Alzheimer disease. *Nature Reviews Neurology*, *11*(8), 457–470. https://doi.org/10.1038/nrneurol.2015.119

Taylor, M. R. (1997). Lactadherin (formerly BA46), a membrane-associated glycoprotein expressed in human milk and breast carcinomas, promotes Arg-Gly-Asp (RGD)- dependent cell adhesion. *DNA and Cell Biology*, *16*(7), 861–869. https://doi.org/10.1089/dna.1997.16.861

Terry, R. D., Masliah, E., Salmon, D. P., Butters, N., DeTeresa, R., Hill, R., Hansen, L. A., & Katzman, R. (1991). Physical basis of cognitive alterations in alzheimer's disease: Synapse loss is the major correlate of cognitive impairment. *Annals of Neurology*, *30*(4), 572–580. https://doi.org/10.1002/ana.410300410

Terzi, E., Hölzemann, G., & Seelig, J. (1997). Interaction of Alzheimer β-amyloid peptide(1-40) with lipid membranes. *Biochemistry*, *36*(48), 14845–14852. https://doi.org/10.1021/bi971843e

Thal, D. R., Capetillo-Zarate, E., Del Tredici, K., & Braak, H. (2006). The development of amyloid beta protein deposits in the aged brain. *Science of Aging Knowledge Environment : SAGE KE*, *2006*(6), re1. https://doi.org/10.1126/sageke.2006.6.re1

Thal, D. R., Griffin, W. S. T., de Vos, R. A. I., & Ghebremedhin, E. (2008). Cerebral amyloid angiopathy and its relationship to Alzheimer's disease. *Acta Neuropathologica*, *115*(6), 599–609. https://doi.org/10.1007/s00401-008-0366-2

Thijssen, D. H. J., Carter, S. E., & Green, D. J. (2016). Arterial structure and function in vascular ageing: Are you as old as your arteries? *Journal of Physiology*, *594*(8), 2275–2284. https://doi.org/10.1113/JP270597

Trujillo-Estrada, L., Jimenez, S., De Castro, V., Torres, M., Baglietto-Vargas, D., Moreno-Gonzalez, I., Navarro, V., Sanchez-Varo, R., Sanchez-Mejias, E., Davila, J., Vizuete, M., Gutierrez, A., & Vitorica, J. (2013). In vivo modification of Abeta plaque toxicity as a novel neuroprotective lithium-mediated therapy for Alzheimer's disease pathology. *Acta Neuropathologica Communications*, *1*(1), 73. https://doi.org/10.1186/2051-5960-1-73

Turkbey, E. B., Jain, A., Johnson, C., Redheuil, A., Arai, A. E., Gomes, A. S., Carr, J., Hundley, W. G., Teixido-Tura, G., Eng, J., Lima, J. A. C., & Bluemke, D. A. (2014). Determinants and normal values of ascending aortic diameter by age, gender, and race/ethnicity in the Multi-Ethnic Study of Atherosclerosis (MESA). *Journal of Magnetic Resonance Imaging*, *39*(2), 360–368. https://doi.org/10.1002/jmri.24183

Uchikado, H., Lin, W.-L., DeLucia, M. W., & Dickson, D. W. (2006). Alzheimer disease with amygdala Lewy bodies: a distinct form of alpha-synucleinopathy. *Journal of Neuropathology and Experimental Neurology*, *65*(7), 685–697.

https://doi.org/10.1097/01.jnen.0000225908.90052.07

Uhlmann, R. E., Rother, C., Rasmussen, J., Schelle, J., Bergmann, C., Ullrich Gavilanes, E. M., Fritschi, S. K., Buehler, A., Baumann, F., Skodras, A., Al-Shaana, R., Beschorner, N., Ye, L., Kaeser, S. A., Obermüller, U., Christensen, S., Kartberg, F., Stavenhagen, J. B., Rahfeld, J. U., … Jucker, M. (2020). Acute targeting of pre-amyloid seeds in transgenic mice reduces Alzheimer-like pathology later in life. *Nature Neuroscience*, *23*(12), 1580–1588. https://doi.org/10.1038/s41593-020-00737-w

Van Cauwenberghe, C., Van Broeckhoven, C., & Sleegers, K. (2016). The genetic landscape of Alzheimer disease: Clinical implications and perspectives. *Genetics in Medicine*, *18*(5), 421–430. https://doi.org/10.1038/gim.2015.117

Van Der Flier, W. M., Skoog, I., Schneider, J. A., Pantoni, L., Mok, V., Chen, C. L. H., & Scheltens, P. (2018). Vascular cognitive impairment. *Nature Reviews Disease Primers*, *4*(Vci), 1–16. https://doi.org/10.1038/nrdp.2018.3

Van Opstal, A. M., Van Rooden, S., Van Harten, T., Ghariq, E., Labadie, G., Fotiadis, P., Gurol, M. E., Terwindt, G. M., Wermer, M. J. H., Van Buchem, M. A., Greenberg, S. M., & Van der Grond, J. (2017). Cerebrovascular function in presymptomatic and symptomatic individuals with hereditary cerebral amyloid angiopathy: a case-control study. *The Lancet Neurology*, *16*(2), 115–122. https://doi.org/10.1016/S1474-4422(16)30346-5

Vassar, R., & Cole, S. (2008). The Basic Biology of BACE1: A Key Therapeutic Target for Alzheimers Disease. *Current Genomics*, *8*(8), 509–530. https://doi.org/10.2174/138920207783769512

Villemagne, V. L., Burnham, S., Bourgeat, P., Brown, B., Ellis, K. A., Salvado, O., Szoeke, C., Macaulay, S. L., Martins, R., Maruff, P., Ames, D., Rowe, C. C., & Masters, C. L. (2013). Amyloid β deposition, neurodegeneration, and cognitive decline in sporadic Alzheimer's disease: A prospective cohort study. *The Lancet Neurology*, *12*(4), 357–367. https://doi.org/10.1016/S1474-4422(13)70044-9

Virchow, R. (1854). Zur Cellulose -Frage. *Archiv Für Pathologische Anatomie Und Physiologie Und Für Klinische Medicin*, *6*(3), 416–426. https://doi.org/10.1007/BF02116546

Viswanathan, A., & Greenberg, S. M. (2011). Cerebral amyloid angiopathy in the elderly. *Annals of Neurology*, *70*(6), 871–880. https://doi.org/10.1002/ana.22516

Wagner, J., Degenhardt, K., Skodras, A., Obermüller, U., Wild, K., Dalmia, A., Häsler, L. M., Lambert, M., Liu, P., Veit, M., Davies, H. A., Madine, J., Feederle, R., Del Turco, D., Nilsson, K. P. R., Lashley, T., Deller, T., Walker, L. C., Heutink, P., … Neher, J. J. (2021). Medin interacts with Aβ to promote cerebral β-amyloid angiopathy. *Submitted*.

Wahl, D., Solon-Biet, S. M., Cogger, V. C., Fontana, L., Simpson, S. J., Le Couteur, D. G., & Ribeiro, R. V. (2019). Aging, lifestyle and dementia. *Neurobiology of Disease*, *130*, 104481. https://doi.org/10.1016/j.nbd.2019.104481

Waldstein, S. R., Rice, S. C., Thayer, J. F., Najjar, S. S., Scuteri, A., & Zonderman, A. B. (2008). Pulse pressure and pulse wave velocity are related to cognitive decline in the Baltimore longitudinal study of aging. *Hypertension*, *51*(1), 99–104. https://doi.org/10.1161/HYPERTENSIONAHA.107.093674

Walker, L. C. (2020). Aβ plaques. *Free Neuropathology*, *1*(0 SE-Review), 1–42. https://doi.org/10.17879/freeneuropathology-2020-3025

Walker, L. C., Callahan, M. J., Bian, F., Durham, R. A., Roher, A. E., & Lipinski, W. J. (2002). Exogenous induction of cerebral β-amyloidosis in βAPP-transgenic mice. *Peptides*, *23*(7), 1241–1247. https://doi.org/10.1016/S0196-9781(02)00059-1

Walsh, D. M., & Selkoe, D. J. (2007). Aβ oligomers - A decade of discovery. *Journal of Neurochemistry*, *101*(5), 1172–1184. https://doi.org/10.1111/j.1471-4159.2006.04426.x

Wan, Y. W., Al-Ouran, R., Mangleburg, C. G., Perumal, T. M., Lee, T. V., Allison, K., Swarup, V., Funk, C. C., Gaiteri, C., Allen, M., Wang, M., Neuner, S. M., Kaczorowski, C. C., Philip, V. M., Howell, G. R., Martini-Stoica, H., Zheng, H., Mei, H., Zhong, X., … Logsdon, B. A. (2020). Meta-Analysis of the Alzheimer's Disease Human Brain Transcriptome and Functional Dissection in Mouse Models. *Cell Reports*, *32*(2), 107908. https://doi.org/10.1016/j.celrep.2020.107908

Wang, J., Gu, B. J., Masters, C. L., & Wang, Y. J. (2017). A systemic view of Alzheimer disease - Insights from amyloid-β metabolism beyond the brain. *Nature Reviews Neurology*, *13*(10), 612–623. https://doi.org/10.1038/nrneurol.2017.111

Wang, M., Fu, Z., Wu, J., Zhang, J., Jiang, L., Khazan, B., Telljohann, R., Zhao, M., Krug, A. W., Pikilidou, M., Monticone, R. E., Wersto, R., Van Eyk, J., & Lakatta, E. G. (2012). MFG-E8 activates proliferation of vascular smooth muscle cells via integrin signaling. *Aging Cell*, *11*(3), 500–508. https://doi.org/10.1111/j.1474-9726.2012.00813.x

Watanabe, T., Totsuka, R., Miyatani, S., Kurata, S. I., Sato, S., Katoh, I., Kobayashi, S., & Ikawa, Y. (2005). Production of the long and short forms of MFG-E8 by epidermal keratinocytes. *Cell and Tissue Research*, *321*(2), 185–193. https://doi.org/10.1007/s00441-005-1148-y

Watson, N. L., Sutton-Tyrrell, K., Rosano, C., Boudreau, R. M., Hardy, S. E., Simonsick, E. M., Najjar, S. S., Launer, L. J., Yaffe, K., Atkinson, H. H., Satterfield, S., & Newman, A. B. (2011). Arterial stiffness and cognitive decline in well-functioning older adults. *Journals of Gerontology - Series A Biological Sciences and Medical Sciences*, *66 A*(12), 1336–1342. https://doi.org/10.1093/gerona/glr119

Watts, J. C., Condello, C., Stöhr, J., Oehler, A., Lee, J., DeArmond, S. J., Lannfelt, L., Ingelsson, M., Giles, K., & Prusiner, S. B. (2014). Serial propagation of distinct strains of Aβ prions from Alzheimer's disease patients. *Proceedings of the National Academy of Sciences of the United States of America*, *111*(28), 10323–10328. https://doi.org/10.1073/pnas.1408900111

Weingarten, M. D., Lockwood, A. H., Hwo, S. Y., & Kirschner, M. W. (1975). A protein factor essential for microtubule assembly. *Proceedings of the National Academy of Sciences of the United States of America*, *72*(5), 1858–1862. https://doi.org/10.1073/pnas.72.5.1858

Westermark, G. T., Johnson, K. H., & Westermark, P. (1999). Staining methods for identification of amyloid in tissue. *Methods in Enzymology*, *309*, 3–25. https://doi.org/10.1016/S0076-6879(99)09003-5

Westermark, G. T., & Westermark, P. (2011). Localized amyloids important in diseases outside the brain - Lessons from the islets of Langerhans and the thoracic aorta. *FEBS Journal*, *278*(20), 3918–3929. https://doi.org/10.1111/j.1742-4658.2011.08298.x

Westermark, P., Mucchiano, G., Marthin, T., Johnson, K. H., & Sletten, K. (1995). Apolipoprotein A1-derived amyloid in human aortic atherosclerotic plaques. *American Journal of Pathology*, *147*(5), 1186–1192.

Wheeler, J. B., Mukherjee, R., Stroud, R. E., Jones, J. A., & Ikonomidis, J. S. (2015). Relation of murine thoracic aortic structural and cellular changes with aging to passive and active mechanical properties. *Journal of the American Heart Association*, *4*(3), e001744. https://doi.org/10.1161/JAHA.114.001744

Willander, H., Hermansson, E., Johansson, J., & Presto, J. (2011). BRICHOS domain associated with lung fibrosis, dementia and cancer - A chaperone that prevents amyloid fibril formation? *FEBS Journal*, *278*(20), 3893–3904. https://doi.org/10.1111/j.1742-

4658.2011.08209.x

Winkler, D. T., Bondolfi, L., Herzig, M. C., Jann, L., Calhoun, M. E., Wiederhold, K. H., Tolnay, M., Staufenbiel, M., & Jucker, M. (2001). Spontaneous hemorrhagic stroke in a mouse model of cerebral amyloid angiopathy. *Journal of Neuroscience*, *21*(5), 1619–1627. https://doi.org/10.1523/jneurosci.21-05-01619.2001

Winklhofer, K. F., Tatzelt, J., & Haass, C. (2008). The two faces of protein misfolding: Gain- and loss-of-function in neurodegenerative diseases. *EMBO Journal*, *27*(2), 336–349. https://doi.org/10.1038/sj.emboj.7601930

Wood, J. G., Mirra, S. S., Pollock, N. J., & Binder, L. I. (1986). Neurofibrillary tangles of Alzheimer disease share antigenic determinants with the axonal microtubule-associated protein tau (τ). *Proceedings of the National Academy of Sciences of the United States of America*, *83*(11), 4040–4043. https://doi.org/10.1073/pnas.83.11.4040

Wu, H. Y., Kuo, P. C., Wang, Y. T., Lin, H. T., Roe, A. D., Wang, B. Y., Han, C. L., Hyman, B. T., Chen, Y. J., & Tai, H. C. (2018). B-Amyloid Induces Pathology-Related Patterns of Tau Hyperphosphorylation At Synaptic Terminals. *Journal of Neuropathology and Experimental Neurology*, *77*(9), 814–826. https://doi.org/10.1093/jnen/nly059

Wuyts, F. L., Vanhuyse, V. J., Langewouters, G. J., Decraemer, W. F., Raman, E. R., & Buyle, S. (1995). Elastic properties of human aortas in relation to age and atherosclerosis: A structural model. *Physics in Medicine and Biology*, *40*(10), 1577–1597. https://doi.org/10.1088/0031-9155/40/10/002

Xu, X., Wang, B., Ren, C., Hu, J., Greenberg, D. A., Chen, T., Xie, L., & Jin, K. (2017). Age-related impairment of vascular structure and functions. *Aging and Disease*, *8*(5), 590–610. https://doi.org/10.14336/AD.2017.0430

Yamada, M., Tsukagoshi, H., Otomo, E., & Hayakawa, M. (1987). Cerebral amyloid angiopathy in the aged. *Journal of Neurology*, *234*(6), 371–376. https://doi.org/10.1007/BF00314080

Yamada, M., Tsukagoshi, H., Otomo, E., & Hayakawa, M. (1988). Systemic amyloid deposition in old age and dementia of Alzheimer type: the relationship of brain amyloid to other amyloid. *Acta Neuropathologica*, *77*(2), 136–141. https://doi.org/10.1007/BF00687423

Yamada, Masahito, Hamaguchi, T., & Sakai, K. (2019). Acquired cerebral amyloid angiopathy: An emerging concept. In D. B. B. T.-P. in M. B. and T. S. Teplow (Ed.), *Progress in Molecular Biology and Translational Science* (Vol. 168, pp. 85–95). Academic Press. https://doi.org/10.1016/bs.pmbts.2019.05.012

Yamaguchi, H., Takagi, J., Miyamae, T., Yokota, S., Fujimoto, T., Nakamura, S., Ohshima, S., Naka, T., & Nagata, S. (2008). Milk fat globule EGF factor 8 in the serum of human patients of systemic lupus erythematosus. *Journal of Leukocyte Biology*, *83*(5), 1300–1307. https://doi.org/10.1189/jlb.1107730

Yan, J., Fu, X., Ge, F., Zhang, B., Yao, J., Zhang, H., Qian, J., Tomozawa, H., Naiki, H., Sawashita, J., Mori, M., & Higuchi, K. (2007). Cross-seeding and cross-competition in mouse apolipoprotein A-II amyloid fibrils and protein A amyloid fibrils. *American Journal of Pathology*, *171*(1), 172–180. https://doi.org/10.2353/ajpath.2007.060576

Yan, R., Blenkowski, M. J., Shuck, M. E., Miao, H., Tory, M. C., Pauley, A. M., Brashler, J. R., Stratman, N. C., Mathews, W. R., Buhl, A. E., Carter, D. B., Tomasselll, A. G., Parodl, L. A., Helnrikson, R. L., & Gurney, M. E. (1999). Membrane-anchored aspartyl protease with Alzheimer's disease β- secretase activity. *Nature*, *402*(6761), 533–537. https://doi.org/10.1038/990107

Yang, B., Wu, Y., Wang, Y., Yang, H., Du, B., Di, W., Xu, X., & Shi, X. (2020). Cerebrospinal fluid

MFG-E8 as a promising biomarker of amyotrophic lateral sclerosis. *Neurological Sciences*, *41*(10), 2915–2920. https://doi.org/10.1007/s10072-020-04416-3

Ye, H., Li, B., Subramanian, V., Choi, B. H., Liang, Y., Harikishore, A., Chakraborty, G., Baek, K., & Yoon, H. S. (2013). NMR solution structure of C2 domain of MFG-E8 and insights into its molecular recognition with phosphatidylserine. *Biochimica et Biophysica Acta - Biomembranes*, *1828*(3), 1083–1093. https://doi.org/10.1016/j.bbamem.2012.12.009

Ye, L., Hamaguchi, T., Fritschi, S. K., Eisele, Y. S., Obermüller, U., Jucker, M., & Walker, L. C. (2015). Progression of Seed-Induced Aβ Deposition within the Limbic Connectome. *Brain Pathology*, *25*(6), 743–752. https://doi.org/10.1111/bpa.12252

Ye, L., Rasmussen, J., Kaeser, S. A., Marzesco, A., Obermüller, U., Mahler, J., Schelle, J., Odenthal, J., Krüger, C., Fritschi, S. K., Walker, L. C., Staufenbiel, M., Baumann, F., & Jucker, M. (2017). Aβ seeding potency peaks in the early stages of cerebral β-amyloidosis. *EMBO Reports*, *18*(9), 1536–1544. https://doi.org/10.15252/embr.201744067

Yi, Y.-S. (2016). Functional Role of Milk Fat Globule-Epidermal Growth Factor VIII in Macrophage-Mediated Inflammatory Responses and Inflammatory/Autoimmune Diseases. *Mediators of Inflammation*, *2016*, 1–12. https://doi.org/10.1155/2016/5628486

Younger, S., Jang, H., Davies, H. A., Niemiec, M. J., Garcia, J. G. N., Nussinov, R., Migrino, R. Q., Madine, J., & Arce, F. T. (2020). Medin Oligomer Membrane Pore Formation: A Potential Mechanism of Vascular Dysfunction. *Biophysical Journal*, *118*(11), 2769–2782. https://doi.org/10.1016/j.bpj.2020.04.026

Yu, F., Li, B. ying, Li, X. li, Cai, Q., Zhang, Z., Cheng, M., Yin, M., Wang, J. fu, Zhang, J. hua, Lu, W. da, Zhou, R. hai, & Gao, H. qing. (2012). Proteomic Analysis of Aorta and Protective Effects of Grape Seed Procyanidin B2 in db/db Mice Reveal a Critical Role of Milk Fat Globule Epidermal Growth Factor-8 in Diabetic Arterial Damage. *PLoS ONE*, *7*(12), e52541. https://doi.org/10.1371/journal.pone.0052541

Yuan, P., Condello, C., Keene, C. D., Wang, Y., Bird, T. D., Paul, S. M., Luo, W., Colonna, M., Baddeley, D., & Grutzendler, J. (2016). TREM2 Haplodeficiency in Mice and Humans Impairs the Microglia Barrier Function Leading to Decreased Amyloid Compaction and Severe Axonal Dystrophy. *Neuron*, *90*(4), 724–739. https://doi.org/10.1016/j.neuron.2016.05.003

Zheng, H., Jiang, M., Trumbauer, M. E., Sirinathsinghji, D. J. S., Hopkins, R., Smith, D. W., Heavens, R. P., Dawson, G. R., Boyce, S., Conner, M. W., Stevens, K. A., Slunt, H. H., Sisodia, S. S., Chen, H. Y., & Van der Ploeg, L. H. T. (1995). B-Amyloid Precursor Protein-Deficient Mice Show Reactive Gliosis and Decreased Locomotor Activity. *Cell*, *81*(4), 525–531. https://doi.org/10.1016/0092-8674(95)90073-X

Zlokovic, B. V. (2011). Neurovascular pathways to neurodegeneration in Alzheimer's disease and other disorders. *Nature Reviews Neuroscience*, *12*(12), 723–738. https://doi.org/10.1038/nrn3114

3. Publications

3.1 Statement of personal contributions

I. Medin aggregation causes cerebrovascular dysfunction in aging wild-type mice

Karoline Degenhardt*, Jessica Wagner*, Angelos Skodras, Michael Candlish, Anna Julia Koppelmann, Katleen Wild, Rusheka Maxwell, Carola Rotermund, Felix von Zweydorf, Christian Johannes Gloeckner, Hannah A. Davies, Jillian Madine, Domenico Del Turco, Regina Feederle, Tammaryn Lashley, Thomas Deller, Philipp Kahle, Jasmin K. Hefendehl, Mathias Jucker, and Jonas J. Neher (2020). *PNAS* *contributed equally

Personal contributions: experimental design of the study (together with K.D., P.K., J.K.H., M.J., and J.J.N); maintenance, preparation and tissue processing of *Mfge8* C2 and WT mouse lines (together with K.D., with assistance from K.W. and A.J.K); TANGO prediction analysis; selection and establishment of human Medin antibody clones for histological and biochemical analysis; histological characterization of aggregates in aorta and brain by double-staining for amyloid-ligands (Methoxy-X04, Congo red) and human Medin (Fig.1, S2) or MFG-E8 (Fig.3, S2, S4) or Aβ; characterization and quantification of cerebrovascular Medin aggregates co-stained with SMA or Alexa hydrazide (Fig.3); biochemical analysis of amyloid in human aorta and APP transgenic mouse brain (Fig.2B, S1); Western Blotting for detection of human Medin, Aβ and mouse MFG-E8 (Fig.2B, S1A/B, S4); data and statistical analysis (together with K.D., J.J.N.); figure and manuscript preparation (together with J.J.N., with contributions from all authors).

Others: K.D. performed histological and biochemical analysis of mouse aorta and serum; A.J.K. performed analyses of astrocytic endfeet coverage and ELISA for brain homogenates; specific anti-human Medin antibody clones were generated and pre-selected by R.F.; A.S. developed tools for data analysis and assisted with image acquisition; *in vivo* 2P experiments were performed by M.C. and J.K.H.; R.M. and C.R. performed epitope mapping; H.A.D. and J.M. performed recombinant human Medin expression and sourced human aortic tissue; F.v.Z. and C.J.G. performed mass-spec analyses; D.D.T. and T.D. performed EM analyses; T.L. selected and sourced human brain tissue; J.J.N. conceived and designed the study.

II. Medin interacts with Aβ to promote cerebral β-amyloid angiopathy

Jessica Wagner*, Karoline Degenhardt*, Angelos Skodras, Ulrike Obermüller, Katleen Wild, Anupriya Dalmia, Lisa M. Häsler, Marius Lambert, Ping Liu, Marleen Veit, Hannah A. Davies, Jillian Madine, Regina Feederle, Domenico Del Turco, K. Peter R. Nilsson, Tammaryn Lashley, Thomas Deller, Lary C. Walker, Peter Heutink, Mathias Jucker, Jonas J. Neher. *Submitted* *contributed equally

Personal contributions: Experimental design of the study (together with K.D., M.J., and J.J.N); maintenance, preparation and tissue processing of APP x *Mfge8* C2 mouse lines (together with K.D., with assistance from K.W.); histological staining and image acquisition for mouse MFG-E8, Aβ, human Medin 1H4 and human MFG-E8, GFAP, Iba1, Aldh1l1, Pu.1 (Fig. 1b/g, 2, 4c-h, S1, S3, S6); amyloid staining with LCO and Methoxy; 3D Imaris reconstruction of human amyloid plaques, CAA and Medin (Fig.1g, 2); stereological quantification of Aβ load, total and plaque-associated microglia (together with K.D.)(Fig.1, S3); staining and quantification of CAA area (together with K.D.), frequency and micro-hemorrhages in APP23 mice (Fig.1); quantification of MFG-E8 in brain homogenates by ELISA and Western Blotting (Fig. 2, S4); characterization of seeding extracts by Western Blotting (6B3 and MFG-E8; Fig.4); amyloid extraction from human aorta and APP23 brain (Fig.4); Medin-depletion; stereotactic intracerebral injections (with U.O. and K.D.); Formic acid (with L.M.H. and M.L.) and DEA extraction of brain homogenates (Fig. S2); biochemical analysis of Aβ, APP and CTF by Western Blotting (together with K.D.) (Fig. S2); microglia isolation via FAC sorting for cytokine and Aβ measurements (with K.D.), Methoxy-X04 injections for *in vivo* phagocytosis experiment with subsequent microglia analysis (with K.D.) (Fig. S3); data and statistical analysis (together with K.D. and J.J.N.); figure and manuscript preparation (together with J.J.N., with contributions from all authors).

Others: D.D.T., T.D. and J.M. performed electron microscopy; H.A.D., J.M., T.L., L.C.W. contributed human tissue; R.F. generated specific anti-human Medin (1H4) antibody clones; Prothena Biosciences Inc. (Dublin, Ireland) provided the anti-human Medin (6B3) antibody; K.P.R.N. contributed LCOs; A.D., P.H. and J.J.N. analyzed expression in ROSMAP cohort; H.A.D. and J.M. performed in vitro aggregation experiments; A.S. developed tools for data analysis and assisted with image acquisition; L.M.H. and M.L. performed immunoassays for chemokines and Aβ; K.D., U.O., K.W., P.L., M.V. and J.J.N performed all other experimental work; J.J.N. conceived and designed the study.

Thesis figures 1-7 were created with BioRender.com.

3.2 Publications

3.2.1 Medin aggregation causes cerebrovascular dysfunction in aging wild-type mice

Karoline Degenhardt*, <u>Jessica Wagner</u>*, Angelos Skodras, Michael Candlish, Anna Julia Koppelmann, Katleen Wild, Rusheka Maxwell, Carola Rotermund, Felix von Zweydorf, Christian Johannes Gloeckner, Hannah A. Davies, Jillian Madine, Domenico Del Turco, Regina Feederle, Tammaryn Lashley, Thomas Deller, Philipp Kahle, Jasmin K. Hefendehl, Mathias Jucker, and Jonas J. Neher (2020). *contributed equally

Medin aggregation causes cerebrovascular dysfunction in aging wild-type mice

Karoline Degenhardt[a,b,c,1], Jessica Wagner[a,b,c,1], Angelos Skodras[a,b], Michael Candlish[d], Anna Julia Koppelmann[b,c], Katleen Wild[a], Rusheka Maxwell[b,e], Carola Rotermund[a,e], Felix von Zweydorf[a], Christian Johannes Gloeckner[a,f], Hannah A. Davies[g,h], Jillian Madine[g,i], Domenico Del Turco[j], Regina Feederle[k,l], Tammaryn Lashley[m,n], Thomas Deller[j], Philipp Kahle[a,e], Jasmin K. Hefendehl[d], Mathias Jucker[a,b], and Jonas J. Neher[a,b,2]

[a]German Center for Neurodegenerative Diseases (DZNE), 72076 Tübingen, Germany; [b]Department of Cellular Neurology, Hertie Institute for Clinical Brain Research, University of Tübingen, 72072 Tübingen, Germany; [c]Graduate School of Cellular and Molecular Neuroscience, University of Tübingen, 72074 Tübingen, Germany; [d]Buchmann Institute for Molecular Life Sciences and Institute of Cell Biology and Neuroscience, Goethe University Frankfurt, 60438 Frankfurt, Germany; [e]Laboratory of Functional Neurogenetics, Department of Neurodegeneration, Hertie Institute for Clinical Brain Research, University of Tübingen, 72076 Tübingen, Germany; [f]Core Facility for Medical Bioanalytics, Institute for Ophthalmic Research, Center for Ophthalmology University of Tübingen, 72076 Tübingen, Germany; [g]Department of Cardiovascular and Metabolic Medicine, Institute of Life Course and Medical Sciences, University of Liverpool, Liverpool L69 3BX, United Kingdom; [h]Liverpool Centre for Cardiovascular Sciences, University of Liverpool, Liverpool L14 3PE, United Kingdom; [i]Department of Biochemistry and Systems Biology, Institute of Systems, Molecular and Integrative Biology, University of Liverpool, Liverpool L69 7ZB, United Kingdom; [j]Institute of Clinical Neuroanatomy, Dr. Senckenberg Anatomy, Neuroscience Center, Goethe University, D-60590 Frankfurt/Main, Germany; [k]Monoclonal Antibody Core Facility, Institute for Diabetes and Obesity, Helmholtz Zentrum München, Research Center for Environmental Health, 85764 Neuherberg, Germany; [l]DZNE, 81377 Munich, Germany; [m]Queen Square Brain Bank for Neurological Disorders, University College London Queen Square Institute of Neurology, London WC1N 1PJ, United Kingdom; and [n]Department of Neurodegenerative Disease, University College London Queen Square Institute of Neurology, London WC1N 1PJ, United Kingdom

Medin is the most common amyloid known in humans, as it can be found in blood vessels of the upper body in virtually everybody over 50 years of age. However, it remains unknown whether deposition of Medin plays a causal role in age-related vascular dysfunction. We now report that aggregates of Medin also develop in the aorta and brain vasculature of wild-type mice in an age-dependent manner. Strikingly, genetic deficiency of the Medin precursor protein, MFG-E8, eliminates not only vascular aggregates but also prevents age-associated decline of cerebrovascular function in mice. Given the prevalence of Medin aggregates in the general population and its role in vascular dysfunction with aging, targeting Medin may become a novel approach to sustain healthy aging.

Medin | MFG-E8 | cerebrovascular dysfunction | aging | amyloid

Amyloids comprise about 36 identified proteins, which under physiological conditions can convert to insoluble aggregates that are often associated with pathological alterations in the amyloid-containing tissue (1). The most common human amyloid described so far is Medin (also known as AMed), which has been found in ~97% of Caucasians above 50 y of age (2), with Medin deposition found predominantly in the thoracic aorta and other arteries of the upper body (3). Medin has been described as a 50-amino acid-long internal fragment of the protein Milk fat globule-EGF factor-8 (MFG-E8) (4), which itself is best known for its role in the phagocytosis of apoptotic cells but is also required for neovascularization, explaining its localization in blood vessels (5). Under which conditions and how Medin is cleaved from MFG-E8 remains unknown, but its exceedingly high prevalence in the aging population begs the question whether Medin—similar to other amyloids—is associated with tissue dysfunction (6). Of note, previous research suggests that age-associated structural and functional alterations of the arteries contribute to cardiovascular diseases (7), and a role of Medin in promoting age-related vascular dysfunction has been hypothesized based on analyses of human autopsy and postmortem aorta samples (8–10). Most recently, evidence of increased Medin levels in patients with vascular dementia compared to cognitively unimpaired individuals was also reported (11). However, mechanistic studies and therefore conclusive evidence for a detrimental role of Medin deposition are so far lacking. This is largely because studies on human tissue lack appropriate controls (due to the presence of Medin deposits in virtually all aged human samples) and could therefore only be correlative in nature, and because no animal model for Medin deposition has so far been described that would enable mechanistic analyses.

Therefore, we analyzed here whether Medin deposition also occurs in the vasculature of aging mice. Indeed, we find extracellular Medin aggregates in C57BL/6J mice, with deposition developing in an age-dependent manner. Notably, Medin aggregates are absent in genetically engineered mice that lack the Medin-containing C2 domain of its precursor protein MFG-E8. Moreover, in these Medin-deficient mice, age-associated vascular dysfunction in cerebral arteries is virtually eliminated. Thus, our data provide direct evidence for a pathological role of this highly prevalent human amyloid.

Significance

Vascular dysfunction, as it develops either during normal aging or vascular disease, remains a major medical problem. The amyloid Medin, which is derived from its precursor protein MFG-E8 (through unknown mechanisms), forms insoluble aggregates in the vasculature of virtually anybody over 50 years of age, and it has been hypothesized that Medin aggregation could contribute to age-associated vascular decline; however, mechanistic analyses have so far been lacking. Our data now demonstrate that reminiscent of humans, mice also develop Medin deposits in an age-dependent manner. Importantly, mice that genetically lack Medin show reduced vascular dysfunction in the aged brain. Therefore, the prevention of Medin accumulation should be investigated as a novel therapeutic approach to preserve vascular health in the aging population.

NEUROSCIENCE

Results

MFG-E8/Medin Aggregates Form in the Mouse Aorta with Age. In humans, Medin aggregates are detectable in blood vessels of the upper body in virtually everyone above the age of 50 (2). While two prior studies in rats and monkeys have reported an increase of aortic levels of the Medin precursor protein MFG-E8 with age (12, 13), it has so far not been investigated whether Medin aggregates are found in other species than humans. Of note, murine and human Medin show 78% amino acid sequence homology (Needleman–Wunsch Global Alignment, BLAST) with the most aggregation-prone region showing high conservation (Fig. 1A) (14, 15). This indicates that mice may be a suitable model to study Medin pathophysiology, although the aggregation propensity of murine Medin may be more limited than its human form (based on TANGO analysis; Fig. 1A).

To assess whether Medin is deposited in the mouse aorta, we collected aorta samples from mice at the age of 2–4, 12, and 20 mo. First, we tested whether levels of MFG-E8 increase with age (using a commercial ELISA). Indeed, aorta homogenates showed a significant increase in MFG-E8 protein levels in 12-mo-old

compared to 2- to 4-mo-old mice and increased even further in 20-mo-old animals (Fig. 1B). Interestingly, at the same time that levels of MFG-E8 increased in the aorta, they decreased in the serum, demonstrating that these changes were not due to blood contamination in the tissue. Immunostaining with a polyclonal antibody against murine MFG-E8, which we found to have high affinity for the C2 and lower affinity for the C1 domain (*SI Appendix,* Fig. S1A and Fig. 1A), confirmed that aortic MFG-E8 staining increases with age (Fig. 1C). Interestingly, MFG-E8 staining revealed irregularly shaped lumps along elastic fibers, reminiscent of findings in human tissue where Medin is found in "nodules and thin streaks" in the aortic media and is closely associated with elastic fibers (2, 16). We also confirmed these previous results in human tissue using a new monoclonal anti-human Medin antibody (1H4) (Fig. 1E). While prior studies could not demonstrate that antibodies were specifically detecting Medin, we here ascertained staining specificity by analyzing tissue from mice that lack the Medin-containing C2 domain of MFG-E8 (*Mfge8* C2 knockout [KO]) (Fig. 1A). In these functional knockout mice, the C2 domain is replaced with a β-galactosidase reporter gene fused to a transmembrane domain.
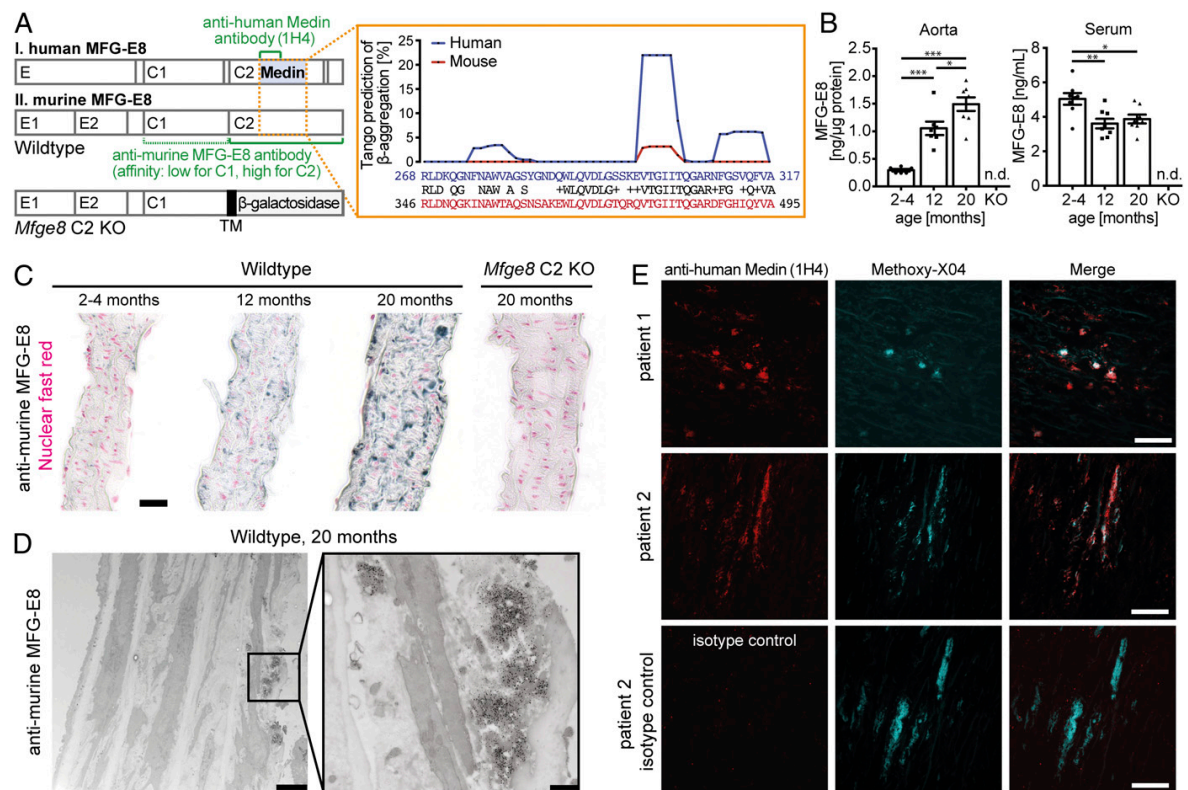

Fig. 1. MFG-E8–positive aggregates accumulate in the mouse aorta with age. (A, *Left*) Schematic structure of human and murine MFG-E8 showing the major protein domains and highlighting protein regions recognized by the two antibodies used throughout this study (green). The structure of the truncated *Mfge8* gene in the C2 domain knockout mice is shown at the bottom, indicating the introduction of a β-galactosidase reporter gene fused to a transmembrane domain (TM), which traps the gene product inside the cell. (*Right*) Amino acid sequence comparison of the reported human Medin sequence with the homologous murine sequence; TANGO prediction of aggregation-prone peptides within the Medin sequence, with high conservation but lower aggregation propensity in the mouse (*Top*). (B) Protein levels in WT mouse aorta and serum in young adult (2–4 mo old; n_{aorta} = 3/3, n_{serum} = 5/3 female/male), adult (12-mo-old, n_{aorta} = 3/4, n_{serum} = 3/5 female/male) and aged (20-mo-old, n_{aorta} = 3/5, n_{serum} = 3/5 female/male) animals and *Mfge8* C2 knockout tissue (n = 1/1 female/male). Data shown are means ± SEM, with one-way ANOVA for aorta: $F_{(2,18)}$ = 29.97, $P < 0.0001$; serum: $F_{(2,21)}$ = 6.85, $P = 0.005$; *$P < 0.05$, **$P < 0.01$, ***$P < 0.001$ for post hoc Tukey test. n.d.: not detectable. (C) Representative immunohistochemical staining for MFG-E8 (black) and cell nuclei (red) of 5-μm sections of the mouse aorta in WT and *Mfge8* C2 KO animals. (D) Immuno-EM for MFG-E8 of aged WT mouse aorta (n = 2 female mice; 24-mo-old); no aggregates were found in young adult (n = 2 male; 3-mo-old) or aged *Mfge8* C2 KO (n = 1/1 male/female; 21–23 mo old) animals. (E) Staining of human aorta sections (5 μm) with anti-human Medin antibody (clone 1H4) or an isotype-control antibody (*Bottom*) and the amyloid-binding dye Methoxy-X04. (Scale bars: C and E, 25 μm; D, *Left*, 2500 nm; D, *Right*, 500 nm.)

73

While this does not prevent gene expression, it effectively traps the truncated MFG-E8/β-galactosidase fusion protein inside the cell, leading to a complete absence of secreted MFG-E8 in *Mfge8* C2 KO animals (as previously confirmed in the aorta and for different cell types; refs. 5, 17, 18 and cp. *SI Appendix*, Fig. S4 for brain tissue). In line with the high affinity of the polyclonal anti-MFG-E8 antibody for the C2 domain (*SI Appendix*, Fig. S1A), staining was absent in the aorta of *Mfge8* C2 KO mice (Fig. 1C) and, accordingly, no signal was found in the ELISA for MFG-E8 (Fig. 1B).

To determine whether the observed staining patterns in wild-type (WT) mice were indeed due to extracellular aggregates, we next performed immuno-electron microscopy (EM) of aortas from young adult and aged WT mice as well as aged *Mfge8* C2 KO mice. As expected from our immunohistochemical analyses, only aged WT animals demonstrated immunolabeling, which was found localized on extracellular aggregates (Fig. 1D). While these aggregates appeared amorphous (rather than fibrillar) under EM, these findings demonstrate that MFG-E8 (or its fragments) forms extracellular aggregates in an age-specific manner in the mouse aorta.

In humans, aortic Medin deposits can be stained with amyloid-binding dyes such as Methoxy-X04, which we also confirmed here (Fig. 1E and see *SI Appendix*, Table S1 for sample information). In apparent contrast, aggregates in the mouse aorta failed to stain with Methoxy-X04 or Congo Red (*SI Appendix*, Fig. S2). However, in our hands, not all Medin-positive aggregates (stained with anti-human Medin antibody 1H4) in human tissue were stained by amyloid-binding dyes (Fig. 1E; n = 3 patients, *SI Appendix*, Table S1 and Fig. S2). Thus, similar to our observations in mice, some Medin deposits in human tissue do not display the characteristic β-sheet structure of other amyloids, possibly representing an earlier aggregation stage.

Aortic Deposits in Mice Show Biochemical Characteristics of Protein Aggregates. Given the amorphous appearance of aortic aggregates in aged mice by EM, we wanted to determine whether these deposits shared biochemical features of other aggregated proteins, i.e., protease resistance and insolubility in aqueous media. Therefore, we used a previously published amyloid purification protocol (19) to determine if the aged aorta would contain aggregated proteins. We first tested this protocol using brains of either aged APP23 or APP Dutch transgenic animals. APP23 mice are a model of Alzheimer's disease pathology with widespread parenchymal and vascular amyloid-β deposition (20) while aged APP Dutch animals show amyloid-β deposition restricted to cerebral blood vessels (21). In brief, homogenates were lysed and subjected to iodixanol gradient centrifugation. Samples were then digested with benzonase and proteinase-K (PK) and were subsequently ultracentrifuged to recover the remaining protease-resistant, insoluble material (Fig. 2A). As expected, this procedure yielded enriched monomeric and oligomeric amyloid-β species from the brains of both aged APP23 and APP Dutch animals (*SI Appendix*, Fig. S1B).

Next, we analyzed fresh-frozen aorta samples from human patients, which showed Medin staining by immunohistochemistry (cp. Fig. 1E). In human aorta samples, Western blotting of the different fractions obtained from the amyloid purification protocol using the monoclonal anti-human Medin antibody (1H4) revealed protein bands corresponding to full-length MFG-E8 but also bands indicating monomeric and possibly oligomeric Medin species (approximately 4, 8, and 12 kDa). After benzonase (P2) and proteinase K (P3) digestion, full-length MFG-E8 and other proteins were degraded, while the protease-resistant material showed distinct bands with molecular mass corresponding to monomeric and oligomeric Medin species as well as a higher molecular mass smear, possibly reflecting higher order aggregates (Fig. 2B).

Analyzing mouse samples next, Western blotting demonstrated full-length MFG-E8 in the total aorta homogenate (TH) of both young and aged WT mice (Fig. 2C; samples are pools of 16 mouse aortas), with significantly stronger signals in the aorta homogenate of aged mice, reflecting our ELISA measurements (Fig. 1B). In contrast, the purification protocol only enriched a protease-resistant MFG-E8–positive fragment from the aorta of aged WT mice, while neither young WT nor aged *Mfge8* C2 KO aortas yielded MFG-E8 species in the final aggregate-containing fractions (Fig. 2C). Notably, the protease-resistant MFG-E8 fragment in the aged mouse aorta showed a molecular mass of approximately 5 kDa, corresponding to the reported size of Medin (4). These results demonstrate that MFG-E8 fragments, which similar to other protein aggregates are protease-resistant as well as insoluble in aqueous buffers and show a molecular mass that corresponds to the reported size of Medin, accumulate in the aging mouse aorta.

Identification of a Medin-Like Fragment in the Aging Mouse Aorta. To ascertain that the ~5-kDa band observed by Western blotting was indeed a Medin-containing peptide, we used a shotgun mass spectrometry approach (Fig. 2D). Briefly, aorta homogenates were prefractionated by protein gel electrophoresis, and only proteins smaller than ~17 kDa were excised to exclude full-length MFG-E8. First, we verified that we could detect Medin peptides in aggregated material by analyzing recombinant human Medin that had been aggregated in vitro. Indeed, following gel electrophoresis and excision of a monomeric as well as an oligomeric band, almost the entire Medin sequence (with the exception of short N- and C-terminal peptides) could be detected by mass spectrometry (*SI Appendix*, Fig. S3).

Next, we compared murine aorta samples (again without further purification procedures) from young and aged WT and aged *Mfge8* C2 KO mice. Here, low molecular mass peptides of MFG-E8 (≤17 kDa) were detectable only in aged WT aortas. Strikingly, the majority of these peptides could be assigned to the C2 domain and were enriched in the sequence corresponding to the originally reported human Medin (Fig. 2D), also consistent with our epitope mapping of the anti-murine MFG-E8 antibody (Fig. 1A and *SI Appendix*, Fig. S1A). Thus, our mass spectrometry results demonstrate that—similar to observations in human patients—Medin-containing fragments are accumulating in the aging mouse aorta, further corroborating our analyses using immunohistochemistry and biochemical purification approaches.

MFG-E8 and Medin in the Aging Brain. In humans, Medin deposition has not only been observed in the thoracic aorta but also other larger arteries of the upper body, including basilar and temporal arteries (3, 22, 23) and most recently also arterioles in the brain parenchyma (11). To confirm Medin deposition in cerebral blood vessels, we stained brain sections of aged patients without any major brain diseases (male and female, 80–86 y old; see *SI Appendix*, Table S2 for details) with the anti-human Medin antibody, 1H4. Strikingly, Medin deposits could be seen within and outside the smooth muscle cell layer in leptomeningeal vessels, larger parenchymal vessels, and even smaller capillaries, where they also showed aggregate-like morphology (Fig. 3A). Of note, these deposits did not show immunoreactivity for amyloid-β nor were they positive for the amyloid-binding dye Methoxy-X04 (Fig. 3 A, Bottom), in contrast to our findings in the human aorta, where both Methoxy-X04–positive and –negative aggregates were found (Fig. 1E).

Next, we analyzed brain tissue from mice to determine whether cerebral blood vessels would display age-related Medin deposition. Indeed, immunohistochemical staining showed MFG-E8–positive blood vessels in the mouse brain, with more intense and aggregate-like staining being observed in aged animals (Fig. 3B). However, these deposits were again not stained by the classical amyloid-binding dyes Methoxy-X04 and Congo Red (*SI Appendix*, Fig. S2). Nevertheless, an age-related increase in cerebral MFG-E8 protein levels could be observed in WT mice by ELISA
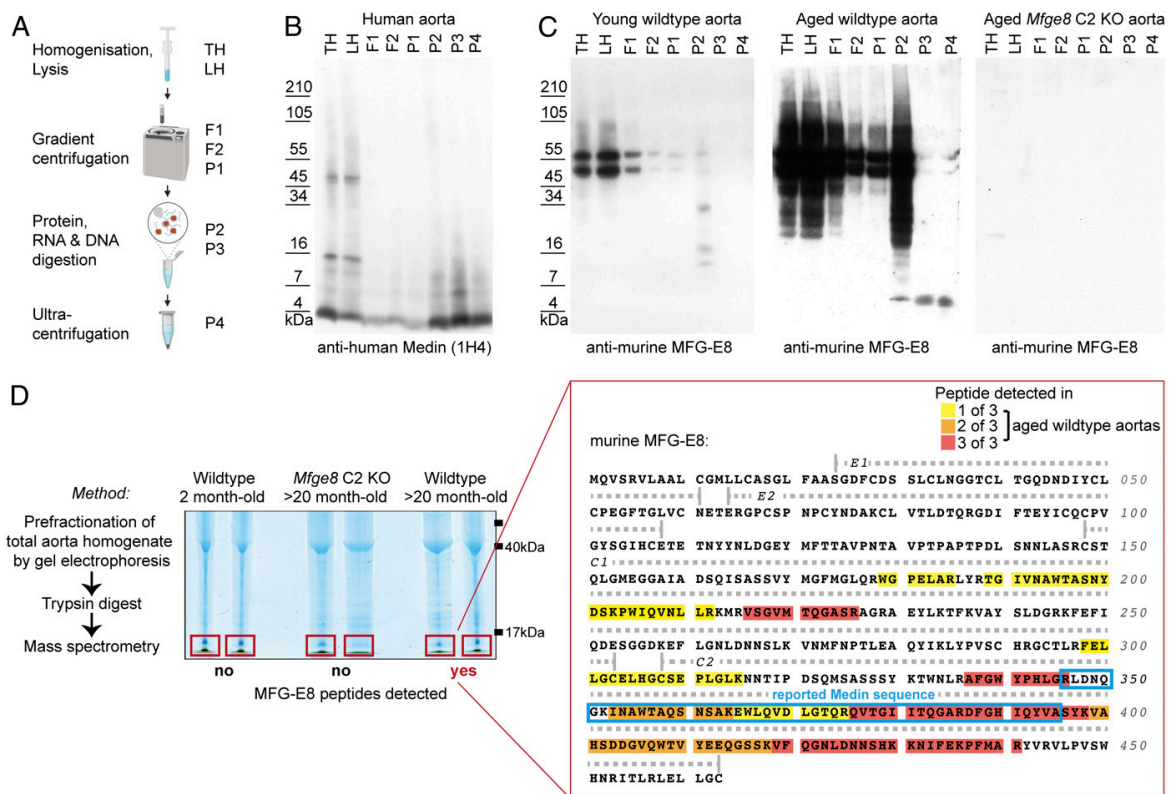
74

Fig. 2. Aortic deposits in mice show biochemical characteristics of protein aggregates and are enriched in Medin-containing fragments of MFG-E8. (*A*) Graphical summary of the purification procedure for the enrichment of protein aggregates from tissue homogenates. (*B*) Analysis of human aorta homogenates (LH, lysed homogenate; TH, total homogenate) reveals enrichment of Medin-positive bands, corresponding to monomeric (∼4 kDa) and oligomeric (∼8/12 kDa) species. (*C*) In mouse aorta samples (pools of 16 aortas were used as input), full-length MFG-E8 is degraded and a ∼5-kDa fragment is enriched only from aged WT but not young WT or aged *Mfge8* C2 KO aortas. (*D*) Mass spectrometry (MS) analysis of total aorta homogenate of young adult WT (2-mo-old; n = 1/1 female/male) and aged (20-mo-old) *Mfge8* C2 KO (n = 2 females) and WT (n = 1/2 female/male) mice. Following prefractionation and in-gel digestions, gel sections containing small proteins (<17 kDa) were excised and subjected to MS analysis. No MFG-E8 peptides were found in samples from young WT or aged *Mfge8* C2 KO animals while aged WT aortas contained ≤17 kDa fragments of MFG-E8, which were most consistently found in the C2 domain (color-code indicates detection in different number of samples; yellow/orange/red = 1/2/3 of 3 samples). The reported human Medin sequence is highlighted with a blue frame.

(Fig. 3*C*), reflecting our findings in the aorta (Fig. 1). Moreover, semiautomated quantification of smooth muscle actin and MFG-E8 staining in serial brain sections revealed no difference in total vascular coverage but showed an increase of cerebrovascular MFG-E8 staining with age (Fig. 3 *D* and *E*). Notably, in brain sections from aged *Mfge8* C2 KO animals, we could detect intracellular MFG-E8-positive puncta both in parenchymal as well as vascular cells, reflecting expression and intracellular retention of the truncated MFG-E8/β-galactosidase fusion protein (*SI Appendix*, Fig. S4*A*). Accordingly, in brain homogenates from aged *Mfge8* C2 KO animals, the fusion protein appeared as a distinct band ∼200 kDa (in line with previous reports; ref. 18), while the band of full-length MFG-E8 observed in WT animals was completely absent (*SI Appendix*, Fig. S4*B*). Thus, our results indicate that in WT mice, the aorta as well as cerebral blood vessels show age-associated deposition of MFG-E8 (fragments) that are likely to contain Medin.

Lack of MFG-E8 Rescues Age-Associated Vascular Dysfunction. We wondered whether Medin deposition could contribute to the decline in vascular function, which occurs with age both in mice and

humans (24–26). Because age-related changes in regional cerebral blood flow are not detectable by positron emission tomography (PET) or MRI measurements in WT animals (27), we assessed cerebral vascular function by two-photon in vivo imaging, which has been shown to detect age-associated cerebrovascular alterations in mice (28). Here, we analyzed the function of cerebral arterioles in living animals, focusing on the middle cerebral artery territory in the sensorimotor cortex, where we also observed Medin deposits in aging mice (Fig. 3*F*). We triggered increases in blood flow to the hindlimb region by evoking neuronal activity using mechanical hindlimb stimulation (Fig. 3*G*), a mechanism called functional hyperemia (29, 30). Indeed, in response to hindlimb stimulation, adult animals (6.4 ± 1.1 mo old) showed a rapid dilation of arteries followed by a slower constriction; this response was indistinguishable between adult WT and *Mfge8* C2 KO animals (Fig. 3*H*). Importantly, in aged WT animals (22.1 ± 2.4 mo old) dilation of the imaged arteries was significantly slower than in adult animals, in line with increased vascular arterial stiffness in aging animals and humans (31, 32). In contrast, both dilation and constriction were significantly improved in aged *Mfge8* C2 KO compared to WT animals (Fig. 3*H*). Thus, our data demonstrate
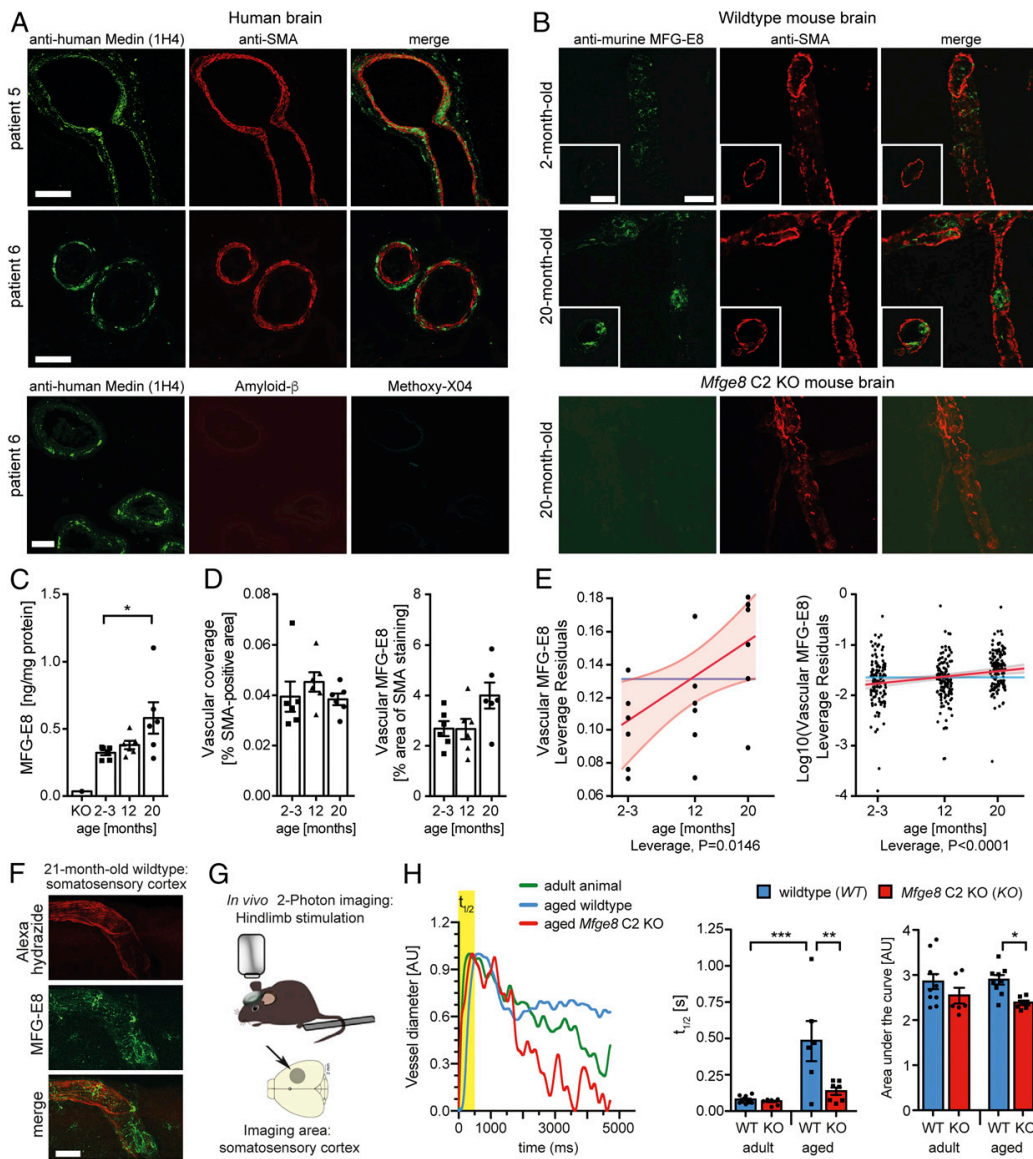
Degenhardt et al.

Fig. 3. MFG-E8/Medin deposition causes age-associated cerebrovascular dysfunction. (*A*) In brain sections of healthy human patients (*n* = 3 patients analyzed), extensive vascular staining of aggregate-like structures is seen with a monoclonal anti-human Medin antibody (1H4). Aggregates are largely localized in the tunica media and the parenchymal side of the vessels. (*Bottom*) Medin-positive deposits do not stain with the amyloid-dye Methoxy-X04 and are negative for amyloid-β. (*B*) In aged (20-mo-old) but not young (2-mo-old) WT mice, aggregate-like structures are also present in the brain vasculature, where they are found mostly in the tunica media and the luminal side of blood vessels. (*C*) Quantification of total MFG-E8 protein levels with age in the WT mouse brain (*n* = 3/3 females/males per group, significant Kruskal–Wallis test: KW statistic = 5.93, *P* = 0.047, followed by Dunn's post hoc comparison, **P* < 0.05). (*D*) Quantification of the overall vascular density (area of smooth muscle actin [SMA] staining) and vascular MFG-E8 staining (% MFG-E8 staining within SMA-positive area) in brain sections with age in WT mice (*n* = 3/3 females/males per group). Data shown are means ± SEM. (*E*) Regression analysis for the impact of age on cerebrovascular accumulation of MFG-E8/Medin (effect leverage plot, where a least squares line [red] and confidence bands [shaded red] are fitted). Analysis for the mean vascular MFG-E8 staining per animal (*Left*) and per brain section (*Right*). (*F*) Representative confocal z-stack of an artery from the middle cerebral artery territory in the somatosensory cortex (horizontal brain section). (*G*) Schematic illustration of in vivo analysis of vascular function in the brain of living mice using two-photon imaging of functional hyperemia. (*H*) Representative traces (*Left*) and quantification of the change in diameter of individual arterioles in adult WT (*n* = 4; 5/6/6/6-mo-old male) or *Mfge8* C2 KO (*n* = 3; 6/6/8-mo-old male) and aged WT (*n* = 4; 21/22/22/22-mo-old male) or *Mfge8* C2 KO (*n* = 3; 19/22/27-mo-old male) animals (*Right*), with $t_{1/2}$ reflecting the speed of vessel dilation, and the area under the curve reflecting the speed of constriction (1–3 arterioles per animal). Arterial dilation and constriction are significantly improved in aged *Mfge8* C2 KO compared to aged WT animals. Two-way ANOVA; $t_{1/2}$: significant main effects of age*genotype/genotype/age: $F_{(1,25)}$ = 7.763/9.369/16.15, *P* = 0.01/0.0052/0.0005; Area under the curve: significant main effect of genotype, $F_{(1,28)}$ = 8.62, *P* = 0.0066; **P* < 0.05, ****P* < 0.01, ******P* < 0.001 for post hoc Bonferroni comparisons. Data shown are means ± SEM (data points are measurements from individual blood vessels). (Scale bars: *A*, 50 μm; *B* and *F*, 25 μm.)

Degenhardt et al.

that the lack of Medin improves vascular function in aging animals.

It has been suggested that vascular amyloid may lead to blood vessel dysfunction through toxic effects on smooth muscle cells (23, 33). However, in contrast to previous reports (33), we did not observe overt loss of smooth muscle cells in cerebrovascular regions with Medin deposits (Fig. 3*A*). Moreover, neither global endothelial cell volume (based on CD31 staining) nor astrocytic endfeet coverage of cerebral blood vessels (based on Aquaporin-4 staining), which is crucial for appropriate neurovascular coupling (25, 30), were affected by aging or in WT versus *Mfge8* C2 KO animals (*SI Appendix*, Fig. S5). While we cannot exclude that the lack of MFG-E8 affected other compartments of the brain, our data strongly suggest that aggregation of Medin (or larger MFG-E8 fragments) contributes to age-related vascular dysfunction in WT mice, possibly through affecting vascular elasticity (34).

Discussion

Our data presented here indicate that the most common human amyloid, Medin (or Medin-containing fragments of MFG-E8), also shows age-associated aggregation in WT mice and demonstrate a pathogenic role of its accumulation in driving age-associated vascular dysfunction. Strikingly, Medin deposits form in aging mice despite their relatively limited lifespan, reflecting the previous finding that Medin deposits can be found in the vast majority of people over 50 y of age (2). However, in mice, Medin aggregates do not stain with classical amyloid dyes (Congo Red, Methoxy-X04) and appear amorphous by EM, possibly reflecting their lower (predicted) aggregation propensity (Fig. 1*A*) or indicating an early stage of fibril formation and/or maturation. It has been reported that in human aortic tissue the amount of Medin in its amyloid state is significantly lower in patients with aortic aneurysm or dissection, while nonfibrillar Medin deposits are significantly higher in the diseased aorta (10) and correlate with reduced aortic elasticity (9). Thus, nonfibrillar forms of Medin could in fact be more pathogenic, and notably, we find that Medin deposits in the human brain vasculature do not stain with amyloid dyes. It has been reported that amyloids can exist as structurally distinct "strains" (with different affinity for common amyloid dyes), which propagate through prion-like mechanisms, i.e., through templated misfolding of the native peptide (e.g., refs. 35, 36). Thus, it is conceivable that different strains of Medin form in the mouse and human vasculature and become (locally) amplified, providing a possible explanation for the differences in amyloid dye affinity observed in our analyses. Further relating to the role of amyloids in vascular dysfunction, it has been shown that soluble amyloid-β monomers and oligomers significantly impair vascular function in Alzheimer's disease (e.g., refs. 37–39), and it will therefore be important to determine which specific types of Medin aggregates are responsible for inducing vascular dysfunction in the aging brain.

Although Medin is the most common human amyloid described so far, little is known about its contribution to disease. Correlative analyses of human tissue suggest that MFG-E8 and Medin may contribute to vasculitis and thoracic aneurysms and dissection (9, 10) as well as vascular dementia (11). Mechanistically, it has been hypothesized that Medin amyloid leads to cell toxicity through promoting inflammatory and oxidative stress, thereby altering the arterial wall structure and predisposing arteries to age-related vascular dysfunction and disease (40–43). However, these studies were unable to determine whether Medin aggregates were cause or consequence of pathological vascular changes. Our observation that Medin deposition occurs in murine blood vessels with age and is absent in *Mfge8* C2 KO animals allowed us to examine in living mice whether this process contributes to vascular dysfunction. Our results now provide direct evidence that Medin aggregation within (cerebral) blood vessels may be causal for vascular dysfunction. Whether this occurs independently or is interlinked with previously reported mechanisms of age-related cerebrovascular dysfunction (including increases in reactive oxygen species; ref. 26) requires further investigation. Nevertheless, our findings indicate that vascular function can be improved by preventing Medin aggregation. Given the high prevalence of cardiovascular, cerebrovascular, and neurodegenerative diseases in the aging population (44, 45), preservation of vascular function remains a major challenge in medical research (46–48). Targeting Medin aggregation should therefore be investigated as a novel therapeutic option to promote healthy aging of the vasculature. Notably, the NMR structure of the Medin-containing C2 domain of human MFG-E8 has been determined (Protein Data Bank ID code 2L9L; ref. 49); this may allow for rational drug design to prevent Medin aggregation through kinetic stabilization of its native structure, as exemplified by recent approaches to prevent transthyretin amyloidosis (50).

Finally, a potential interaction between Medin and amyloids in the brain is also of interest, because amyloidosis is prevalent in many neurodegenerative diseases. Previous experiments showed that Medin can act as a heterologous seed for the aggregation of serum amyloid A (51), but whether it interacts with other extracellular amyloids and in particular amyloid-β, which deposits both in the parenchyma as well as in blood vessels of the brain, remains unknown. Despite their structural similarities, amyloids do not necessarily coaggregate and can even show cross-inhibitory effects (52, 53). Therefore, understanding if and how Medin may contribute to age-related amyloidosis in the brain will be investigated in future studies.

Materials and Methods

1. M. D. Benson *et al*., Amyloid nomenclature 2018: Recommendations by the international society of amyloidosis (ISA) nomenclature committee. *Amyloid* **25**, 215–219 (2018).
2. G. Mucchiano, G. G. Cornwell 3rd, P. Westermark, Senile aortic amyloid. Evidence for two distinct forms of localized deposits. *Am. J. Pathol.* **140**, 871–877 (1992).
3. S. Peng *et al*., Medin and medin-amyloid in ageing inflamed and non-inflamed temporal arteries. *J. Pathol.* **196**, 91–96 (2002).
4. B. Häggqvist *et al*., Medin: An integral fragment of aortic smooth muscle cell-produced lactadherin forms the most common human amyloid. *Proc. Natl. Acad. Sci. U.S.A.* **96**, 8669–8674 (1999).
5. J.-S. Silvestre *et al*., Lactadherin promotes VEGF-dependent neovascularization. *Nat. Med.* **11**, 499–506 (2005).
6. D. Eisenberg, M. Jucker, The amyloid state of proteins in human diseases. *Cell* **148**, 1188–1203 (2012).
7. S. S. Najjar, A. Scuteri, E. G. Lakatta, Arterial aging: Is it an immutable cardiovascular risk factor? *Hypertension* **46**, 454–462 (2005).
8. T. J. Muckle, Giant cell inflammation compared with amyloidosis of the internal elastic lamina in temporal arteries. *Arthritis Rheum.* **31**, 1186–1189 (1988).
9. H. A. Davies *et al*., Idiopathic degenerative thoracic aneurysms are associated with increased aortic medial amyloid. *Amyloid* **26**, 148–155 (2019).
10. S. Peng *et al*., Role of aggregated medin in the pathogenesis of thoracic aortic aneurysm and dissection. *Lab. Invest.* **87**, 1195–1205 (2007).
11. N. Karamanova *et al*., Endothelial immune activation by medin: Potential role in cerebrovascular disease and reversal by monosialoganglioside-containing nanoliposomes. *J. Am. Heart Assoc.* **9**, e014810 (2020).
12. Z. Fu *et al*., Milk fat globule protein epidermal growth factor-8: A pivotal relay element within the angiotensin II and monocyte chemoattractant protein-1 signaling cascade mediating vascular smooth muscle cells invasion. *Circ. Res.* **104**, 1337–1346 (2009).
13. M. Wang *et al*., MFG-E8 activates proliferation of vascular smooth muscle cells via integrin signaling. *Aging Cell* **11**, 500–508 (2012).
14. A.-M. Fernandez-Escamilla, F. Rousseau, J. Schymkowitz, L. Serrano, Prediction of sequence-dependent and mutational effects on the aggregation of peptides and proteins. *Nat. Biotechnol.* **22**, 1302–1306 (2004).
15. A. Larsson *et al*., Unwinding fibril formation of medin, the peptide of the most common form of human amyloid. *Biochem. Biophys. Res. Commun.* **361**, 822–828 (2007).
16. I. Kholová, H. W. M. Niessen, Amyloid in the cardiovascular system: A review. *J. Clin. Pathol.* **58**, 125–133, 10.1136/jcp.2004.017293 (2005).
17. K. Atabai *et al*., Mfge8 is critical for mammary gland remodeling during involution. *Mol. Biol. Cell* **16**, 5528–5537 (2005).
18. E. F. Nandrot *et al*., Essential role for MFG-E8 as ligand for αvβ5 integrin in diurnal retinal phagocytosis. *Proc. Natl. Acad. Sci. U.S.A.* **104**, 12005–12010 (2007).
19. J. Stöhr *et al*., Purified and synthetic Alzheimer's amyloid beta (Aβ) prions. *Proc. Natl. Acad. Sci. U.S.A.* **109**, 11025–11030 (2012).
20. C. Sturchler-Pierrat *et al*., Two amyloid precursor protein transgenic mouse models with Alzheimer disease-like pathology. *Proc. Natl. Acad. Sci. U.S.A.* **94**, 13287–13292 (1997).
21. M. C. Herzig *et al*., Abeta is targeted to the vasculature in a mouse model of hereditary cerebral hemorrhage with amyloidosis. *Nat. Neurosci.* **7**, 954–960 (2004).
22. S. Peng, "Medin amyloid in human arteries and its association with arterial diseases," Dissertation, Uppsala Universitet, Uppsala, Sweden (2006).
23. S. Peng, J. Glennert, P. Westermark, Medin-amyloid: A recently characterized age-associated arterial amyloid form affects mainly arteries in the upper part of the body. *Amyloid* **12**, 96–102 (2005).
24. S. Tarantini, C. H. T. Tran, G. R. Gordon, Z. Ungvari, A. Csiszar, Impaired neurovascular coupling in aging and Alzheimer's disease: Contribution of astrocyte dysfunction and endothelial impairment to cognitive decline. *Exp. Gerontol.* **94**, 52–58 (2017).
25. C. Iadecola, M. Nedergaard, Glial regulation of the cerebral microvasculature. *Nat. Neurosci.* **10**, 1369–1376 (2007).
26. H.-M. Kang, I. Sohn, J. Jung, J.-W. Jeong, C. Park, Age-related changes in pial arterial structure and blood flow in mice. *Neurobiol. Aging* **37**, 161–170 (2016).
27. F. C. Maier *et al*., Longitudinal PET-MRI reveals β-amyloid deposition and rCBF dynamics and connects vascular amyloidosis to quantitative loss of perfusion. *Nat. Med.* **20**, 1485–1492 (2014).
28. L. Park, J. Anrather, H. Girouard, P. Zhou, C. Iadecola, Nox2-derived reactive oxygen species mediate neurovascular dysregulation in the aging mouse brain. *J. Cereb. Blood Flow Metab.* **27**, 1908–1918 (2007).
29. A. Y. Shih *et al*., Two-photon microscopy as a tool to study blood flow and neurovascular coupling in the rodent brain. *J. Cereb. Blood Flow Metab.* **32**, 1277–1309 (2012). Correction in: *J. Cereb. Blood Flow Metab.* **33**, 319 (2013).
30. D. Attwell *et al*., Glial and neuronal control of brain blood flow. *Nature* **468**, 232–243 (2010).
31. M. A. Hajdu, D. D. Heistad, J. E. Siems, G. L. Baumbach, Effects of aging on mechanics and composition of cerebral arterioles in rats. *Circ. Res.* **66**, 1747–1754 (1990).
32. A. Paini *et al*., Carotid and aortic stiffness: Determinants of discrepancies. *Hypertension* **47**, 371–376 (2006).
33. D. T. Winkler *et al*., Spontaneous hemorrhagic stroke in a mouse model of cerebral amyloid angiopathy. *J. Neurosci.* **21**, 1619–1627 (2001).
34. A. Larsson *et al*., Lactadherin binds to elastin–A starting point for medin amyloid formation? *Amyloid* **13**, 78–85 (2006).
35. C. Condello *et al*., Structural heterogeneity and intersubject variability of Aβ in familial and sporadic Alzheimer's disease. *Proc. Natl. Acad. Sci. U.S.A.* **115**, E782–E791 (2018).
36. M. Jucker, L. C. Walker, Propagation and spread of pathogenic protein assemblies in neurodegenerative diseases. *Nat. Neurosci.* **21**, 1341–1349 (2018).
37. R. Nortley *et al*., Amyloid β oligomers constrict human capillaries in Alzheimer's disease via signaling to pericytes. *Science* **365**, eaav9518 (2019).
38. Z. Suo *et al*., Soluble Alzheimers β-amyloid constricts the cerebral vasculature in vivo. *Neurosci. Lett.* **257**, 77–80 (1998).
39. K. Niwa *et al*., Abeta 1-40-related reduction in functional hyperemia in mouse neocortex during somatosensory activation. *Proc. Natl. Acad. Sci. U.S.A.* **97**, 9735–9740 (2000).
40. J. Madine, D. A. Middleton, Comparison of aggregation enhancement and inhibition as strategies for reducing the cytotoxicity of the aortic amyloid polypeptide medin. *Eur. Biophys. J.* **39**, 1281–1288 (2010).
41. H. Chiang, P. Chu, T. Lee, MFG-E8 mediates arterial aging by promoting the proinflammatory phenotype of vascular smooth muscle cells. *J. Biomed. Sci.* **26**, 61 (2019).
42. M. Wang, H. H. Wang, E. G. Lakatta, Milk fat globule epidermal growth factor VIII signaling in arterial wall remodeling. *Curr. Vasc. Pharmacol.* **11**, 768–776 (2013).
43. R. Q. Migrino *et al*., Amyloidogenic medin induces endothelial dysfunction and vascular inflammation through the receptor for advanced glycation endproducts. *Cardiovasc. Res.* **113**, 1389–1402 (2017).
44. S. W. Wen, C. H. Y. Wong, Aging- and vascular-related pathologies. *Microcirculation* **26**, e12463 (2019).
45. World Health Organization, "*Global status report on noncommunicable diseases 2014*" (World Health Organization, Geneva, Switzerland, 2014).
46. J. A. H. R. Claassen, Cognitive decline and dementia: Are we getting to the vascular heart of the matter? *Hypertension* **65**, 505–506 (2015).
47. M. P. Pase *et al*., Association of aortic stiffness with cognition and brain aging in young and middle-aged adults: The Framingham third generation cohort study. *Hypertension* **67**, 513–519 (2016).
48. J. C. de la Torre, Cerebral hemodynamics and vascular risk factors: Setting the stage for Alzheimer's disease. *J. Alzheimers Dis.* **32**, 553–567 (2012).
49. H. Ye *et al*., NMR solution structure of C2 domain of MFG-E8 and insights into its molecular recognition with phosphatidylserine. *Biochim. Biophys. Acta* **1828**, 1083–1093 (2013).
50. M. M. Alhamadsheh *et al*., Potent kinetic stabilizers that prevent transthyretin-mediated cardiomyocyte proteotoxicity. *Sci. Transl. Med.* **3**, 97ra81 (2011).
51. A. Larsson, S. Malmström, P. Westermark, Signs of cross-seeding: Aortic medin amyloid as a trigger for protein AA deposition. *Amyloid* **18**, 229–234 (2011).
52. T. Bachhuber *et al*., Inhibition of amyloid-β plaque formation by α-synuclein. *Nat. Med.* **21**, 802–807 (2015).
53. J. Coomaraswamy *et al*., Modeling familial Danish dementia in mice supports the concept of the amyloid hypothesis of Alzheimer's disease. *Proc. Natl. Acad. Sci. U.S.A.* **107**, 7969–7974 (2010).
54. J. K. Hefendehl *et al*., Long-term in vivo imaging of β-amyloid plaque appearance and growth in a mouse model of cerebral β-amyloidosis. *J. Neurosci.* **31**, 624–629 (2011).
55. J. K. Hefendehl *et al*., Repeatable target localization for long-term in vivo imaging of mice with 2-photon microscopy. *J. Neurosci. Methods* **205**, 357–363 (2012).
56. P. Füger *et al*., Microglia turnover with aging and in an Alzheimer's model via long-term in vivo single-cell imaging. *Nat. Neurosci.* **20**, 1371–1376 (2017).

Degenhardt et al.   PNAS | **September 22, 2020** | vol. 117 | no. 38 | **23931**

78

NEUROSCIENCE

Supplementary Information for

Medin aggregation causes cerebrovascular dysfunction in aging wildtype mice

Karoline Degenhardt, Jessica Wagner, Angelos Skodras, Michael Candlish, Anna Julia Koppelmann, Katleen Wild, Rusheka Maxwell, Carola Rotermund, Felix von Zweydorf, Christian Johannes Gloeckner, Hannah A. Davies, Jillian Madine, Domenico Del Turco, Regina Feederle, Tammaryn Lashley, Thomas Deller, Philipp Kahle, Jasmin K. Hefendehl, Mathias Jucker, Jonas J. Neher

Dr. Jonas J. Neher
Email: jonas.neher@dzne.de

This PDF file includes:

> Supplementary Materials and Methods
>
> Figures S1 to S5
>
> Tables S1 to S2
>
> SI References

1

Supplementary Materials and Methods

Human tissue

Ascending aortic tissue samples (Supplementary Table S1) were rapidly frozen in dry ice and isopentane slurry after collection, and immediately stored at –80°C prior to use. For histology, the tissue was formalin-fixed and paraffin-embedded and cut into 10 μm-thick sections.

Human brain tissue (Supplementary Table S2) was obtained from the Queen Square Brain Bank for Neurological Disorders (UCL Institute of Neurology, London, UK). 12-15 μm thick, FFPE brain sections from the frontal or temporal cortex were used for analysis.

Informed consent from all patients and ethical approval was obtained for all experiments (see main text for details).

Tissue collection

For brain and aorta preparation, mice were deeply anesthetized and transcardially perfused with phosphate-buffered saline (PBS). Brain hemispheres were separated, with one hemisphere freshly frozen on dry ice for biochemical analyses and the other stored for 24 h in 4 % paraformaldehyde (PFA). The PFA-fixed hemisphere was then transferred to 30% sucrose for another 48 h, and subsequently frozen in 2-methyl-butane. Coronal sections of 25 μm or horizontal sections of 40 μm thickness were cut with a freezing sliding microtome (Leica).

After removal of the perivascular adipose tissue, the aorta was also either freshly frozen on dry ice or fixed in PFA overnight followed by paraffin embedding and microtome sectioning at 5 μm thickness. Sections were mounted on glass slides and dried at 60°C overnight.

Blood was collected from deeply anesthetized mice by cardiac puncture (before perfusion) and serum samples were obtained by coagulation at room temperature for 10 min, centrifugation for 10 min at 2,000 rpm and collection of the cell-free supernatant.

For gel electrophoresis and ELISA analyses, tissue samples were homogenized in PBS using a Precellys® lysing kit for 20 % w/v brain homogenates in Tris-HCl buffer (50 mM Tris pH 8, 150 mM NaCl, 5 mM EDTA) or 1% (w/v) aorta homogenates in PBS, containing phosphatase and protease inhibitors (Pierce). Brain homogenates were sonicated in three cycles for 35 s each, at 4°C (Bioruptor, Diagenode). Total protein concentration of homogenates was quantified using a BCA assay (Pierce).

Electron microscopy

For electron microscopy, animals were perfused with PBS, followed by a mixture of 4% PFA and 0.5% glutaraldehyde in 0.1 M cacodylate buffer (pH 7.4, Science Services) for 15 min. Serial frontal brain sections were cut with a vibratome (Leica VT1000S), washed in TBS, incubated in 0.1% NaBH4 (Sigma-Aldrich), and blocked with 5% BSA for 1 h at room temperature (RT) to reduce non-specific staining. For MFG-E8 staining, goat polyclonal anti-murine MFG-E8 (R&D systems, 1:1,000) was used as primary antibody followed by a biotinylated specific anti-IgG (Vector

2

Laboratories, 1:200) as secondary antibody. After washing in TBS, sections were incubated in avidin–biotin– peroxidase complex (ABC-Elite; Vector Laboratories) for 90 min at RT and were reacted with diaminobenzidine (DAB) solution (Vector Laboratories) at RT. Sections were silver-intensified by incubation in 3% hexamethylenetetramine (Sigma-Aldrich), 5% silver nitrate (AppliChem), and 2.5% disodium tetraborate (Sigma-Aldrich) for 10 min at 60°C, in 1% tetrachlorogold solution (AppliChem) for 3 min, and in 2.5% sodium thiosulfate (Sigma-Aldrich) for 3 min. After staining, sections were washed in 0.1 M cacodylate buffer, osmicated (0.5% OsO_4 in cacodylate buffer), dehydrated (70 % ethanol containing 1% uranyl acetate (Serva)), and embedded in Durcupan (Sigma-Aldrich). Ultrathin sections were collected on single-slot Formvar-coated copper grids that were contrast enhanced with lead citrate for 4 min and examined using a Zeiss electron microscope (Zeiss EM 900).

Anti-human Medin antibody

For the custom-made anti-human Medin antibody, rats were immunized with synthetic ovalbumin-coupled Medin peptide aa 268-287 (RLDKQGNFNAWVAGSYGNDQ). Hybridoma supernatants were screened by ELISA on biotinylated peptides and positive clones were further validated by Western blotting and IF. Clone MFGS 1H4 (rat IgG2b) was recloned by limiting dilution to obtain a stable monoclonal cell line to be used for further experiments (cell culture supernatant 1:10 WB, 1:2 IF). As isotype control, cell culture supernatant of rat IgG2b was used.

Immunohistochemistry and quantification

Paraffin sections were deparaffinized and rehydrated using standard protocols. Free-floating brain sections were washed in PBS and endogenous peroxidase was quenched by incubation of the sections with 0.3% hydrogen peroxide (AppliChem) in PBS for 30 min. For enhancement of vascular Medin and MFG-E8 staining, brain sections were pretreated with 1 µg/mL proteinase K (in 1 mM $CaCl_2$, 50 mM Tris buffer, pH 7.6) at 37°C for 30 min, followed by deactivation in 10 mM EDTA (pH 6) at 90°C for 10 min (1). Human aorta paraffin sections were boiled in citrate buffer (1.8 mM citric acid, 8.2 mM trisodium citrate, pH 6) at 90°C for 30 min. Unspecific antibody binding was blocked by incubation with 2% normal donkey serum (DS) in PBS containing 0.3% Triton X-100, and primary antibody (diluted in the same medium) was incubated at 4°C overnight with agitation, followed by washing and incubation with the secondary antibody (diluted in 1% DS-PBS) using either ABC and Peroxidase Substrate kits (Vectastain) or appropriate fluorescently labelled secondary antibodies (according to the manufacturer's instructions, Invitrogen or Jackson ImmunoResearch, 1:250). To reduce autofluorescence (from various sources such as lipofuscin, elastin or collagen) in brain sections, TrueBlack™ Quencher (Biotium) was applied (1:20 in 70% ethanol) for 5-10 s according to the manufacturer's instructions.

Primary antibodies used were an anti-human Medin antibody (clone 1H4; see above), a goat polyclonal anti-murine MFG-E8 antibody, with high affinity for the C2 domain (R&D systems,

3

1:1,000; cp. epitope mapping Suppl. Fig. 1), anti-SMA (Dako, 1:200), anti-AQP4 (Merck, 1:1000), anti-CD31 (BD Biosciences, 1:50). For nuclear staining, sections were incubated in Nuclear Fast Red (1%, Fluka, in 5% AlSO$_4$, Merck) for 5 min. Amyloid staining was performed using Methoxy-X04 (4% vol of 10 mg/ml in DMSO and 7.7% vol CremophorEL in 88.3% PBS) for 30 min at RT or Congo red, as described (2). For labelling of arterioles, Alexa hydrazide (1:1000 from 2 mM stock solution) was added for 90 s (3).

Images were acquired using a Zeiss Axioplan 2 with the AxioVision 4.7 software (Zeiss) using 40x/0.75 objective, with fixed camera exposure time and lamp intensity for comparative stainings. Image background was subtracted using an inbuilt Fiji plugin (Rolling-Ball background correction). Optical sections were acquired on a Zeiss LSM 510 META (Axiovert 200M) confocal microscope with a 20x/0.5 (air) or an oil immersion 40x/1.3 or 63x/1.4 objective on the LSM software 4.2 (Carl Zeiss), using sequential excitation of fluorophores (A488, A568, A647) or amyloid ligands (Methoxy-X04, Congo red). Maximum intensity projections were generated with Fiji.

For automated quantification of vascular MFG-E8, fluorescence images were acquired on a Zeiss AxioObserver.Z1 Slide Scanner, using a 20x/0.8 objective for image acquisition of whole brain sections, followed by semi-automated and blinded analysis with Fiji using custom-written plugins (available on request). For this automated, low magnification analysis, a rat monoclonal anti-murine MFG-E8 (R&D systems, 1:500) was used in combination with the anti-SMA antibody (Dako, 1:200), as this monoclonal anti-murine MFG-E8 showed higher signal in the vasculature compared to the parenchyma. Automated selection of the whole brain area as region of interest (ROI) was manually checked and corrected if necessary. Fluorescence channels for MFG-E8 and SMA were split and if needed, intensity thresholds were manually adjusted to exclude unspecific background signal. For every section, the area of MFG-E8 and SMA staining in the ROI was measured. To determine the vascular MFG-E8 signal, thresholded SMA area was converted to a binary mask and the area and intensity of the masked MFG-E8 signal was determined. For each animal, the total vascular MFG-E8 area (μm^2) was normalized to the total area of SMA (μm^2) in a random set of every 12th systematically sampled coronal brain sections (excluding olfactory bulb and cerebellum).

Volume of endothelial cells and astrocytic endfeet coverage on blood vessels were determined by 3D-reconstruction (Imaris software with XTension "Surface Surface Contact Area" by Matthew Gastinger, Bitplane) of endothelial cells (CD31) and astrocytic end feet (AQP4) signal in 5 µm z-stacks (6 images in three different sections per animal, 40x/1.3 objective).

4

Medin purification protocol

Amyloid was extracted from human and mouse aortic tissue according to a previous published protocol for Amyloid-β purification from mouse brain (4). Briefly, 50 mg of human aortic tissue or 75 mg of pooled fresh-frozen aortas from 16 mice were homogenized in 2 ml calcium- and magnesium-free PBS using a Glass-Teflon homogenizer (total homogenate =TH). TH was then incubated with citrate lysis buffer (10 mM citrate pH 6, 1 mM EDTA, 1% wt/vol Triton X-100) for 30 min on ice. The aorta lysate (Lysed homogenate = LH) was adjusted to 18% (wt/vol) iodixanol (OptiPrep, Sigma-Aldrich) and centrifuged twice through an iodixanol gradient (SW41 Ti rotor, Beckmann, 60.000 x g, 4°C). The top layer was discarded; the next two layers and their interphases were collected (Fraction 1 and 2 = F1, F2) and diluted in citrate buffer (10 mM citrate pH 6, 137 mM NaCl, 1 mM EDTA). After centrifugation for 1 hour at 21,000 x g, the pellet was resuspended in 400 µl Tris buffer (10 mM, pH 8.3, 1.71 M NaCl) containing 1% (wt/vol) zwittergent 3-14 (P1). After centrifugation for 30 min at 135,000 x g, the supernatant was discarded, and the pellet was resuspended in 100 µl TMS buffer (50 mM Tris–HCl, pH 7.8; 100 mM NaCl, 10 mM MgCl2) and treated with 300 units/mL of Benzonase at 37°C overnight (P2). Samples were ultracentrifuged for 30 min at 135,000 x g. Residual proteins in the pellet were digested with 40 µg/ml proteinase K (Fisher Scientific) in TMS buffer for 1 h at 37 °C and stopped by the addition of 2 mM PMSF. The digested samples (P3) were adjusted to 1.71 M NaCl and centrifuged for 30 min at 135,000 x g through a 1 M sucrose layer. The pellet, P4, was then resuspended in 0.1 M sodium acetate buffer.

Cloning of MFG-E8 domains and Transfection of HEK cells

The psd44-iGFP-MFGE8-long vector (generated by A. Mariotti, Université Lausanne (5) and distributed by AddGene) was amplified for full-length MFG-E8 expression after Ex-Taq PCR and verification via gel electrophoresis (FL-MFG-E8). Additionally, the four different MFG-E8 domains (E1, E2, C1, C2) were subcloned and amplified by Ex-Taq-PCR using specifically designed primers and transformed into *E. coli* DH5α cells. Sequences were verified using BigDye Terminator v.3.1 and an ABI 3130xl Genetic Analyzer (Applied Biosystems). Primer sequences can be obtained on request. DNA of FL-MFG-E8 and its individual domains were cloned using SalI/NotI restriction sites into pCMV-3xFLAG for transfection of HEK293E cells, which were cultured in Dulbecco's modified Eagle's medium (DMEM) with 10% FCS at 37 °C in 5% CO2. Transient transfections with DNA were performed with FuGENE and OptiMEM (Roche Applied Science) following the manufacturer's instructions. HEK293E cells were lysed in RIPA buffer (50 mM Tris-HCl pH 8.0, 150 mM NaCl, 1% NP-40, 0.5% NaDesoxycholate, 0.5% SDS) and pelleted at 18,000rpm for 15 min at 4 °C. Total protein concentration of RIPA lysates was determined with the bicinchoninic acid (BCA) protein assay kit (Pierce).

5

Western Blotting

Samples were diluted and denatured in loading buffer (10 % glycerol, 2 % SDS, 2 % β-mercaptoethanol, 0.1 M Tris-HCl pH 8.6), boiled at 95°C for 5 min and loaded on a Tris-Tricine 10-20 % or Bis-Tris 4-12% gradient gel (Invitrogen). For detection of MFG-E8 in total homogenates, brain samples (15µg total protein per sample) were preheated for 5 min in 8M Urea at 70°C before denaturation in loading buffer. After electrophoresis, gels were transferred to a nitrocellulose membrane in a semi-dry blotting system. Transfer was confirmed by Ponceau-S staining. Blocking was performed either with 5% milk (FLAG-M2, 1H4, 6e10) or 5% donkey serum (polyclonal anti-murine MFG-E8) in PBS-T for 1 h. For detection of Medin or Aβ, membranes were boiled in PBS for 5 min at 90°C. Subsequently, membranes were incubated overnight at 4°C with the primary antibody in PBS-T. Primary antibodies used were goat polyclonal anti-murine MFG-E8 (R&D systems, 1:1,000), anti-Flag M2-Peroxidase (HRP) (Sigma, 1:30,000), anti-human Medin 1H4 (1:10) and anti-Aβ 6e10 (Covance, 1:2,500). Membranes were then probed with the respective secondary horseradish peroxidase (HRP)-labelled antibodies (1:20,000, Jackson ImmunoLaboratories). Protein bands were detected using chemiluminescent peroxidase substrate (ECL prime, GE Healthcare).

Enzyme-linked immunosorbent assay (ELISA)

Quantification of mouse MFG-E8 by ELISA (R&D Systems) in serum, aorta and brain was performed according to the manufacturer's instructions. Serum samples were pre-diluted 1:3, 20% brain homogenates 1:10 and 1% aorta homogenates 1:500 before the measurements. Protein levels were normalized to the total protein content as measured by BCA protein assay (Pierce). Measurements were performed on a FLUOstar Omega reader (BMG Labtech).

Preparation and aggregation of recombinant human Medin

Recombinant human Medin was produced as previously reported (6) and was aggregated *in vitro* at a concentration of 27 µg/ml in Tris-HCl buffer (50 mM Tris pH 8, 150 mM NaCl, 5 mM EDTA) for 48h at 37°C without agitation.

Mass spectrometry (LC-MSMS)

Prefractionation of 10% aorta homogenates in PBS was performed via SDS-polyacrylamid gel electrophoresis according to standard methods on the Invitrogen NuPAGE system (10% gel). The separated proteins were fixed in 50% MeOH containing 12% acetic acid for 30 min followed by staining with 0.4% Coomassie Brilliant Blue G250 prior to dissection of gel bands of <17 kDa protein size. Protein bands were de-stained and washed by incubation in 40% acetonitrile in HPLC grade water for 20 min and shortly dehydrated in 100% acetonitrile. Dried gel plugs were exposed to 5 mM DTT for 15 min at 60°C, which was replaced by 25 mM iodacetamid for 45 min at ambient temperature in the dark. Washing with 40% and 100% acetonitrile was repeated. After drying,

6

proteins were subjected to in-gel proteolysis using trypsin (Sigma-Aldrich, 10 ng/µl in 50 mM ammonium bicarbonate buffer) over night at 37°C. Peptides were extracted by subsequent incubation of the gel plugs in 2.5% trifluoracetic acid (TFA), 0.5% TFA in 50% acetonitrile and 0.5% TFA in 100% acetonitrile each for 15 min at room temperature and concentrated via Speed Vac (35°C, vacuum).

Extracted peptides were analyzed by LC/MSMS using a nanoflow HPLC system (Ultimate 3000 RSLC; Thermo Fisher) coupled to an Orbitrap Q-Excative (Thermo Fisher) tandem mass spectrometer. Peptides were separated by reversed C-18 chromatography and 180-min gradients. MS1 spectra were acquired in the Orbitrap at 70K resolution. After selection of the 10 most intense precursor ions from the MS1 scans for HCD fragmentation (Top 10 method), MS2 spectra were acquired at 17.5K. For database search, tandem mass spectra were extracted by MSConvert (ProteoWizard version 3.0.7331). Charge state deconvolution and de-isotoping were not performed. All MS/MS samples were analyzed using Mascot (Matrix Science; version 2.5.1). Mascot was set up to search the SwissProt database (version 2019_08, selected for either homo sapiens [20431 entries] or mouse [17030 entries]) assuming the proteolytic enzyme trypsin. Mascot was searched with a fragment ion mass tolerance of 0.60 Da and a parent ion tolerance of 10.0 PPM. Carbamidomethyl of cysteine was specified in Mascot as a fixed modification. Deamidation of asparagine and glutamine, oxidation of methionine were specified in Mascot as variable modifications. Scaffold (version 4.4.5, Proteome Software Inc.) was used for downstream analysis and visualization.

2-photon imaging of vascular function

Cranial window surgeries were carried out as previously described in detail (7–9). Briefly, animals were anaesthetised (fentanyl, 0.05 mg / kg; midazolam, 5 mg / kg; medetomidine, 0.5 mg / kg) and a circular cranial window (4 mm diameter) was placed over the right somatosensory cortex hindlimb region. A titanium ring was then positioned over the cranial window, allowing for precise fixation of the cranial window at the 2-photon imaging setup. After completion of surgery, anaesthesia was terminated via an i.p. injection of antidote (atipamezole, 2.5 mg / kg; flumazenil, 0.5 mg / kg).

For *in vivo* 2-photon imaging, mice were anaesthetised (isoflurane; 5 % for induction, 1 - 1.5 % for maintenance) and administered an i.v. injection of fluorescein-conjugated dextran in sterile saline (70 kDa; Sigma Aldrich 46945) to visualise the cerebrovasculature as described previously (9). The mouse was then secured in a custom head-fixation device (8) positioned underneath the objective lens at the imaging setup. Imaging was performed using a motorized custom 2-photon microscope (10) equipped with a Chameleon Ultra II laser (Coherent). Motor control and image acquisition were controlled using an MP285A (Sutter Instrument Company) and ScanImage software (Vidrio Technologies). 2-photon excitation of fluorescein-conjugated dextran was performed at 800 nm (laser power <50 mW). Emission was detected using a non-descanned detector (Hamamatsu Photonics), a T560lpxr-UF2 dichroic and an ET525/50m-2p bandpass filter

7

(Chroma Technology Corporation). Z-stack images (512 x 512, 2 µm steps) were taken using either a Plan-Apochromat 5x/0.16 (Zeiss) or a HC Fluotar 25x/0.95 W (Leica Microsystems) objective. Line scans (positioned perpendicularly across the arterioles within the somatosensory cortex hindlimb region) were acquired using the 25x objective at 99.99 Hz using the arbitrary line scan function in ScanImage. A 50 s recording was taken for each vessel analyzed. Mechanical stimulation of the left hindlimb was triggered 5 s after the start of each recording as a single pulse using a Master-9 pulse stimulator (A.M.P.I), with a minimum interval of 2 min between subsequent hindlimb stimulations.

For quantification, the 16-bit fluorescence intensity signal along the line over the scan time was visualized in ImageJ in the form of a 2-dimensional image ('kymograph') (11). A custom-made plugin was written in ImageJ to automatically import the data to kymographs, apply a Gaussian Blur filter of 3 pixel radius to remove spike noise and threshold the resulting image using an automated threshold based on Shannon's entropy. Pixels of the resulting binary image of the kymograph were added along the time-dimension, creating a sequence of values that constitute the vessel diameter changes over the scan time. In order to render the data comparable across ROIs and animals, they were normalized to a scale of 0 to 1. To exclude higher frequency artifacts, as well as breathing and heartbeat capillary changes, the normalized data were further filtered using MATLAB. Using the Fourier power spectrum, we could determine a prominent frequency of 0.8 Hz and a subsequently broad high-frequency component thereafter. We thus designed a low-pass filter to attenuate frequencies higher than 0.75 Hz. The filtered data were time-shifted to correct for the low-pass filter phase response (group delay). The area under the curve of the filtered capillary diameter changes over time were further calculated in MATLAB, by approximating the curve integral via the trapezoidal method. Finally, in order to calculate the initial response of the blood vessels, the time constant $t_{1/2}$ of the response was obtained using a One-phase exponential fit directly implemented in GraphPad Prism, on the first 5 s of the normalized filtered capillary diameter change curves.

As it is currently not possible to label Medin deposits during *in vivo* imaging, arterioles of similar diameter were selected at random from the MCA territory. For this reason, we considered each blood vessel as an independent measurement, as we observed strong intra-individual differences in wildtype animals that may result from the presence/absence of Medin deposits, which we found to be unevenly distributed throughout the blood vessels.

TANGO analysis

The TANGO algorithm (12) was used to predict β-aggregation propensity of the Medin peptide. For this calculation the following parameters were chosen: pH 7.4, temperature 298.15 K, ionic strength 0.02 M and 1 mM concentration.

8

Statistics

Statistical analysis was performed using Prism 6 software. Data were tested for normal distribution (Shapiro-Wilk test) and statistical outliers were identified and removed (ROUT method). If data were normally distributed, ANOVA was performed, followed by Tukey's multiple comparison test. If data were not normally distributed, a non-parametric test (Kruskal-Wallis) was performed, followed by multiple comparison of the mean ranks with Dunn's correction if $P<0.05$. As we did not observe differences between male and female animals regarding Medin/MFG-E8 levels/deposition etc., we did not test further for gender effects in any of our analyses. All data shown are means ± S.E.M.

Linear regressions to analyze the impact of aging on vascular accumulation of MFG-E8/Medin were generated using JMP software (version 14.2.0). If necessary, data were first log10 transformed to achieve a normal distribution. Data were then analyzed using the 'Fit model' function, generating residual vs. leverage plots, where a least squares line (red) and confidence bands (shaded red) provide a visual representation of the statistical significance (at the 5% level) of the effect of X ("Age"); a significant effect is evident by the crossing of the confidence lines (shaded red/red) through the blue line in the graph in the graph, which indicates the mean of the Y leverage residuals. To calculate the data points in the graph, the mean value of Y is added to the Y-residuals and the mean of the X-value is added to the X-residuals, generating "leverage residuals", and these pairs of residuals are then used to generate the effect leverage plots shown (see e.g. [13]).
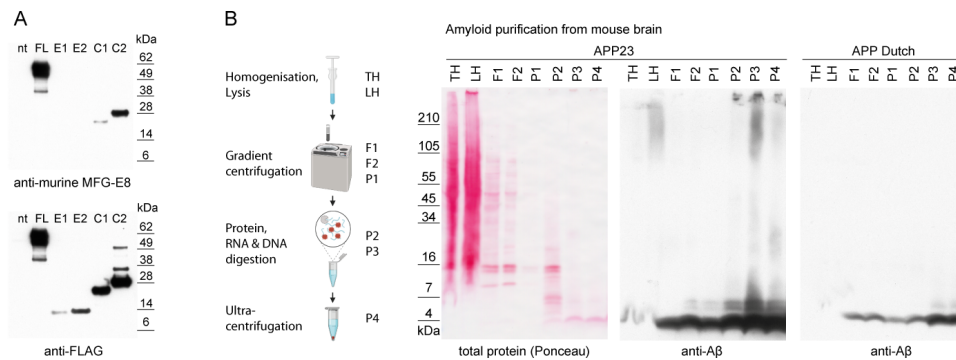
9

Fig. S1: Epitope mapping of the polyclonal anti-murine MFG-E8 antibody used throughout this study and amyloid extraction from transgenic mouse brain.

A, *top*: Western blotting of recombinantly expressed full-length (FL) MFG-E8 and its individual domains (E1, E2, C1, C2) demonstrates that the polyclonal anti murine-MFG-E8 antibody has the highest affinity for epitope(s) within the Medin-containing C2 domain, with low affinity also for the C1 domain and no detection of the E1 and E2 domains. *bottom,* Input control using the FLAG-tag of recombinantly expressed proteins. **B**, *left:* Graphical summary of the purification procedure for the enrichment of amyloids from tissue homogenates. *Right*, Proof-of-principle experiment demonstrating the elimination/digestion of soluble proteins during the procedure (Ponceau staining of total protein) while enriching amyloid-β from APP23 and APP Dutch transgenic mouse brains (anti-Aβ staining).
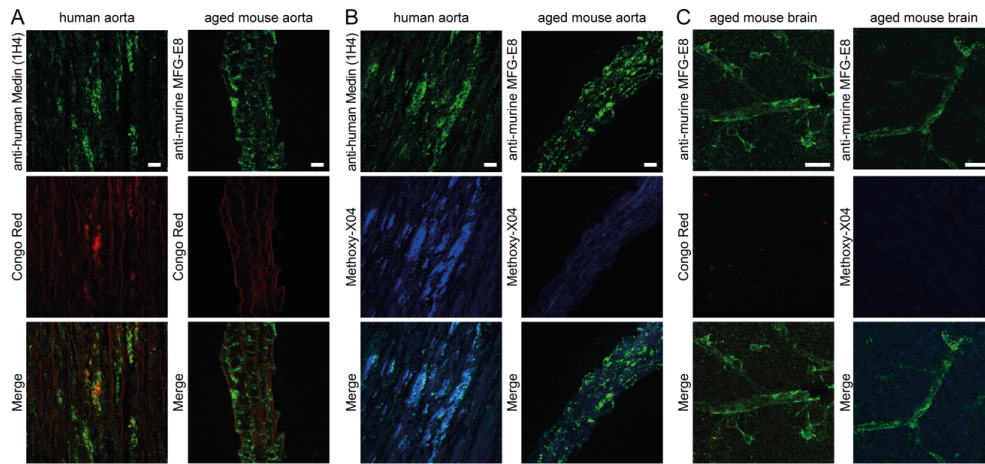
10

Fig. S2: Lack of affinity for amyloid dyes in the aged mouse aorta and brain.

A/B, The amyloid binding dyes Congo Red (A) and Methoxy-X04 (B) stain Medin+ aggregates in the human aorta but not MFG-E8+ aggregates the aged mouse aorta. **C**, In the aged mouse brain, MFG-E8+ vascular aggregates are not stained by Congo Red or Methoxy-X04 (cp. Fig. 3 for human brain). Scale bar: 20 µm.
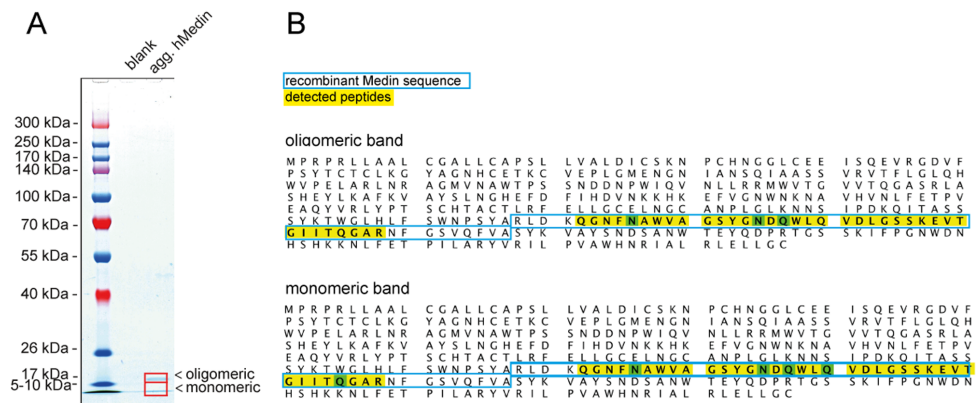
Fig. S3: **Mass spectrometry analysis of aggregated recombinant human Medin.** Recombinant human Medin (hMedin) was aggregated for 48 h at 37°C and **A**, pre-fractionated by gel electrophoresis, showing monomeric and oligomeric bands, which were excised and analyzed by **B**, mass spectrometry. The coverage of the recombinant Medin sequence (blue frame) by detected peptides is marked in yellow (green= post-translational modification i.e. deamidation).
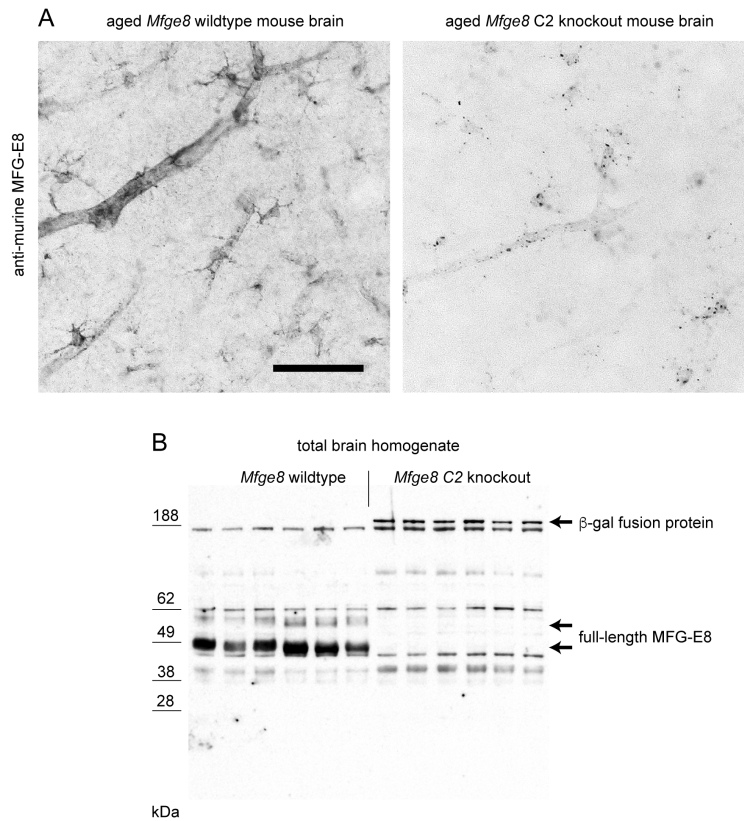
12

Fig. S4: MFG-E8 is retained within cells in Mfge8 C2 knockout animals

A, MFG-E8 staining in aged wildtype brain (>20-month-old) is widespread and evident both in blood vessels as well as astrocytes. In contrast, *Mfge8* C2 KO animals show only a punctate intracellular staining pattern (in parenchymal as well as vascular cells; a blood vessel is recognizable in the center of the image), in line with retention of the MFG-E8/β-galactosidase fusion protein inside the cells, resulting from the introduction of a transmembrane domain (cp. Fig. 1). **B**, Western Blotting of total brain homogenate. In wildtype animals two isoforms of the full-length MFG-E8 protein are clearly visible as two distinct bands ~50/60 kDa, but are absent in *Mfge8* C2 KO animals, where the fusion protein appears as a distinct band ~200 kDa. Scale bar = 50 μm.
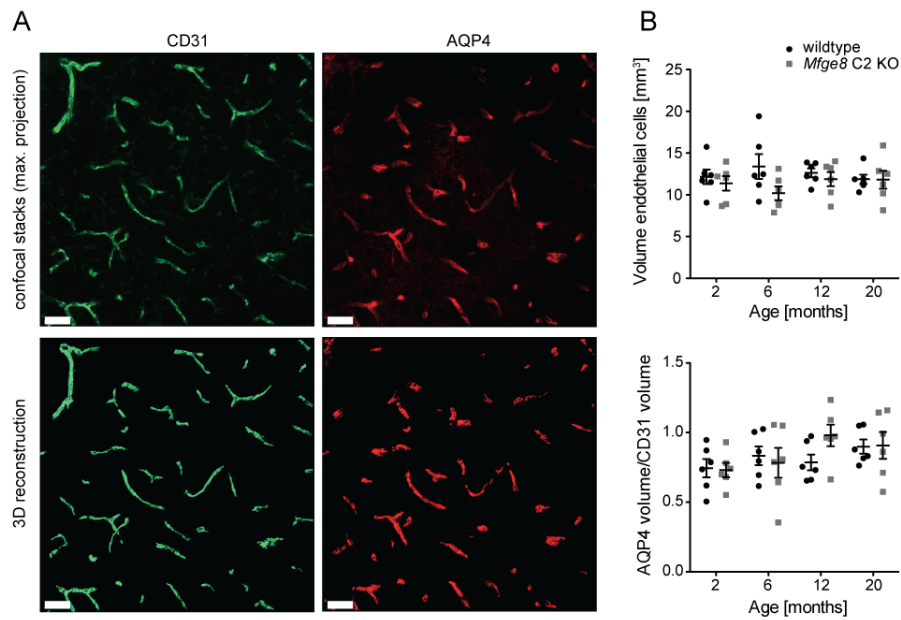
13

Fig. S5: Astrocytic endfeet coverage of brain blood vessels does not change with age or *Mfge8* **C2 knockout.**

A, Anatomically matched brain sections of wildtype and *Mfge8* C2 KO animals (3 sections per mouse with 3 males and 3 females per age group) were stained for endothelial cells (CD31) and astrocytic endfeet (Aquaporin-4, AQP4). Confocal z-stacks (5 µm; 6 per animal; *top images*) were acquired and 3D-reconstructed using Imaris software (*bottom images*) to quantify **B**, the volume of endothelial cells (*top*) and the astrocytic endfeet coverage (AQP4) of endothelial cells (*bottom*). Scale bar: 30 µm.

14

Table S1: Patient information of aorta donors

Case	Age (years)	Sex	Clinical presentation	Tissue source	Histology	Extraction
Patient 1	69	F	Aneurysm	Surgery	X	X
Patient 2	70	F	Cardiac arrest, hypoxic brain injury	Post-mortem	X	
Patient 3	67	M	Aneurysm	Surgery	X	X
Patient 4	81	F	Aneurysm	Surgery		X

Table S2: Patient information of brain donors

Case	Age (years)	Sex	Clinical presentation	Braak and Braak	CERAD	THAL	ABC score
Patient 5	80	F	Normal/ path ageing	2	none	0	A0B1C0
Patient 6	86	F	Normal/ path ageing	2	none	0	A0B1C0
Patient 7	84	M	Control	0	none	0	A0B0C0

SI References

1. H. Kai, *et al.*, Enhanced Antigen Retrieval of Amyloid β Immunohistochemistry: Re-evaluation of Amyloid β Pathology in Alzheimer Disease and Its Mouse Model. *J. Histochem. Cytochem.* **60**, 761–769 (2012).

2. S. Peng, *et al.*, Role of aggregated medin in the pathogenesis of thoracic aortic aneurysm and dissection. *Lab. Invest.* **87**, 1195–1205 (2007).

3. Z. Shen, Z. Lu, P. Y. Chhatbar, P. O'Herron, P. Kara, An artery-specific fluorescent dye for studying neurovascular coupling. *Nat. Methods* **9**, 273–276 (2012).

4. J. Stohr, *et al.*, Purified and synthetic Alzheimer's amyloid beta (Abeta) prions. *Proc. Natl. Acad. Sci. U. S. A.* **109**, 11025–11030 (2012).

5. C. Carrascosa, *et al.*, MFG-E8/lactadherin regulates cyclins D1/D3 expression and enhances the tumorigenic potential of mammary epithelial cells. *Oncogene* **31**, 1521–1532 (2012).

6. H. A. Davies, *et al.*, Oxidative Stress Alters the Morphology and Toxicity of Aortic Medial Amyloid. *Biophys. J.* **109**, 2363–2370 (2015).

7. J. K. Hefendehl, *et al.*, Long-term in vivo imaging of β-amyloid plaque appearance and growth in a mouse model of cerebral β-amyloidosis. *J. Neurosci.* **31**, 624–629 (2011).

8. J. K. Hefendehl, *et al.*, Repeatable target localization for long-term in vivo imaging of mice with 2-photon microscopy. *J. Neurosci. Methods* **205**, 357–363 (2012).

9. P. Füger, *et al.*, Microglia turnover with aging and in an Alzheimer's model via long-term in vivo single-cell imaging. *Nat. Neurosci.* **20**, 1371–1376 (2017).

10. D. G. Rosenegger, C. H. T. Tran, J. LeDue, N. Zhou, G. R. Gordon, A High Performance, Cost-Effective, Open-Source Microscope for Scanning Two-Photon Microscopy that Is Modular and Readily Adaptable. *PLoS One* **9**, e110475 (2014).

11. K. Kisler, *et al.*, In vivo imaging and analysis of cerebrovascular hemodynamic responses and tissue oxygenation in the mouse brain. *Nat. Protoc.* **13**, 1377–1402 (2018).

12. A.-M. Fernandez-Escamilla, F. Rousseau, J. Schymkowitz, L. Serrano, Prediction of sequence-dependent and mutational effects on the aggregation of peptides and proteins. *Nat. Biotechnol.* **22**, 1302–1306 (2004).

13. J. Sall, Leverage Plots for General Linear Hypotheses. *Am. Stat.* **44**, 308–315 (1990).

16

3.2.2 Medin interacts with Aβ to promote cerebral β-amyloid angiopathy

Jessica Wagner*, Karoline Degenhardt*, Angelos Skodras, Ulrike Obermüller, Katleen Wild, Anupriya Dalmia, Lisa M. Häsler, Marius Lambert, Ping Liu, Marleen Veit, Hannah A. Davies, Jillian Madine, Regina Feederle, Domenico Del Turco, K. Peter R. Nilsson, Tammaryn Lashley, Thomas Deller, Lary C. Walker, Peter Heutink, Mathias Jucker, Jonas J. Neher. *contributed equally

Submitted

Medin interacts with Aβ to promote cerebral β-amyloid angiopathy

Jessica Wagner[1,2,3,14], Karoline Degenhardt[1,2,3,14], Angelos Skodras[1,2], Ulrike Obermüller[2], Katleen Wild[1], Anupriya Dalmia[1], Lisa M. Häsler[1,2], Marius Lambert[1,2], Ping Liu[1,2], Marleen Veit[1,2,3], Hannah A. Davies[4,5], Jillian Madine[5,6], Regina Feederle[7,8], Domenico Del Turco[9], K. Peter R. Nilsson[10], Tammaryn Lashley[11,12], Thomas Deller[9], Lary C. Walker[13], Peter Heutink[1], Mathias Jucker[1,2], Jonas J. Neher[1,2*]

[1]German Center for Neurodegenerative Diseases (DZNE), Tübingen, Germany
[2]Department of Cellular Neurology, Hertie Institute for Clinical Brain Research, University of Tübingen, Germany
[3]Graduate School of Cellular and Molecular Neuroscience, University of Tübingen, Germany;
[4]Department of Cardiovascular and Metabolic Medicine, Institute of Life Course and Medical Sciences, University of Liverpool, United Kingdom;
[5]Liverpool Centre for Cardiovascular Sciences, University of Liverpool, Liverpool L14 3PE, United Kingdom;
[6]Department of Biochemistry and Systems Biology, Institute of Systems, Molecular and Integrative Biology, University of Liverpool, United Kingdom
[7]Monoclonal Antibody Core Facility, Institute for Diabetes and Obesity, Helmholtz Zentrum München, Research Center for Environmental Health, 85764
Neuherberg, Germany;
[8]DZNE, Munich, Germany;
[9]Institute of Clinical Neuroanatomy, Dr. Senckenberg Anatomy, Neuroscience Center, Goethe University, Frankfurt/Main, Germany;
[10]Department of Physics, Chemistry and Biology, Linköping University, Linköping, Sweden;
[11]Queen Square Brain Bank for Neurological Disorders, University College London Queen Square Institute of Neurology, London WC1N 1PJ, United Kingdom
[12]Department of Neurodegenerative Disease, University College London Queen Square Institute of Neurology, London WC1N 1PJ, United Kingdom
[13]Department of Neurology and Yerkes National Primate Research Center, Emory University, Atlanta, GA 30322
[14] equal contribution

*correspondence to: jonas.neher@dzne.de

Aggregates of Medin amyloid (a fragment of the protein MFG-E8) are found in the vasculature of virtually every person over 50 years of age[1,2], making it the most common amyloid known to date. We recently reported that Medin aggregates also form in the vasculature of ageing wildtype mice and cause dysfunction of cerebral blood vessels[3]; here, we find in two mouse models of β-amyloidosis, that Medin co-localises with amyloid-β deposits and that genetic Medin-deficiency reduces amyloid deposition, in particular vascular β-amyloidosis. Moreover, we demonstrate that brain levels of MFG-E8 increase with vascular but not parenchymal β-amyloidosis in mice. Accordingly, we show that in patients with Alzheimer's disease, increased *MFGE8* expression predicts cognitive decline independent of plaque load and tau pathology, and that Medin localises primarily to cerebral blood vessels with vascular β-amyloidosis. Therefore, we tested if Medin may directly interact with amyloid-β to drive vascular amyloidosis, and show that i) lack of Medin alters amyloid structure in mice, ii) amyloid-β and Medin form heterologous amyloid fibrils *in vitro*, and iii) intracerebral injection of aorta-derived Medin induces premature

β-amyloidosis in mice. Our data highlight Medin aggregation as a vascular risk factor and therapeutic target for Alzheimer's disease.

Amyloidosis is caused by local or systemic accumulation of insoluble, misfolded and aggregated proteins; 36 amyloids have so far been identified, many of them associated with tissue dysfunction and disease[4], including major neurodegenerative diseases[5,6]. The most common human amyloid known to date is Medin, a 50 amino acid peptide cleaved (by unknown mechanisms) from the protein Milk fat globule EGF-like factor-8 (MFG-E8; also known as lactadherin). Medin amyloid was first described in the aorta but is also found in other arteries of the upper body of ~97 percent of the Caucasian population above 50 years of age[1,2,7]. Previous studies implied that Medin aggregates may weaken and lead to the degeneration of the arterial wall, and may cause arterial stiffening and cerebrovascular dysfunction[8–12]. In line with these studies, we recently demonstrated that Medin also exists in ageing wildtype mice, where it forms vascular aggregates that directly contribute to cerebrovascular dysfunction[3]; therefore, Medin deposition may be a risk factor for vascular dementia. Independently, a recent study of post-mortem human samples demonstrated that Medin aggregates are increased in cerebral arterioles of vascular dementia and AD patients compared to cognitively healthy controls, and that amongst cerebrovascular pathologies, arteriolar Medin was the best predictor of AD diagnosis[13]. These findings raise the question of whether elevated Medin levels are the cause or consequence of AD pathology. Therefore, we here studied the role of Medin in mouse models of cerebral β-amyloidosis and in post-mortem human brain tissue.

Medin deficiency reduces β-amyloidosis in APP transgenic mice

To study if Medin contributes to AD pathology, we first stained tissue from two APP transgenic mouse lines, APPPS1 and APP23[14,15], using a polyclonal anti-murine MFG-E8 antibody; we previously established that this antibody recognises extracellular Medin aggregates in ageing wildtype animals due to its high affinity for epitopes located in the Medin-containing C2 domain, but also detects epitopes in the C1 domain with lower affinity[3] (Fig. 1a). Staining with this antibody co-localised extensively with amyloid plaques in both APP transgenic models (Figs. 1b/c), being detectable throughout the plaques by confocal microscopy (Fig. 1d). In contrast, amyloid plaque co-staining was absent when we genetically eliminated Medin by cross-breeding the APP transgenic lines with mice lacking the Medin-containing C2 domain of *Mfge8* (*Mfge8* C2 KO)[16]. However, due to the presence of the truncated MFG-E8 C2 KO variant (which is retained intracellularly in the *Mfge8*-expressing cells), APPPS1/APP23 x *Mfge8* C2 KO animals still showed

punctate staining in astrocytes, reflecting the recognition of C1 domain epitopes by the polyclonal MFG-E8 antibody (Figs. 1b-c and Extended Data Fig. 1). Notably, the lack of extracellular MFG-E8/Medin significantly reduced plaque deposition at early stages of pathology in both APP mouse lines. In particular, Aβ plaque load was reduced by ~40% in 2-month-old APPPS1 x *Mfge8* C2 KO compared to APPPS1 x *Mfge8* wildtype (WT) animals (Fig. 1e; with APPPS1 mice showing first plaques around 6 weeks) and by ~50% in 6- and 9-month-old APP23 x *Mfge8* C2 KO compared to APP23 x *Mfge8* WT mice (Fig. 1f; with APP23 mice showing first plaques around 6 months of age). These changes in plaque load were also reflected by Aβ protein levels (measured either by immunoassay in formic acid extracts or by Western Blotting analysis), but with the exception of 6-month-old APP23 animal. In these animals, Aβ levels were indistinguishable between *Mfge8* WT and C2 KO mice despite the reduction in plaque load (Extended Data Figs. 2a-d), possibly due to the limited effect of a small number of plaques on total Aβ levels. To exclude an effect of endogenous murine Aβ, we also compared Aβ levels in (APP non-transgenic) *Mfge8* WT and *Mfge8* C2 KO animals but could not detect a genotype effect (Extended Data Fig. 2e). Moreover, protein levels and processing of (transgenic) human amyloid-β precursor protein (APP) appeared unchanged between *Mfge8* genotypes in APP transgenic animals (Extended Data Figs. 2b/d). To exclude that plaque clearance was altered, we also analysed microglial phagocytosis of Aβ plaques and, again, could not detect any genotype effects (Extended Data Figs. 3a/b).

These results indicated that the absence of Medin was probably affecting Aβ aggregation directly. However, because the genotype differences in plaque load became less prominent with progressing pathology (Figs. 1e/f), and because Medin aggregates have so far only been described in the vasculature[7,13], we also analysed cerebral β-amyloid angiopathy (CAA), i.e. vascular amyloid deposition that develops in APP23 mice starting from ~12 months of age[14,17,18] (but does not develop in APPPS1 animals to any robust degree). Indeed, in APP23 animals, we also found considerable co-localisation of MFG-E8- and Aβ-staining in blood vessels (Fig. 1g), which we corroborated in a second model with extensive CAA, APP Dutch animals[19] (Fig. 1g). To delineate the impact of MFG-E8/Medin on CAA, we quantified CAA in 12-month-old APP23 animals, and despite the high variability in CAA at this age, *Mfge8* C2 KO animals showed a reduction of ~85% in CAA burden compared to *Mfge8* WT animals (Fig. 1h). To study if this reduction of CAA would persist with progressing pathology, we aged APP23 animals to 24 months; at this age, severe CAA develops, resulting in microhaemorrhages[20]. Notably, CAA burden as well as microhaemorrhages were reduced by ~65% in 24-month-old *Mfge8* C2 KO compared to *Mfge8* WT animals (Figs. 1h/i). These data indicate that MFG-E8/Medin modulates cerebral β-amyloidosis, particularly in the vasculature.

MFG-E8 levels increase with CAA in mice and predict cognitive decline in AD patients, where Medin co-localises with vascular amyloid

We wanted to examine the role of Medin in human pathology next, but currently no assays exist that would allow direct quantification of Medin. However, previous genetic studies have identified polymorphisms that modulate gene expression of the Medin precursor MFG-E8 and, in turn, result in a corresponding modulation of the risk for vascular disease[21–24]. We therefore wondered whether MFG-E8 levels could serve as a surrogate marker for Medin-associated vascular pathology in the brain. We first examined this relationship in our mouse models, leveraging their well-defined and quantifiable pathological alterations. Measuring total MFG-E8 levels in the brains of wildtype animals as well as APPPS1 mice and APP23 mice, we found that MFG-E8 levels increased with ageing in the brain of wildtype mice, as expected from our previous work[3]. In APPPS1 animals, which develop pronounced plaque pathology but no CAA[15], MFG-E8 levels were indistinguishable from wildtype animals. In contrast, APP23 animals, which develop both extensive plaque pathology and severe CAA[14,20], had significantly higher brain MFG-E8 levels than did age-matched wildtype and APPPS1 mice (Fig. 2a, Extended Data Fig. 4). This indicated that MFG-E8 levels may reflect CAA rather than parenchymal plaque load. Indeed, analysing the relationship between MFG-E8 protein levels and stereological counts of CAA and plaque burden, we found that in 12-month-old APP23 animals, which show large variations in CAA burden, MFG-E8 levels correlated positively with CAA levels but negatively with plaque load. While in 20-month-old APP23 animals, where CAA burden is more similar amongst animals, the correlation between MFG-E8 levels and CAA was no longer evident, the negative correlation between MFG-E8 levels and plaque burden was still apparent (Fig. 2b). Therefore, increased levels of cerebral MFG-E8 may be indicative of CAA severity, at least before the end-stage of cerebral β-amyloidosis.

Having established a potential relationship between brain MFG-E8 levels and CAA, we next examined the relevance of our findings for AD patients. To this end, we analysed *MFGE8* gene expression of dorsolateral prefrontal cortex samples from 566 patients of the ROSMAP cohort[25], focussing on patients with AD as the only known cause of cognitive impairment (based on the final clinical diagnosis, i.e. *cogdx* 1 vs. 2 vs. 4 [26]). In ROSMAP patients, *MFGE8* expression increased significantly in AD patients (85.9±3.7 years; 69% female) compared to non-demented controls (82.9±5.0 years; 61% female) (Fig. 2c and Supplementary Data Table 1); in contrast, it did not change in an age-dependent manner in frontal lobe samples from a control cohort of 116 patients between the ages of 15-95 years[27] (Extended Data Fig. 5a and Supplementary Data Table 1), demonstrating that the increase in *MFGE8* expression occurred due to AD-associated pathology

rather than age. Moreover, linear regression analysis revealed a significant association of *MFGE8* expression levels with cognitive decline in ROSMAP patients (measured by the Mini Mental State Examination test battery, 'mmse30'; Fig. 2d). Notably, this effect of *MFGE8* expression on cognitive dysfunction was independent of amyloid load ('CERAD score') and tau pathology ('Braak and Braak score') (Fig. 2d), and also remained significant when adjusted for age, sex, education, post-mortem interval, *APOE* genotype, RNA-sequencing batch, and ROS versus MAP study (Extended Data Fig. 5b). To determine whether *MFGE8* expression was increased as part of its known molecular response pathway, we analysed whether 10 genes in the network of MFG-E8 would also predict cognitive decline in patients but found no significant impact of these genes on cognitive performance (Extended Data Fig. 5c), indicating that MFG-E8 may act through an unknown pathway or that its normal function may be subverted in AD, possibly through its conversion to Medin.

To delineate which brain compartment might be affected by Medin in AD patients, we performed immunostaining of frontal brain tissue from 6 human AD patients (see Extended Data Table 1 for patient information). First, we stained brain sections with an antibody against full-length human MFG-E8, which (in line with our mouse models) strongly labelled astrocytes and also showed some localised vascular immunoreactivity (Extended Data Fig. 6). In contrast, an anti-human Medin antibody (1H4 [3]) showed prevalent immunoreactivity on aggregate-like structures in the cerebral vasculature but did not detectably stain amyloid plaques in AD patients (Fig. 2e) – in line with the reported predominant vascular localisation of Medin in humans[2,3,8]. Interestingly, co-staining for Medin, Aβ and Methoxy-X04 revealed that Medin deposits often co-localised with CAA and showed partial overlap with vascular Aβ deposits (Fig. 2e). Thus, both in mouse models of cerebral β-amyloidosis as well as in human AD patients, Medin may contribute to pathology through promoting vascular amyloid formation.

Medin co-aggregates with Aβ, altering amyloid structure

The evident co-localisation of Medin and Aβ both in mouse and human tissue indicated a possible interaction of these two amyloids. To examine this possibility, we first analysed the subcellular localisation of Medin/MFG-E8 (fragments) on/around amyloid plaques using immuno-electron microscopy (EM) for MFG-E8/Medin on brain tissue from APPPS1 x *Mfge8* WT/C2 KO animals. In APPPS1 x *Mfge8* WT animals, we found conspicuous labelling of amyloid fibrils, which was absent in APPPS1 x *Mfge8* C2 KO animals (Fig. 3a), in line with our immunohistochemical analysis (cp. Fig. 1c). Moreover, amyloid plaques showed a less pronounced fibril structure in APPPS1 x *Mfge8* WT compared to APPPS1 x *Mfge8* C2 KO animals (Fig. 3a; magnification). This indicated that Medin –

which often forms amorphous rather than fibrillar aggregates *in vivo*[3] – could lead to a less ordered structure of amyloid deposits. To further assess this, we used two conformation-sensitive amyloid dyes (luminescent conjugated oligothiophenes, LCOs)[28]. For this analysis, we focussed specifically on age groups with similar plaque burden (namely 4-month-old APPPS1 and 12-month-old APP23 animals, cf. Figs. 1e/f) to determine whether Medin would affect Aβ aggregation independent of the change in plaque/CAA load, and to avoid confounding effects resulting from plaque size, which is known to affect LCO affinity[28] (average plaque size analysed in APPPS1 mice: 695±209/783±170 a.u. in *Mfge8* WT/C2 KO; APP23 mice: 1,549±72/1,554±65 a.u. in *Mfge8* WT/C2 KO). Indeed, we observed a significant change towards more compact amyloid in Medin-deficient animals (Fig. 3b), consistent with the EM analysis and indicating that Medin influences Aβ aggregation.

Since plaque morphotype can also be affected by microglia[29] and because full-length MFG-E8 is best known for its function as an opsonin[30], we further analysed microglial plaque-association as well as cytokine levels but could not detect genotype effects in either mouse model (Extended Data Figs. 3c-e). This indicated that the change in plaque morphotype was likely due to an interaction between Medin and Aβ. Therefore, we next tested whether recombinant Aβ and Medin would co-aggregate *in vitro*, using a Thioflavin-T (ThT) affinity assay. Medin (15 µM) aggregated significantly faster than Aβ(40) (20 µM) while their mixture aggregated with the same speed as Medin alone and did not show a biphasic ThT fluorescence profile (Fig. 3c), as might be expected if the peptides were aggregating independently. Moreover, immuno-EM of the aggregated peptides showed labelling for Medin and Aβ in close vicinity on the same amyloid fibrils (Fig. 3c), indicating co-aggregation. Interestingly, these heterologous fibrils were also morphologically distinct from the individually aggregated peptides, corroborating our *in vivo* analyses (Figs. 3a/b). Thus, our data indicate that Medin and Aβ can interact directly both *in vitro* and *in vivo*. Remarkably, endogenous levels of Medin appear to be able to influence Aβ aggregation *in vivo* despite the substantial overexpression of APP in these mouse models[14,15].

Exogenous Medin aggregates precipitate cerebral β-amyloidosis

Considering that Medin aggregate formation appears to start relatively early in life[1,2] and could therefore precede Aβ aggregation in the vasculature, we wondered if Medin aggregates might also be able to induce Aβ aggregation, that is if they might act as a "seed" for β-amyloidosis[31] (Fig. 4a). We have previously shown that vehicle injections do not induce detectable Aβ seeding[31,32]; therefore, we here opted instead to compare the efficacy of Medin-containing aorta-derived material against homologous seeding of Aβ, using hippocampal injections with brain extract from an end-stage APP transgenic animal as the gold standard. As expected, the injection of APP23 brain

extract resulted in overt Aβ deposition 6 months later, at an age where no endogenous Aβ aggregates have formed in host mice (Fig. 4c). To test whether Medin could induce heterologous Aβ seeding, we extracted Medin from two human aorta samples (using the same amount of starting material) from a 69-year-old female and 67-year-old male patient, who showed significant aortic Medin deposition (Fig. 4b and [3]). Analysis of these extracts by EM revealed numerous particles in the range of ~50-100 nm that were labelled heavily by an anti-human Medin antibody (1H4 [3]; Fig. 4b), and were occasionally still attached to collagen or elastic fibres, reflecting their tissue localisation (Extended Data Fig. 7a). Hippocampal injection of these aortic extracts also induced significant, premature Aβ aggregation 6 months later (Figs. 4c/d). In fact, the extent of hippocampal Aβ deposition was comparable to material extracted from the aged APP23 brain for one of the aorta samples, while the reduced seeding efficacy of the second sample reflected its lower Medin content (Figs. 4c/d). To confirm that Medin species were responsible for Aβ seeding, we immuno-depleted Medin from the highly seeding-active aorta extract (using the 1H4 antibody); this resulted in a complete absence of Medin in the extract (Fig. 4e; as confirmed by Western Blotting using a second anti-Medin antibody, 6B3) and fully abolished Aβ seeding (Figs. 4f/g). Previous reports found small amounts of Aβ in the human aorta[33,34]; however, using highly sensitive ELISA measurements, we were unable to detect any Aβ in formic acid extracts of the human aorta samples used for injections (data not shown). These results indicate that human Medin aggregates are capable of inducing human Aβ aggregation *in vivo*.

Since it is possible that amyloid extraction and immuno-depletion approaches are not entirely specific for Medin, we also injected aorta samples from (APP non-transgenic) aged *Mfge8* WT or *Mfge8* C2 KO animals, using total aorta homogenates to avoid any potential confounds introduced by extraction procedures (Fig. 4h). Corroborating our human Medin-depletion experiments, aorta homogenate from aged *Mfge8* WT animals was significantly more potent in seeding Aβ deposition than aorta homogenate from aged *Mfge8* C2 KO animals, although some non-specific seeding was observed using these complex samples (Figs. 4i/j).

Thus, Medin aggregates can accelerate Aβ pathology via a heterologous seeding mechanism. Therefore, formation of vascular Medin aggregates, which are prevalent in AD patients, could promote cerebral β-amyloid angiopathy and as a result vascular damage. Through such vascular effects, Medin could significantly contribute to brain injury and cognitive decline in AD[35,36].

Discussion

Despite its exceedingly high prevalence in the ageing population[1], it remains unknown how Medin amyloid is generated, and it is poorly understood whether it contributes to disease. Our recent work demonstrated that during ageing, Medin deposition leads to vascular stiffening in the brain of wildtype mice[3]. Two recent independent studies on post-mortem human tissue further indicated that Medin levels are not only increased in the brain vasculature of patients with vascular dementia but also are better predictors of AD diagnosis than other cerebrovascular pathologies[8,13]. However, it remained unknown how Medin may contribute to brain dysfunction in AD and how it relates to other hallmarks of this disorder (e.g. parenchymal plaques or tauopathy). Through independent lines of investigation, we here provide evidence that Aβ and Medin interact *in vivo*, thereby promoting cerebral β-amyloidosis – with a notable contribution to β-amyloid angiopathy and, as a result, damage of the brain vasculature (as evidenced by cerebral microbleeds). We demonstrate an ability for Medin to co-aggregate with Aβ *in vitro* (Fig. 3) and to cross-seed Aβ *in vivo* (Fig. 4), with effects on aggregation kinetics as well as amyloid structure. This new amyloid-amyloid interaction of Medin and Aβ may be explained by their reported shared structural and physicochemical characteristics: Both are small fragments (Aβ 40-42 aa, Medin 50 aa) of much larger proteins, and interestingly, human Medin and Aβ share some amino acid sequences, particularly in the aggregation-prone region of Medin[37,38].

Even though amyloids do not necessarily cross-seed[39] and can even cross-inhibit each other's aggregation *in vivo*[40], previous studies have indicated that Medin can cross-seed Serum amyloid A[41] and that Aβ can be cross-seeded by Amylin (IAPP) *in vivo*[42,43]. While it is unclear how IAPP would reach the brain from the periphery, we and others have previously reported the presence of Medin aggregates in the human brain vasculature (even in cognitively healthy patients)[3,8,13], and here we demonstrate co-localisation of Aβ and Medin aggregates within the same blood vessels both in mouse models of cerebral β-amyloidosis as well as in human AD tissue. While we also found strong co-localisation of MFG-E8 staining with Aβ plaques in APP transgenic mice, we were unable to detect Medin staining on parenchymal Aβ deposits in the brains of AD patients – whether this is due to species differences or a result of antibody affinity requires further investigation.

Thus, it currently appears most likely that in the human brain, a contribution of Medin to AD would be driven by its effects on the vasculature, in line with our finding that *MFGE8* expression levels predict cognitive decline in AD patients even when adjusted for plaque pathology and tauopathy. Further in support of this hypothesis, there is so far no genetic evidence that would directly link MFG-E8 or Medin to AD; however, expression quantitative trait loci (eQTLs) have been

identified that enhance or reduce *MFGE8* expression levels and thereby increase and decrease the risk for vascular disease[21–24], respectively. This supports a crucial role for MFG-E8 in vascular health, which could also be driving its impact on cognitive decline in human patients. Notably, a recent data-driven analysis of multimodal biomarker changes in >1000 patients found that vascular dysfunction (even in the periphery) is the earliest and strongest change detectable in AD[44]. Furthermore, epidemiological studies have shown that vascular dysfunction – in particular during midlife when Medin deposition is reportedly ongoing[1] – is a strong risk factor for late-onset AD[45,46]. Thus, in view of our data demonstrating a role for Medin in driving age-associated vascular dysfunction[3] as well as CAA (this study), targeting Medin might be a new therapeutic approach to preserve brain function during aging and Alzheimer's disease through improving vascular health.

References

1. Mucchiano, G., Cornwell, G. G. & Westermark, P. Senile aortic amyloid: Evidence for two distinct forms of localized deposits. *Am. J. Pathol.* **140**, 871–877 (1992).

2. Häggqvist, B. O. *et al.* Medin: An integral fragment of aortic smooth muscle cell-produced lactadherin forms the most common human amyloid. *Proc. Natl. Acad. Sci. U. S. A.* **96**, 8669–8674 (1999).

3. Degenhardt, K. *et al.* Medin aggregation causes cerebrovascular dysfunction in aging wild-type mice. *Proc. Natl. Acad. Sci. U. S. A.* **117**, 23925–23931 (2020).

4. Benson, M. D. *et al.* Amyloid nomenclature 2020: update and recommendations by the International Society of Amyloidosis (ISA) nomenclature committee. *Amyloid* **27**, 217–222 (2020).

5. Eisenberg, D. & Jucker, M. The amyloid state of proteins in human diseases. *Cell* **148**, 1188–1203 (2012).

6. Iadanza, M. G., Jackson, M. P., Hewitt, E. W., Ranson, N. A. & Radford, S. E. A new era for understanding amyloid structures and disease. *Nat. Rev. Mol. Cell Biol.* **19**, 755–773 (2018).

7. Peng, S., Glennert, J. & Westermark, P. Medin-amyloid: A recently characterized age-associated arterial amyloid form affects mainly arteries in the upper part of the body. *Amyloid* **12**, 96–102 (2005).

8. Karamanova, N. *et al.* Endothelial Immune Activation by Medin: Potential Role in Cerebrovascular Disease and Reversal by Monosialoganglioside-Containing Nanoliposomes. *J. Am. Heart Assoc.* **9**, e014810 (2020).

9. Davies, H. A. *et al.* Idiopathic degenerative thoracic aneurysms are associated with increased aortic medial amyloid. *Amyloid* **26**, 148–155 (2019).

10. Peng, S. *et al.* Medin and medin-amyloid in ageing inflamed and non-inflamed temporal arteries. *J. Pathol.* **196**, 91–96 (2002).

11. Peng, S. *et al.* Role of aggregated medin in the pathogenesis of thoracic aortic aneurysm and dissection. *Lab. Investig.* **87**, 1195–1205 (2007).

12. Migrino, R. Q. *et al.* Amyloidogenic medin induces endothelial dysfunction and vascular inflammation through the receptor for advanced glycation endproducts. *Cardiovasc. Res.* **113**, 1389–1402 (2017).

13. Migrino, R. Q. *et al.* Cerebrovascular medin is associated with Alzheimer's disease and vascular dementia. *Alzheimer's Dement. Diagnosis, Assess. Dis. Monit.* **12**, 1–10 (2020).

14. Sturchler-Pierrat, C. *et al.* Two amyloid precursor protein transgenic mouse models with Alzheimer disease-like pathology. *Proc. Natl. Acad. Sci. U. S. A.* **94**, 13287–92 (1997).

15. Radde, R. *et al.* Abeta42-driven cerebral amyloidosis in transgenic mice reveals early and robust pathology. *EMBO Rep.* **7**, 940–6 (2006).

16. Silvestre, J.-S. *et al.* Lactadherin promotes VEGF-dependent neovascularization. *Nat. Med.* **11**, 499–506 (2005).

17. Calhoun, M. E. *et al.* Neuronal overexpression of mutant amyloid precursor protein results in prominent deposition of cerebrovascular amyloid. *Proc. Natl. Acad. Sci. U. S. A.* **96**, 14088–14093 (1999).

18. Beckmann, N. *et al.* Age-dependent cerebrovascular abnormalities and blood flow disturbances in APP23 mice modeling Alzheimer's disease. *J. Neurosci.* **23**, 8453–8459 (2003).

19. Herzig, M., Winkler, D. & Bürki, K. Abeta is targeted to the vasculature in a mouse model of hereditary cerebral hemorrhage with amyloidosis. *Nat. Neurosci.* **7**, 954–960 (2004).

20. Winkler, D. T. *et al.* Spontaneous hemorrhagic stroke in a mouse model of cerebral amyloid angiopathy. *J. Neurosci.* **21**, 1619–1627 (2001).

21. Nelson, C. P. *et al.* Association analyses based on false discovery rate implicate new loci for coronary artery disease. *Nat. Genet.* **49**, 1385–1391 (2017).

22. Van Der Harst, P. & Verweij, N. Identification of 64 novel genetic loci provides an expanded view on the genetic architecture of coronary artery disease. *Circ. Res.* **122**, 433–443 (2018).

23. Nikpay, M. *et al.* A comprehensive 1000 Genomes-based genome-wide association meta-analysis of coronary artery disease. *Nat. Genet.* **47**, 1121–1130 (2015).

24. Soubeyrand, S. *et al.* Regulation of MFGE8 by the intergenic coronary artery disease locus on 15q26.1. *Atherosclerosis* **284**, 11–17 (2019).

25. Mostafavi, S. *et al.* A molecular network of the aging human brain provides insights into the

pathology and cognitive decline of Alzheimer's disease. *Nat. Neurosci.* **21**, 811–819 (2018).

26. De Jager, P. L. *et al.* Data descriptor: A multi-omic atlas of the human frontal cortex for aging and Alzheimer's disease research. *Sci. Data* **5**, 180142 (2018).

27. Blauwendraat, C. *et al.* Comprehensive promoter level expression quantitative trait loci analysis of the human frontal lobe. *Genome Med.* **8**, 65 (2016).

28. Rasmussen, J. *et al.* Amyloid polymorphisms constitute distinct clouds of conformational variants in different etiological subtypes of Alzheimer's disease. *Proc. Natl. Acad. Sci. U. S. A.* **114**, 13018–13023 (2017).

29. Yuan, P. *et al.* TREM2 Haplodeficiency in Mice and Humans Impairs the Microglia Barrier Function Leading to Decreased Amyloid Compaction and Severe Axonal Dystrophy. *Neuron* **90**, 724–739 (2016).

30. Brown, G. C. & Neher, J. J. Microglial phagocytosis of live neurons. *Nat. Rev. Neurosci.* **15**, 209–216 (2014).

31. Meyer-Luehmann, M. *et al.* Exogenous induction of cerebral β-amyloidogenesis is governed bf agent and host. *Science (80-.).* **313**, 1781–1784 (2006).

32. Fritschi, S. K. *et al.* Highly potent soluble amyloid-β seeds in human Alzheimer brain but not cerebrospinal fluid. *Brain* **137**, 2909–2915 (2014).

33. Kokjohn, T. A. *et al.* Chemical characterization of pro-inflammatory amyloid-beta peptides in human atherosclerotic lesions and platelets. *Biochim. Biophys. Acta - Mol. Basis Dis.* **1812**, 1508–1514 (2011).

34. Roher, A. E. *et al.* Amyloid beta peptides in human plasma and tissues and their significance for Alzheimer's disease. *Alzheimer's Dement.* **5**, 18–29 (2009).

35. Greenberg, S. M. *et al.* Cerebral amyloid angiopathy and Alzheimer disease — one peptide, two pathways. *Nat. Rev. Neurol.* **16**, 30–42 (2020).

36. Boyle, P. A. *et al.* Cerebral amyloid angiopathy and cognitive outcomes in community-based older persons. *Neurology* **85**, 1930–1936 (2015).

37. Larsson, A. *et al.* Unwinding fibril formation of medin, the peptide of the most common form of human amyloid. *Biochem. Biophys. Res. Commun.* **361**, 822–828 (2007).

38. Davies, H. A., Madine, J. & Middleton, D. A. Comparisons with Amyloid-β Reveal an Aspartate Residue That Stabilizes Fibrils of the Aortic Amyloid Peptide Medin. *J. Biol. Chem.* **290**, 7791–7803 (2015).

39. Rasmussen, J. *et al.* Infectious prions do not induce Aβ deposition in an in vivo seeding model. *Acta Neuropathologica* **135**, 965–967 (2018).

40. Bachhuber, T. *et al.* Inhibition of amyloid-β plaque formation by α-synuclein. *Nat. Med.* **21**, 802–807 (2015).

41. Larsson, A., Malmström, S. & Westermark, P. Signs of cross-seeding: Aortic medin amyloid as a trigger for protein AA deposition. *Amyloid* **18**, 229–234 (2011).

42. Moreno-Gonzalez, I. *et al.* Molecular interaction between type 2 diabetes and Alzheimer's disease through cross-seeding of protein misfolding. *Mol. Psychiatry* **22**, 1327–1334 (2017).

43. Ly, H. *et al.* The association of circulating amylin with β-amyloid in familial Alzheimer's disease. *Alzheimer's Dement. Transl. Res. Clin. Interv.* **7**, e12130 (2021).

44. Iturria-Medina, Y. *et al.* Early role of vascular dysregulation on late-onset Alzheimer's disease based on multifactorial data-driven analysis. *Nat. Commun.* **7**, 11934 (2016).

45. Akoudad, S. *et al.* Association of cerebral microbleeds with cognitive decline and dementia. *JAMA Neurol.* **73**, 934–943 (2016).

46. Gottesman, R. F. *et al.* Association between midlife vascular risk factors and estimated brain amyloid deposition. *JAMA - J. Am. Med. Assoc.* **317**, 1443–1450 (2017).

47. Sall, J. Leverage plots for general linear hypotheses. *Am. Stat.* **44**, 308–315 (1990).
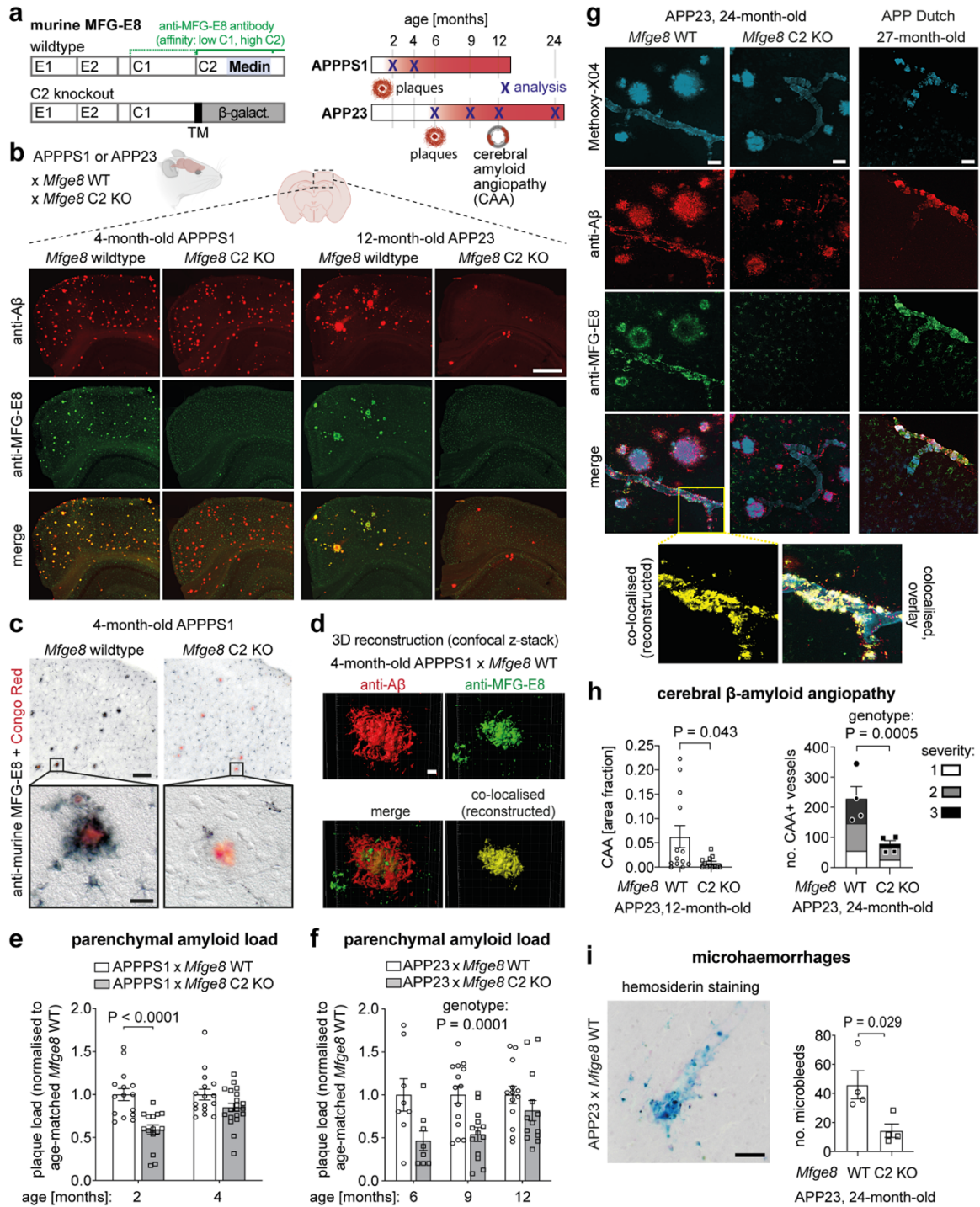
Figure 1: Medin strongly co-localises with Aβ deposits and promotes cerebral β-amyloidosis.

a, *left*: Schematic structure of the murine MFG-E8 protein domains in *Mfge8* wildtype (WT) and *Mfge8* C2-domain knockout (C2 KO) animals; indicated are a genetically inserted transmembrane domain ('TM') and the binding sites of the anti-murine MFG-E8 antibody, which strongly recognises epitopes in the C2 domain and thus Medin-containing fragments of MFG-E8 (green); *right*: timeline of pathological changes and analysis time-points in APPPS1 and APP23 transgenic mouse models. b, Immunofluorescent overview images of cortical brain sections from APPPS1/APP23 x *Mfge8* WT/C2 KO animals demonstrate substantial overlap of Aβ (red) and MFG-E8 or its fragments (green). c, Histological analysis of cortical brain sections from APPPS1 x *Mfge8* WT/C2 KO animals shows staining of MFG-E8 (fragments) on plaques as well as cells; extracellular plaque staining is completely absent in *Mfge8* C2 KO mice, while punctate cellular staining is visible due to the

truncated *Mfge8* C2 KO gene product being retained intracellularly. **d**, Representative 3D reconstruction of a confocal z-stack demonstrates co-localisation of Aβ/MFG-E8 (fragments) throughout the plaque. **e/f**, Stereological quantification shows significantly delayed plaque deposition in *Mfge8* C2 KO animals compared to *Mfge8* WT littermates in APPPS1 (e) and APP23 (f) mice (APPPS1: 2-month-old: n=7f/8m WT, 6f/9m C2 KO; 4-month-old: n=8f/8m WT, 12f/8m C2 KO; APP23 animals: 6-month-old: n=8f WT, 8f C2 KO, males have no plaques yet; 9-month-old: n=7f/7m WT, 7f/6m C2 KO; 12-month-old: n=4f/9m WT; 6f/7m C2 KO; APPPS1: 2-way-ANOVA: significant interaction and main effects of age*genotype/age/genotype $F_{(1,62)}$=4.79/4.79/22.06, p=0.032/0.032/<0.0001; APP23 significant main effect of genotype $F_{(1,63)}$=16.80, P=0.0001; P-values shown in *e* are for Sidak's posthoc comparison). **g**, In 24-25 month-old APP23 mice (n=4 males analysed) as well as 27-month-old APP Dutch mice (n=2 females analysed), staining for MFG-E8 (fragments) co-localises substantially with CAA. **h**, Medin deficiency in APP23 x *Mfge8* C2 KO animals reduces CAA burden both in 12- and 24-month-old animals (12-month-old: n=4f/9m *Mfge8* WT, n=5f/7m Mfge8 C2 KO; Mann-Whitney U test for genotype; 24-month-old: n=4m/4m *Mfge8* WT/C2 KO animals; 2-way ANOVA for genotype and severity, with significant main effect for genotype: $F_{(1,18)}$=18.07; data points indicate the average total number of CAA-laden vessels, independent of severity). **i**, In the same 24-month-old animals, Medin deficiency also reduces microhaemorrhages (Mann-Whitney U test). Data shown are means ± S.E.M. Scale bars: 500 μm in *b*, 100/20 μm in *c* (top/bottom), 5 μm in *d*, 100 μm in *e/f*. β-galact.: β-galactosidase gene.
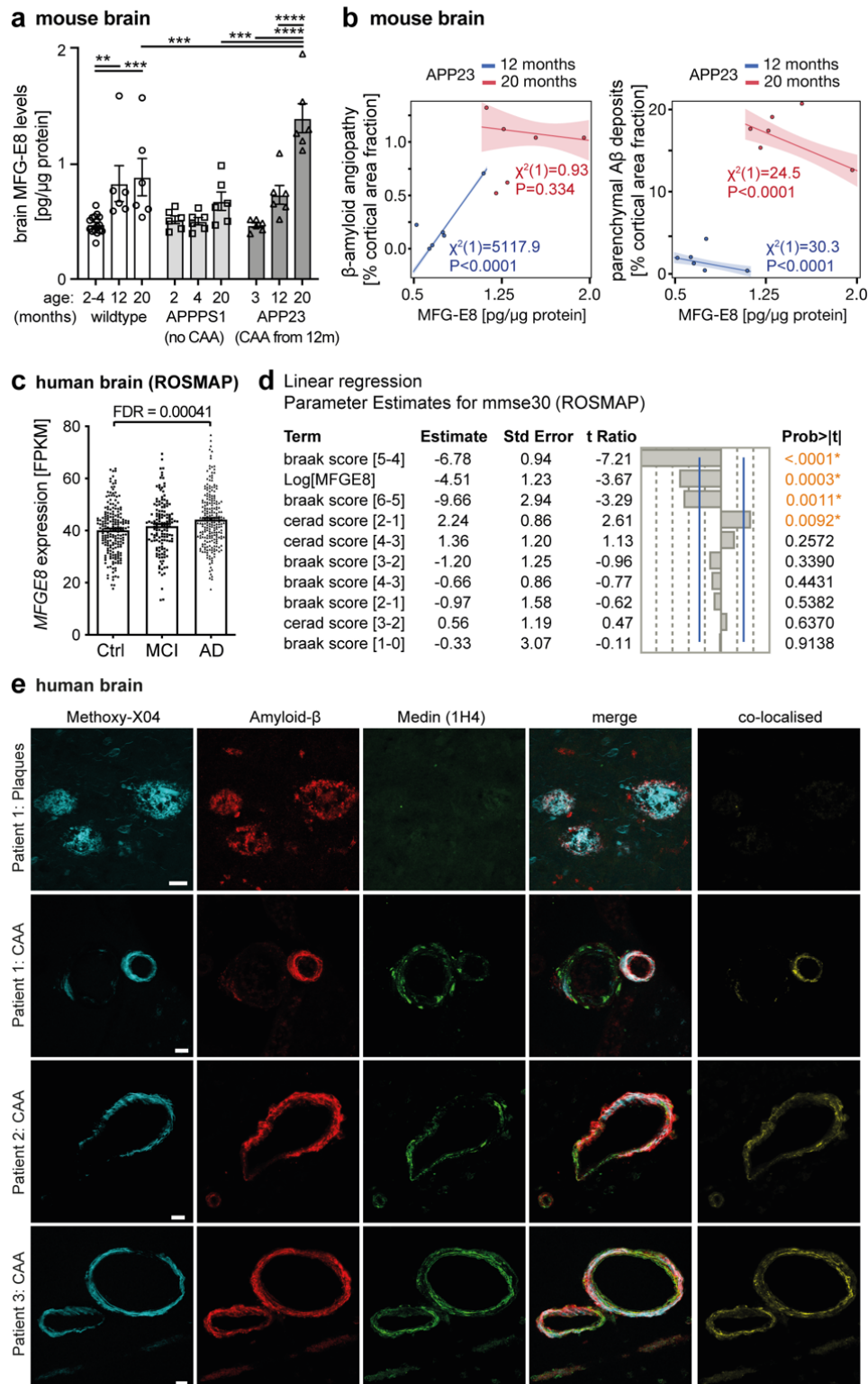
a mouse brain

brain MFG-E8 levels [pg/µg protein]

** *** *** *** **** ****

age: 2-4 12 20 | 2 4 20 | 3 12 20
(months) wildtype | APPPS1 | APP23
(no CAA) | (CAA from 12m)

b mouse brain

β-amyloid angiopathy [% cortical area fraction]

APP23 — 12 months — 20 months

$\chi^2(1)=0.93$
P=0.334

$\chi^2(1)=5117.9$
P<0.0001

MFG-E8 [pg/µg protein]

parenchymal Aβ deposits [% cortical area fraction]

APP23 — 12 months — 20 months

$\chi^2(1)=24.5$
P<0.0001

$\chi^2(1)=30.3$
P<0.0001

MFG-E8 [pg/µg protein]

c human brain (ROSMAP)

MFGE8 expression [FPKM]

FDR = 0.00041

Ctrl   MCI   AD

d Linear regression
Parameter Estimates for mmse30 (ROSMAP)

Term	Estimate	Std Error	t Ratio		Prob>|t|
braak score [5-4]	-6.78	0.94	-7.21		<.0001*
Log[MFGE8]	-4.51	1.23	-3.67		0.0003*
braak score [6-5]	-9.66	2.94	-3.29		0.0011*
cerad score [2-1]	2.24	0.86	2.61		0.0092*
cerad score [4-3]	1.36	1.20	1.13		0.2572
braak score [3-2]	-1.20	1.25	-0.96		0.3390
braak score [4-3]	-0.66	0.86	-0.77		0.4431
braak score [2-1]	-0.97	1.58	-0.62		0.5382
cerad score [3-2]	0.56	1.19	0.47		0.6370
braak score [1-0]	-0.33	3.07	-0.11		0.9138

e human brain

Methoxy-X04 | Amyloid-β | Medin (1H4) | merge | co-localised

Patient 1: Plaques
Patient 1: CAA
Patient 2: CAA
Patient 3: CAA

Figure 2: MFG-E8 levels predict CAA in mice and cognitive decline in AD patients, where Medin co-localises with β-amyloid angiopathy.

a, MFG-E8 protein levels in the mouse brain increase with ageing in wildtype and with cerebral β-amyloid angiopathy (CAA) in APP23 animals, but not in response to plaque deposition alone in APPPS1 mice (n=6f/10m for 2-4 month-old WT, all other groups n=3f/3m; two-way ANOVA with significant interaction and main effects for age*genotype/age/genotype: F(4,55)=6.36/F(2,55)=27.20/F(2,55)=8.81, P=0.0003/<0.0001/0.0005;

109

/*/**** P<0.01/0.001/0.0001 for Tukey posthoc comparisons). **b**, Linear regression (Robust Cauchy fit) demonstrates that MFG-E8 levels correlate positively with CAA in 12-month-old APP23 mice but not in 20-month-old animals (left panel), while showing negative correlations with plaque load (right panel). **c**, In 566 patients of the ROSMAP cohort[26], *MFGE8* expression levels gradually increase from cognitively normal controls ('Ctrl'; n=123f/78m) through mild cognitive impairment ('MCI'; n=94f/49m) and diagnosed AD ('AD'; n=152f/68m). **d**, Linear regression analysis demonstrates a significant impact of *MFGE8* expression levels on predicting cognitive decline, even when adjusted for plaque load (CERAD: 'cerad score') and tau pathology (Braak and Braak: 'braak score'; cp. Extended Data Fig. 5 for inclusion of additional factors). **e**, In brain sections from AD patients (n=6; see Table S1), Medin staining (1H4 antibody; green) is not detectable on amyloid plaques but is prevalent in blood vessels, where it partially co-localises with Aβ (red) and the amyloid dye, Methoxy-X04 (blue). Data shown are means ± S.E.M. Scale bars: 20 μm in e.
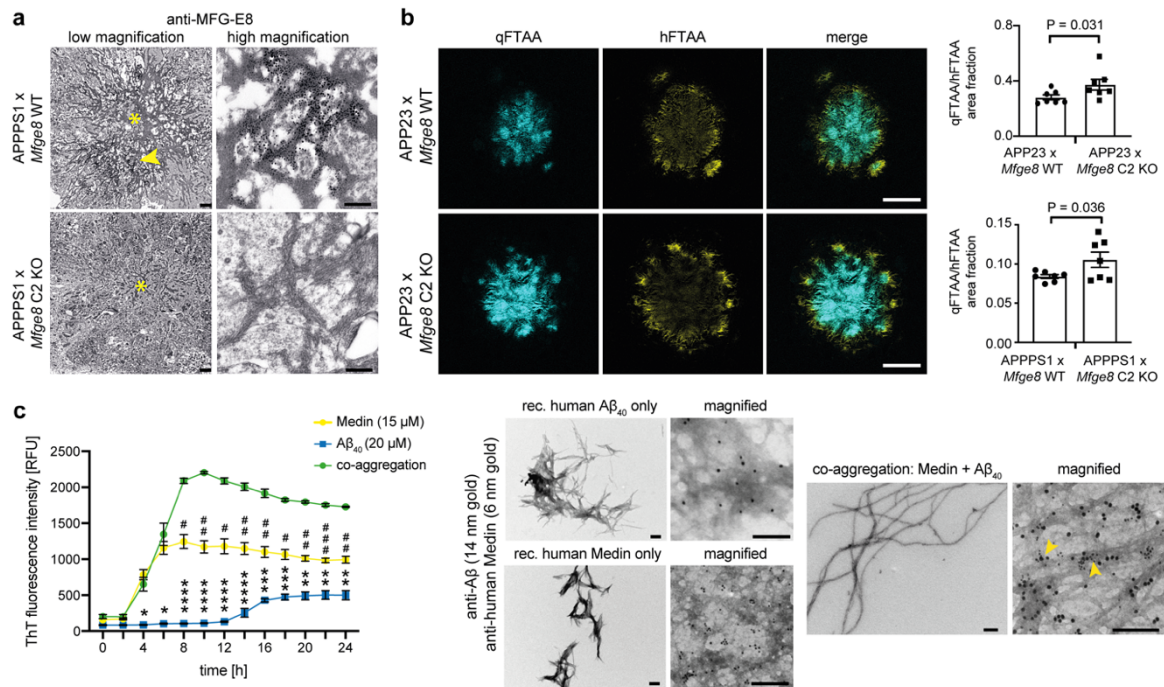
Figure 3: Medin alters plaque structure *in vivo* and co-aggregates with Aβ *in vitro*.

a, Immuno-electron microscopic (EM) images showing silver-enhanced anti-MFG-E8 (fragment) staining of plaques in 4-month-old APPPS1x*Mfge8* WT/C2 KO animals (asterisks indicate the plaque core, the arrowhead indicates MFG-E8 (fragment) staining on the plaque; staining is absent in *Mfge8* C2 KO animals; n=1f/1m *Mfge8* WT and n=1f/1m *Mfge8* C2 KO analysed). **b**, *left*: Representative amyloid staining with two luminescent conjugated oligothiophenes, which recognise compact (qFTAA) and more diffuse (hFTAA) amyloid species. In *Mfge8* C2 KO animals, qFTAA area fraction is increased, indicating more compact amyloid. *Right*: Ratio of plaque area stained with qFTAA/hFTAA in 12-month-old APP23 and 4-month-old APPPS1 animals (for both: n=3f/4m WT, 3f/4m C2 KO; unpaired t-test: APP23 t(12)=2.150, APPPS1 t(12)=2.134). **c**, *In vitro* co-aggregation assay based on Thioflavin T (ThT) fluorescence, showing faster aggregation of Medin compared to Aβ and a mono-phasic profile indicative of co-aggregation when peptides were aggregated together (n=3; 2-way repeated measures ANOVA; significant interaction and main effects for time*aggregating peptide(s)/time/aggregating peptide: F(24, 72)=49.76/F(2.686, 16.12)=182.1/F(2, 6)=400.8, P<0.0001/P<0.0001/P<0.0001; Tukey's multiple comparisons: */**/***/**** P<0.05/0.01/0.001/0.0001 compared with 'co-aggregation'). Immuno-EM analysis of aggregated recombinant peptides, demonstrating a conspicuous change in fibril morphology of the co-aggregated peptides as well as staining of Aβ and Medin on the same fibrils (yellow arrowheads indicate Aβ/Medin staining in close proximity). Data shown are means ± S.E.M. Scale bars: 1 μm (left) and 250 nm (right) in *a*; 40 μm in *b*, 200 nm in *c*.
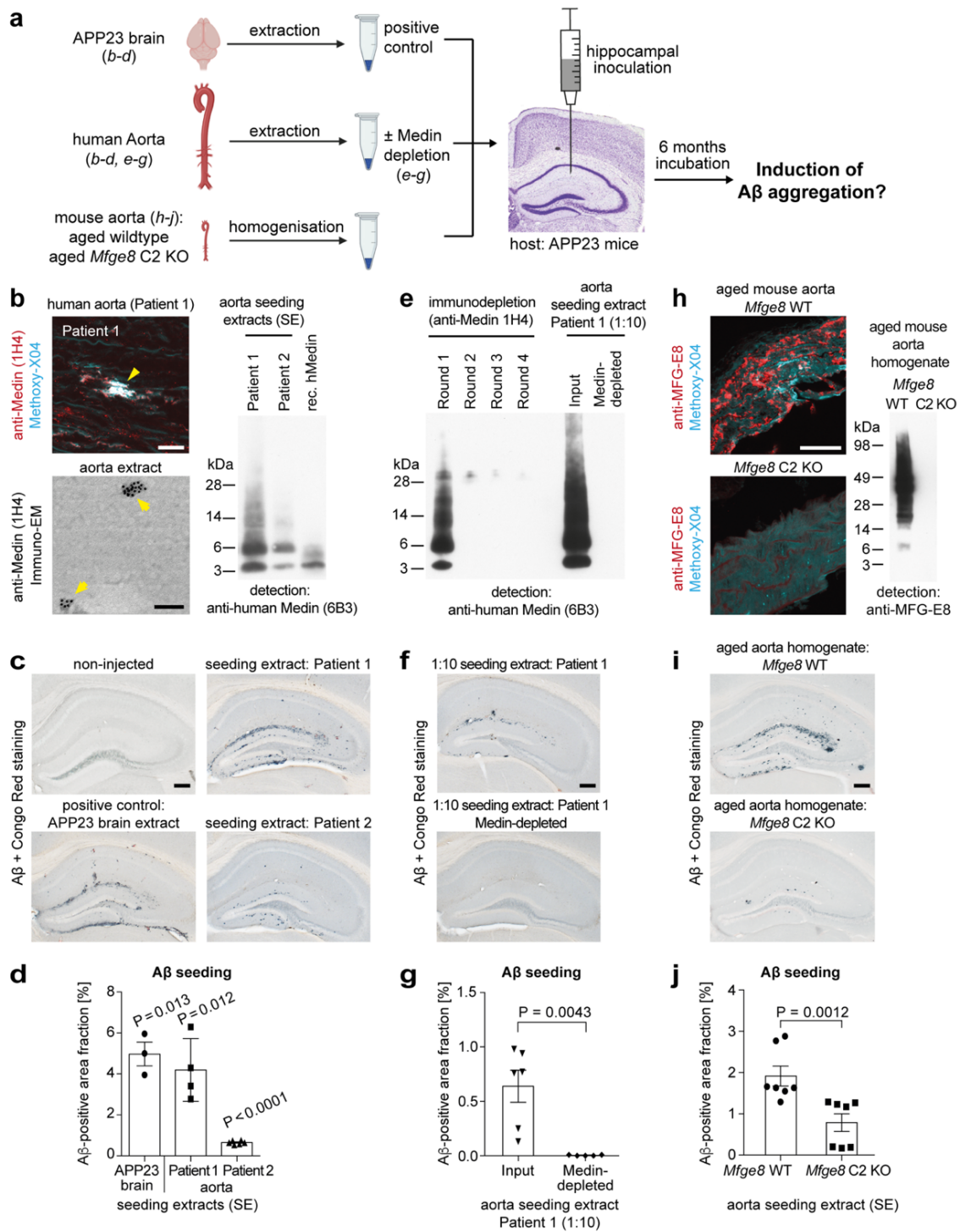
**Figure 4: Intracerebral inoculation with Medin aggregates induces premature β-amyloidosis.**
a, Experimental design: Samples from human Aorta, Aβ-laden APP23 brain and (APP non-transgenic) *Mfge8* WT/*Mfge8* C2 KO mouse aorta were injected into young, pre-depositing APP23 hosts. Cerebral β-amyloidosis was assessed 6 months later, when no endogenous amyloid deposits have formed yet in host mice. **b**, *top left:* aorta tissue section stained for Medin (1H4 antibody) and amyloid (Methoxy-X04; note that collagen fibres are auto-fluorescent), showing a prominent Medin deposit (yellow arrowhead); *bottom left*: immuno-electron microscopy of human aorta extract shows abundant and heavily labelled Medin-aggregates (1H4 antibody). *right*, Western blotting analysis independently confirms presence of Medin (using a different anti-Medin antibody, 6B3), with higher levels in Patient 1 extract. **c**, Analysis of cerebral β-amyloidosis 6 months after intra-hippocampal injection. Representative images of Aβ deposition induced by APP23 brain extract (positive

control) and aorta extract of patients 1 and 2, in comparison to an age-matched un-injected APP23 animal, which shows no endogenous deposits. **d**, Stereological quantification of Aβ deposition shows significant seeding of Aβ with both extracts, patient 1 extract being similarly potent as extract from an aged APP23 mouse brain (n=3/4/6 for APP23/patient1/patient2 extract; One sample t-test against 0: APP23 t(2)=8.563; patient 1 t(3)=5.485; patient 2 t(5)=18.57). **e**, Patient 1 aorta extract was diluted 1:10 (for technical reasons) and Medin was immuno-depleted using anti-human Medin 1H4 antibody (in 4 rounds of incubation). Successful depletion was verified by Western Blotting with anti-human Medin antibody 6B3. **f/g**, Medin-depletion virtually abolishes Aβ seeding (analysis as in *c/d*; n=6/5 extract/depleted-extract; Mann Whitney U test). **h**, *left:* aged mouse aorta stained for MFG-E8/Medin and amyloid (Methoxy-X04, which mostly shows autofluorescence). *Right*: Western Blotting for MFG-E8 (fragments) in aged mouse aortas demonstrates prominent MFG-E8 and its fragments in aged *Mfge8* WT but not *Mfge8* C2 KO aorta. **i/j**, Aorta homogenate from aged *Mfge8* C2 KO mice is less seeding-active than is homogenate from aged *Mfge8* WT aorta, although some non-specific seeding is observed (analysis as in *c/d*; n=7/7 animals injected with *Mfge8* WT/C2 KO aorta homogenate; Mann Whitney U test). Data shown are means ± S.E.M. Scale bars: 25 μm/100 nm in b (top/bottom); 250 μm in c/f/i; 25 μm in h.
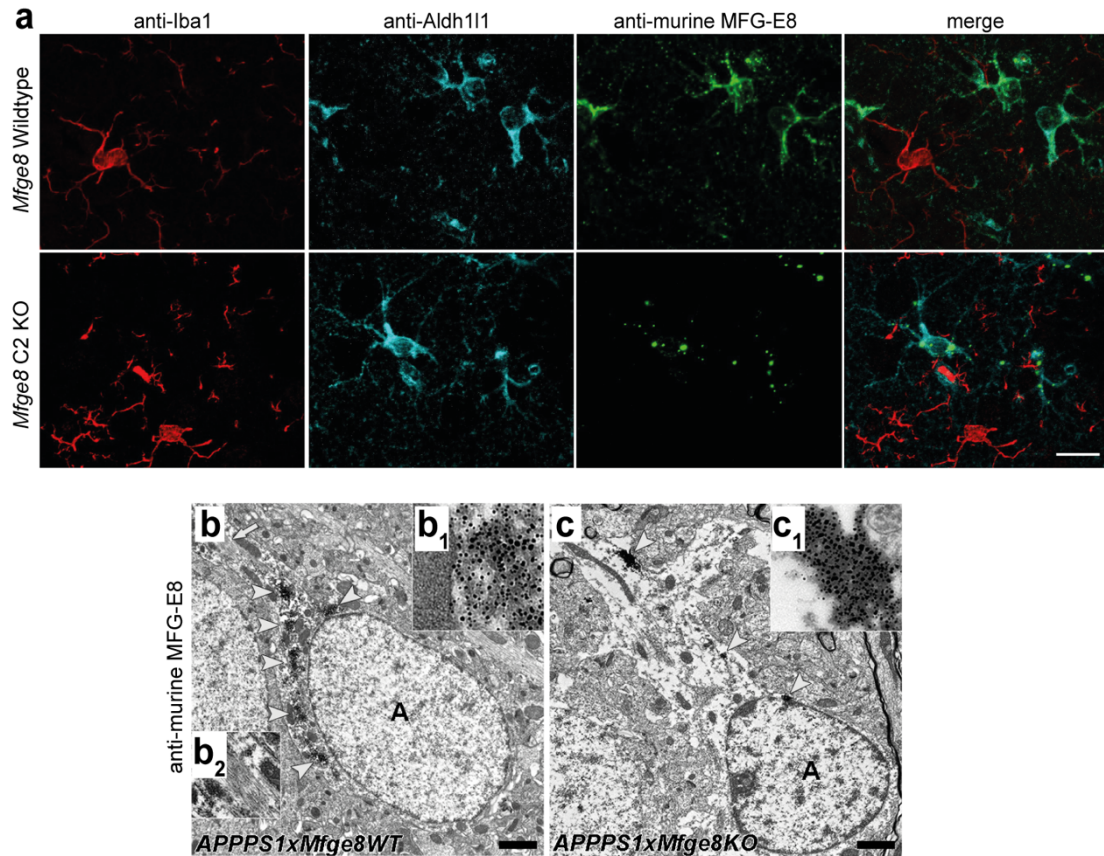
**Extended Data Figure 1: MFG-E8 is expressed by astrocytes in APP transgenic mice.**
a, Immunofluorescent co-staining of MFG-E8 (green) with astrocytic (Aldh1l1, cyan) and microglial (Iba1, red) markers demonstrates co-localisation only with astrocytes. Note that in *Mfge8* C2 KO mice, the truncated MFG-E8/β-galactosidase fusion protein (cp. Fig. 1a) is still expressed but is retained inside the cell (due to an inserted transmembrane domain), causing a punctate staining pattern. **b**, Astrocytic ('A') staining is also evident by immuno-electron microscopy in 4-month-old APPPS1 x *Mfge8* wildtype (WT) animals. The arrow *(top left)* indicates bundles of intermediate filaments in the astrocytic cytoplasm, which are shown at higher magnification in b2. **c**, Astrocytes in *Mfge8* C2 KO animals also contain heavily labelled punctate structures, indicating intracellular accumulation of the truncated MFG-E8 protein (arrowheads indicate positively stained structures, which are magnified in b1/c1 inserts; n=1f/1m *Mfge8* WT and n=1f/1m *Mfge8* C2 KO animals analysed). Scale bar; 15 μm in a, 500 nm in b.
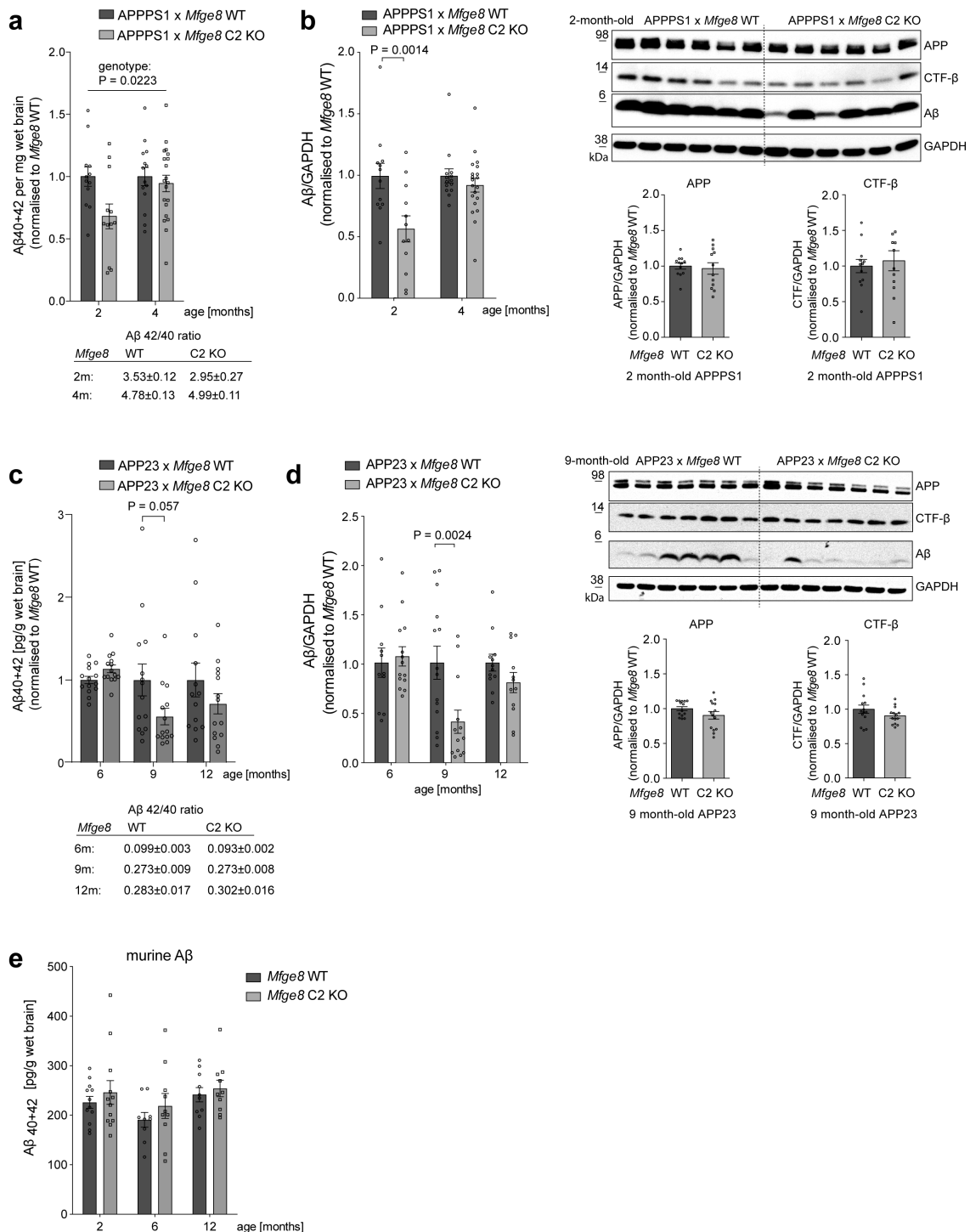
**Extended Data Figure 2: MFG-E8/Medin deficiency reduces Aβ protein levels at early stages of pathology.**
a, Aβ 40 and 42 levels in brain homogenate were quantified by immunoassay in APPPS1 x *Mfge8* wildtype (WT) vs. APPPS1 x *Mfge8* C2 knockout (KO) animals (2 months: n=6f/6m APPPS1 x *Mfge8* WT and n=6f/6m *Mfge8* C2 KO, 4 months n=6f/8m WT and n=12f/8m C2 KO; 2-way ANOVA significant main effect for genotype $F_{(1,54)}=5.54$). **b**, Quantification of Aβ, C-terminal fragment-β (CTF-β) and Amyloid Precursor Protein (APP) by Western Blotting analysis (using 6E10 antibody) in brain homogenates from APPPS1 x *Mfge8* WT/C2 KO animals; data were pooled from different blots after normalisation to the average wildtype level (2 months: n=6f/6m APPPS1 x *Mfge8* WT and n=6f/6m APPPS1 x *Mfge8* C2 KO, 4 months: n=6f/8m APPPS1 x *Mfge8* WT

and n=12f/8m APPPS1 x *Mfge8* C2 KO; 2-way ANOVA with significant interaction and main effects for age*genotype/age/genotype: $F_{(1,54)}=5.067/F_{(1;54)}=10.30/F_{(1,54)}=5.067$; P=0.0285/0.0022/0.0285; followed by Sidak's posthoc comparison). A representative blot for 2-month-old animals is shown. **c**, Aβ 40 and 42 levels in brain homogenate were quantified by immunoassay in APP23 x *Mfge8* wildtype (WT) vs. APP23 x *Mfge8* C2 KO animals (6 months n=8f/6m WT and n=8f/6m *Mfge8* C2 KO, 9 months n=7f/7m WT and n=7f/6m C2 KO; 12 months n=7f/7m WT and n=7f/7m *Mfge8* C2 KO; 2-way ANOVA significant interaction and main effect for genotype*age/genotype: $F_{(2,77)}=3.834/F_{(1,77)}=4.160$, P=0.0259/P=0.0448; followed by Sidak's posthoc comparison). **d**, Quantification of Aβ, C-terminal fragment-β and Amyloid Precursor Protein (APP) by Western Blotting analysis (using 6E10 antibody) in brain homogenates from APP23 x *Mfge8* WT/C2 KO animals; data were pooled from different blots after normalisation to the average wildtype level (6 months: n=7f/4m APP23 x *Mfge8* WT and n=7f/6m APP23 x *Mfge8* C2 KO, 9 months: n=7f/7m APP23 x *Mfge8* WT and n=7f/6m APP23 x *Mfge8* C2 KO, 12 months: n=5f/7m APP23 x *Mfge8* WT and n=5f/7m APP23 x *Mfge8* C2 KO; 2-way ANOVA with significant interaction and main effects for age*genotype/age/genotype: $F_{(2,70)}=3.652/F_{(2,70)}=3.652/F_{(1,70)}=5.757/$; P=0.0310/0.0310/0.0191; followed by Sidak's posthoc comparisons). A representative blot for 9-month-old animals is shown. **e**, murine Aβ 40 and 42 levels were quantified with an immunoassay in (APP non-transgenic) *Mfge8* WT vs. *Mfge8* C2 KO animals (2 months: n=6m/6f *Mfge8* WT and n=6m/6f *Mfge8* C2 KO, 6 months n=4m/5f *Mfge8* WT and n=4m/6f *Mfge8* C2 KO; 12 months n=4m/6f *Mfge8* WT and n=3m/7f *Mfge8* C2 KO). Data shown are means ± S.E.M.
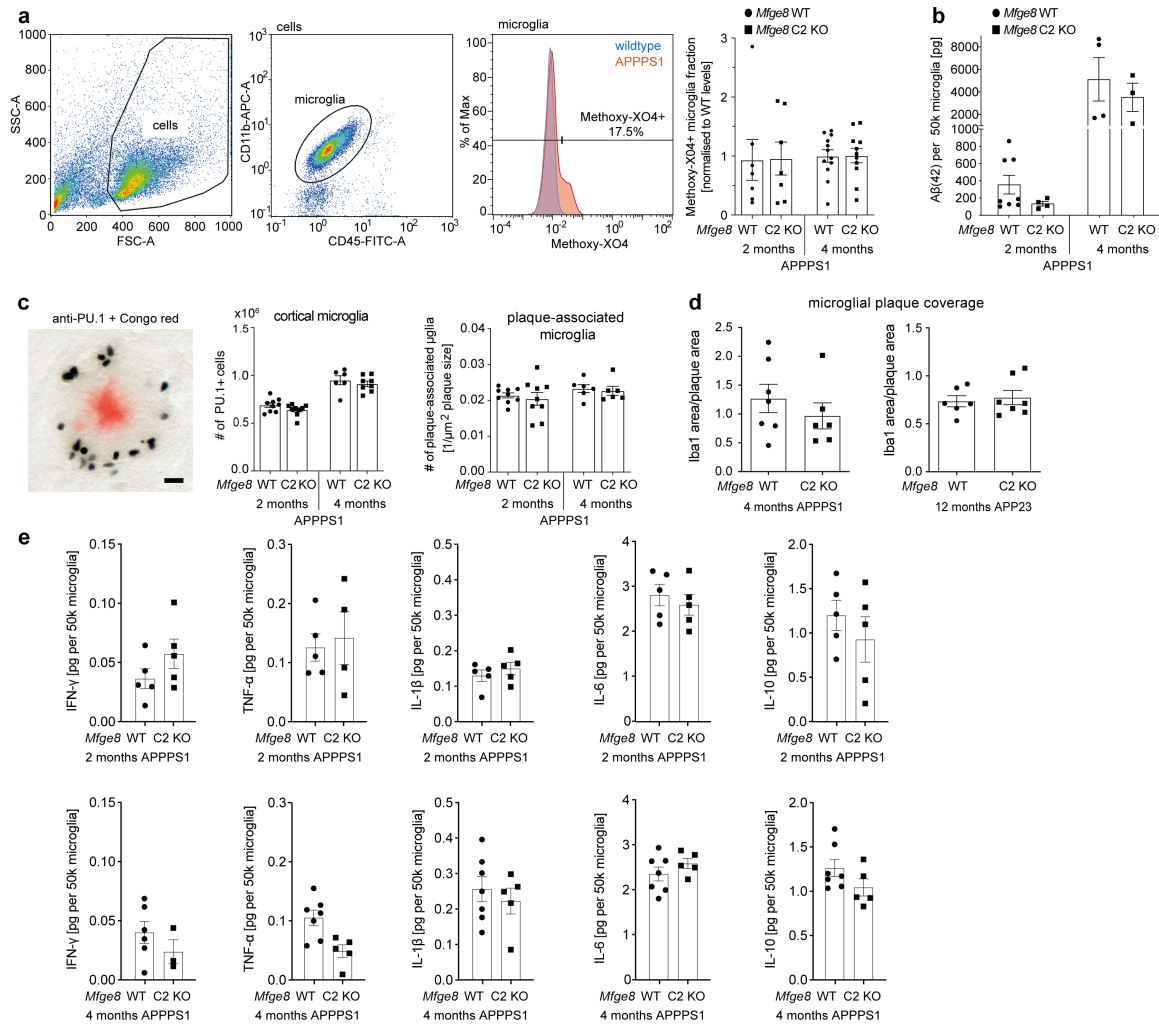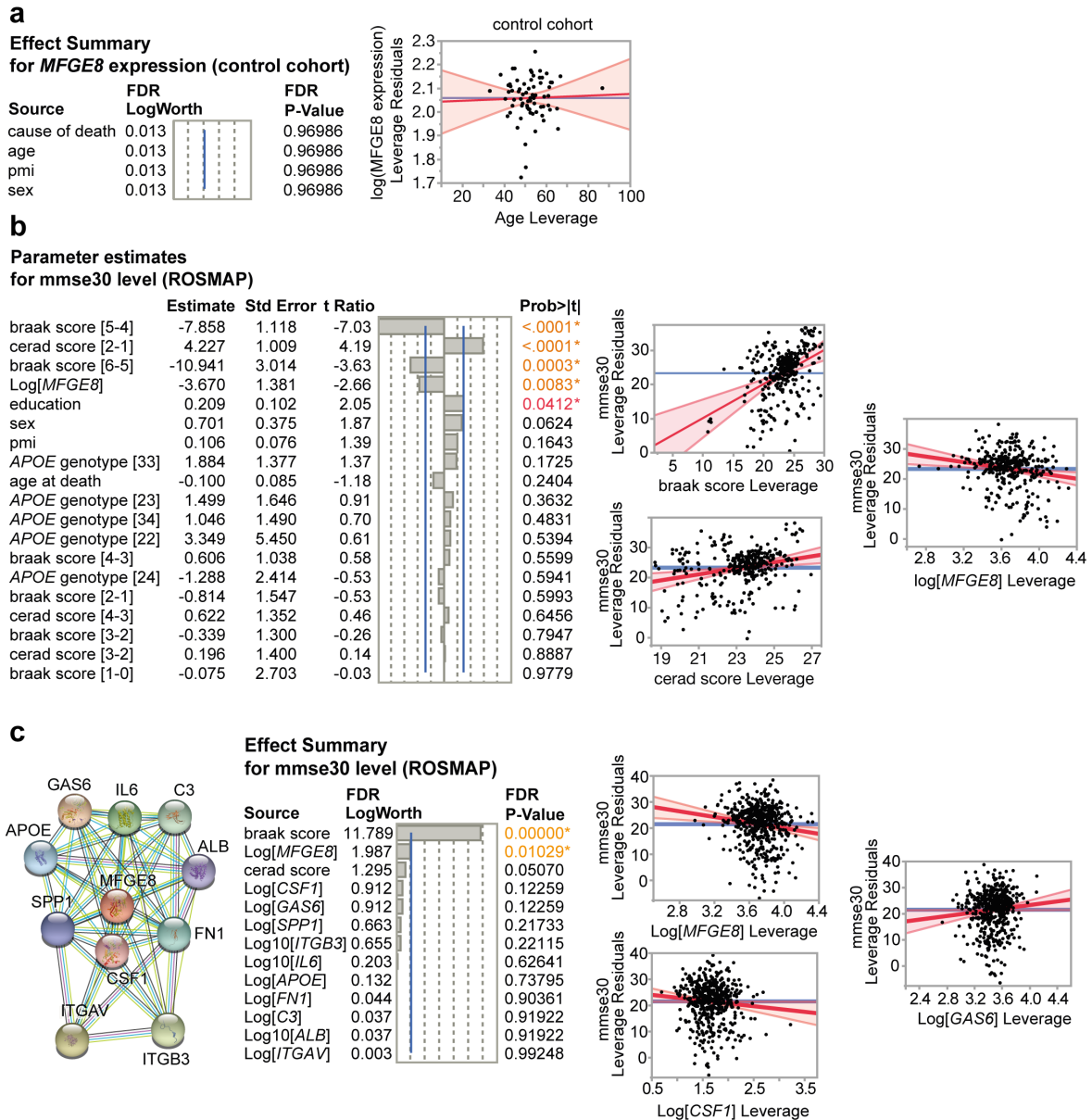
Extended Data Figure 3: MFG-E8/Medin deficiency does not affect microglial responses to cerebral β-amyloidosis.

a, Microglial phagocytosis of Aβ is not affected by *Mfge8* C2 KO in APPPS1 animals, as evidenced by FACS-based analysis of the amyloid-specific Methoxy-X04 signal (2 months: n=4f/4m *Mfge8* WT n=5f/2m *Mfge8* C2 KO; 4 months: n=9f/3m *Mfge8* WT, n=6f/5m *Mfge8* C2 KO) in microglia (identified based on CD11b^{high}, CD45[intermediate] cells) or by **b**, ultra-sensitive ELISA measurements of Aβ42 levels in purified microglia (as in *a*) (2 months APPPS1: n=5f/3m *Mfge8* WT, n=3f/2m *Mfge8* C2 KO; 4 months APPPS1: n=1f/3m *Mfge8* WT, n=2f/1m *Mfge8* C2 KO). **c**, Stereological quantification of total cortical microglia (Pu.1 staining, black; *middle*) or around plaques (Congo Red staining, *right*) shows no differences in total and plaque-associated numbers of microglia in APPPS1 x *Mfge8* WT versus APPPS1 x *Mfge8* C2 KO animals at 2/4 months of age (for total microglia in 2-month-old animals: n=5f/4m APPPS1 x *Mfge8* WT and n=6f/3m APPPS1 x *Mfge8* C2 KO and in 4-month-old animals: n=3f/3m APPPS1 x *Mfge8* WT and 6f/2m APPPS1 x *Mfge8* KO; for plaque-associated microglia in 2-month-old animals: n=5f/4m APPPS1 x *Mfge8* WT and n=6f/3m APPPS1 x *Mfge8* KO; in 4-month-old animals: 5f/1m APPPS1 x *Mfge8* WT and 3f/3m APPPS1 x *Mfge8* C2 KO). **d**, The coverage of the plaque surface by microglia (measured as the overlap of Iba1- and Methoxy-X04 staining for individual plaques) is not altered in 4-month-old APPPS1 x *Mfge8* WT vs. APPPS1 x *Mfge8* C2 KO animals nor in 12-month-old APP23 x *Mfge8* WT vs. APP23 x *Mfge8* C2 KO animals (n=3f/4m analysed for each group). **e**, Cytokine levels measured in purified microglia (cf. panel *a*), are indistinguishable in 2 and 4 months old APPPS1 x *Mfge8* WT and APPPS1 x *Mfge8* C2 KO animals APPPS1 (2 months: n=5f/3m *Mfge8* WT, n=3f/2m *Mfge8* C2 KO; 4 months: n=3f/4m *Mfge8* WT, n=3f/2m *Mfge8* C2 KO). Data shown are means ± S.E.M. Scale bar: 20 μm in b.

117
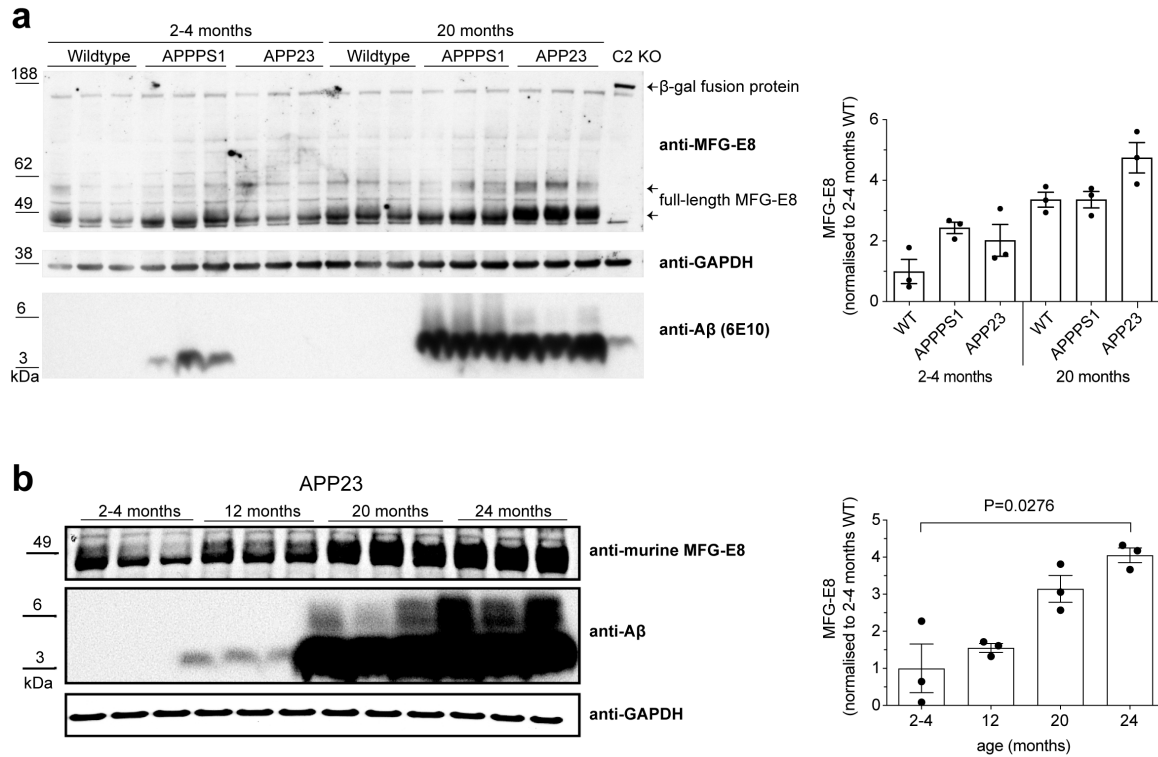
Extended Data Figure 4: MFG-E8 levels increase with age and cerebral β-amyloidosis.
Validation of ELISA measurements of MFG-E8 protein levels in the brain of wildtype, APPPS1 and APP23 mice (cf. Fig. 2a). **a**, Western Blotting confirms increasing levels of full-length MFG-E8 protein with age and cerebral β-amyloidosis (evident by Aβ staining using the 6E10 antibody). Note the absence of MFG-E8 bands in the far-right sample of an *Mfge8* C2 KO animal, which however shows the MFG-E8/β-galactosidase (β-gal) fusion protein. For semi-quantitative analysis (right), the MFG-E8 signal was normalised to GAPDH. **b**, Analysis of MFG-E8 protein levels in the brain of APP23 animals confirms increases of MFG-E8 with pathology. For semi-quantitative analysis (right), MFG-E8 signal was normalised to GAPDH (Kruskal-Wallis statistic=9.051, P=0.0032; followed by Dunn's posthoc comparison). Blots were repeated at least 2 times.

a

Effect Summary
for *MFGE8* expression (control cohort)

Source	FDR LogWorth	FDR P-Value
cause of death	0.013	0.96986
age	0.013	0.96986
pmi	0.013	0.96986
sex	0.013	0.96986

control cohort

b

Parameter estimates
for mmse30 level (ROSMAP)

	Estimate	Std Error	t Ratio		Prob>|t|
braak score [5-4]	-7.858	1.118	-7.03		<.0001*
cerad score [2-1]	4.227	1.009	4.19		<.0001*
braak score [6-5]	-10.941	3.014	-3.63		0.0003*
Log[*MFGE8*]	-3.670	1.381	-2.66		0.0083*
education	0.209	0.102	2.05		0.0412*
sex	0.701	0.375	1.87		0.0624
pmi	0.106	0.076	1.39		0.1643
APOE genotype [33]	1.884	1.377	1.37		0.1725
age at death	-0.100	0.085	-1.18		0.2404
APOE genotype [23]	1.499	1.646	0.91		0.3632
APOE genotype [34]	1.046	1.490	0.70		0.4831
APOE genotype [22]	3.349	5.450	0.61		0.5394
braak score [4-3]	0.606	1.038	0.58		0.5599
APOE genotype [24]	-1.288	2.414	-0.53		0.5941
braak score [2-1]	-0.814	1.547	-0.53		0.5993
cerad score [4-3]	0.622	1.352	0.46		0.6456
braak score [3-2]	-0.339	1.300	-0.26		0.7947
cerad score [3-2]	0.196	1.400	0.14		0.8887
braak score [1-0]	-0.075	2.703	-0.03		0.9779

c

Effect Summary
for mmse30 level (ROSMAP)

Source	FDR LogWorth	FDR P-Value
braak score	11.789	0.00000*
Log[*MFGE8*]	1.987	0.01029*
cerad score	1.295	0.05070
Log[*CSF1*]	0.912	0.12259
Log[*GAS6*]	0.912	0.12259
Log[*SPP1*]	0.663	0.21733
Log10[*ITGB3*]	0.655	0.22115
Log10[*IL6*]	0.203	0.62641
Log[*APOE*]	0.132	0.73795
Log[*FN1*]	0.044	0.90361
Log[*C3*]	0.037	0.91922
Log10[*ALB*]	0.037	0.91922
Log[*ITGAV*]	0.003	0.99248

Extended Data Figure 5: The impact of *MFGE8* gene expression on cognitive decline in AD patients.
Linear regressions were performed to analyse **a**, the impact of aging on *MFGE8* gene expression in a control cohort of 116 patients who died without dementia, and **b**, the impact of *MFGE8* gene expression on cognitive performance ('mmse30') adjusted for amyloid load (CERAD: 'cerad score'), tau pathology (Braak and Braak: 'braak score'), education level, post-mortem interval ('pmi'), sex, age at death, *APOE* genotype, RNA-sequencing batch ('batch') as well as the study (ROS vs. MAP) in 566 patients. **c**, The impact of gene expression of *MFGE8* and 10 genes within its known molecular network (https://string-db.org/) on cognitive performance ('mmse30') was analysed in the same patients as in *b*, adjusted for amyloid load ('cerad score') and tau pathology ('braak score'). Selected regression plots are shown as so-called residual vs. leverage plots[47] (see Methods for details): crossing of a least squares line (red) and confidence bands (shaded red) through the mean of the Y leverage residuals (blue line) indicates statistical significance. FDR: False Discovery Rate (adjusted P-value using the Benjamini-Hochberg correction). FDR LogWorth: -log10(FDR P-Value) for each model effect.
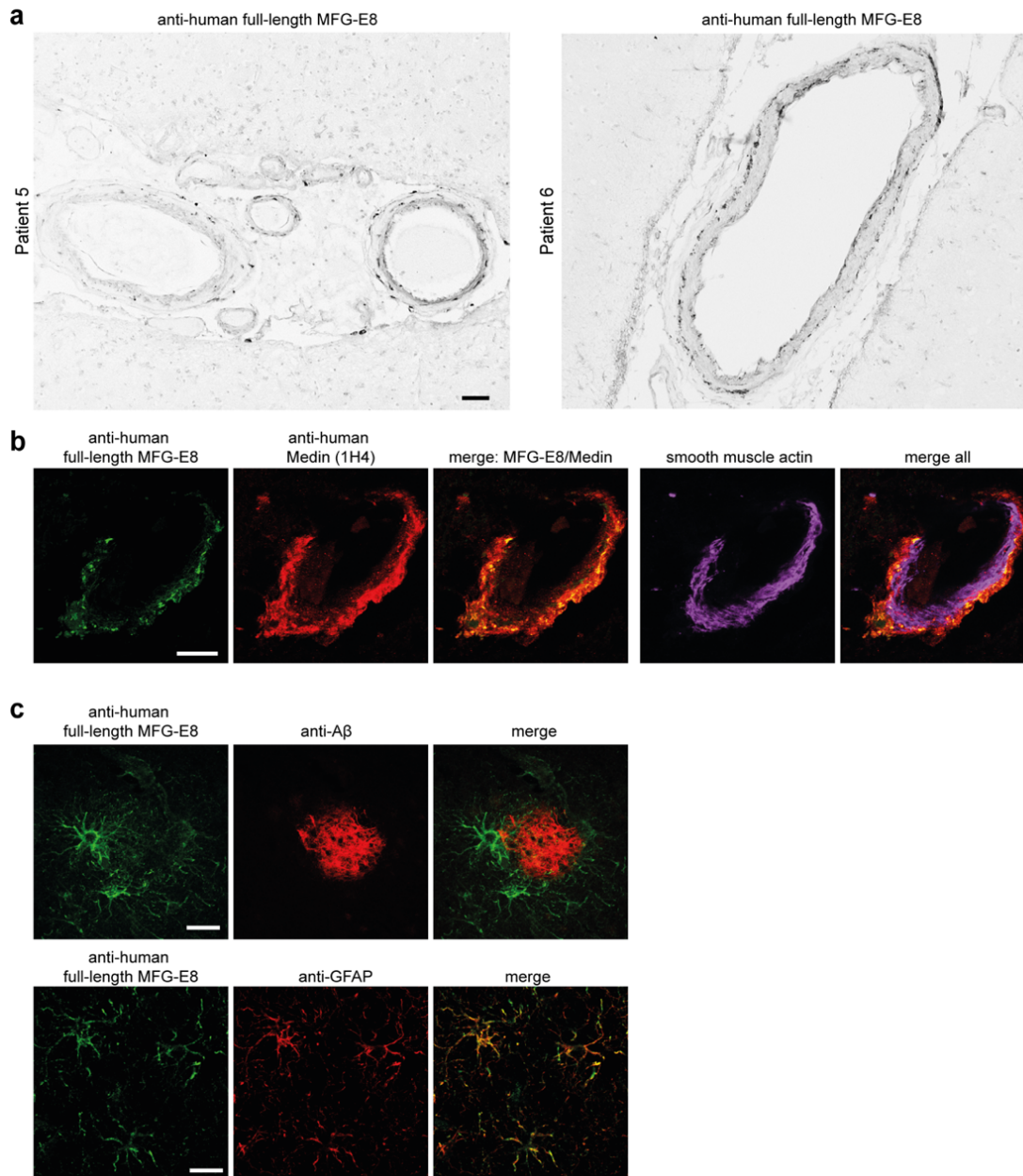
Extended Data Figure 6: Immunostaining with an anti-human full-length MFG-E8 antibody shows cellular staining of vascular cells and astrocytes.

a, Brain sections of two sporadic AD patients were stained with a monoclonal antibody raised against human full-length MFG-E8. b, Exemplary image of co-staining for human full-length MFG-E8 (green), and human Medin (1H4, red) showing limited overlap between full-length MFG-E8 and Medin in a cerebral blood vessel (stained with smooth muscle actin; tissue sections are from Patient 4, cf. Fig. 4). c, Staining for full-length MFG-E8 (green) in human AD brain sections also labels cells around amyloid plaques (anti-Aβ, red), which are identified as astrocytes by co-staining for glial fibrillary acidic protein (GFAP). Scale bars: 50 μm in a, 20 μm in b, 50 μm in c.
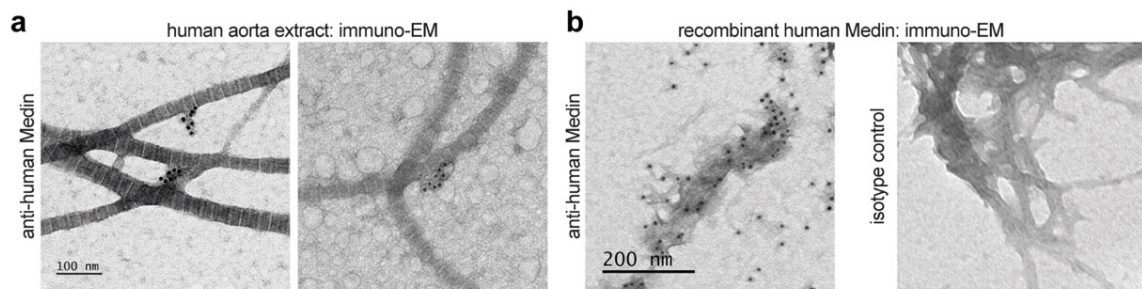
Extended Data Figure 7: Medin aggregates extracted from human aorta.
a, Immuno-electron microscopic analysis of amyloid extract from human aorta shows Medin aggregates still associated with collagen and/or elastic fibres. b, Immuno-gold labelling of recombinant Medin is only observed with the Medin-specific 1H4 antibody (left) but not with an isotype control antibody (right).

Extended Data Table S1: Human tissue.

Aorta (surgical resection tissue)			
Case	Age (years)	Sex	Clinical pres.
Patient 1	69	F	Aneurysm
Patient 2	67	M	Aneurysm

Brain (post-mortem tissue)						
Case	Age (years)	Sex	Clinical pres.	Braak score	CERAD score	Additional pathology
Patient 1	67	M	Sporadic AD	6	frequent	Lewy body pathology, moderate CAA
Patient 2	77	M	Sporadic AD	6	frequent	Severe CAA, amygdalar Lewy body pathology, hippocampal sclerosis with TDP-43 proteinopathy
Patient 3	88	M	Sporadic AD	6	frequent	Microinfarct
Patient 4	64	M	Sporadic AD	6	frequent	Amygdalar Lewy body pathology
Patient 5	68	F	Sporadic AD	6	frequent	Moderate CAA, mild small vessel disease, incidental Lewy body pathology
Patient 6	88	F	Sporadic AD	5	frequent	Mild CAA

Materials and Methods

Human tissue

Ascending aortic tissue samples were obtained from patients undergoing elective aneurysmal repair at Liverpool Heart and Chest Hospital (Extended Data Table 1). This study was ethically approved by Liverpool Bio-Innovation Hub (project approval reference 15-06 and 18-07). The LBIH Biobank confers ethical approval for the use of samples through their ethical approval as a Research Tissue Bank (REC reference 14/NW/1212, NRES Committee North West–Haydock). After collection, samples were rapidly frozen in dry ice and isopentane slurry, and immediately stored at –80°C prior to use.

Human brain tissue (Extended Data Table 1) was obtained from the Queen Square Brain Bank for Neurological Disorders (UCL Institute of Neurology, London, UK; approval protocol No: EXTMTA5/16) and the Emory University Alzheimer's Disease Research Center (IRB 00045782) with informed consent from families. 12-15 µm thick, FFPE brain sections from the frontal or temporal cortex were used for analysis.

This study was also approved by the ethical committee of the Medical Faculty, University of Tübingen, Germany (Protocol No: 354/2016BO2). Informed consent was obtained from all participants.

Mice

Male and female C57BL/6J and *Mfge8* C2 knockout (C57BL/6J-Mfge8 Gt[(KST227)Byg]) mice[1] (generously provided by Dr. Clotilde Théry, INSERM U932, Institute Curie, France) were bred in-house in a specific pathogen free (SPF) facility. Heterozygous *Mfge8* C2 knockout animals were crossed with hemizygous APP transgenic mice. The APP transgenic mouse lines, APPPS1 (C57BL/6J-Tg(Thy1-APP$_{K670N;M671L}$ and Thy1-PS1$_{L166P}$)[2] and APP23 (C57BL/6J-Tg(Thy1-APP$_{K670N;M671L}$)[3], have been backcrossed with C57BL/6J for >20 generations and were bred in-house were bred in-house in a specific pathogen free (SPF) facility. Where possible, littermate controls were used. All mice were maintained under specific pathogen-free conditions. Experiments were performed in accordance with German veterinary office regulations (Baden-Württemberg) and were approved by the local authorities for animal experimentation (Regierungspräsidium) of Tübingen, Germany (Approval numbers: N03/14, N02/15, N03/15, N07/16, N3/19, §4MIT v. 05.03.2018, §4MIT v. 18.08.2016).

Tissue preparation

For brain and aorta preparations, mice were deeply anesthetized and transcardially perfused with phosphate-buffered saline (PBS). Brains were stored for 24 h in 4% paraformaldehyde (PFA). Optional, one hemisphere was freshly frozen on dry ice for biochemical analysis. The PFA-fixed hemisphere was then transferred to 30% sucrose for another 48 h, and subsequently frozen in 2-methyl-butane. Coronal sections of 25 µm were cut with a freezing sliding microtome (Leica). After removal of the perivascular adipose tissue, the aorta was freshly frozen on dry ice.

For gel electrophoresis and ELISA analyses, tissue samples were homogenized using a Precellys® lysing kit for 10% or 20% w/v brain homogenates in Tris-HCl buffer (50 mM Tris pH 8, 150 mM NaCl, 5 mM

EDTA, phosphatase and protease inhibitors (Pierce)) or 10% (w/v) aortic homogenates in PBS. Total protein concentration of homogenates was quantified using the BCA assay (Pierce) according to standard protocols.

Microglial isolation and *in vivo* phagocytosis assay

One day prior to microglial isolation, mice were intraperitoneally injected with 17.5 µl per g bodyweight of the amyloid dye Methoxy-X04 (4% vol of 10 mg/ml Methoxy-X04 in DMSO, 7.7% vol CremophoreEL in 88.3% vol PBS). Microglia were isolated as previously described[4,5]. Briefly, the neocortex was dissected and minced in ice-cold Hanks Buffered Salt Solution (HBSS, 15 mM HEPES, 0.54% D-Glucose, 0.1% DNase (w/v)). The minced tissue was sequentially homogenized in glass Dounce and Potter homogenizers (Wheaton). Tissue suspension was filtered through a 70 µm cell strainer (BD Biosciences) and centrifugated at 300 g for 15 min at 4°C in a swinging-bucket rotor. The pellet was resuspended in 70% Percoll solution (Healthcare) and centrifuged for 30 min at 800 g at 4°C through a 70%, 37% and 30% isotonic Percoll gradient. Cells were recovered from the 70/37% interphase and washed with fluorescence-activated cell sorting (FACS) buffer (1xHBSS, 2% FCS, 10 mM EDTA) by centrifugation at 300 g for 15 min at 4°C. For blocking of non-specific Fc receptor-mediated antibody binding, the cell pellet was resuspended in FACS buffer, and Fc-block (BD, 1:400) was added for 10 min. Cells were stained with anti-mouse CD45 A700 (Biolegend, 1:200) or anti-mouse CD45 FITC (Affymetrix Bioscience, 1:100) and anti-CD11b APC (Biolegend, 1:200) for 15 min at 4°C. After washing, the pellet was resuspended in FACS buffer containing 25 mM HEPES. CD11b^{high}/CD45^{low}-positive microglial cells were sorted with a Sony SH800 flow cytometer in FACS buffer containing 25 mM HEPES. Isolated cells were pelleted (800 g for 7 min) and stored at -80°C.

For quantification of Aβ phagocytosis *in vivo*, microglia were isolated and the proportion of Methoxy-positive microglia was analyzed by flow cytometry with MACSQuant Analyser (Miltenyi Biotec). Since 2-month-old APP transgenic mice contain lower Aβ plaque burden, Methoxy-X04 (1:250) was additionally added during the staining procedure. Background signals were excluded by gating based on APP non-transgenic mice for each separate experiment. Signals of APPPS1x*Mfge8* C2 KO were normalized to the APPPS1x*Mfge8* C2 WT mean of each experiment to reduce batch effects. The Methoxy-positive fraction of APPPS1x*Mfge8* C2 KO was normalized to the mean of the entire experimental wildtype group. Additionally, phagocytosed Aβ was measured in isolated microglia by SIMOA Human Aβ42 2.0 Kit (Quanterix) after formic acid extraction (see section on Protein Extraction), following the manufacturer's protocol.

Thioflavin T fluorescence aggregation assay:

Thioflavin T (ThT) fluorescence assays were carried out on a Flexstation 3 microplate reader (Molecular Devices Ltd., San Jose, CA, USA). Experiments were carried out in sealed 96-well, black-walled, clear-bottomed microplates (Nunc). Data were recorded every 5 min using bottom read mode, with excitation at 440 nm and emission at 490 nm. The assay was carried out using 20 µM Medin (produced recombinantly as previously described[6]) or 15 µM Aβ40 (BioLegend) alone or co-incubated in 50 mM Tris, 150 mM NaCl, 5 mM EDTA, pH8 with 2 µM ThT at 37°C under quiescent conditions with 5 sec shaking before each reading.

Protein extraction

In wildtype mice, soluble Aβ was extracted from 20% brain homogenates by adding an equal volume of 0.4% diethylamine (DEA, in 100 mM NaCl) followed by rigorous vortexing. After ultracentrifugation for 1 hour at 135,000 x g (TLA-55 rotor with fixed-angle, Beckman Coulter) at 4°C, the supernatant was neutralized with 0.5 M Tris-HCl (pH 6.8, 1:10 ratio) and flash-frozen on dry-ice[7].

For extraction of insoluble protein aggregates in whole brain or isolated microglia (50,000 cells) from APP transgenic mice, samples were treated with formic acid (Sigma-Aldrich, final concentration 70% (vol/vol)), sonicated for 30 seconds on ice and centrifugated at 25,000 x g for 1h at 4°C. Supernatant was then mixed with neutralization buffer (1 M Tris base, 0.5 M Na_2HPO_4, 0.05% NaN_3 (w/v)) and measurements were performed.

Enzyme-linked immunosorbent assay (ELISA)

MFG-E8 protein levels in mouse brain were measured by commercial ELISA (R&D Systems) according to the manufacturer's instructions. Brain homogenates (10%) were prediluted 1:5. MFG-E8 levels were normalised to the total protein content as measured by the BCA protein assay (Pierce). Measurements were performed on a FLUOstar Omega reader (BMG Labtech).

Quantification of human Aβ was performed by Aβ Peptide Panel 1 (6E10) V-Plex assay (Meso Scale Discovery, MSD) or by the SIMOA Human Aβ42 2.0 Kit (Quanterix) in FA-extracted samples (brain homogenates or isolated microglia, 50,000 cells) according to manufacturer's instructions[5,8]. Murine Aβ was measured by Abeta Peptide Panel 1 (4G8) V-Plex assay (MSD) in diethylamine (DEA)-extracted brain homogenates (see section on Protein extraction).

Cytokines of microglial cells (50,000 cells in 50mM Tris pH8, 150 mM NaCl, 5 mM EDTA) were measured using the Proinflammatory Panel 1 (mouse) V-Plex Kit (MSD) according to the manufacturer's protocol.

Western Blotting

Samples were diluted and denatured in loading buffer (10 % glycerol, 2 % SDS, 2 % β-mercaptoethanol, 0.1 M Tris-HCl pH 8.6), sonicated 3x5 seconds (LabSonic, B. Braun Biotech International GmbH, 0.5 mm diameter sonotrode, cycle 1, amplitude 8), and heated to 95°C for 5 min. For detection of MFG-E8 in total homogenates, brain samples were preheated for 5 min in 8M urea at 70°C before denaturation in loading buffer. Total protein was adjusted to 10-15 µg for Western Blot analysis and loaded on a Bis-Tris 4-12% or Tris-Tricine 10-20% gradient gel (Invitrogen). After electrophoresis, gels were transferred to a nitrocellulose membrane in a semi-dry blotting system. Transfer was confirmed by Ponceau-S staining. Blocking was performed either with 5% milk (6E10, CTF-β, GAPDH, 6B3) or 5% donkey serum (polyclonal anti-murine MFG-E8) in PBST for 1 h. For detection of Aβ, membranes were boiled in PBS for 5 min at 90°C. Subsequently, membranes were incubated overnight at 4°C with the primary antibody in PBST. Primary antibodies used

were goat polyclonal anti-murine MFG-E8 (R&D systems, 1:1,000), anti-GAPDH (Acris Antibodies GmbH, 1:100,000), anti-human Medin 6B3 (Prothena, 1:2500 in 5% BSA-PBST), anti-CTF-β (Sigma Aldrich, 1:2,000) and anti-Aβ 6e10 (Biolegend, 1:2,500). Membranes were then probed with the respective secondary horseradish peroxidase (HRP)-labelled antibodies (1:20,000, Jackson ImmunoLaboratories). Protein bands were detected using chemiluminescent peroxidase substrate (ECL prime, GE Healthcare). Densitometric values of protein band intensities were analysed with the software package Aida (Stella 3200, Raytest) or ImageJ and normalised to GAPDH.

Medin-depletion of aortic extracts

Medin depletion was performed similarly to a previous publication[9]. 200 µl of paramagnetic beads coated with Protein G (Dynabeads) were washed 3 times in sterile PBS (+0.02% Tween) and incubated overnight with 1 mL tissue-culture supernatant of the monoclonal 1H4 antibody. Aortic extract was prediluted 1:10 in sterile PBS and 100 µl of the diluted extract were incubated for 2 hrs with one quarter of the 1H4-Protein G-Dynabeads-complex. This step was then repeated three times, with the final incubation taking place overnight at 4°C. The final supernatant was used for injection. Paramagnetic beads from each step were washed 3 times with PBS and subjected to elution in loading buffer. Final supernatant and eluted bead material from each step were collected for Western blotting using 6B3 as detection antibody.

***In vivo* inoculations**

Medin aggregates were purified from fresh-frozen 100mg human aorta (Medin, n=2 patients, 2 extractions per patient were pooled before injection) and Aβ was purified from the brain of one 28-month-old APP23 transgenic mouse, as previously described[10]. Quantification of Aβ in the extracts was performed after FA extraction using the MesoScale Discovery platform, yielding no detectable signals. For mouse aorta seeding extracts, aortas from aged *Mfge8* C2 KO and WT mice were homogenised in sterile PBS (10 mg tissue/100 µl; using a Precellys homogeniser) and sonicated three times for 5 s; samples were adjusted to the same total protein concentration (~2 µg/µl).

Intrahippocampal injections (2.5 µl per hippocampus) were done bilaterally in pre-depositing 2-4-month-old female and male APP23 mice[3]. Whenever possible, age-matched littermates were used for injections. After anesthesia with ketamine/xylazine (100 mg/kg to 10 mg/kg of body weight), injections were targeted to the hippocampus (anteroposterior, −2.5 mm; left/right, ±2.0 mm; dorsoventral, −1.8 mm) and delivered with a Hamilton syringe at a speed of 1.25 µL/min[11]. The syringe was kept in place for an additional 2 min and then slowly withdrawn. The surgical incision was closed, and the mice were closely monitored until regaining consciousness. After 6 months of incubation, the mice were sacrificed and the brains processed for histologic staining with anti-Aβ (CN6[14], 1:1,000) and Congo Red and Aβ plaque load was quantified stereologically (as described[12]).

Histology and immunostaining

Paraffin sections were deparaffinized and rehydrated using standard protocols. Free-floating brain sections were washed in PBS and endogenous peroxidase was quenched by incubation of the sections with 0.3% hydrogen peroxide (AppliChem) in PBS for 30 min. For staining of human brain tissue, sections were pretreated with 1 µg/mL proteinase K (in 1 mM $CaCl_2$, 50 mM Tris buffer, pH 7.6) at 37°C for 30 min, followed by deactivation in 10 mM EDTA (pH 6) at 90°C for 10 min[10,13]. Human aorta paraffin sections were boiled in citrate buffer (1.8 mM citric acid, 8.2 mM trisodium citrate, pH6) at 90°C for 30 min. For immunohistochemical (IHC) detection, sections were quenched 30 min with 0.3% H_2O_2. Unspecific antibody binding was blocked by incubation with 5% normal serum of the secondary antibody-species (in 0.3% Triton X-100 in PBS), and primary antibody was incubated at 4°C overnight with agitation, followed by washing and incubation with the secondary antibody (diluted in 1% serum-PBS) using either ABC and Peroxidase Substrate kits (Vectastain) or appropriate fluorescently labelled secondary antibodies (according to the manufacturer's instructions, Invitrogen or Jackson ImmunoResearch, 1:250). To reduce autofluorescence (from various sources such as lipofuscin, elastin or collagen) in human brain sections, TrueBlack™ Quencher (Biotium) was applied (1:20 in 70% ethanol) for 5s according to the manufacturer's instructions.

Primary antibodies used were anti-human Medin antibody (clone 1H4, 1:2), goat polyclonal anti-murine MFG-E8 antibody, with high affinity for the C2 domain (R&D Systems, 1:1,000), anti-Iba1 (WAKO, 1:1,000), anti-PU.1 (Cell Signaling, 1:1,000 for IHC, 1:250 for IF), anti-Aldh1l1 (abcam, 1:100), anti-GFAP, anti-human MFG-E8 (R&D Systems, 1:500), anti-SMA (abcam, 1:200) and anti-Aβ (CN6[14], 1:1,000). Amyloid staining was performed using Methoxy-X04 (4% vol of 10 mg/ml in DMSO and 7.7% vol CremophorEL in 88.3% PBS) for 15 min at RT, Congo red or LCO staining (2.4 µM qFTAA and 0.77 µM hFTAA in PBS[11]), according to standard protocols. Prussian blue staining was used to visualize cerebral microbleeds by staining ferric iron in hemosiderin[15].

Image analysis

Images were acquired using a Zeiss Axioplan 2 with the AxioVision 4.7 software (Zeiss) using a 4x/0.10 or 40x/0.75 objective, with fixed camera exposure time and lamp intensity for comparative stainings. Image background was subtracted using an inbuilt Fiji plugin (Rolling-Ball background correction). Optical sections were acquired on a Zeiss LSM 510 META (Axiovert 200M) confocal microscope with a 20x/0.5 (air) or an oil immersion 40x/1.3 or 63x/1.4 objective on the LSM software 4.2 (Carl Zeiss), using sequential excitation of fluorophores (A488, A568, A647) or Leica SP8 on the software LAS X (Leica, Germany). Mosaics of whole sections were acquired on a Zeiss AxioObserver.Z1 Slide Scanner, using a 20x/0.8 objective for image acquisition. Maximum intensity projections were generated with Fiji or Imaris software.

Aβ (compact and diffuse, CAA) load was determined based on Congo red and anti-Aβ (CN6) staining using the area fraction fractionator technique[9]. Stereological analysis was performed by a blinded observer on sets of every 36th systematically sampled brain sections throughout the neocortex (for quantification of cortical Aβ load in the 2- to 4-month-old APPPS1xMfge8 or in the 9- to 12-month-old APP23xMfge8 mice,

respectively) or in a set of every 12th sampled section for quantification of hippocampal seeding induction using an Axioskop microscope (Zeiss, Germany) equipped with a motorized x-y-z-stage coupled to a video-microscopy system (Microfire, Optronics, California, USA). Analysis was conducted using the Stereo Investigator 6 (MBF Bioscience). Aβ load was calculated as area (%) covered by Congo red and anti-Aβ staining (20x/0.45 air objective). Since the 6-month-old female APP23xMfge8 mice only had 1-8 plaques per set of every 12th section, plaque number was quantified by blinded counting and not by stereological analysis. Male 6-month-old APP23x*Mfge8* WT-C2 KO mice were not included, as they virtually never show plaques at this age. For ease of visual comparison, stereological counts were normalised to the mean value of the *Mfge8* WT animals for each age-group.

Frequency of CAA (positive for Aβ and Congo Red) and hemosiderin-positive microhaemorrhages were manually assessed throughout the region of interest (every 36th section in the cortex for CAA and every 12th section for hemosiderin; and every 12th section of the hippocampus, striatum, and thalamus by a blinded observer, according to previous descriptions[15,16].

For analysis of LCO staining, 8μm-thick z-stacks of 30-40 plaques per animal were acquired with a Leica SP8 microscope using an 40x/1.3 oil-immersion objective on the software LAS X, using sequential excitation of the A647 fluorophore (for Iba1 costaining) and LCOs. qFTAA and hFTAA were excited with the 405 laser. Maximum intensity projections of the images were semi-automatically analyzed by a blinded observer with a custom plugin written in Fiji. After selecting plaques with surrounding Iba1-staining as region of interest, fluorescence channels were split and fixed intensity thresholds were applied to each channel. For every plaque, plaque size and area of the different stainings within the region of interest were determined based on thresholded areas.

For the determination of the number of microglia per brain, Iba1-positive cells were determined with the optical fractionator technique with three dimensional dissectors as previously described[5,12]. For the assessment of plaque-associated PU.1-positive cells, the diameter of the Congo Red-positive plaques was determined and microglial nuclei were counted in the two-fold radius of the plaque diameter.

Electron microscopy

For electron microscopy, animals were perfused with PBS, followed by a mixture of 4% PFA and 0.5% glutaraldehyde in 0.1 M cacodylate buffer (pH 7.4, Science Services) for 15 min. Following a brief postfixation period, serial frontal brain sections were cut with a vibratome (Leica VT1000S), washed in TBS, incubated in 0.1% NaBH4 (Sigma-Aldrich), and blocked with 5% BSA for 1 h at room temperature (RT) to reduce non-specific staining. For MFG-E8 staining, goat polyclonal anti-murine MFG-E8 (R&D systems, 1:1,000) was used as primary antibody followed by a biotinylated specific anti-IgG (Vector Laboratories, 1:200) as secondary antibody. Specificity of labeling was further verified in control experiments without antibodies. After washing in TBS, sections were incubated in avidin–biotin–peroxidase complex (ABC-Elite; Vector Laboratories) for 90 min at RT and were reacted with diaminobenzidine (DAB) solution (Vector Laboratories) at RT. Sections were silver-intensified by incubation in 3% hexamethylenetetramine (Sigma-Aldrich), 5% silver nitrate

(AppliChem), and 2.5% disodium tetraborate (Sigma-Aldrich) for 10 min at 60°C, in 1% tetrachlorogold solution (AppliChem) for 3 min, and in 2.5% sodium thiosulfate (Sigma-Aldrich) for 3 min. After staining, sections were washed in 0.1M cacodylate buffer, osmicated (0.5% OsO4 in cacodylate buffer), dehydrated (70% ethanol containing 1% uranyl acetate (Serva)), and embedded in Durcupan (Sigma-Aldrich). Ultrathin sections were collected on single-slot Formvar-coated copper grids that were contrast-enhanced with lead citrate for 4 min and examined using a Zeiss EM 900 electron microscope.

For immuno-electron microscopy of recombinant fibrils, peptides were aggregated by incubating Medin and Aβ40 alone or together under the same conditions as used for ThT analysis at 37°C for 7 days. 4 μL aliquots of fibrils were loaded onto carbon-coated copper grids and left for 2 min, the excess was removed by filter paper, and blocked in 1:10 goat serum in PBS+ (phosphate-buffered saline, pH 8.2, containing 1 % BSA, 500 mL/L Tween-20, 10 mM Na EDTA, and 0.2 g/L NaN3) for 15 min. Grids were then incubated with 1:500 Medin antibody (custom antibody from GenicBio Hong Kong) and Aβ antibody (6E10, BioLegend) for 2 h at room temperature, rinsed in 3x2 min PBS+, and then immunolabelled using 6 nm gold particle-conjugated goat anti-rabbit and 14 nm donkey anti-mouse IgG secondary probe (1:50) for 1 h at room temperature. After 5x2 min PBS+ and 5x2 min distilled water rinses, the grids were negatively stained using 4% uranyl acetate for 30 sec. Samples were visualized on a Tecnai 10 electron microscope at 100 kV.

For immuno-electron microscopy of human aorta extracts, grids were prepared as above using 1H4 Medin antibody or isotype control and 10 nm goat anti-rat IgG secondary probe (1:50).

Statistics

A priori power analyses were performed (using G*Power software, version 3.1.9.6) to determine the minimum number of animals for each experiment to achieve a power of 80%. Statistical analysis was performed using Prism 8 software. Data were tested for normal distribution (Shapiro-Wilk test) and statistical outliers were identified and removed (ROUT method), where necessary. If data were normally distributed, one- or two-way ANOVAs were performed, followed by Tukey's or Sidak's multiple comparison test (as suggested by the software). Because we could not detect overt gender effects in our data sets, we did not consider sex as an independent variable in our analyses. If data were not normally distributed, a non-parametric test (Kruskal-Wallis) was performed, followed by multiple comparison of the mean ranks with Dunn's correction if $P < 0.05$. For pairwise comparisons, only non-parametric Mann-Whitney tests were used in this manuscript. All data shown are means ± S.E.M.

Linear regressions were performed using JMP software (version 14.2.0). If necessary, data were first log10-transformed to achieve a normal distribution. Data were then analyzed using the 'Fit model' function, generating parameter estimates as well as residual vs. leverage plots, where a least squares line (red) and confidence bands (shaded red) provide a visual representation of the statistical significance (at the 5% level) of the effect of X ("Age"); a significant effect is evident by the crossing of the confidence lines (shaded red/red) through the blue line in the graph, which indicates the mean of the Y leverage residuals. To calculate the data points in the graph, the mean value of Y is added to the Y-residuals and the mean of the X-value is

added to the X-residuals, generating "leverage residuals", and these pairs of residuals are then used to generate the effect leverage plots shown (see e.g. [17]).

References

1. Silvestre, J.-S. *et al.* Lactadherin promotes VEGF-dependent neovascularization. *Nat. Med.* **11**, 499–506 (2005).
2. Radde, R. *et al.* Abeta42-driven cerebral amyloidosis in transgenic mice reveals early and robust pathology. *EMBO Rep.* **7**, 940–6 (2006).
3. Sturchler-Pierrat, C. *et al.* Two amyloid precursor protein transgenic mouse models with Alzheimer disease-like pathology. *Proc. Natl. Acad. Sci. U. S. A.* **94**, 13287–92 (1997).
4. Füger, P. *et al.* Microglia turnover with aging and in an Alzheimer's model via long-term in vivo single-cell imaging. *Nat. Neurosci.* **20**, 1371–1376 (2017).
5. Wendeln, A.-C. *et al.* Innate immune memory in the brain shapes neurological disease hallmarks. *Nature* **556**, 332–338 (2018).
6. Davies, H. A. *et al.* Oxidative Stress Alters the Morphology and Toxicity of Aortic Medial Amyloid. *Biophys. J.* **109**, 2363–2370 (2015).
7. Casali, B. T. & Landreth, G. E. Aβ Extraction from Murine Brain Homogenates. *Bio-protocol* **6**, e1787 (2016).
8. Ye, L. *et al.* Aβ seeding potency peaks in the early stages of cerebral β-amyloidosis. *EMBO Rep.* **18**, 1536–1544 (2017).
9. Meyer-Luehmann, M. *et al.* Exogenous induction of cerebral beta-amyloidogenesis is governed by agent and host. *Science* **313**, 1781–1784 (2006).
10. Degenhardt, K. *et al.* Medin aggregation causes cerebrovascular dysfunction in aging wild-type mice. *Proc. Natl. Acad. Sci.* 202011133 (2020). doi:10.1073/pnas.2011133117
11. Rasmussen, J. *et al.* Amyloid polymorphisms constitute distinct clouds of conformational variants in different etiological subtypes of Alzheimer's disease. *Proc. Natl. Acad. Sci.* **114**, 13018 LP – 13023 (2017).
12. Varvel, N. H. *et al.* Replacement of brain-resident myeloid cells does not alter cerebral amyloid-β deposition in mouse models of Alzheimer's disease. *J. Exp. Med.* **212**, 1803–1809 (2015).
13. Kai, H. *et al.* Enhanced Antigen Retrieval of Amyloid β Immunohistochemistry: Re-evaluation of Amyloid β Pathology in Alzheimer Disease and Its Mouse Model. *J. Histochem. Cytochem.* **60**, 761–769 (2012).
14. Eisele, Y. S. *et al.* Peripherally applied Abeta-containing inoculates induce cerebral beta-amyloidosis. *Science* **330**, 980–982 (2010).
15. Winkler, D. T. *et al.* Spontaneous Hemorrhagic Stroke in a Mouse Model of Cerebral Amyloid Angiopathy. *J. Neurosci.* **21**, 1619 LP – 1627 (2001).
16. Schelle, J. *et al.* Early Aβ reduction prevents progression of cerebral amyloid angiopathy. *Ann. Neurol.* **86**, 561–571 (2019).
17. Sall, J. Leverage plots for general linear hypotheses. *Am. Stat.* **44**, 308–315 (1990).

Author contributions

Conflict of interest

T.D. received funding from Novartis for a lecture on human brain anatomy. The other authors declare no competing interest.

Supplementary Information is available for this paper.
All data generated or analysed during this study are included in this published article (and its supplementary information files).

Correspondence and requests for materials should be addressed to Dr Jonas Neher (jonas.neher@dzne.de).

4. Appendix

4.1 Acknowledgements

4.2 Abbreviations

2D, 3D	two, three-dimensional
AA	(serum) amyloid A
aa	amino acid
AD	Alzheimer's disease
AICD	APP intracellular domain
AMed	Medin amyloid
ApoE	Apolipoprotein E
APP	amyloid precursor protein
APPs	soluble APP ectodomain fragment
Aβ	amyloid-β
BACE	β-site APP cleaving enzyme
BBB	blood brain barrier
BLAST	Basic Local Alignment Search Tool
BM	basement membrane
C1/2	discoidin domain 1/2
CAA	cerebral amyloid angiopathy
CTF	C-terminal fragment
DNA	deoxyribonucleic acid
EC	endothelial cell
ECM	extracellular matrix
EGF	epidermal growth factor
EOAD	early-onset AD
IAPP	islet amyloid polypeptide
kDa	kilodalton
KO	knockout
LCO	luminescent conjugated oligothiophenes
LOAD	late-onset AD
MAPT	microtubule-associated protein tau
MFG-E8	milk fat globule-EGF factor-8
MMP	matrix metalloproteinase
MRI	magnetic resonance imaging
MMSE	mini-mental state examination
NO	nitric oxide
P/T	proline/ threonine
PD	Parkinson's disease
PET	positron emission tomography
PrP	prion protein
PS	phosphatidylserine
PSEN	presenilin
qFTAA/hFTAA	quadro/hepta-formyl thiophene acetic acid
RAGE	receptor for advanced glycation end products
RGD	arginine-glycine-aspartate
ROS	reactive oxygen species
SMC	smooth muscle cell
SOD	superoxide dismutase
SS	signal peptide sequence
T2D	type-2 diabetes
TDP-43	TAR DNA-binding protein 43

tg	transgenic
ThT	Thioflavin T
Thy1	thymocyte differentiation antigen 1
TM	transmembrane domain
TTR	transthyretin
VaD	vascular dementia
VCI	vascular cognitive impairment
VEGF	vascular endothelial growth factor
VSMC	vascular smooth muscle cell
WT	wild-type
y	years
β-gal	β-galactosidase